

**A theoretical and experimental investigation
of a solid desiccant air dehumidification
system using shell-tube heat and mass
exchanger configuration**

By

Adrian Rosseno Katili

Sarjana Teknik (BEng), MSc

Thesis Submitted to the University of Nottingham

for the Degree of Doctor of Philosophy

June 2018

Abstract

The building sectors represent about 40% of total primary energy consumption and more than 30% of CO₂ emissions globally. In hot and humid climates, the need for air conditioning for thermal comfort contributes to around 60% of domestic buildings energy consumption. This is aggravated by the widespread use of inefficient and energy intensive mechanical vapour compression air conditioning systems and the way air humidity is controlled. An extensive literature review of air dehumidification systems was conducted to map out the state of existing technology. This re-enforced the status of existing passive cooling technologies operating according to the principle of adsorption, absorption and evaporation as offering promising solutions but of limited performance.

This research aims to investigate potential design enhancement of solid desiccant based air dehumidification systems that can extend the applicability of evaporative cooling systems to hot and humid regions. However, this requires overcoming the common problems associated with solid desiccant systems in regards to removing large amount of heat released during the adsorption process and residual heat from the regeneration process. Therefore, this thesis proposes an innovative solid desiccant air dehumidification system arranged in the form of a shell-tube heat and mass exchanger configuration. The proposed air dehumidification arrangement is designed to enhance both heat and mass transfer between the solid desiccant layer and its surrounding during the adsorption and regenerations process. The design incorporates a solid desiccant annular layer inside the heat exchanger tubes. A bundle of these desiccant filled tubes was enclosed in cylinder with two openings to form a tube-shell heat and mass exchanger. A rolled thin copper mesh was used to support the solid desiccant particles against the tube wall while allowing air to flow through the centre of the tube.

Abstract

A comprehensive mathematical model expressing heat and mass transfer balance of the system was developed and the governing equations were discretised into a MATLAB codes program. The results of the mathematical model were presented in details investigating the effects of different operating parameters such as tube length, diameter, air temperature, humidity ratio and flow velocity. To validate the computer results, a proof-of-concept laboratory prototype and test rig were built and tested under controlled air temperature and humidity. It was particularly noted that while optimum tube length was found for better overall performance, it was also observed that moisture removal was more efficient under smaller air velocity. For higher dehumidification capacity and efficiency, shorter cycle time was however more favourable.

Furthermore, the experimental test results emphasized the importance of the removal of heat of adsorption from the desiccant layer. By using secondary air to help remove heat during moisture adsorption and to evacuate residual heat from preceding regeneration process, the prototype was able to provide air with constant humidity ratio of around 8 g/kg lower than the ambient air for a dehumidification cycle of 5 minutes. It was also shown that dehumidification performance would be severely reduced if secondary air / post-regeneration cooling was not employed. Furthermore, the investigations under different testing conditions revealed that dehumidification capacity increased 50% with higher airflow while moisture removal would be more efficient under lower air velocity, and higher regeneration temperature improved dehumidification rate by up to 28% at the expense of higher heating energy. It was also noted that while drier outlet air could be provided with lower inlet air humidity, dehumidification effect was more significant with higher inlet air humidity.

Last but not least, the experimental test results were also used to refine the mathematical model and introduce corrections to the governing equations mainly concerning heat storage of the system's structure and its effect on moisture adsorption and desorption rates.

Publications

- A.R. Katili, R. Boukhanouf, R. Wilson, Space Cooling in Buildings in Hot and Humid Climates – a Review of the Effect of Humidity on the Applicability of Existing Cooling Techniques, in: 14th International Conference on Sustainable Energy Technologies – SET 2015, Nottingham, 2015. doi:10.13140/RG.2.1.3011.5287.

Acknowledgement

First of all, I would like to express my utmost gratitude to my supervisor Dr. Rabah Boukhanouf for his immense and invaluable guidance throughout my unforgettable four-year-long academic journey in Nottingham. From back then when I was applying for PhD until the writing up of this thesis, his endless support, advices and encouragement have always helped me gain knowledge and confidence to progress during my research project.

I am greatly thankful for the assistance of Tony Gospel, Andrew Mathews, and Jonathan Moss during my time in the laboratory. They have been very helpful during the design and fabrication of my experimental setup. The prototype would not be finished without their support.

I am deeply indebted to the Indonesian Ministry of Finance for sponsoring my study. I chose my research topic on air dehumidification to address the need of energy efficient solution for buildings in hot and humid climate, and I sincerely hope this thesis would be beneficial for Indonesia. I also hope that experience and skills I acquired during my study will help me contribute further to the knowledge and research in this area.

Finally, I would like to express my sincerest appreciation and thanks to my wife Xandra for her support and patience during my study. She came to my life at the perfect time and her being my companion has given me the extra motivation to keep working hard. Also, the endless encouragement and support from my father, mother, sister, family, friends and colleagues are hugely appreciated.

Table of Contents

Abstract.....	I
Publications	III
Acknowledgement.....	IV
Table of Contents	V
Nomenclature	IX
List of Figures.....	XI
List of Tables.....	XIV
Chapter 1: Introduction.....	15
1.1 Background	15
1.2 Project aims and objectives.....	20
1.3 Problem definition	20
1.4 Research methodology.....	21
1.5 Novelty and contribution to knowledge	23
1.6 Thesis layout	23
Chapter 2: Review of solid desiccant air dehumidification technologies.....	25
2.1 Introduction	25
2.1.1. Thermal condensation dehumidification systems.....	25
2.1.2. Desiccant-based dehumidification systems	26
2.1.3. Membrane-based dehumidification systems.....	27
2.2 Solid desiccant materials.....	28
2.2.1. Adsorption characteristic of solid desiccant materials.....	28
2.2.2. Advancement on desiccant material	31
2.3 Solid desiccant dehumidification systems	32
2.3.1. Rotary desiccant wheel.....	34
2.3.2. Fixed desiccant bed/channel.....	39
2.3.3. Internally cooled desiccant dehumidifier	44
2.3.4. Analysis of reviewed work of solid desiccant systems.....	54
2.4 Governing equations for solid desiccant dehumidifier.....	60
2.4.1. Gas-side resistance and solid-side resistance models.....	60
2.4.2. Equilibrium adsorption equation.....	64
2.4.3. Governing equations for solid desiccant dehumidifier with internal heat exchanger	65
2.5 Summary	71

Table of Contents

Chapter 3: Design and computer modelling	74
3.1 Introduction	74
3.2 Outline configuration of the shell-tube solid desiccant heat and mass exchanger	75
3.3 Mathematical formulation.....	79
3.3.1. Energy balance of secondary air in the shell side.....	81
3.3.2. Heat and mass balance of process air.....	82
3.3.3. Heat and energy balance of the desiccant layer	83
3.3.4. Boundary conditions.....	85
3.4. Numerical solutions and computer model	87
3.4.1. Discretisation of equations in sub-region 1 and sub-region 3 (air channels).....	88
3.4.2. Discretization of equations in sub-region 2 (desiccant layer).....	90
3.4.3. Computer model algorithm	96
3.4.4. Validation of the computer model.....	100
3.5. Performance indices	101
3.5.1. Dehumidification Coefficient of Performance (DCOP).....	102
3.5.2. Dehumidification Capacity (DC).....	102
3.5.3. Overall relative moisture removal efficiency	102
3.6. Computer model results of a single shell-tube heat and mass exchanger configuration modelling	103
3.6.1. Cyclical steady state.....	103
3.6.2. Temperature and humidity distribution along the air channels.....	105
3.6.3. Temperature and humidity distribution in the desiccant layer	109
3.6.4. Performance improvement of the shell-tube configuration.....	111
3.6.5. Effect of channel length.....	114
3.6.6. Effect of air velocity.....	115
3.6.7. Effect of cycle time	117
3.7. Summary	118
Chapter 4: Small scale laboratory prototype construction.....	121
4.1. Earlier design prototype.....	121
4.2. Design and construction of the shell-tube desiccant rig.....	125
4.3. Desiccant filling.....	129
4.4. Auxiliary components.....	132
4.5. Test rig	133
4.6. Measuring instruments.....	134

Table of Contents

4.7.	Experimental setup and operating modes.....	136
4.8.	Test conditions	139
4.9.	Test procedure and health and safety checks.....	141
4.10.	Experimental observations and limitations	142
4.10.1.	Desiccant tubes handling	142
4.10.2.	Heating of regeneration air	143
4.10.3.	Measurement limits	144
4.10.4.	Heat storage of system's structure.....	144
4.11.	Preliminary results	145
4.12.	Summary	147
Chapter 5:	Results analysis and discussion	148
5.1.	Uncertainty of experimental data	148
5.2.	Effect of secondary air stream on dehumidification performance	152
5.2.1.	Case a – air dehumidification with no secondary (shell side) air flow and no cooling period	152
5.2.2.	Case b – air dehumidification with secondary (shell side) air flow and no cooling period	154
5.2.3.	Case c – air dehumidification with secondary (shell side) air flow and a cooling period	156
5.2.4.	Comparative analysis.....	158
5.3.	Parametric analysis.....	159
5.3.1.	Effect of airflow rate.....	159
5.3.2.	Effect of regeneration temperature.....	161
5.3.3.	Effect of inlet air humidity	163
5.4.	Simplified energy assessment.....	164
5.5.	Mathematical model refinement	166
5.5.1.	New energy balance for secondary air stream.....	166
5.5.2.	Energy balance for the shell-side surface.....	167
5.5.3.	Discretization of the new equations	167
5.5.4.	Results of updated model	168
5.6.	Summary	172
Chapter 6:	Conclusion and future work.....	175
6.1.	Conclusions	175
6.1.1.	Contribution	175
6.1.2.	The main findings.....	177
6.2.	Future work.....	180

Table of Contents

6.2.1. Further refinement on mathematical model	180
6.2.2. Heat storage and further testing possibilities	180
6.2.3. Integration with cooling systems for building application	181
References.....	184
Appendices	190
Appendix A – Computer Algorithm written in MATLAB script file.....	190
Appendix B – Thomas Algorithm to solve tridiagonal system of desiccant side heat balance	224
Appendix C - Thomas Algorithm to solve tridiagonal system of desiccant side moisture balance	224

Nomenclature

Abbreviations

ADI	Alternating direction implicit method
CC	Concentric channels
DCOP	Dehumidification coefficient of performance
DC	Dehumidification capacity
DW	Desiccant wheel
GSR	Gas-side resistance model
GSSR	Gas and solid-side resistance model
HMX	Heat and mass exchanger
RH	Relative humidity
SC	Single channel

Nomenclature

A_{ic}	Cross section for primary air channel, m ²
A_{oc}	Cross section area for air flow in shell side, m ²
c_a	Specific heat of air, J kg ⁻¹ K ⁻¹
c_d	Specific heat of desiccant, J kg ⁻¹ K ⁻¹
c_v	Specific heat of water vapour, J kg ⁻¹ K ⁻¹
D_h	Hydraulic diameter, m
D_{va}	Moisture diffusivity in air, m ² s ⁻¹
D_s	Effective moisture diffusion coefficient, m ² s ⁻¹
h_{ic}	Convective heat transfer coefficient for primary air channel, W m ⁻² K ⁻¹
h_{oc}	Convective heat transfer coefficient in shell side, W m ⁻² K ⁻¹
h_m	Convective mass transfer coefficient in primary channel, kg m ⁻² s ⁻¹
$h_{r,inlet}$	Inlet enthalpy of regeneration air, J kg ⁻¹
$\bar{h}_{r,outlet}$	Mean outlet enthalpy of regeneration air, J kg ⁻¹
L_v	Latent heat of vaporization, J kg ⁻¹
$\dot{m}_{p,ic}$	Mass flow rate of dehumidified process air, kg s ⁻¹
$\dot{m}_{r,ic}$	mass flow rate of regeneration air, kg s ⁻¹
$\dot{m}_{r,oc}$	mass flow rate of heating air, kg s ⁻¹
p_{id}	Perimeter of primary air channel (desiccant layer), m
p_{od}	Contact perimeter between secondary air and desiccant tube, m
q_{st}	Latent heat of adsorption of the desiccant layer, J kg ⁻¹
t_{ad}	Adsorption time, s
t_{cyc}	Total cycle time, s
T_{aic}	Temperature of primary air, K
T_{aoc}	Temperature of secondary air, K
$T_{p,inlet}$	Inlet temperature of process air, K
$T_{c,inlet}$	Inlet temperature of cooling air, K
$T_{r,inlet}$	Inlet temperature of regeneration air, K
$T_{r,oc,inlet}$	Inlet temperature of heating air, K
$\bar{T}_{r,oc,outlet}$	Mean outlet temperature of heating air, K
T_{sdic}	Temperature of desiccant surface in contact with primary air stream, K
T_{sdoc}	Temperature of desiccant surface at the interface with the tube wall, K

Nomenclature

u_{aic}	Velocity of primary air, m s^{-1}
u_{aoc}	Velocity of secondary air, m s^{-1}
Y_{aic}	Humidity ratio of primary air kg kg^{-1}
$Y_{p,inlet}$	Inlet humidity of process air, kg kg^{-1}
$\bar{Y}_{p,outlet}$	Mean outlet humidity of process air, kg kg^{-1}
$Y_{r,inlet}$	Inlet humidity ratio of regeneration air, kg kg^{-1}
Y_{sdc}	gas phase equilibrium moisture content at the surface in contact with primary air, kg kg^{-1}

Greek symbols:

ρ_a	Air density, kg m^{-3}
ρ_d	Desiccant density, kg m^{-3}
λ_a	Air heat conductivity, $\text{W m}^{-1} \text{K}^{-1}$
λ_d	Desiccant heat conductivity, $\text{W m}^{-1} \text{K}^{-1}$
η	Moisture removal efficiency

List of Figures

Fig 1-1 Typical Building Energy Consumption in Tropical Countries [7]	16
Fig 1-2 Distribution of sensible and latent cooling load throughout the day [8].....	16
Fig 1-3 Contributor to building's cooling load [8].....	17
Fig 1-4 Monthly average outdoor condition for various climates in Asia during the hottest month of the year [7]	17
Fig 1-5 Latent load for South East Asian climate	18
Fig 2-1 Schematic of common desiccant dehumidifier [19]	27
Fig 2-2 Adsorption isotherms classified according to IUPAC [26].....	29
Fig 2-3 Comparison between adsorption isotherms of Type 1 extreme (1E), Type 1 moderate (1M), linear, Type 3 moderate (3M), and Type 3 extreme (3E) [25]	31
Fig 2-4 Desiccant wheel schematics [25]	33
Fig 2-5 Pennington cycle [25]	34
Fig 2-6 Honeycomb air channels of desiccant wheel [28].....	35
Fig 2-7 Examples of desiccant wheel's channel shapes considered in the study by Narayanan [34].....	35
Fig 2-8 Moisture removal for different channel shapes [34]	36
Fig 2-9 Radial blade rotary desiccant wheel design [36]	38
Fig 2-10 Wind tower with desiccant rotary wheel integration concept [36]	39
Fig 2-11 Geometry of honeycomb type adsorbent bed studied by Zhang et al. [37]	39
Fig 2-12 Schematic of a desiccant packed bed [38]	42
Fig 2-13 Configuration of (a) vertical, and (b) radial flow packed bed [40]	43
Fig 2-14 Pressure drop comparison between two packed desiccant bed [40].....	44
Fig 2-15 Schematic of desiccant packed bed with internal heat exchanger in cross- flow arrangement [43]	46
Fig 2-16 Cross-cooled compact solid desiccant dehumidifier [44].....	47
Fig 2-17 Conceptual diagram of cross-flow heat exchanger type adsorbent bed investigated in [45]	48
Fig 2-18 Desiccant-coated fin-tube heat exchanger [46]	49
Fig 2-19 Air conditioning system with silica gel coated heat exchanger [47]	50
Fig 2-20 Multi-pass honeycomb rotary desiccant regenerated by a direct hot water heating [48]	51
Fig 2-21 Process diagram of the multi-pass rotary dehumidifier [48].....	52
Fig 2-22 Non-adiabatic desiccant wheel [49]	53
Fig 2-23 Water cooled desiccant wheel [50]	54
Fig 2-24 cylindrical coordinate system and a model of control volume of the desiccant wheel [51]	61
Fig 2-25 Non-adiabatic desiccant wheel channel cross section geometry and model heat and mass transfer resistances [49].....	68
Fig 2-26 Schematic of the representative channel used in the mathematical model of [50].....	70
Fig 3-1 Arrangement of the proposed shell-tube HMX (adsorption mode).....	75

List of Figures

Fig 3-2 Schematics for (a) adsorption and (b) regeneration process	76
Fig 3-3 Shell-tube desiccant heat and mass exchanger replacing the desiccant wheel and heat exchanger in Pennington cycle configuration.....	77
Fig 3-4 STHMX combined with a dew-point indirect evaporative cooler	78
Fig 3-5 Control volume for mathematical modelling	80
Fig 3-6 Control volume of the model	87
Fig 3-7 Computer model flow chart.....	97
Fig 3-8 Validation of computer model: (a) Process air average outlet humidity ratio; and (b) Process air average outlet temperature.....	101
Fig 3-9 Outlet air (a) temperature and (b) humidity over multiple cycles	104
Fig 3-10 Primary air temperature profile along the channel for (a) dehumidification and (b) regeneration process.....	106
Fig 3-11 Secondary air temperature profile along the channel for (a) dehumidification and (b) regeneration process	107
Fig 3-12 Primary air humidity profile along the channel for (a) dehumidification and (b) regeneration process.....	108
Fig 3-13 Temperature profile of desiccant surface in contact with primary air for (a) dehumidification and (b) regeneration process	109
Fig 3-14 Moisture profile of desiccant layer for (a) adsorption and (b) desorption process.....	110
Fig 3-15 Variation of outlet (a) air humidity ratio and (b) temperature	112
Fig 3-16 Performance comparison of different working scenario.....	113
Fig 3-17 Dehumidification performance for different air channel length.....	115
Fig 3-18 Dehumidification performance for different air velocities	116
Fig 3-19 Dehumidification performance for various cycle time	117
Fig 4-1 Schematic of earlier prototype with single tube-side channel	121
Fig 4-2 Constructed early prototype rig and the flow diagram	122
Fig 4-3 Test results of the first prototype: Primary air humidity profile over time for both adsorption and desorption process	123
Fig 4-4 3D sketch of the tubes and shell arrangement	125
Fig 4-5 Air flow paths through the heat exchanger	126
Fig 4-6 CAD drawing of the prototype: (a) front view and (b) side view	127
Fig 4-7 Construction shell-tube heat and mass exchanger	128
Fig 4-8 Shell-side casing	128
Fig 4-9 Air flow separator.....	129
Fig 4-10 Desiccant tube filling process: (a) wire copper mesh, (b) cutting wire mesh into small sections, (c) Rolling mesh with help of metal rod, (d) insertion of rolled mesh into the tube, (e) desiccant tube ready for filling, (f) aluminium tube filled with desiccant powder	130
Fig 4-11(a) desiccant powder sieving, (b) sieved powder to be poured inside the tube	131
Fig 4-12 Hot air blower.....	132
Fig 4-13 Assembled test rig	133
Fig 4-14 Positioning of measurement instrument	134

List of Figures

Fig 4-15 Measurement instruments (a) thermocouple,(b) hot wire anemometer,(c) temperature and humidity sensor, and(d) hand held temperature and humidity meter	135
Fig 4-16 Experimental setup	136
Fig 4-17 Airflow schematics for regeneration process.....	137
Fig 4-18 Airflow schematic during cool down period.....	138
Fig 4-19 Airflow schematics during dehumidification period	138
Fig 4-20 Integration of dew point evaporative cooler	139
Fig 4-21 Testing scenarios	140
Fig 5-1 Uncertainty in inlet air temperature and humidity	150
Fig 5-2 Uncertainty in outlet air temperature and humidity	151
Fig 5-3 Case a - Primary air temperature and humidity ratio variation for dehumidification process ($T_{cyc}/2=5$ min, $v_p=11.02$ m ³ /h, $T_{inlet}=30^{\circ}\text{C}$, $Y_{inlet}=22$ g/kg)	153
Fig 5-4 Case a - Primary air temperature and humidity ratio variation for regeneration process ($T_{cyc}/2=5$ min, $v_p=11.02$ m ³ /h, $T_{inlet}=30^{\circ}\text{C}$, $Y_{inlet}=22$ g/kg).	154
Fig 5-5 Case b - Primary air temperature and humidity ratio variation for dehumidification process ($T_{cyc}/2=5$ min, $v_p=4.07$ m ³ /h, $V_{secondary}=12.09$ m ³ /h, $T_{inlet}=30^{\circ}\text{C}$, $Y_{inlet}=22$ g/kg)	155
Fig 5-6 Case b - Primary air temperature and humidity ratio variation for regeneration process ($T_{cyc}/2=5$ min, $v_p=4.07$ m ³ /h, $V_{secondary}=12.09$ m ³ /h, $T_{inlet}=30^{\circ}\text{C}$, $Y_{inlet}=22$ g/kg)	156
Fig 5-7 Case c - Primary air temperature and humidity ratio variation for dehumidification process ($T_{cyc}/2=5$ min, $v_p=4.07$ m ³ /h, $v_{secondary}=12.09$ m ³ /h, $T_{inlet}=30^{\circ}\text{C}$, $Y_{inlet}=22$ g/kg)	157
Fig 5-8 Case c - Primary air temperature and humidity ratio variation for regeneration process ($T_{cyc}/2=5$ min, $v_p=4.07$ m ³ /h, $v_{secondary}=12.09$ m ³ /h, $T_{inlet}=30^{\circ}\text{C}$, $Y_{inlet}=22$ g/kg)	158
Fig 5-9 Dehumidification performance for different types of working cycle.....	159
Fig 5-10 Dehumidification performance with different flow rates	161
Fig 5-11 Dehumidification performance with varied regeneration temperature ...	162
Fig 5-12 Effect on inlet air humidity on dehumidification performance	164
Fig 5-13 Humidity ratio of primary air stream (dehumidification and regeneration process).....	169
Fig 5-14 Temperature of primary air stream (dehumidification and regeneration process).....	170
Fig 5-15 Temperature of secondary air stream (dehumidification and regeneration process).....	171
Fig 5-16 Air humidity ratio - comparison between simulation and experimental results	172

List of Tables

Table 2-1 Properties of various desiccants studied by Zhang et al. [37] 40

Table 2-2 Summary of reviewed work on solid desiccant systems 56

Table 3-1 Properties of solid desiccant material [32] 85

Table 3-2 Desiccant wheel parameters used for validation [32,63]..... 100

Table 3-3 Base operating parameters of the computer model..... 103

Table 4-1 Dehumidifier prototype specification 126

Table 4-2 Silica gel properties (Sigma Aldrich 214396) 131

Table 4-3 Hot air blower specification..... 132

Table 4-4 Measurement summary 135

Table 4-5 Testing results for inlet air at 30°C, 80% RH, heating set value 120°C,
airflow level 1 146

Table 5-1 Estimated relative uncertainty in air humidity ratio..... 150

Table 5-2 Measured air conditions for different airflow settings 160

Table 5-3 Air temperature and humidity profile for different regeneration
temperature set values..... 161

Table 5-4 Measured air conditions for different inlet humidity set values 163

Table 5-5 Simplified energy assessment of the dehumidifier prototype 165

Table 5-6 Operating parameters for the updated computer model 168

Chapter 1: Introduction

1.1 Background

Thermal comfort is essential for the wellbeing and enhanced living conditions of building occupants. A recent survey conducted by Frontczak [1] showed that thermal comfort ranked above visual and acoustic comfort and indoor air quality. However, the drive towards better thermal comfort conditions within built environments leads to significant increase in the use of active HVAC mechanical systems. This coupled with people spending most of the time indoor; the building sector becomes one of the largest energy consumer worldwide. Globally, energy consumption of building accounts for about 40% of total primary energy consumption and more than 30% of CO₂ emissions [2]. In many countries, HVAC systems share an important proportion in building energy consumption. For example, in the US, space heating contributes 37% of residential energy consumption and more than 25% of service sector energy consumption, while in the EU, contribution of space heating accounts for 66% of residential use and 39% of service sector [3]. Furthermore, in regions with hot climate, around 60% of building energy consumption is used for space cooling [4]. Energy consumption of buildings is also becoming more and more important in developing countries such as in South East Asia due to population growth and improvement of economic prosperity. With prediction that the energy consumption in this region will exceed that of developed countries, there is therefore a strong interest to utilize energy resources efficiently [5,6]. As South East Asian region has hot and humid climate, typical building energy consumption is dominated by the use of air conditioning systems, as shown in Fig 1-1.

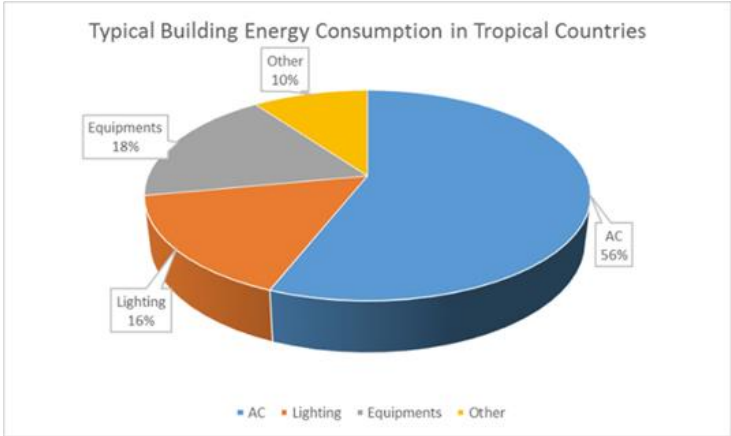


Fig 1-1 Typical Building Energy Consumption in Tropical Countries [7]

Cooling loads in buildings are characterised with sensible heat load (air temperature) as well as latent heat load (air moisture). High latent heat load means that a considerable amount of cooling load in buildings is attributed to reducing air humidity. Fig 1-2 shows an example of daily profile of building cooling loads in Hong Kong [8]. It can be observed that the latent heat load is comparable to sensible heat load, especially during the morning period where the latent heat load is almost as high as the sensible heat load. Moreover, while the sensible heat load fluctuates throughout the day, the latent heat load is rather constant.

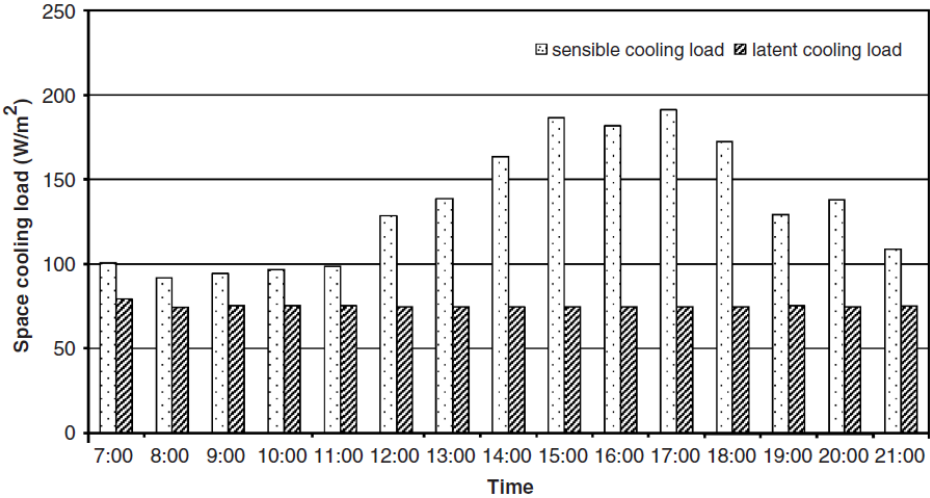


Fig 1-2 Distribution of sensible and latent cooling load throughout the day [8]

Chapter 1: Introduction

Humid fresh air from the ventilation system is noted to be the biggest contributor of the latent heat load, followed by the building occupant (though not as significant). The heat gain through the building envelope, meanwhile, is the most dominant sensible load. Such cooling load profile is typical in hot and humid climate as illustrated in Fig 1-3.

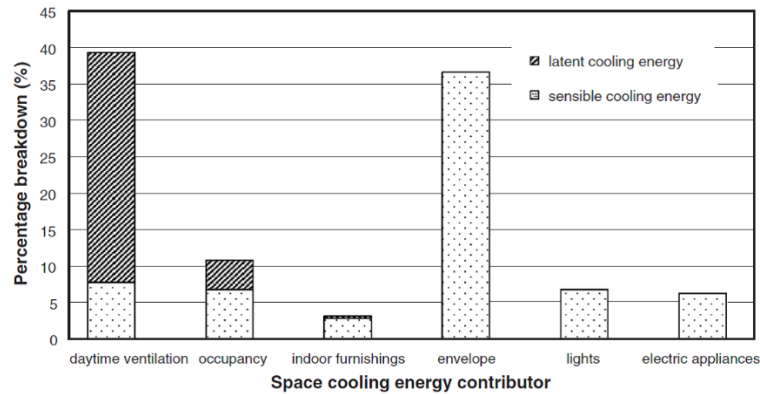


Fig 1-3 Contributor to building's cooling load [8]

Figure Fig 1-4 shows the characteristics of outdoor air in areas with tropical climate (Manila, Singapore, Bangkok, Kuala Lumpur, and Jakarta) compared to summer conditions of other climates such as sub-tropical climate (Hong Kong), temperate climate (Tokyo, Beijing, Seoul), and desert climate (Riyadh, Abu Dhabi) [7].

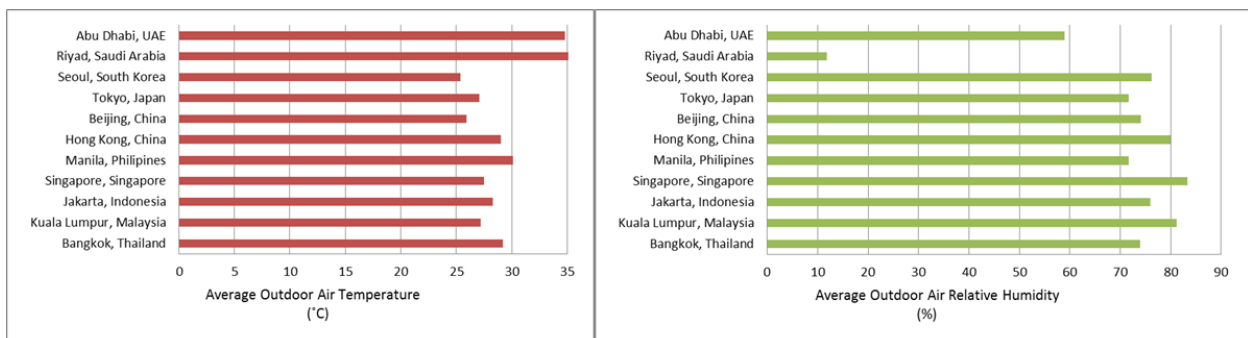


Fig 1-4 Monthly average outdoor condition for various climates in Asia during the hottest month of the year [7]

Chapter 1: Introduction

With outdoor air temperature range of 27 to 30°C and relative humidity higher than 70%, the tropical weather conditions mean that latent cooling load of buildings in most East Asian and South East Asian countries is high. In such climate, using common standard for air conditioned building with space temperature of 24°C and relative humidity of 50%, the cooling system needs to remove 9-10 g/kg of moisture from the air (Fig 1-5).

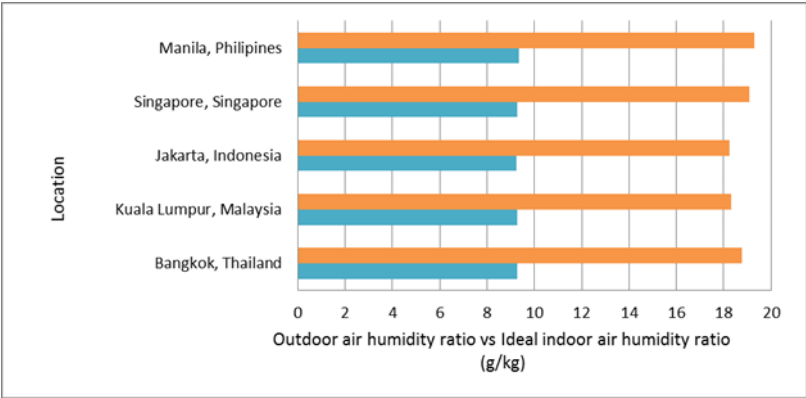


Fig 1-5 Latent load for South East Asian climate

The market for building indoor air conditioning system is mostly dominated by the mechanical vapour-compression refrigeration systems. These systems are popular with residential and commercial buildings operators as they provide good performance and controllability of indoor climate as well as reliability and cost effectiveness. However, it's also known to consume large amount of energy, especially in hot and humid climate where the system has to deal with both sensible and latent load. Mechanical vapour compression air conditioning (AC) systems reduce air humidity by cooling the air below its dew point to condensate the water vapour from the air, thus reducing its moisture content. In tropical climate, such approach means the air is cooled way below the required temperature for thermal comfort. For example, if outdoor air at temperature of 30°C and relative humidity (RH) of 80% is required to be conditioned at 24°C, 50% RH, the AC system would have to reduce the air temperature to below 15°C in order to remove the water vapour, followed by re-heating to achieve the required temperature and humidity. This leads to significant use of energy.

Various low energy alternative/passive cooling systems have been considered, notably evaporative cooling, radiant cooling and ground cooling (earth-to-air heat exchangers). However, those systems do not have capability of treating latent heat load, thus hinder their applicability in hot and humid climate [7,9–13]. Desiccant materials are known for their affinity to adsorb moisture from the air and hence can be found used for air dehumidification. Such systems can be used in conjunction with mechanical vapour compression systems for air conditioning or as alternative cooling system so that latent and sensible cooling loads can be treated independently thus increasing overall energy performance of HVAC system, while it can also be driven by low heat source such as heat recovery systems or solar energy, adding its potential for energy saving [14–16].

The desiccant material can be either solid or liquid type desiccant, with solid desiccant rotating wheel as the most adopted configuration for air dehumidification. By passing humid air stream through the desiccant coated/impregnated wheel, the desiccant can adsorb water vapour from the air stream to achieve air dehumidification. Since desiccant materials need to be regenerated to allow continuous operation, desiccant wheel is usually divided into two sections, the air dehumidification section and the desiccant regeneration section.

Desiccant regeneration can be achieved by applying heat to the desiccant in order to desorb moisture. Thus, by using the rotating wheel configuration, the two process can be performed simultaneously. However, while the regeneration process is essential for the working cycle of desiccant dehumidification systems, high temperature of desiccant (due to residual heat of regeneration process as well as adsorption heat during air dehumidification) is the common disadvantage of such system, as it limits the adsorption capacity of the desiccant. Furthermore, it also increases air temperature, thus adding the sensible cooling load of air cooling/conditioning system.

This research work addresses the importance of air humidity treatment and building HVAC performance, as both are strongly dependent to each other, especially in hot and humid climate. Increasing demand for air conditioning in buildings has a big contribution to global energy consumption, and latent heat load can have severe impacts on cooling system's

thermal performance. It is thus necessary to explore and develop energy efficient means of air dehumidification to cope with high air conditioning load, and more importantly, to “enable” various alternative/passive cooling systems.

1.2 Project aims and objectives

The main aim of the research project is to investigate a novel configuration of shell-tube heat exchanger based solid desiccant dehumidifier system. The choice of the heat exchanger design centres on heat exchange capabilities of shell-tube configuration and the suitability of integrating solid desiccant material layer while the shell-side serves to enhance cooling and regeneration of the desiccant material. This design addresses some heat transfer limitations commonly found in solid desiccant systems such as rejection of heat of adsorption. It is also anticipated that this shell-tube dehumidifier can form part of an integrated passive cooling strategy using evaporative cooling. The specific research objectives are described as follows:

- 1) A thorough literature review with the context of air dehumidification in building, with focus in solid desiccant dehumidification.
- 2) Computer modelling of thermal performance of air dehumidification system using complex formulation of heat and mass transfer processes of the solid desiccant.
- 3) Design, building and testing a laboratory scale shell-tube air dehumidification arrangement under controlled conditions of temperature, humidity and air flow rate.

1.3 Problem definition

Conventional mechanical vapour compression systems are overwhelmingly the preferred technology for air-conditioning in building because they offer simple control of thermal comfort. However, this disguises the fact that the technology is energy intensive in hot and humid climates (e.g., tropics and sub-tropics) as the air latent heat is treated by overcooling air, followed by reheating, leading to further energy waste. On the other hand, most of the

existing passive and low energy alternative cooling techniques can only deal with sensible heat, while latent load left untreated (or in some cases, increased). Therefore, air dehumidification process can play an important role in reducing energy consumption both of active and passive air-conditioning systems. Solid desiccant materials are commonly used in buildings for air dehumidification and heat recovery in the form of a rotary wheel. The desiccant is usually an inert solid material that doesn't cause any health issues.

For continuous operation however, the desiccant material requires energy in the form of low grade heat for regeneration and expelling desorbed moisture. A solid desiccant air dehumidifier thus operates between two states: adsorption and regeneration. In continuous cycle, the desiccant material must be cooled immediately after the regeneration process. It is also vital that during the adsorption process the desiccant material's temperature is not allowed to increase unbound as it limits its adsorption capacity and increases treated air temperature. Therefore, removing heat of adsorption during the adsorption process is required to improve performance and energy efficiency of the system.

1.4 Research methodology

This thesis addresses the aims and objectives of the project by carrying out a stepwise research methodology as follows:

1) Literature review

An overview of adoption of air conditioning for buildings in hot and humid climate is provided with particular focus on desiccant materials based air dehumidification for treating supply air moisture. Additionally, more detailed review of solid desiccant dehumidifier is presented including working principles, configurations, materials, integration with cooling systems, and performance of each systems.

This literature review provides the prerequisite understanding on air dehumidification principle, classification of various systems and advances. A research gap and innovations were identified, leading to the formulation of the research hypothesis of the proposed system design using shell-tube arrangement incorporation with desiccant material for effective air dehumidification and as an enabling technology for evaporative cooling system.

2) Mathematical formulations and simulations for the proposed systems

From the literature review, mathematical formulations were developed for the modelling of heat and mass transfer of the adsorption and desorption processes. Governing equations of energy and mass conservation were derived for the proposed configuration to formulate a mathematical model and associated boundary conditions. The mathematical model was then discretised into computer codes written using MATLAB software. The computer codes were then run iteratively until target convergence criteria were achieved and performance parameters determined.

3) Test rig constructions and experimental tests

A small-scale laboratory test rig was built to evaluate the performance of solid desiccant air dehumidification system. An environmental chamber supplying air at controlled temperature and humidity and air flow rate was used to assess the thermal performance of the desiccant material and the shell-tube mechanical arrangement. The desiccant system can be integrated to an indirect evaporative cooler. The experimental results provide realistic insight into the assumptions made in the formulation of the mathematical model and how to improve the accuracy of the computer model and system design for maximum dehumidification performance.

1.5 Novelty and contribution to knowledge

Research and development of adsorption systems for air dehumidification and other application have been reported in many literature using many different types of adsorbents, bed configurations, mathematical modelling and experimental investigations. However, the formulation of mathematical models of heat and mass transfer in adsorption systems remains complex and is application specific. In this work, adapted mathematical formulation of solving heat and mass transfer processes in the adsorption layer carried out with extensive boundary conditions. The work also attempted to address the problem of adsorption heat removal using a novel counter-flow tube-shell heat exchanger configuration. In this configuration, the solid desiccant forms a concentric thin layer around the inner diameter of the tube walls. This configuration allows fast desiccant material regeneration and heat removal during the adsorption process.

Therefore, this work contributes to advancing knowledge and understanding of design and mathematical modelling of adsorption for energy efficient air dehumidification systems, and providing alternative low carbon solutions for thermal comfort in buildings.

1.6 Thesis layout

The thesis is structured into 6 chapters:

Chapter 1 covers general background of the building energy consumption with focus on the energy demand of air conditioning in hot and humid climate. This chapter also includes the research aims and objectives, problem statement, the research methodology, and the contribution to the knowledge.

Chapter 2 provides an overview of the most common air dehumidification methods including the working principles. Furthermore, desiccant based dehumidification cooling system is considered as the main interest in this research work, with advance in materials, various configuration will be covered.

Chapter 1: Introduction

Chapter 3 is about the design and mathematical formulation of the proposed design, describing the working schematics and the governing heat and mass transfer equations. Furthermore, the numerical method of the equations is presented, and the computer model is developed to perform simulations of the operation and performance of the proposed dehumidifier.

Chapter 4 concerns the fabrications of small scale test rig and experimental work conducted of the proposed dehumidification system. This chapter describes test schematics, the components of the system, fabrication process, assembly and integration to evaporative cooling system, and experiment set-up. Additionally, step-by-step testing procedure and some experimental results are highlighted as well.

Chapter 5 analyses and discusses the results of the experiments data. The system's behaviour during different process and continuous cycles is evaluated, and a parametric study of the dehumidifier thermal performance is conducted under different operational parameters to assess its performance. Short viability assessment of the system will also be presented. Then, feedback from the test rig data will be used to improve the mathematical model.

Chapter 6 concludes the research findings and highlights the main features of the air dehumidification system. In addition, recommendation for future work to be conducted will be provided, based on any limitations of the systems as well as potential for further improvement.

Chapter 2: Review of solid desiccant air dehumidification technologies

2.1 Introduction

Thermal comfort and wellbeing of buildings' occupants are achieved through implementing narrow controls of air dry bulb temperature, humidity, air movement speed and radiation. The air relative humidity in building is an important factor as breathing problems and skin irritation can be caused by a dry microclimate whereas a high level of air relative humidity can lead to condensation and mould growth. Therefore, air relative humidity needs to be kept in the range of 30-70% [7]. In hot and humid climates where air relative humidity is approaching saturation, latent heat in form of air moisture has a significant proportion in air conditioning (AC) load. The commonly used mechanical vapour compression AC system removes water vapour from air by cooling it below its dew point, which is energy intensive. Alternative ways have been investigated to decouple sensible and latent heat energy of air. For example, solid and liquid desiccant materials for air dehumidification have gained popularity as they can be driven by low grade heat. On the other hand, recent studies also focus on isothermal air dehumidification incorporating highly selective membranes.

2.1.1. Thermal condensation dehumidification systems

The most common air dehumidification process is based on cooling. If humid air comes into contact with a cooling coil whose surface temperature is lower than the dew point of air, condensation of water vapour from the air will occur on the surface of the coil, thus dehumidification is obtained. This type of dehumidification is widely used in mechanical

vapour compression AC system, thus air cooling and dehumidification can be achieved with one single unit. However, this type of AC system is very energy intensive, as air is conditioned to appropriate thermal comfort level by overcooling the air below its dew point (usually much lower than required temperature for thermal comfort), then followed by re-heating of the air to the required temperature. Moreover, the refrigerant used in the MVC systems has raised environmental concerns [17]. While alternative systems (to replace the use of refrigerant) have been proposed, such as adsorbent and absorbent AC systems, they still rely on overcooling and reheating to dehumidify air.

2.1.2. Desiccant-based dehumidification systems

With a high affinity to absorb water vapour from air, desiccant materials can be employed to separate moisture from air, thus cooling and dehumidification can be treated independently. The moisture removal process with desiccant materials, or the sorption process (adsorption or absorption process), is an interaction between the sorbent and sorbate molecules through intermolecular interaction [18]. Desiccant materials at low water vapour concentration can attract and capture air moisture content to the surface of the desiccant due to vapour pressure difference between them, until equilibrium is reached. As desiccant approach saturation, its ability to adsorb moisture will decrease. Thus, for continuous air dehumidification, desiccant material needs to be reactivated / regenerated by applying thermal energy to remove moisture from the desiccant so that it can be used again. Fig 2-1 shows the schematic of desiccant dehumidifier in combination with a cooling system. Humid air is drawn from the ambient and passed through desiccant packed beds / desiccant coated channels, where moisture is adsorbed from the air stream by the desiccant material. The dried air is then sensibly cooled before being supplied to building. To regenerate the desiccant, air is heated to the required temperature and passed through the dehumidifier to expel moisture from the desiccant.

Desiccant-based air dehumidification is commonly accomplished using solid or liquid desiccant materials. Liquid desiccant systems generally require lower regeneration temperature and have lower pressure drop in air side. Solid desiccant systems, in the other hand, are compact, less subject to corrosion and carryover of liquid solution [19]. La et al. [14] conducted a case study of a hybrid desiccant cooling system and vapour compression air-conditioning for Shanghai weather condition. The author reported that by using solar energy to provide regeneration heating of the desiccant, the desiccant cooling system was able to handle about 33% of the cooling load and removed about 69% of the moisture load, saving 34% in electrical energy.

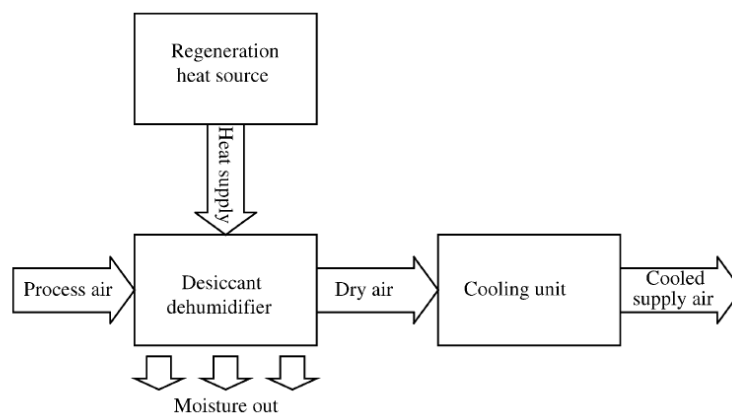


Fig 2-1 Schematic of common desiccant dehumidifier [19]

2.1.3. Membrane-based dehumidification systems

While desiccant-based dehumidification systems incorporate heat of adsorption, thus converting latent heat to sensible heat, the isothermal nature of water vapour separation in membrane technology has gained interest for HVAC application. The membranes for dehumidification process need to be permeable to water vapour while selective to water vapour over other matter/species. Studies have been conducted on different concept membrane-based dehumidification system, such as membrane-based liquid desiccant dehumidification system, vacuum membrane dehumidification systems, and membrane-

based electrochemical air dehumidification system. While incorporation of membrane in liquid desiccant system could overcome the carry-over problem, the other two concept previously mentioned have gained interest due to their capability to perform isothermal air dehumidification, thus removing latent heat of process air without adding more sensible heat. However, there are still several limitations for practical use in buildings, such as the intensive energy use for the compressor in the vacuum dehumidification system and low electrical efficiency in the electrochemical dehumidification system. Additionally, membrane-based heat and mass exchanger, or total heat recovery system, has been proposed and studied for pre-cooling and pre-dehumidification of air [17,20–22].

2.2 Solid desiccant materials

In general, solid desiccant material can be classified into two main categories: a) substances with porous structure (e.g. silica gel, zeolite, etc.), which realizes water adsorption based on difference of water vapour pressure between pores within the desiccant material and surrounding air. b) Substances that can form solid crystalline hydrate, such as LiCl, CaCl₂, LiBr, etc. [23,24].

Choice of adsorbent/desiccant materials is one of important factor in the development of solid desiccant air dehumidification system. Various criteria is considered when choosing proper desiccant material, such as water adsorption quantity, regeneration ability, long-term stability, non-toxicity, cost, etc. Silica gel and zeolite are the most widely adopted material for solid desiccant dehumidifier, while other commonly used materials are activated carbon, activated alumina, molecular sieve, lithium chloride, calcium chloride, etc. [23,25].

2.2.1. Adsorption characteristic of solid desiccant materials

Generally, adsorbent material can be characterized based on its affinity to water or its hydrophilicity. The hydrophilicity of various material is classified according to IUPAC (International Union of Pure and Applied Chemistry) based on the type of sorption isotherm

of the material, which presents the affinity of water vapour in respect to different water vapour pressure and temperature [26].

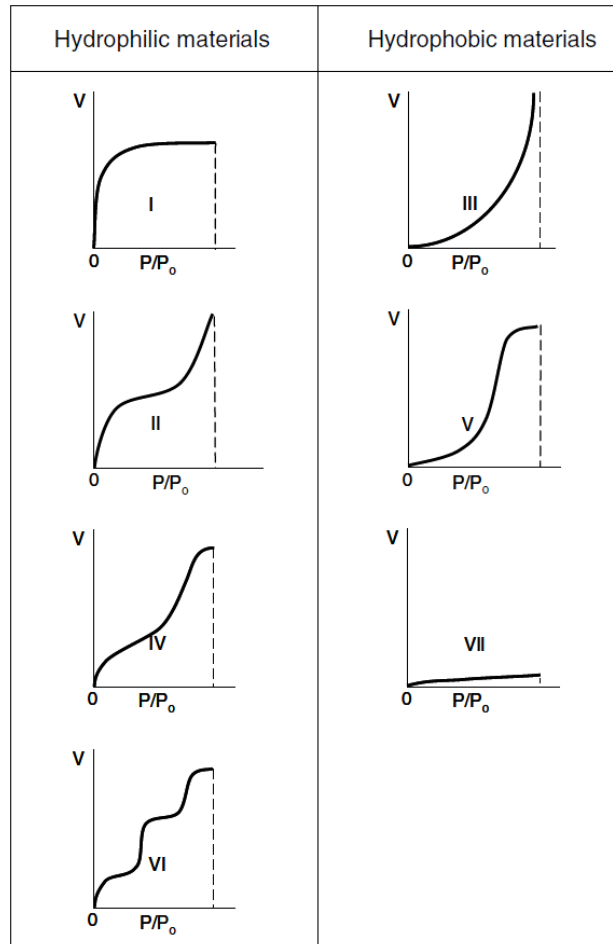


Fig 2-2 Adsorption isotherms classified according to IUPAC [26]

As shown in Fig 2-2, the water sorption isotherms are divided into seven types. The isotherm type I, II, IV, and VI represent hydrophilic material with moderate to high water sorption capacity even at low partial pressure (P/P_0). Type I materials, in particular, are classified as very hydrophilic due to high affinity to water and very fast saturation at low P/P_0 , followed by consistent adsorption over a wide range of P/P_0 due to water saturation in the pores. There are also materials with unusual step-like type VI isotherm. On the other hand, materials with isotherm type III, V, and VII are considered hydrophobic or low hydrophilic materials. Type III and type V materials have low sorption at low P/P_0 followed by increase of sorption at

moderate P/P_0 , then high water adsorption at P/P_0 close to 1. Very hydrophobic materials are characterized with type VII isotherm, with low sorption throughout the entire P/P_0 and finite water sorption capacity less than the available pore volume [26].

It should be noted that the most hydrophilic material is not necessarily the best material for air dehumidification system. Zheng and Wang [23] argued that the optimal desiccant material should have type V isotherm. For example, even though materials with type I isotherm has very high sorption capacity, they are also more difficult to be regenerated since they are more hydrophilic and have higher water adsorption amount at low P/P_0 . Materials with type III isotherm, meanwhile, have high water adsorption only at very high P/P_0 .

Examples of material with sorption characteristic approaching isotherm type I are silica gel and zeolite (NaA), while mesoporous material such as the A1MCM-41 has type V isotherm [26]. However, silica gels and zeolites are still generally more preferable for air dehumidification system due to higher long-term stability of the material. Zeolites generally have higher adsorption capacity compared to silica gels. However, zeolites have the disadvantage of much higher required temperature for regeneration ($>200^\circ\text{C}$) [26].

The capability of desiccant materials can also be characterized based on another adsorption isotherm curve as shown in Fig 2-3. It is suggested that the ideal adsorption performance of desiccant materials for air conditioning application should approach Type 1M isotherm. Even though the normalized loading fraction (actual desiccant water content at corresponding Relative Humidity (RH)/maximum desiccant water content at $\text{RH} = 100\%$) of materials with Type 1E isotherm is higher than that of type 1M, it also means type 1E materials are more difficult to regenerate due to its nearly complete loading at very low RH [25].

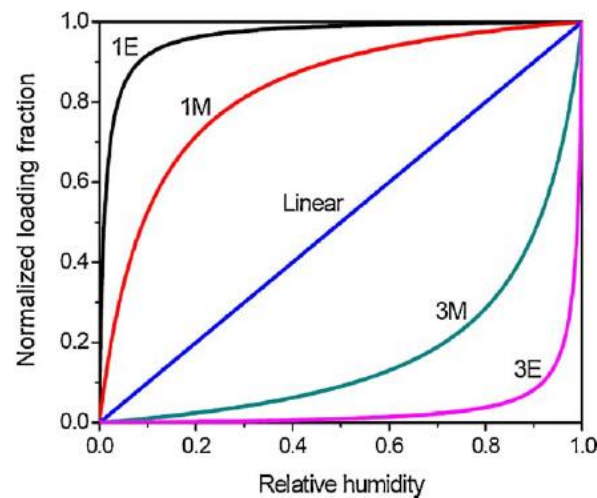


Fig 2-3 Comparison between adsorption isotherms of Type 1 extreme (1E), Type 1 moderate (1M), linear, Type 3 moderate (3M), and Type 3 extreme (3E) [25]

2.2.2. Advancement on desiccant material

Recently, researchers have investigated different ways to improve performance of common desiccant materials, as well as developing new materials with higher adsorption capacity and/or lower required regeneration temperature. Among the novel desiccants, a lot of investigations have focused on composite desiccant materials, which are formed by confining salt to porous host adsorbent. The main idea of developing composite desiccants is to combine advantages of different desiccant materials, while overcoming their drawbacks. For example, while silica gels are widely used due to long term stability and low cost, their disadvantages of low adsorption capacity leads to relatively huge size of dehumidification unit [23]. Moreover, adsorption capacity of silica gel decreases quickly with the rise of temperature, especially when the partial pressure of water vapour is low [27]. Other material such as lithium chloride and calcium chloride have higher hygroscopic capacity compared to silica gel, however, the formation of solid crystalline hydrate during adsorption process could lead to the loss of desiccant material and may reduce performance [27].

By forming composite of these silica gel- and haloids-based materials, the limited adsorption capacity of silica gel and crystallization and corrosion problem of haloids can be overcome. Additionally, lower regeneration can be used, thus facilitating the usage of low-grade heat sources [25]. Jia et al [27] developed a composite desiccant of SG-LiCl and reported that the adsorption capacity of the composite was 2-3 times higher than conventional SG at high humidity. When applied to a desiccant wheel, it was reported that under practical operation, the dehumidification amount of the composite wheel was 20–40% higher compared to conventional wheel [28]. Other composite desiccants, as well as other advanced desiccant materials such as nano porous inorganic materials and polymeric desiccant materials were summarized by Zheng, Wang [23].

2.3 Solid desiccant dehumidification systems

In solid desiccant-based air conditioning / cooling systems, the desiccant unit acts as air dehumidifier prior to the following cooling unit, thus latent and sensible heat are treated independently. The most common arrangement for solid desiccant dehumidifier is slowly rotating wheel impregnated/coated with desiccant material. Fig 2-4 shows the schematics of a desiccant wheel. The desiccant wheel is usually divided into 2 parts, the adsorption section, where process air is passed through to be dehumidified; and regenerating section, where heated air flows through to remove adsorbed water. Thus, by rotating the wheel, adsorption and regeneration process can be performed together, allowing continuous air dehumidification process. Alternatively, packed adsorbent bed can also be used by exposing it to ambient air, or by forcing humid air through the bed. For continuous process, at least 2 beds are required, e.g. 1 bed used for air dehumidification while the other is regenerated, and then switching the bed to complete the cycle.

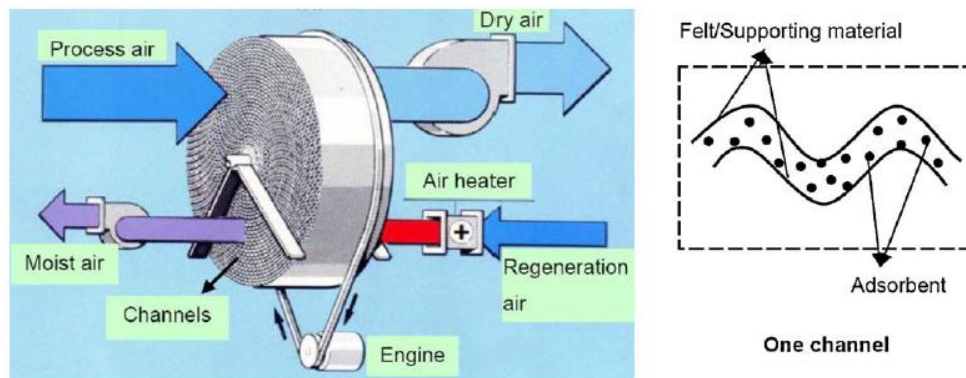


Fig 2-4 Desiccant wheel schematics [25]

Desiccant dehumidification process is close to an isenthalpic procedure, as it merely converts latent energy to sensible energy and produce no useful cooling [25]. This is especially true in case of common desiccant wheel, where adsorption and regeneration process performed continuously switching between the two processes, thus desiccant material is usually at higher temperature than the ambient air. Thus, to form a desiccant air conditioning system that is able to treat both sensible and latent heat, cooling unit is usually incorporated to remove the sensible heat of dehumidified air.

Pennington cycle, or ventilation cycle was the first patented rotary desiccant air conditioning system [25,29]. Fig 2-5 shows the schematics of the Pennington cycle. Hot and humid ambient air at state point 1 is passed through a desiccant wheel (DW), where its moisture is adsorbed by the desiccant, while its temperature is increased due to sensible heat transfer as well as adsorption heat. The hot and dry air at state 2 is then pre-cooled using a sensible heat exchanger (HE), followed by further cooling by direct evaporative cooling (DEC) before supplied to building at state point 4. Return air at state point 5 is cooled by evaporation by another DEC for process air pre-cooling in the HE, before heated by the heat source (HS). The hot air at state 8 regenerate the DW and then the hot and humid air is exhausted.

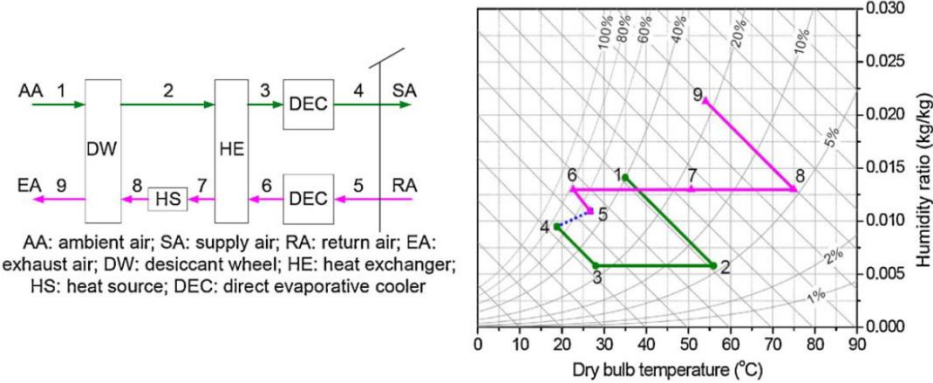


Fig 2-5 Pennington cycle [25]

As in Pennington cycle systems, the cooling capacity in any type of solid desiccant cooling system will be largely affected by state of air exiting the dehumidification unit. Thus, the performance of the desiccant dehumidifier has a very important role on overall cooling capacity. On the other hand, the dehumidifier performance is mainly determined by its configuration and operating conditions.

2.3.1. Rotary desiccant wheel

Desiccant wheel usually consists of a frame which has multiple small channels. Those channels are fabricated in shapes like sinusoidal, triangular, or honeycomb [30]. Honeycomb type channels are commonly adopted as they offer high contact area between the desiccant and process air stream [31]. Fig 2-6 shows desiccant wheel air channels with honeycomb configuration. One of the drawbacks of packed desiccant beds is high pressure loss. Goldsworthy et al. [32] studied this factor in a rotating desiccant cooling system and found that the benefits of using a desiccant wheel could be offset by the increased fan energy consumption.



Fig 2-6 Honeycomb air channels of desiccant wheel [28]

Al-Sharqawi et al. [33] numerically analysed the effect of flow-duct geometry on solid desiccant dehumidification, comparing heat and mass transfer between humid transient-laminar air stream and silica gel ducts with different cross-section geometries such as circular, square and triangular. It was reported that the highest heat and mass transfer occurred inside the triangular duct, with 42% more moisture adsorbed compared to the square and circular ducts. However, the largest velocity gradient of the triangular duct was also the largest, which is 6.6% and 19.6% larger than the square and circular ducts respectively. The average pressure drop of the triangular duct was also the most significant, 69% and 73.5% more than the square and circular ducts.

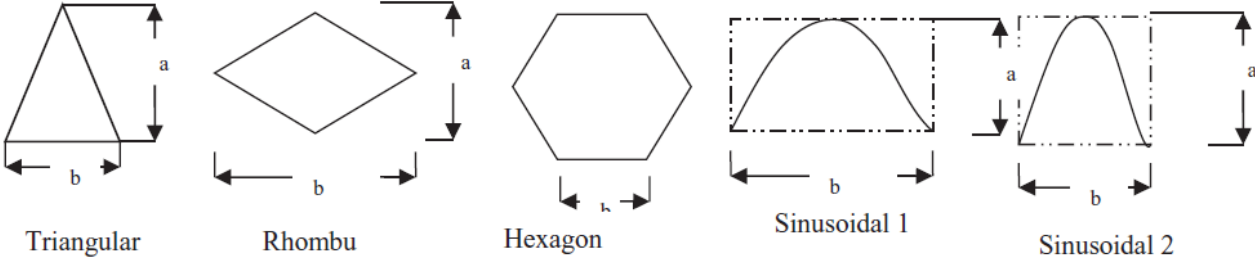


Fig 2-7 Examples of desiccant wheel's channel shapes considered in the study by Narayanan [34]

Narayanan [34] investigated the dehumidification performance of desiccant wheels with different duct shapes including hexagonal, rhombus and sinusoidal (Fig 2-7). The cross-section area was kept for identical for each shape. As shown in Fig 2-8, desiccant wheels with triangular, sinusoidal and rectangular cross-sections have higher moisture removal capacity than the hexagonal circular, and square shaped channels. It was reported that, with identical cross section area, the difference in performance was attributed to combined effect of hydraulic diameter and thus the Nusselt number for different channels, which effect their heat transfer coefficients.

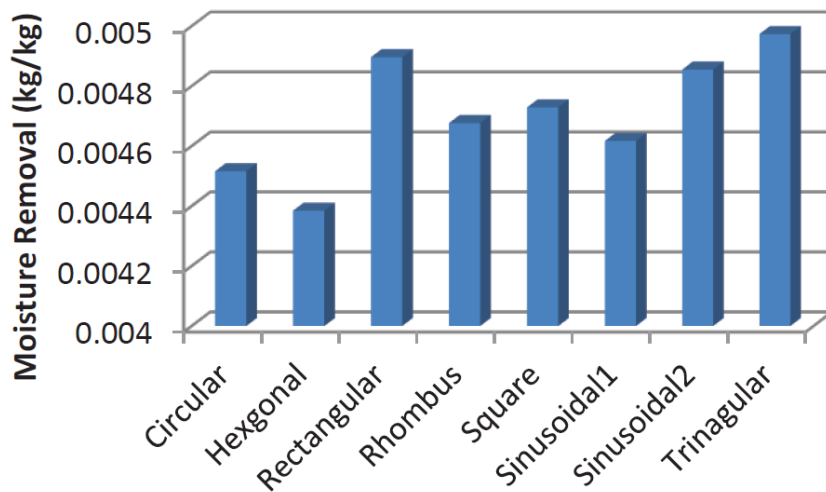


Fig 2-8 Moisture removal for different channel shapes [34]

Ge et al. [35] developed a mathematical model to predict the performance of a compound desiccant wheel proposed by Jia et al. [27,28]. The model was adopted to analyse the effect of some operation parameters on dehumidification performance. In the analysis, some parameters were varied while others were kept constant to investigate their impact on moisture removal capacity per unit mass of process air D , relative moisture removal efficiency η (the ratio of D to inlet moisture ratio of process air) and dehumidification coefficient of performance ($DCOP$ – which reflects the dehumidification capacity and energy utilization for regeneration at the same time).

When the central angle of regeneration section of the desiccant wheel θ_r was increased – which means for fixed air velocity, more regeneration air is adopted to remove moisture of less process air–, D was also increased until it reached its maximum value, after which it kept constant with further increase of θ_r . On the other hand, optimum θ_r was found for maximum $DCOP$. When θ_r was too small, the desiccant was not properly regenerated and consequently low moisture removal even with high process air flow. More effective regeneration could be achieved with higher θ_r , at the expense of decreased process air flux as well as increased thermal energy needed to heat the regeneration air, and when θ_r was bigger than 100° , the negative effects on $DCOP$ compensated the positive effect on D , then $DCOP$ decreased. Considering the trade-off between D and $DCOP$, θ_r between 100° and 160° was recommended.

It was also reported that the compound desiccant wheel had better dehumidification performance under a climate with lower temperature, as the desiccant was better cooled at lower process air inlet temperature, thus can adsorb more moisture. On the other hand, optimum regeneration temperature for maximum $DCOP$ was found at about 85°C , after which the energy required to provide the regeneration heat was more significant than the increase of D . The desiccant wheel was also found to perform better when regeneration air with lower humidity was used. Rotation speed of the wheel was also reported to be crucial parameter. When the rotation speed was too high, the desiccant did not have enough time to remove air moisture, while adsorbed moisture wasn't completely desorbed. Conversely, when the rotation speed was too low, desiccant would already reach saturation before it arrived at the regeneration section. Optimum rotation speed for maximum D was reported to be about 12 r/h.

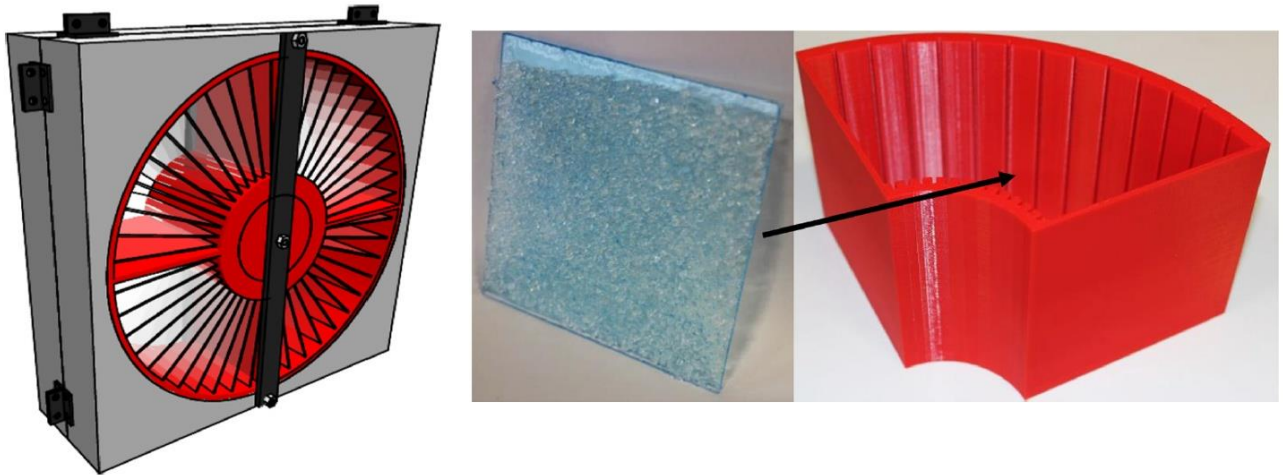


Fig 2-9 Radial blade rotary desiccant wheel design [36]

To address common wheel desiccant wheel limitation due to high pressure drop, O'Connor et al. [36] designed radial blade rotary desiccant wheel with silica gels applied to the faces of thin plastic sheets, which form the radial blades of the wheel (Fig 2-9). With typical pressure drop of common desiccant wheel up to 100 Pa, It was expected that the individual volumes between the blades would ensure that the pressure drop did not exceed the aim of 2 Pa, which would facilitate the application of the radial blade rotary desiccant into passive ventilation (wind tower) system as shown in Fig 2-10. It was reported that pressure drop of 2.06 Pa and 2.10 Pa was measured for the adsorption and desorption tests respectively. The low pressure drop suggested that integration into passive ventilation was possible with further improvement. It was also reported that for temperate climate, the desiccant wheel was able to achieve acceptable dehumidification performance. However, further investigation is necessary for hotter and more humid climates.

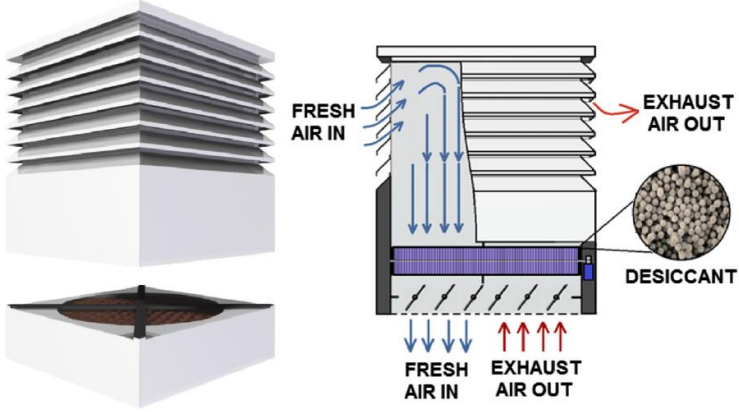


Fig 2-10 Wind tower with desiccant rotary wheel integration concept [36]

2.3.2. Fixed desiccant bed/channel

As in desiccant wheel, fixed desiccant bed usually consists of desiccant coated/impregnated channel(s). Packed desiccant arrangements have also been investigated, where air is forced through the densely packed desiccant beads/granules in order to maximise contact between air and desiccant particles in expense of higher pressure drop. However, while single rotary desiccant bed can perform continuous dehumidification, at least 2 fixed beds in tandem are required for continuous supply of dehumidified air, alternatively performing adsorption and desorption process.

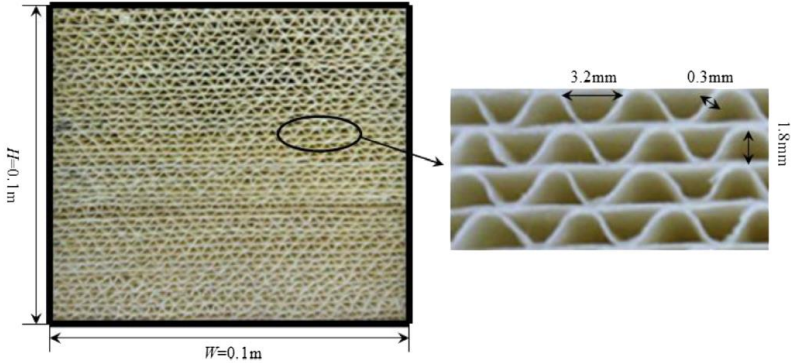


Fig 2-11 Geometry of honeycomb type adsorbent bed studied by Zhang et al. [37]

Chapter 2: Review of solid desiccant air dehumidification technologies

Zhang et al. [37] conducted performance comparisons of honeycomb-type adsorbent beds with different desiccant materials. A mathematical model was developed to predict the performance of fabricated bed, with impregnated desiccant materials, formed by a series of parallel sinusoidal straight ducts packed together (Fig 2-11). The validated model was then used to compare different materials (see Table 2-1) from a viewpoint of a "system", thus cyclical adsorption-desorption were performed under different operating conditions such as varying regeneration between 40°C to 90°C. Three performance indices were considered: the dehumidification coefficient of performance (*COP*– ratio of the useful dehumidification energy to required heat energy during regeneration), specific dehumidification power (*SDP* – amount of adsorbed moisture for every complete cycle per unit mass of desiccant) and dehumidification efficiency (ratio of moisture removal, per unit mass of air, to ideal moisture removal).

Table 2-1 Properties of various desiccants studied by Zhang et al. [37]

Material	Density (kg m ⁻³)	Max water content (kg kg ⁻¹)	Adsorption heat (kJ kg ⁻¹)	Mass (kg)
Silica gel B	790	0.40	2362	0.231
Silica gel 3A	770	0.35	2380	0.225
Silica gel RD	800	0.37	2370	0.234
Silica gel / LiCl	875	0.60	2476	0.256
Silica gel / CaCl ₂	976	0.55	2620	0.285
Zeolite 5A	680	0.19	3974	0.199
Zeolite 13X	650	0.22	3843	0.190
Zeolite 13X / CaCl ₂	1100	0.46	3398	0.322
CaCl ₂	2150	0.33	3675	0.628
LiCl	2068	0.43	2957	0.705

Chapter 2: Review of solid desiccant air dehumidification technologies

It was reported that, under hot and humid operating condition (inlet of process air at temperature 30°C and 85% relative humidity), varying the regeneration temperature had little impact on system *COP*, as more energy required for higher regeneration heat was compensated by higher useful energy output. Highest *COP* at 0.8 was reported for Silica gels 3A and RD, while lowest *COP* at 0.45 were obtained for zeolites 5A and 13X. It was argued that as the adsorption heat of zeolites 5A and 13X were higher than others, they require more driving heat to desorb the same amount of water vapour.

SDP was reported to be increased monotonically with higher regeneration temperature, as water vapour was desorbed faster at higher desorption temperatures, thus more water vapour to be adsorbed during the next adsorption process. Again, *SDP* of silica gels 3A and RD were higher than others, while CaCl_2 and LiCl obtained the lowest value. This was attributed to their high adsorption heat, as well as large density compared to other, which lead to a larger mass loading (volume of the desiccant bed is fixed). Since *SDP* reflected dehumidification performance per unit mass of desiccant, when dehumidification amount was similar, larger mass would lead to lower *SDP*.

At regeneration temperature below 80°C, the dehumidification efficiency of silica gels B, 3A, and RD were reported to be higher than the other. However, at regeneration temperature equal to 90°C, silica gel/ LiCl and silica gel/ CaCl_2 composites reached the highest value of 46%. It was stated that the lowest efficiency was obtained for zeolites 5A and 13X, due to their maximum equilibrium water content which was the lowest among other materials. It was concluded that under hot and humid operating conditions, silica gels 3A and RD would be the better choices.

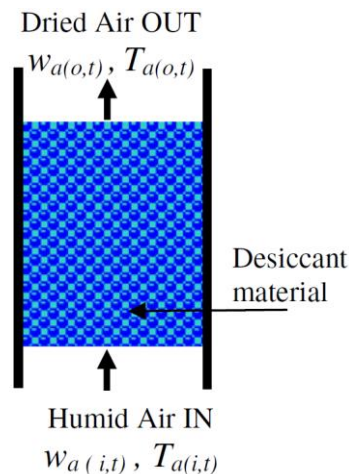


Fig 2-12 Schematic of a desiccant packed bed [38]

Ramzy et al. [39] investigated the cyclic operation of adsorption-desorption for air dehumidification using two packed beds of silica gel particles.

Fig 2-12 shows an air channel filled with packed desiccant materials. Mathematical model was developed to study the heat mass transfer for a cyclic operation of a desiccant packed bed and validated experimentally. In addition, theoretical investigations were also carried out to reveal the effect of different operating conditions such as regeneration air temperature, process air temperature, bed length and process to regeneration air flow ratio on the exit process air conditions and the cycle efficiency of the bed.

The main performance indicator used in this study was the cycle efficiency, which was essentially similar to the previously mentioned term DCOP and COP used in Ref. [35] and Ref. [37], respectively. Different channel length was varied from 50 mm to 300 mm. It was found that the humidity ratio of the exit process air decreased as bed length increased. On the other hand, higher exit air temperatures are obtained for longer beds due to higher adsorption rates. Moreover, the cycle efficiency increased as length increased. However, it was also noted that pressure drop was higher in longer beds, thus optimum bed length should be selected to provide minimum pressure drop and maximum cycle efficiency. Similarly to Ref. [35,37], optimum regeneration temperature was found when considering the trade-off between heat

energy required for regeneration and dehumidification effect. In this study, the optimum regeneration temperature was about 90°C when desiccant particles of 2 mm was used, while optimum regeneration for larger particles (3 mm to 5 mm) was slightly higher in the range of 90-100°C. As it was found that the system obtained higher efficiency with lower inlet process air, a sensible cooling for the process air prior dehumidification was recommended. However, the dew point temperature of the process air stream imposes a limitation on the pre-cooling. Effect of different ratio of dehumidification to regeneration air flow rates was also analysed, and smaller flow rate ratio was recommended to obtain lower process air humidity ratio at the exit. Moreover, the cycle efficiency was found to be increased with an increase in the velocity of process air. On the other hand, the required humidity ratio of the exit process air stream imposed a limitation on using higher process air flow.

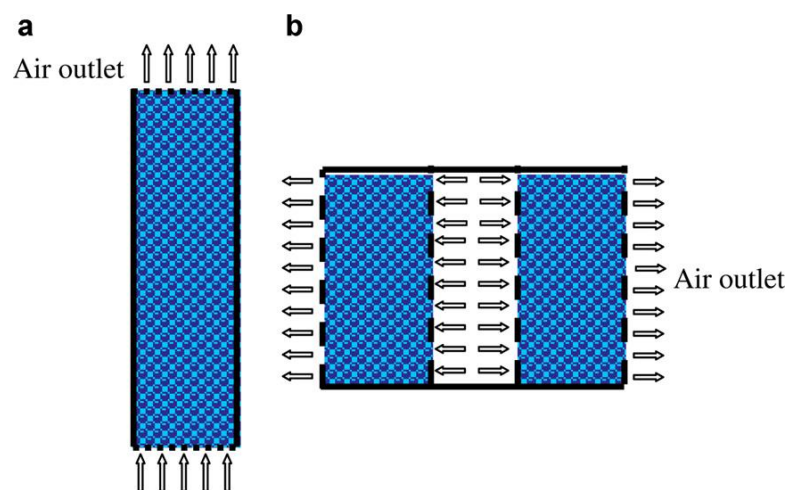


Fig 2-13 Configuration of (a) vertical, and (b) radial flow packed bed [40]

With large pressure drop being the main disadvantage of vertical packed desiccant bed, Awad et al. [40] proposed the radial flow desiccant dehumidification bed. Fig 2-13 shows the difference between a vertical packed desiccant bed and a hollow cylindrical packed bed dehumidifier with radial flow. The radial flow bed was proposed with the main idea of reducing the travelled distance of process air, thus significant decrease in pressure drop through the dehumidifier. As shown in Fig 2-14, it was observed that the pressure drop in for the radial

configuration was too small compared with that for the vertical packed bed. Thus, the blowing energy for the hollow cylindrical bed will be minimum compared with that required for the vertical. Additionally, five experimental test models of the hollow bed with different inner to outer diameter ratios were experimentally investigated. It was demonstrated that bed design parameters should be considered in accordance with the objective function of the process. In cases of minimum pressure drop, lower values of bed diameter ratio should be selected. On the other hand, to maximize the reduction in air humidity it was recommended to use desiccant bed with higher bed diameter ratio.

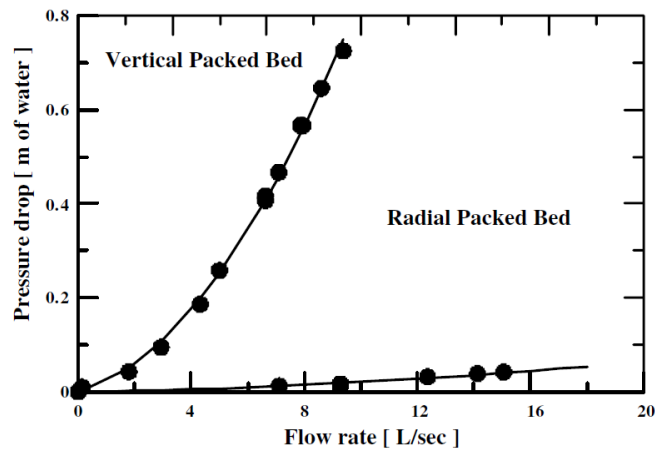


Fig 2-14 Pressure drop comparison between two packed desiccant bed [40]

2.3.3. Internally cooled desiccant dehumidifier

While used for air dehumidification process, the adsorption heat released by desiccant material increases the process air temperature. Moreover, as solid desiccant dehumidifier's operation switches between adsorption and regeneration process, the dehumidified temperature exiting the dehumidifier unit is usually at much higher temperature than the required temperature for comfort level. On the other hand, while heat is required to regenerate saturated desiccant material, the desiccant need to be at lower temperature for

optimum adsorption, making cooling and heating of desiccant material crucial to its dehumidification performance.

For example, Ref. [35] reported that the performance of desiccant wheel was lower when higher inlet air temperature was used during adsorption process. They reported that the system would perform better in a climate with relatively low temperature, as desiccant could be cooled better during dehumidification process, thus could adsorb more water vapour. However, they also reported that higher regeneration temperature also increased the dehumidification capacity due to better regeneration process. Similar argument was also stated in Ref. [39]. Another example from Fernandez-Hernandez et al. [41] demonstrates how the continuous cycle of desiccant dehumidification system can affect the sensible load of the cooling system. They reported that with air temperature at about 30°C entering a desiccant channel, the outlet temperature reached 50°C during the drying process. With regeneration temperature at above 60°C, the temperature of desiccant material became much higher than the process air, thus releasing a lot of sensible heat, as well as sorption heat during adsorption. These emphasize the role of desiccant cooling on the dehumidification performance.

La et al. [25] reported that heat exchangers have been incorporated to pre-cool/pre-heat the process/regeneration air to improve the performance of desiccant air conditioning systems. However, not only that they increase the overall size of the system, in such adiabatic system, heat transfer is limited between the desiccant material and process/regeneration air stream. Thus, system configurations with internal heat exchanger have gained interest. Such system can be generally called direct cooling and heating desiccant system [42] or DCHDS. In DCHDS, adsorption heat is that occurs during dehumidification can be discharged directly by the heat exchanger, hence more effective moisture removal from the air stream. Additionally, better regeneration process can also be achieved due to improved heating.

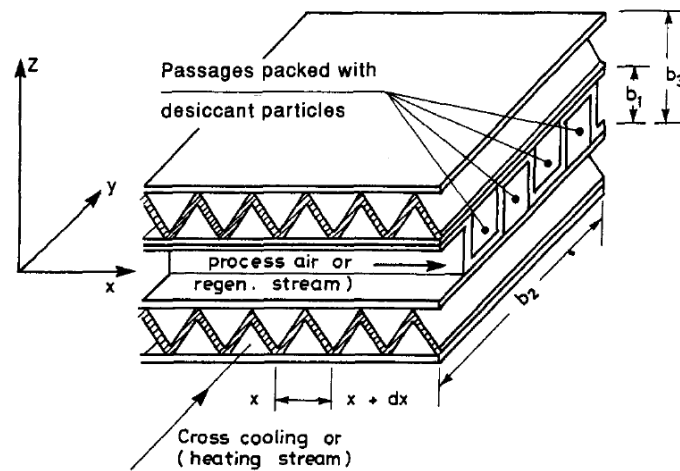


Fig 2-15 Schematic of desiccant packed bed with internal heat exchanger in cross-flow arrangement [43]

One of the early works on DCHDS was proposed by Fathalah and Aly [43] who investigated packed desiccant bed dehumidifier with cross-flow arrangement. The analysis was based on employing two identical stationary solid desiccant beds working alternately between the adsorption and desorption mode. As shown in Fig 2-15, process (or regeneration) air stream flows through the channels along the x -coordinate, which are packed with silica gel particles with an average diameter of 4 mm at an average porosity of 42%. The neighbouring channels along the y -coordinate have no desiccant in them, and they are assigned for cross cooling (or heating) air stream. It was reported that during adsorption process, with inlet process air stream at 28.6°C , $0.0158 \text{ kg}_{\text{H}_2\text{O}}/\text{kg}_a$ and inlet cooling air stream at 31°C , the process air exited the bed at average 45°C , $0.0075 \text{ kg}_{\text{H}_2\text{O}}/\text{kg}_a$. During desorption process, with inlet regeneration air stream at 70°C , $0.024 \text{ kg}_{\text{H}_2\text{O}}/\text{kg}_a$ and inlet heating air stream at average temperature 70°C , the regeneration air stream exited the bed at average 48°C , $0.0327 \text{ kg}_{\text{H}_2\text{O}}/\text{kg}_a$. The dehumidification performance gain was not demonstrated, as comparison with other desiccant bed / operating conditions wasn't done. Additionally, it was also mentioned that pressure drop in the passage with packed desiccant should be considered.

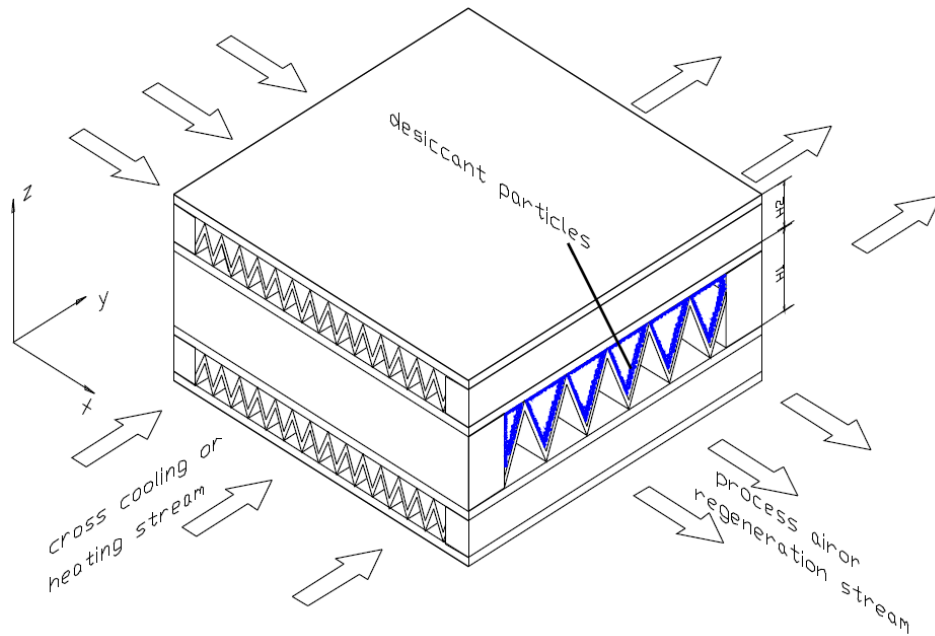


Fig 2-16 Cross-cooled compact solid desiccant dehumidifier [44]

Weixing et al. [44] proposed a desiccant coated cross-cooled compact solid desiccant dehumidifier (DCCCCD), consisting of multiple aluminium alloy channels in cross flow arrangement (Fig 2-16). In the primary channels, process/regeneration air flows through and exchange heat and moisture with fine silica gel particles is glued onto the inner surface of the channels. Secondary channels, meanwhile, are used for cooling/heating air stream, with no desiccant materials. The DCCCCD was numerically investigated under fixed dehumidification and regeneration period at 1000 s each, with inlet temperature of process air (PA) at 35°C, secondary-side cooling air at 20°C, and inlet temperature of regeneration air (RA) at 65°C, secondary-side heating air at 80°C, (inlet humidity ratio of PA and RA kept constant at 0.015 kg/kg). The minimal outlet humidity of PA reached 6.4 g/kg, with average outlet humidity was about 7.8 g/kg.

The dehumidification performance of the DCCCCD was also compared with that of a desiccant packed type (DPCCCD), and it was reported that for mass flow rate above 180 kg/h, a DPCCCD would present a better performance due to more gross desiccant mass compared to

the DCCCCD. However, under the same flow velocity, the pressure drop of PA in DPCCCD was approximately more than seven times larger than that in DCCCCD. A prototype of DCCCCD was manufactured and experimentally tested under varied air inlet temperature and humidity to compare the performance between scenarios with and without secondary cooling. The dehumidification capacity of DCCCCD with secondary cooling was reported to be 50% higher than that without secondary cooling [44].

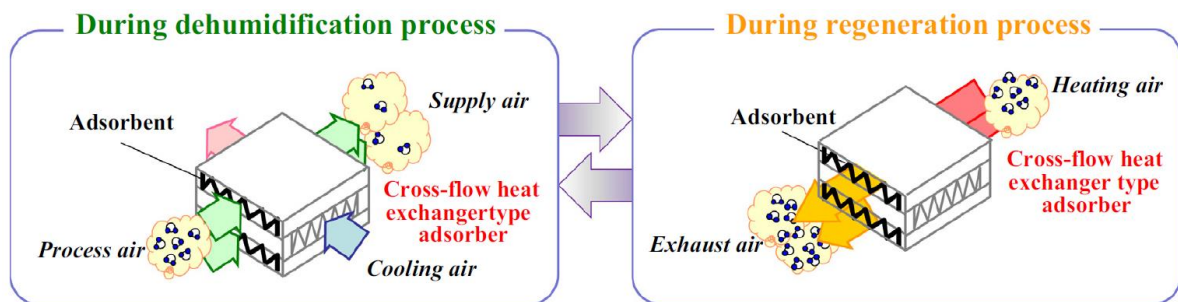


Fig 2-17 Conceptual diagram of cross-flow heat exchanger type adsorbent bed investigated in [45]

Kubota et al. [45] experimentally tested a cross-flow aluminium heat exchanger coated with Aluminophosphate (AIPO) zeolite. The material was chosen as it was expected to regenerate sufficiently even with low-temperature heat source of around 333 K. As shown in Fig 2-17, the secondary channels are used only as cooling air passage, the regeneration heat was provided solely by the heated air in the primary channels. The experiment was carried out with process and cooling air at temperature 303 K and regeneration air at temperature 333 K directed to the bed. Air velocity for air flows in primary channels was maintained at 1 m/s, while inlet absolute humidity was maintained around 16 g/kg for each air flow.

Effect of cooling air velocity on dehumidification was investigated by varying the velocity between 0-3 m/s. In case of no cooling, outlet absolute humidity was maintained at 13 g/kg after slight decrease initially, and then increased gradually. It was found that the minimum absolute humidity of the process air at the outlet decreased as the cooling air velocity increased; i.e., for air velocity 1 m/s, the minimum absolute humidity was 10.6 g/kg, whereas it attained 7.8 g/kg with cooling air velocity equal to 3 m/s. It was reported that over 91% of

heat can be removed by cooling air during dehumidification process, depending on cooling air velocity [45].

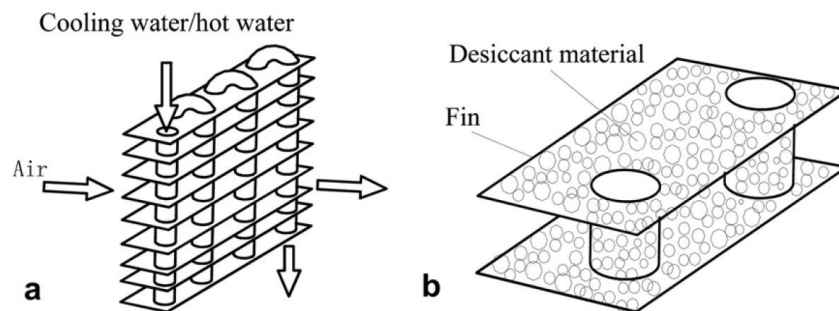


Fig 2-18 Desiccant-coated fin-tube heat exchanger [46]

With better heat transfer than air-to-air heat exchanger, desiccant dehumidifier with air-liquid heat exchanger configuration, such as the desiccant coated fin-tube heat exchanger (DCHE) has also gained interest. Better cooling effect can be achieved in expense of more complicated structure (to include water circulation system). Ge et al. [46] proposed and experimentally investigated two DCHEs with silica gels and polymer, respectively. Fig 2-18 shows the schematic figure of (a) fin-tube heat exchanger and (b) structure of DCHE. The DCHE was proposed by coating desiccant material to the outside surface of conventional fin-tube heat exchanger. When cooling water is pumped into the tube, ambient air flows through DCHE to be dehumidified by the adsorbent. On the other side, hot water is pumped into the tube to regenerate the desiccant materials. Thus, in this particular DCHE, cooling and heating are provided solely from the water flowing through the tubes, while air is directly sourced from ambient and flows to the outside surface of the DCHE.

It was expected that, if temperature of the cooling water was much lower than that of inlet air, the air could be cooled in the DCHE during dehumidification. When tested with inlet air temperature at 30°C and humidity at 14.5 g/kg, water temperature of 25°C during dehumidification and 60°C during regeneration, minimum humidity at the outlet of the DCHE with silica gels was 7.7 g/kg while the minimum outlet humidity ratio for polymer coated DCHE was 8.5 g/kg.

Chapter 2: Review of solid desiccant air dehumidification technologies

For both silica gels and polymer, outlet air temperature reached steady-state of about 26.5°C, indicating that the system was able to treat both latent and sensible heat. It was reported that due to the internal cooling, moisture removal capacity could be increased by 2.5 g/kg compared to similar system without the extra cooling. When tested under various testing conditions, the silica gel coated DCHE performed better than the polymer coated system. It was also reported that the performance of the two DCHEs increased considerably when higher inlet humidity ratio (17.5 g/kg) was used.

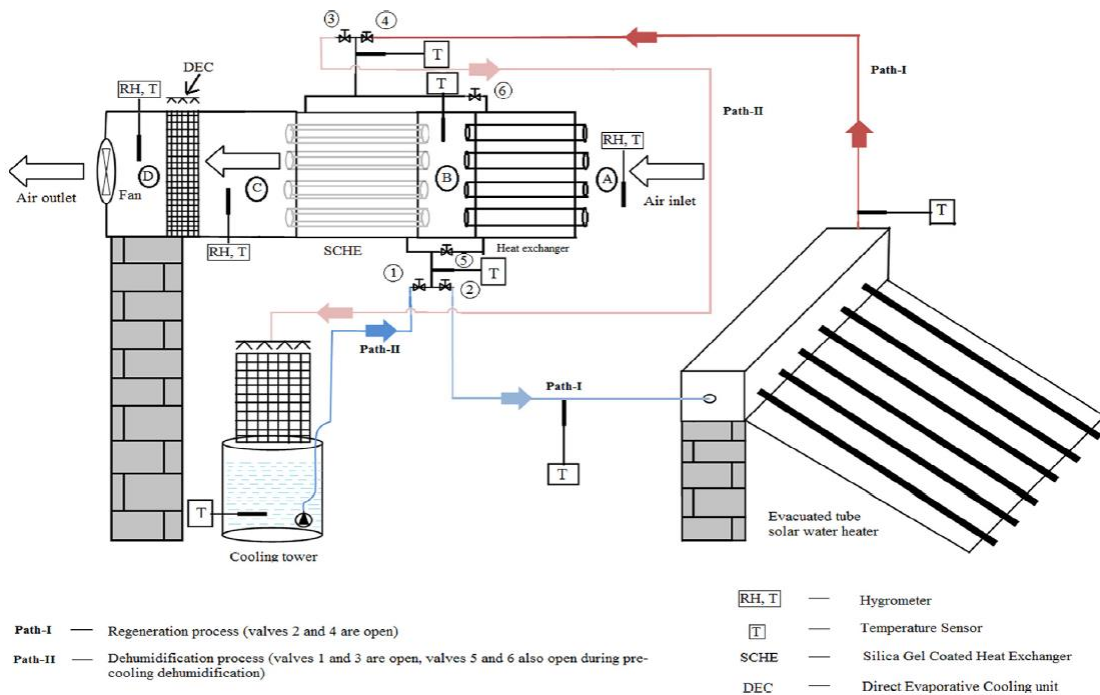


Fig 2-19 Air conditioning system with silica gel coated heat exchanger [47]

Kumar and Yadav [47] proposed water cooled, silica gel heat exchanger (SCHE) with the basic structure of shell and tube type heat exchanger, with silica gel coated inside the tubes. Water is circulated through the shell side to help cooling of the desiccant during adsorption period, while hot water is used for regeneration. To form a solid desiccant cooling system, a heat exchanger is used to pre-cool process air prior to dehumidification system, as well as direct evaporative cooling unit (DEC) to cool down the dehumidified air (Fig 2-19).

Chapter 2: Review of solid desiccant air dehumidification technologies

During the testing, the desiccant was first regenerated by exposing the experimental setup for 5 hours. The hot water with average temperature of 64.1°C was produced using a solar panel heater. The hot water was then transferred to the shell side of the SCHE, heating up the desiccant coated tubes, and regeneration air was flown through the tubes to desorb the moisture. After regeneration process was completed, the hot water was drained out of the SCHE, followed by 1 hour rest period to let the SCHE to transfer its regeneration heat to the atmosphere. The dehumidification process was started by circulating the cooling water at average temperature of 27.6°C in the SCHE and heat exchanger. Process air at average temperature varying between 36.2-34°C and average humidity of 19.3-20.7 g/kg was first pre-cooled by the heat exchanger to around 31°C. Then, the air is cooled and dehumidified to temperature and humidity about 29.5°C and 16.8 g/kg. The DEC further cooled down the dehumidified air, with temperature and humidity between 27-26°C and 15.9-20.5 g/kg at the outlet of the system. It was reported that even though the supply air condition does not lie in the comfort zone, the results demonstrated potential at domestic level [47].

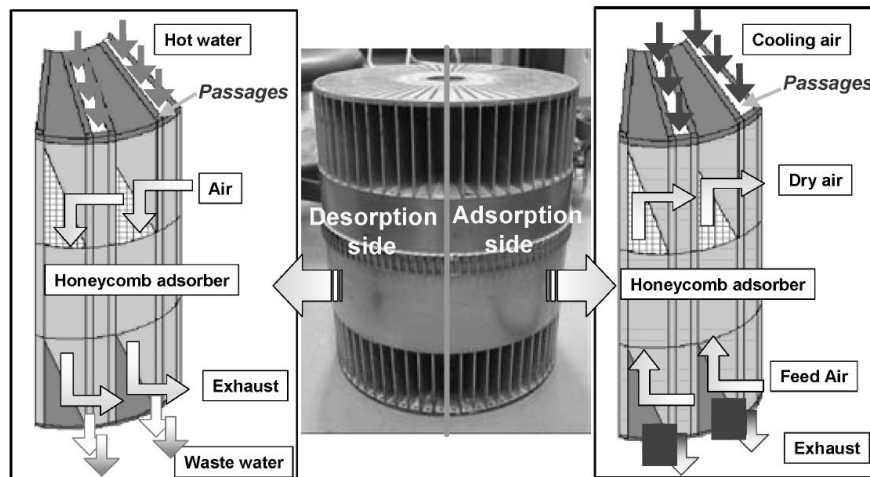


Fig 2-20 Multi-pass honeycomb rotary desiccant regenerated by a direct hot water heating [48]

Rotary desiccant wheels with internal heat exchanger have also been proposed. One of the earliest design was the water heated, air cooled adsorbent wheel proposed by Kodama et al.[48], as shown in Fig 2-20. The wheel was designed with multiple passes in cross flow

arrangement, which allow process air and cooling air to flow separately in the adsorption section, as well as regeneration air and heating water in the desorption side (Fig 2-21). When regeneration heat was provided by regeneration hot water only (feed air and cooling air at 32°C, 22 g/kg), it was reported that satisfactory dehumidification performance could be obtained with regeneration temperature of 45°C. The dehumidification performance of the multi-pass wheel was reported to be 1.3 times higher than that of conventional wheel, however the complex design and the high heat capacity of the structure limit its potential [48].

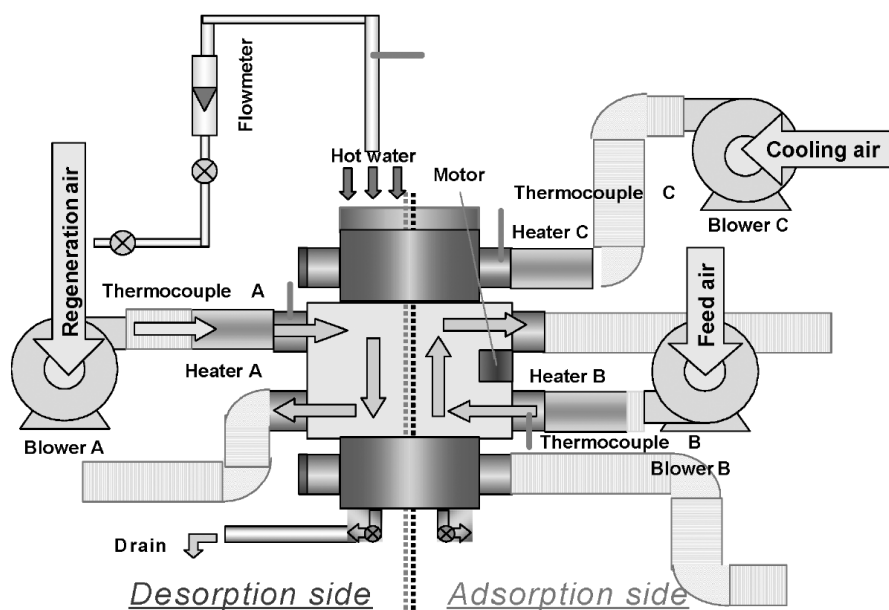


Fig 2-21 Process diagram of the multi-pass rotary dehumidifier [48]

Narayanan et al. [49] designed and investigated non-adiabatic silica gel wheel design as shown in Fig 2-22. Based on parallel plate arrangement, cooling air enters through the central shaft of the wheel and exits in secondary channels perpendicular to the axis of shaft. The primary channel, is used as passage of process air in dehumidification process, while during regeneration process they are used as passage of heated regeneration air. The adsorption and desorption process of the proposed wheel design was simulated in COMSOL Multiphysics software, with chosen rotational speed of 20 rev/h and regeneration temperature of 60°C, while inlet temperature of process air was set to 30°C (inlet humidity airflow for both airflows

Chapter 2: Review of solid desiccant air dehumidification technologies

set to 18 g/kg). The flowing cooling stream was 15°C during dehumidification period, while during regeneration, it was assumed that stagnant air at 30°C occupied the cooling channel. During dehumidification process, the minimum humidity ratio at the outlet of 12.7 g/kg was obtained, with average outlet air temperature below the inlet temperature, indicating the wheel was able to treat both sensible and latent heat of process air. Moreover, dehumidification level of the internally cooled wheel was reported to be between 45-53% higher compared to that of a conventional wheel [49].

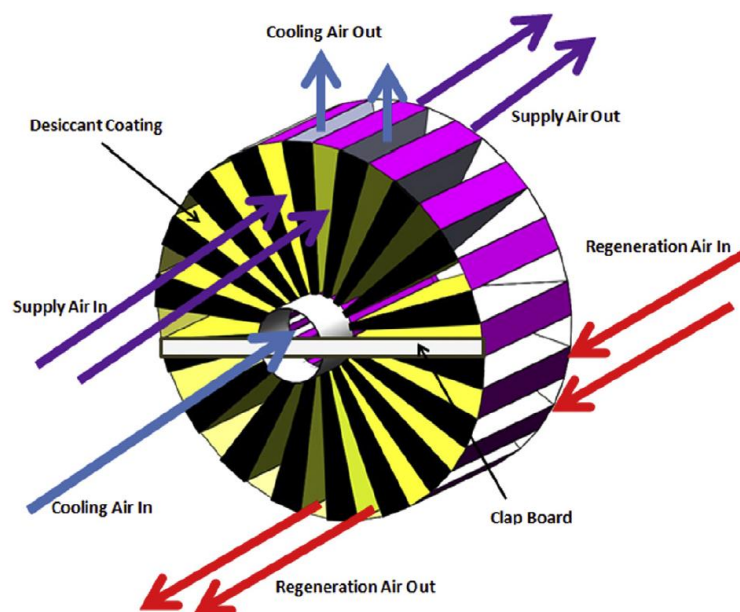


Fig 2-22 Non-adiabatic desiccant wheel [49]

Goldsworthy and White [50] developed an internally cooled desiccant wheel based on a shell and tube heat exchanger housed between two circular plates as shown in

Fig 2-23. The wheel consists of polymer desiccant coated aluminium tubes for process/regeneration air flow, and water passage through the central shaft of the wheel to allow water travel through the lower half of the wheel (the adsorption passage area) outside the tubes before exiting through holes in the shell at the other end of the wheel. This helps sensible cooling of the desiccant during dehumidification, while heating for desorption is only provided by high temperature regeneration air. Compared to conventional desiccant wheel,

dehumidification performance of the water cooled configuration was 40% higher [50] for 35°C process air, 80°C regeneration air and 16 g/kg inlet conditions with average cooling water temperature of 26.9°C.

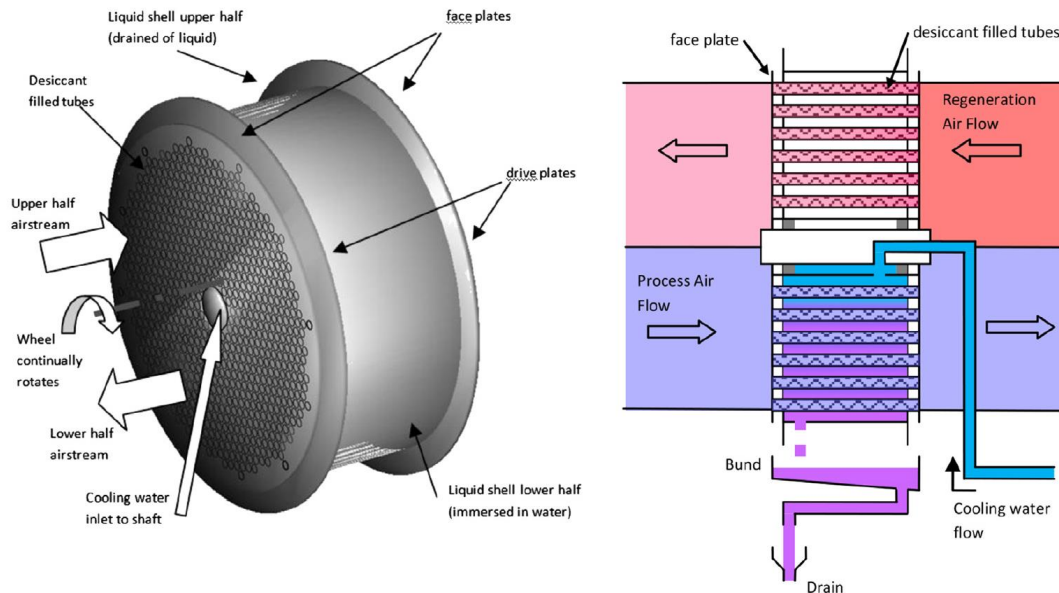


Fig 2-23 Water cooled desiccant wheel [50]

2.3.4. Analysis of reviewed work of solid desiccant systems

The solid desiccant based air conditioning systems have gained interest due to their ability to attract moisture directly from air without having to overcool the process air thus separating the sensible and latent load of air conditioning systems. Moreover, desiccant systems also facilitate the use of alternative cooling techniques that offer low-cost solution to reduce air temperature but unable to treat humidity such as evaporative coolers.

In desiccant air conditioning systems, as dehumidification of process air is usually performed prior to subsequent cooling process, the desiccant dehumidifier unit is the main component that can significantly affect the overall performance of the whole systems. The dehumidification performance of the desiccant unit depends on several factor such as the

Chapter 2: Review of solid desiccant air dehumidification technologies

choice of desiccant material, incorporation of the desiccant material into the air channel(s), channel geometry and construction, as well as operating parameters.

While honeycomb wheel/bed configuration has been widely adopted due to high contact surface area between air stream and desiccant surface, concerns regarding high pressure loss and heat released during dehumidification have led to research for alternative desiccant arrangement for better dehumidification performance. Table 2-2 summarised recent studies of various configuration including common wheel and bed as well as internally cooled systems. It includes the design features of various systems, such as type of desiccant unit, flow pattern, research method, and performance parameters.

Chapter 2: Review of solid desiccant air dehumidification technologies

Table 2-2 Summary of reviewed work on solid desiccant systems

Study	Method	Material	Configuration	Performance parameters	Design features
Ge et al. [35]	Sim. with exp. validation	Silica gel – LiCl composite	Honeycomb rotary wheel	COP: 0.1-0.6 D: 2-9 g/kg Eff: 0.2-0.35	Conventional configuration
O'Connor et al. [36]	Sim. and exp.	Silica gel	Radial blade rotary wheel	N/A	Silica gels applied to the face of thin plastic sheet to form the radial plates of the wheel. Low pressure drop (around 2 Pa) compared to common desiccant wheel (up to 100 Pa)
Zhang et al. [37]	Sim. with exp. validation	Silica gel, zeolites, etc. (see Table 2-1)	Honeycomb bed	COP: 0.45-0.8 SDP: 50-800 g kg ⁻¹ h ⁻¹ Eff: 7.5-46%	Conventional honeycomb channel impregnated with desiccant material
Ramzy et al. [39]	Sim. and exp.	Silica gel	Packed beds	COP: 0.15-0.6	Two desiccant vertical beds in tandem to perform dehumidification and regeneration process simultaneously
Awad et al. [40]	Sim. and exp.	Silica gel	Radial flow bed	N/A	Hollow cylindrical packed bed with radial flow. Negligible pressure loss compared to that for vertical packed bed
Weixing et al. [44]	Sim. with exp. Validation	Silica gel	Cross-flow heat exchanger	N/A	Desiccant particles are glued onto the inner surface of the primary channels. Secondary channels (without desiccant) are used for cooling/heating air stream
Kubota et al. [45]	Exp.	AIPO Zeolite	Cross-flow heat exchanger	N/A	Desiccant is coated on the primary air flow channel. During dehumidification process, cooling air flows in the secondary channel, while on regeneration process, heated air flows only in primary channels

Chapter 2: Review of solid desiccant air dehumidification technologies

Ge et al. [46]	Exp.	Silica gel, polymer	Fin-tube heat exchanger	D: 0.5-5 g/kg	Desiccant is coated on the fin-side of the heat exchanger. Water is circulated through to the tube-side to improve cooling and heating of the desiccant
Kumar, Yadav. [47]	Exp.	Silica gel	Shell-tube heat exchanger	COP: 0.45 A _d : 0.42 kg/h	Desiccant is coated on the inner surface of the tubes. Cooling water is circulated through the shell-side during adsorption. Heating of desiccant achieved only with hot water
Kodama et al. [48]	Exp.	Zeolite	Multi-pass, cross-flow wheel	N/A	Wheel with alternate arrangement of honeycomb desiccant air channels and passages for hot water during desorption and cooling air during adsorption process
Narayanan et al. [49]	Sim. with exp. Validation	Silica gel	Non-adiabatic wheel	N/A	Desiccant coated wheel with alternate rectangular channels. The supply air flows through the desiccant (primary) channels in axial direction, while cooling air flows in radial direction. Heat for regeneration provided only by heated air stream in the primary channel
Goldsworthy, White [50]	Sim. with exp. Validation	Polymer desiccant	Rotary shell and tube wheel	N/A	Desiccant materials are packed inside aluminium tubes which are held in place by metal plates to form a wheel. Cooling water travels through the adsorption side of the wheel. Regeneration heat is provided by high temperature air that flows through the tubes in the desorption side.

Sim: Simulation, Exp: Experiment, COP: Coefficient of performance, D: moisture removal, Eff: Efficiency, SDP: specific dehumidification power, A_d: adsorption rate

Chapter 2: Review of solid desiccant air dehumidification technologies

From the aforementioned reviewed works, it can be summarised that the current numerical and/or experimental studies on solid desiccant dehumidification systems concern the following activities:

- i. Investigations of different desiccant materials , like [35], [37], [45], [46], and [50])
- ii. Parametric studies for system optimisation like [35], [37], [39], [44], [45], [46], and [48]
- iii. Desiccant unit geometric and structural arrangement as in [36], [40], [44], [45], [46], [47], [48], [49], and [50]

From the recent studies summarised above, it can be noted that while pressure loss could have considerable impact on overall energy efficiency of solid desiccant systems, the dehumidification performance mainly depends by moisture desorption rate during regeneration as well as heat released during adsorption, which is also affected by the regeneration process during continuous cycle. Concerning the common desiccant honeycomb wheel/bed, the following disadvantages and limitations are identified as follows:

- Significant pressure loss through the densely packed channels, especially with higher airflows or longer air channels
- Adsorption heat released by desiccant during air dehumidification
- Residual heat left inside the desiccant from regeneration
- Heat transfer is limited between the airstream and desiccant layer

Several alternative arrangements to limit the pressure loss were proposed by [36] and [40], which were essentially improving the opening area for air stream or reducing the travel distance. However, this also lead to reduction of contact area between air stream and desiccant layer, which could limit adsorption/desorption rate, especially as these configurations didn't address the heat transfer limitation of common wheel/bed arrangement. In order to improve heat evacuation during adsorption, desiccant arrangements with internal heat exchanger have been proposed. Several studies have shown that by using either air/water as secondary fluid to remove sensible heat from desiccant (without direct contact), dehumidification performance can be considerably improved [44–50]. Moreover, the use of

secondary fluid in addition to the primary air stream to add heat to desiccant during regeneration process could also improve desorption rate, as reported in [44], [46], and [48]. From various proposed arrangement, the shell-tube desiccant arrangement proposed in [47] and [50] offers the highest heat transfer contact area between the secondary fluid and the desiccant material. However, their structure was rather complicated, especially due to the fact that they require a water circulating system which add complexity to the system. It can be also be noted that the relatively large tube diameter (around 25 mm) used in in [47] would limit the contact between the air stream and the desiccant layer on the inner surface of the tube, thus limiting the adsorption rate. Furthermore, even though hot water that circulate through the shell-side was used to heat the desiccant, the air stream wasn't heated prior entering the desiccant coated tubes, which means the advantage of using two heat transfer fluid was not demonstrated during regeneration process. Similar problem was encountered with the shell-tube wheel of [50]. Due to the complicated structure of the wheel, the shell-tube feature was only applied to the adsorption side of the wheel, thus heat required for regeneration could only be provided by heated air stream through the tubes in the desorption side.

In this research, the proposed shell-tube desiccant arrangement is intended to benefit the advantages of shell-tube heat exchanger configuration, while also overcoming the disadvantages mentioned above. For this project, shell-tube desiccant bed is adopted as it offers simpler structure than the wheel-type. However, instead of water, air will be used as secondary fluid. This will further simplify the structure of the system while also keep it compact. Moreover, the system configuration also takes into account the possibility to heat both the primary and secondary airstream. This will ensure that the advantage of enhanced heat transfer of the desiccant system can be fully demonstrated, thus improving dehumidification performance and its applicability in air conditioning systems.

2.4 Governing equations for solid desiccant dehumidifier

Solid desiccant dehumidifier, with either the common rotary or bed type configuration, usually consists of multiple small channels for air passage. These channels are coated/packed with desiccant material. The governing equations for these channels concern principally the heat and mass transfer between the air stream and the desiccant. Mathematical modelling for solid desiccant dehumidifier systems for either types are usually pretty similar in that the governing equations concern only one channel, while it is assumed that the air stream is uniformly distributed to all channels, thus the heat and mass transfer for one channel is considered to be representative of the whole system. In such case, the governing equations for rotary type desiccant dehumidifier can also be applied to fixed desiccant beds.

2.4.1. Gas-side resistance and solid-side resistance models

Ge et al. [51] summarized different types of governing equations for rotary desiccant dehumidification systems. Those equations are usually distinguished between gas-side resistance (GSR) describing the heat and mass transfer of the fluid stream (usually air) and solid-side resistance (SSR) describing the heat and mass transfer in the solid desiccant. Generally, one dimensional assumption and Euler cylindrical coordinate system are used to describe the wheel, as shown in Fig 2-24.

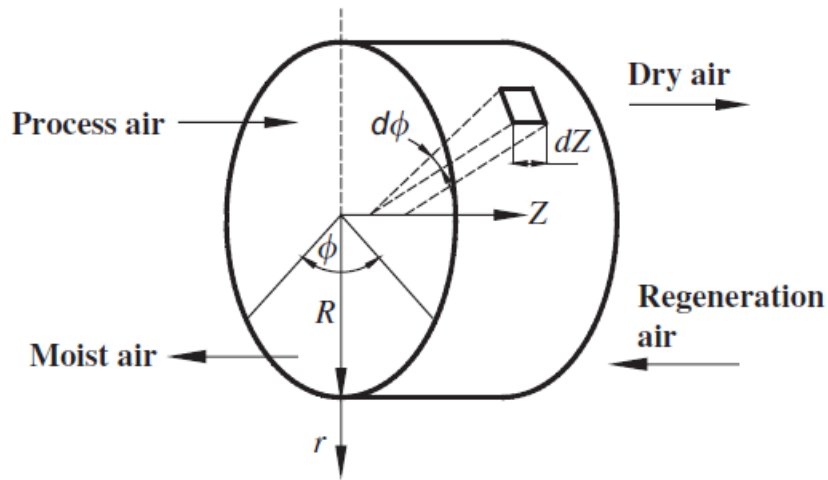


Fig 2-24 cylindrical coordinate system and a model of control volume of the desiccant wheel [51]

In general, the moisture balance in the air can be described as [51]:

$$d_e \rho_a \left(\frac{\partial Y_a}{\partial t} + u \frac{\partial Y_a}{\partial z} \right) = K_y (Y_d - Y_a) \quad (2.1)$$

The first term on the left-hand side (LHS) of equation (2.1) is the moisture storage term in the air, while the second term represents the rate of moisture variation in the air due to the axial flow (z direction) of the air stream. d_e is hydraulic diameter (m), ρ_a is density of dry air (kg/m^3), Y_a is absolute humidity ratio of the air stream ($\text{kg}_{\text{water vapour}} / \text{kg}_{\text{dry air}}$), t is time (s), u is air velocity (m/s), z is axial distance through matrix measured from period entrance (m). The term on the right-hand side (RHS) of the equation above describes the rate of moisture variation in the air caused by mass transfer by conduction, with K_y is gas-side mass transfer coefficients ($\text{kg}/\text{m}^2\text{s}$), Y_d is humidity ratio in equilibrium with the desiccant ($\text{kg}_{\text{water vapour}} / \text{kg}_{\text{dry air}}$).

The general energy conservation in the air stream can be expressed as [51]:

$$d_e c_{pa} \rho_a \left(\frac{\partial T_a}{\partial t} + u \frac{\partial T_a}{\partial z} - \frac{k_a}{c_{pa} \rho_a} \frac{\partial^2 T_a}{\partial z^2} \right) = h(T_d - T_a) + c_{pv} K_y (Y_d - Y_a) (T_d - T_a) \quad (2.2)$$

The first term on the LHS of equation (2.2) is the energy storage in the humid air, while the second term represents the rate of energy variation in the air due to the axial flow of the air,

Chapter 2: Review of solid desiccant air dehumidification technologies

and the third term calculates the heat conduction in the air. c_{pa} is the specific heat of air (J/kgK), T_a is temperature of air (K), k_a is conductivity of air (W/mK). The first term on RHS of is the convective heat transfer between the air and solid desiccant, while the second term indicates the sensible heat transfer between the air and solid desiccant, with h is air-side convective heat transfer coefficient (W/m²K), T_d is temperature of the desiccant (K), c_{pv} is specific heat of water vapour (J/kgK).

The moisture balance in the desiccant is given by the following general equation [51]:

$$\rho_d \delta \left(\frac{\partial W}{\partial t} + D_e \frac{\partial^2 W}{\partial z^2} \right) = K_y (Y_a - Y_d) \quad (2.3)$$

The first term on the LHS of equation (2.3) represents the moisture storage term inside desiccant; the second term is mass diffusion within the solid desiccant in axial direction, while the term on the RHS shows the convective mass transfer between the air and desiccant. ρ_d is density of desiccant (kg/m³), δ is thickness of the desiccant felt (m), W is desiccant adsorption mass (kg_{adsorbate} / kg_{adsorbent}), D_e is desiccant effective diffusivity (m² / s).

Generally, the heat balance in the desiccant can expressed as follow [51]:

$$c_{pd} \rho_d \delta \left(\frac{\partial T_d}{\partial t} + \frac{k_d}{c_{pd} \rho_d} \frac{\partial^2 T_d}{\partial z^2} \right) = h(T_a - T_d) + K_y (Y_a - Y_d) q_{st} + c_{pv} K_y (Y_a - Y_d) (T_a - T_d) \quad (2.4)$$

The first term on the LHS of equation (2.4) represents the energy storage term of the desiccant, while the second term is the heat transfer due to heat conduction within desiccant, with c_{pd} is the specific heat of the desiccant (J/kgK), k_d is the conductivity of the desiccant (W/mK). On the RHS, the first term shows the convective heat transfer between the solid desiccant and air, while the second term calculates the influence of adsorption heat, and the third term represents the sensible heat transfer between the solid desiccant and air, with q_{st} is the heat of adsorption (J/kg_{adsorbate}).

In general, mathematical models for desiccant dehumidifier can be divided into 2 categories, models that assume GSR only and models that assume both GSR and SSR, thus called GSSR models. In GSR only models, it is thought that the heat and mass transfer processes from air stream to desiccant are controlled by GSRs only, thus gradient of temperature and vapour

concentration within solid desiccant are ignored. GSR models also generally assume that convection is the dominant heat and mass transfer process, while heat conduction and moisture diffusion in the air can be neglected.

Kravchik et al. [52] developed a model for solid desiccant bed, which assumes that gas-side resistance controls the mass and heat transfer rate. Awad et al. [40] conducted theoretical and experimental investigation on the radial flow desiccant dehumidification bed, in which heat and mass transfer were assumed to be dominated only by forced convection to the flowing air through the bed. In their modelling for solid desiccant wheel, Nia et al. [53] also assumed that heat conduction and mass diffusion in the desiccant can be neglected. In these studies, heat and mass balance formulations for both the air stream and the desiccant layer are thus described mainly as the convective heat and mass transfer equations.

For higher accuracy of modelling, GSSR model is more preferable than GSR model for GSSR model is able to represent the temperature and moisture distribution within the solid desiccant due to heat and mass diffusion. Ge et al. [51] summarised that typical diffusion theory holds that water vapour molecule has three types of diffusion in porous medium: ordinary diffusion, Knudson diffusion and surface diffusion. In solid desiccant dehumidifiers, all three mechanisms are applicable. Several researchers distinguish these three types of diffusion in their modelling, while there are also those who assume one effective mass diffusivity coefficient [35,37,54–56].

Ge et al. [35] developed mathematical modelling to predict the performance of a compound desiccant wheel. The gas side resistance and the solid side resistance were considered in the model. While convection was assumed to be the dominant heat and mass transfer process for the gas side resistance, the solid side resistance considered the temperature and moisture content gradients due to heat conduction and mass diffusion along the length of the channel. The model was developed to improve the accuracy of GSR-only model developed by Zhang et al. [57]. This GSR-only model was employed by Jia et al. [28] for studying a compound desiccant wheel, and it was reported that the discrepancy between the simulation results and the experimental data was around 15-20%. Ge et al. [35] reported that their model was able

to achieve improvement in accuracy, with 9% discrepancy with the experimental data of Jia et al. [28].

While some researchers opted to neglect the temperature and moisture gradients other than in axial direction / length of the channel (as done by [35], [55], and [56]), there are also those who believe that the moisture diffusion along the thickness of desiccant cannot be neglected. Goldsworthy et al. [32] argued that while a lumped capacitance thermal model of the solid material in the radial direction would be appropriate, the slow moisture diffusion through the desiccant could limit the rate of moisture transfer between the solid and the air stream. Consequently, a 2-D model would be required to determine the moisture profile through the wall. Zhang et al. [37] developed 1-D GSSR model, which considered heat and mass gradients of air (due to convective transfer only) in axial direction; while the desiccant temperature and water content gradient due to heat conduction and mass diffusion is considered along the desiccant thickness. It was argued that the heat conduction and moisture diffusion in solid along the axial direction is several magnitudes lower than those in thickness and can be neglected. Moreover, even with this 1-D model, the change of temperature in the solid along air flow can be reflected due to coupling with the air-side heat and mass balance. The model was validated with their self-developed desiccant bed and it was reported that the maximum differences between calculated values and tested values are 9.8% for temperature and 12% for humidity, respectively [37].

2.4.2. Equilibrium adsorption equation

As mentioned previously, governing equations of solid desiccant systems mainly consist of air-side resistance and desiccant-side resistance models. It should be noted that while the air-side mass balance describes the change of air humidity ratio (in $\text{kg}_{\text{water vapour}} / \text{kg}_{\text{dry air}}$), the desiccant-side moisture conservations describe the adsorbed moisture in the desiccant ($\text{kg}_{\text{adsorbate}} / \text{kg}_{\text{adsorbent}}$). Thus, auxiliary equations are necessary to relate the two moisture balance equations. One of them is the equilibrium equation which determines the amount of moisture that will be adsorbed by the desiccant. Under different operating conditions such as

relative humidity and desiccant temperature, desiccant has different adsorption capacity and thus different equilibrium adsorption quantity. One of the main methods to determine the equilibrium equation for desiccant is through experiments to obtain the dynamic adsorption data for specific materials.

For regular density silica gel, the equilibrium relative humidity on the surface of the material is fitted by Pesaran and Mills [58] and written as follow:

$$RH = 0.0078 - 0.05759W + 24.16554W - 124.78W^3 + 204.226W^4 \quad (2.5)$$

With RH is relative humidity (RH) of air in equilibrium with the surface. Thus, using known the desiccant temperature (T_d), the humidity ratio in equilibrium with the desiccant (Y_d) can also be calculated, allowing the coupling of heat and mass balance of both air-side and desiccant-side. This equation was also employed in other studies on silica gel dehumidifier such as in [32], [49], and [57]. Other examples of equilibrium equation for other materials such as compound desiccant and polymer desiccant materials can be found in [35] and [50].

On the other hand, there is also a general sorption equation written as follow [37,44,51,59]:

$$\frac{W}{W_{max}} = \frac{RH}{r+(1-r)RH} \quad (2.6)$$

With W_{max} is the maximum water content of desiccant ($\text{kg}_{\text{adsorbate}} / \text{kg}_{\text{adsorbent}}$) and r is the separation factor, or a constant that determines the isotherm shape as shown in Fig 2-3. This equation can be applied for different desiccant materials if their maximum water content and isotherm curve is known. For example, the W_{max} for regular density silica gel is 0.37 $\text{kg}_{\text{water vapour}}/\text{kg}$, while its separation factor is 1.1 [37].

2.4.3. Governing equations for solid desiccant dehumidifier with internal heat exchanger

While the governing equations for common desiccant wheel / bed configuration primarily concern heat and mass exchange between one air stream and the desiccant in one channel, the governing equations for internally cooled desiccant should also consider the heat transfer

taking place in the secondary channel (for sensible heating/cooling of desiccant) in addition to the heat and mass balance equations for the primary channel where dehumidification and regeneration process is taking place.

For example, Weixing et al. [44] developed a GSR-dominated mathematical model for a desiccant coated cross-cooled compact solid desiccant dehumidifier (DCCCD, see also Fig 2-16). For the primary channel, the mass and energy balance equations are written as follow [44]:

$$\frac{1}{u_{pf}} \cdot \frac{\partial Y}{\partial \tau} + \frac{\partial Y}{\partial x} = \frac{K_{mpc} \cdot F_{mpc}}{\dot{m}_{pf} \cdot L_x} \cdot (Y_{ad} - Y) \quad (2.7)$$

$$\frac{1}{u_{pf}} \cdot \frac{\partial t_a}{\partial \tau} + \frac{\partial t_a}{\partial x} = \frac{K_{hpc} \cdot F_{hpc}}{\dot{m}_{pf} \cdot (Cp_a + Y \cdot Cp_v) L_x} \cdot (t_{de.o} - t_a) \quad (2.8)$$

With u_{pf} is velocity of primary flow (m/s), Y is humidity ratio of process air (kg/kg a), τ is time (s), x is coordinate component of primary side, K_{mpc} is convective mass transfer coefficient in primary channel (kg/m²s), F_{mpc} is area of mass transfer in primary channel (m²), \dot{m}_{pf} is mass flow rate of primary air (kg/s), L_x is length of side of dehumidifier in x coordinate (m), Y_{ad} is the humidity ratio of process air close to the surface of the desiccant (kg / kg a), t_a is dry bulb temperature (°C), K_{hpc} is convective heat transfer coefficient (W/m² °C), F_{hpc} is area of heat transfer in primary channel (m²), Cp_a and Cp_v are specific heat of air and that of water vapour, respectively (J/kg °C), and $t_{de.o}$ is temperature of desiccant in contact with air flow in primary channel (°C). The mass and energy balance equations for the desiccant are written as follow [44]:

$$\frac{\partial W}{\partial \tau} = \frac{K_{mpc} \cdot F_{mpc}}{M_{de}} \cdot (Y - Y_{ad}) \quad (2.9)$$

$$\frac{\partial t_{av.de}}{\partial \tau} = \frac{1}{(Cp_{de} + W \cdot Cp_w)} \times [K_{hpc} \cdot F_{hpc} (t_a - t_{de.o}) + \alpha \cdot F_{hpc.f} \cdot \eta_{pc} (t_{sp} - t_{de.i.f}) + \alpha \cdot F_{hpc.sp} (t_{sp} - t_{de.i.sp}) + K_{mpc} \cdot F_{mpc} (Y - Y_{ad}) Q_{ad}] \quad (2.10)$$

With W is water content of desiccant (kg/kg de), M_{de} is mass of desiccant (kg), $t_{av.de}$ is average temperature of desiccant (°C), Cp_{de} and Cp_w are the specific heat of desiccant and water, respectively (J/kg °C), α is equivalent heat exchange coefficient between desiccant

and the fins of primary side ($W/m^2 \text{ } ^\circ C$), $F_{hpc.f}$ is area of heat transfer between the fin in primary channel and desiccant (m^2), η_{pc} is efficiency of the fins in the primary channel, t_{sp} and $t_{de.i.f}$ are temperature of separator and desiccant in contact with the fins, respectively ($^\circ C$), $F_{hpc.sp}$ is area of heat transfer between the separator in primary channel and desiccant (m^2), $t_{de.i.sp}$ is the temperature of desiccant in contact with separator ($^\circ C$), and Q_{ad} is adsorption ($J/kg \text{ w}$). The heat balance equations for air in secondary flow and the separator metal are written as follow [44]:

$$\frac{1}{u_{sf}} \cdot \frac{\partial t_{sf}}{\partial \tau} + \frac{\partial t_{sf}}{\partial y} = \frac{K_{hsc} \cdot F_{hsc} \cdot \eta_{sc}}{Cp_{sf} \cdot \dot{m}_{sf} \cdot L_y} \cdot (t_{sp} - t_{sf}) \quad (2.11)$$

$$\frac{\partial (M_{mt} Cp_{mt} \cdot t_{av.mt})}{\partial \tau} = K_{hsc} \cdot (\eta_{sc} \cdot F_{hsc.f} + F_{hsc.sp}) (t_{sf} - t_{sp}) + \alpha \cdot F_{hpc.f} \cdot \eta_{pc} (t_{de.i.f} - t_{sp}) + \alpha \cdot F_{hpc.sp} (t_{de.i.sp} - t_{sp}) \quad (2.12)$$

With u_{sf} is velocity of secondary flow (m/s), t_a is dry bulb temperature in secondary side ($^\circ C$), y is coordinate component of secondary side, K_{hsc} is convective heat transfer coefficient in secondary side ($W/m^2 \text{ } ^\circ C$), F_{hpc} is area of heat transfer in secondary channel (m^2), η_{sc} is efficiency of the fins in the secondary channel, Cp_{sf} is specific heat of secondary air ($J/kg \text{ } ^\circ C$), \dot{m}_{sf} is mass flow rate of secondary air (kg/s), L_y is length of side of dehumidifier in y coordinate (m), M_{mt} is mass of metal (kg), Cp_{mt} is specific heat of metal ($J/kg \text{ } ^\circ C$), $t_{av.mt}$ is average temperature of metal ($^\circ C$), $F_{hpc.f}$ is area of heat transfer between the fins in secondary channel and desiccant (m^2), and $F_{hpc.sp}$ is area of heat transfer between the separator in secondary channel and desiccant (m^2). There is no mass transfer in secondary side. The model was validated with a constructed test rig and it was reported that both outlet humidity ratio and temperature values of process airflow agreed well between simulation and experiment [44], however, the discrepancy wasn't explicitly given.

Narayanan et al. [49] developed a GSSR model for a non-adiabatic desiccant wheel. The channels of the wheel were approximated as rectangular cross section as shown in Fig 2-25. For the air side, it was assumed that only convective heat and mass transfer took place. On the other hand, it was also assumed that moisture and temperature variation of air other than

Chapter 2: Review of solid desiccant air dehumidification technologies

in the direction of flow could be neglected. The heat and mass balance equations for the primary air flow (control volume CV1) are written as follows [49]:

$$\frac{1}{u_g} \frac{\partial Y_g}{\partial t} + \frac{\partial Y_g}{\partial x} = \frac{\beta P_{in}}{u_g \rho_g A_g} (Y_d - Y_g) \tag{2.13}$$

$$\frac{1}{u_g} \frac{\partial T_g}{\partial t} + \frac{\partial T_g}{\partial x} = \frac{\alpha P_{in}}{u_g \rho_g A_g c_{p_g}} (T_d - T_g) \tag{2.14}$$

With u_g is air velocity (m/s), Y_g and Y_d are humidity ratio of air and that of air in equilibrium with desiccant, respectively (kg/kg), β is convective mass transfer coefficient (kg/m² s), P_{in} is inner perimeter of the desiccant channel (m), ρ_g is the density of air (kg/m³), A_g is cross section area of air channel (m²), T_g and T_d are temperature of air and desiccant, respectively (K), α is the convective heat transfer coefficient (W/m² K), and c_{p_g} is specific heat of air (J/kg K). For the secondary air, it was assumed that due to the large airflow during dehumidification process, the rise of temperature could be neglected. On the other hand, it was assumed that stagnant air at 30°C occupied the secondary channel during regeneration process.

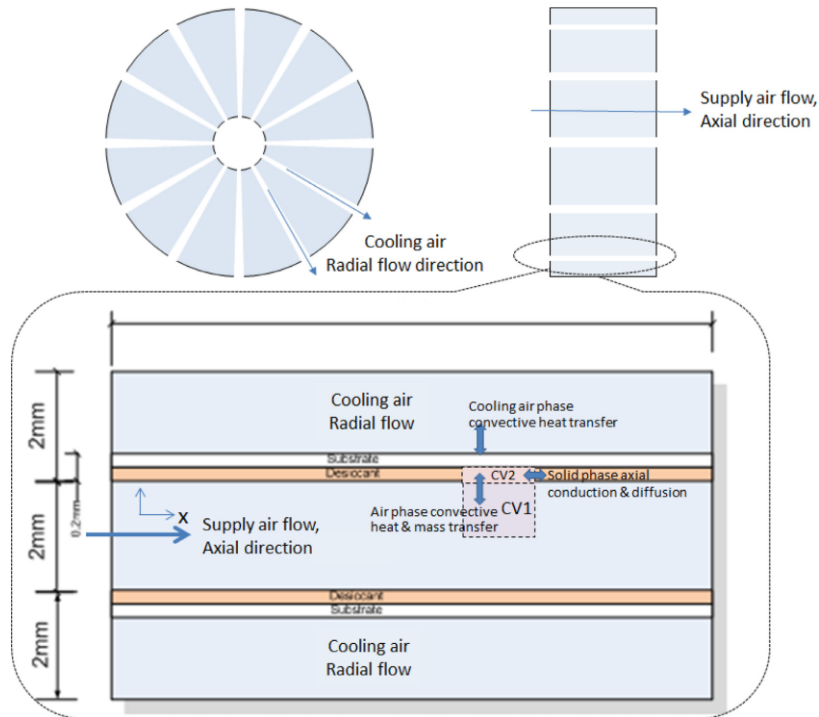


Fig 2-25 Non-adiabatic desiccant wheel channel cross section geometry and model heat and mass transfer resistances [49]

For the solid side, the desiccant layer was assumed to contain interconnected pores filled with air that has moisture content in equilibrium with the desiccant material, and the moisture diffusion included gas diffusion through pore spaces and surface diffusion through the solid. The desiccant layer was also assumed to be very thin such that solid side transport diffusion resistances are in the axial direction only, while the conductive resistance of the substrate layer was also neglected. The resulting mass and energy balance equations in solid side (control volume CV2) are written as follow [49]:

$$\rho_d(1 - \varepsilon) \frac{\partial W_d}{\partial t} = \rho_g D_a \left(\frac{\partial^2 Y_d}{\partial x^2} \right) + \rho_d D_s \left(\frac{\partial^2 W_d}{\partial x^2} \right) + \frac{\beta P_{in}}{A_d} (Y_g - Y_d) \quad (2.15)$$

$$\rho_d c_{pt} \frac{\partial T_d}{\partial t} = \lambda_d \left(\frac{\partial^2 T_d}{\partial x^2} \right) + q_a \rho_d \left(\frac{\partial W_d}{\partial t} \right) + \frac{\alpha P_{in}}{A_d} (T_g - T_d) + \frac{\alpha_c P_{out}}{A_d} (T_c - T_d) \quad (2.16)$$

With ρ_d is density of desiccant (kg/m^3), ε is porosity of desiccant, W_d is water content of desiccant (kg/kg), D_a and D_s are gas and surface diffusivity, respectively (m^2/s), c_{pt} is total heat capacity of solid side (J/kg K), λ_d is heat conductivity of desiccant (W/m K), q_a is adsorption heat (J/kg), α_c is the convective heat transfer coefficient in secondary side ($\text{W/m}^2 \text{K}$), P_{out} is outer perimeter of the desiccant channel (m), and T_s is temperature of secondary air (K). The model was validated with test rig consisting of two channels arranged in cross-flow arrangement which represent the non-adiabatic wheel. Although no explicit discrepancy value was given between the numerical results and the experimental data, it was reported that the simulation results agreed very closely with the measured humidity and temperature data under different operating conditions [49].

Goldsworthy et al. [50] developed a simplified mathematical model for water cooled desiccant wheel which considered heat and mass transfer process in a single representative channel. The model consists of air-side convection heat and mass transfer equations coupled to a two-dimensional calculation of heat and moisture diffusion inside the desiccant material lining the air channel. The desiccant material was assumed to transfer heat to the channel wall, which, on the other hand, was also assumed to exchange heat with the cooling water during dehumidification process. The schematic of the representative channel used for the model is shown at Fig 2-26.

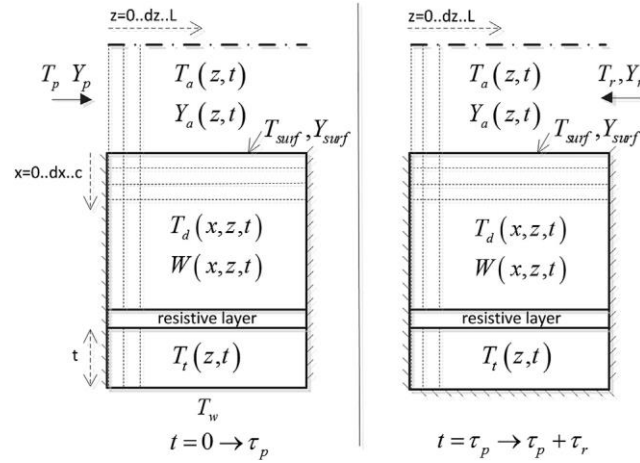


Fig 2-26 Schematic of the representative channel used in the mathematical model of [50]

The conservation equations of energy and moisture for the air side are written as follow [50]:

$$\rho_a \left(\frac{\partial h_a}{\partial t} + u_a \frac{\partial h_a}{\partial z} \right) = \frac{4}{D_h} (T_{surf} - T_a) [\beta_a + \beta_m c_{p_v} (Y_{surf} - Y_a)] \quad (2.17)$$

Where $h_a = \int (c_{p_a} + c_{p_v} Y_a) dT_a$

$$\rho_a \left(\frac{\partial Y_a}{\partial t} + u_a \frac{\partial Y_a}{\partial z} \right) = \frac{4}{D_h} \beta_m (Y_{surf} - Y_a) \quad (2.18)$$

With ρ_a is air density (kg/m^3), h_a is enthalpy of air (J/kg), c_{p_a} and c_{p_v} are specific heat of air and vapour, respectively (J/kg K), u_a is air velocity (m/s), D_h is channel hydraulic diameter (m), T_a and T_{surf} are temperature of air and desiccant-air surface, respectively (K), β_a is convective heat transfer coefficient ($\text{W/m}^2 \text{K}$), β_m is convective mass transfer coefficient ($\text{kg/m}^2 \text{s}$), Y_a and Y_{surf} are absolute humidity of air and desiccant-air surface, respectively (kg/kg). The energy balance equation for the tube / channel is written as [50]:

$$\frac{\partial T_t}{\partial t} = \frac{k_t}{\rho_t c_{p_t}} \frac{\partial^2 T_t}{\partial z^2} + \frac{1}{\rho_t c_{p_t} a} [\beta_t (T_d - T_t) + \beta_w (T_w - T_t)] \quad (2.19)$$

With T_t , T_d , and T_w are temperature of tube, desiccant, and water, respectively (K), k_t is thermal conductivity of tube (W/m K), ρ_t is tube density (kg/m^3), c_{p_t} is specific heat of tube (J/kg K), a is tube thickness (m), β_t and β_w are average heat transfer coefficient for tube and water, respectively ($\text{W/m}^2 \text{K}$). The term involving T_w is set to 0 during regeneration process,

while fixed water temperature is assumed during air dehumidification process. The desiccant energy and moisture conservation equations are written as follow [50]:

$$\rho_d \frac{\partial e_d}{\partial t} = \nabla \cdot (k_d \nabla T_d) \quad (2.20)$$

Where $e_d = \int (c_{p_d} + c_{p_w} W) dT_d$

$$\frac{\partial W}{\partial t} = \nabla \cdot (D_{eff} \nabla W) \quad (2.21)$$

With ρ_d is density of desiccant (kg/m^3), e_d is internal energy of desiccant (J/kg), c_{p_d} and c_{p_w} are specific heat of desiccant and water, respectively (J/kg K), k_d is thermal conductivity of desiccant (W/m K), W is desiccant moisture loading (kg/kg), and D_{eff} is effective moisture diffusivity (m^2/s). The model was validated using experimental data of the wheel, and it was reported that the discrepancy between the simulated results and test data was generally within ± 1 g/kg for humidity and ± 2 °C for temperature [50].

2.5 Summary

This chapter provided a review of solid desiccant-based air dehumidification systems, covering the brief overview of other air dehumidification techniques, desiccant materials, and working principles. Additionally, a review was carried out of different dehumidifier configurations.

The most common air dehumidification technique is the thermal condensation dehumidification, which is applicable in the widely adopted mechanical vapour compression air conditioning system. The dehumidification in this system is achieved by cooling air below its dew-point, followed by re-heating, which is very energy intensive. Desiccant-based dehumidifiers attract interest due to the material affinity to attract and hold moisture. Moreover, desiccant material can be driven by low-grade heat source such as solar energy or waste heat. By employing low-heat driven desiccant material and efficient cooling system to treat sensible and latent heat independently, significant energy saving could be achieved. Desiccant material can be distinguished between liquid desiccant and solid desiccant material. While liquid desiccants offer favourable performance, solid desiccants are easier to handle as

they are inert and non-toxic. Alternatively, membrane-based dehumidification offers great potential of isothermal air dehumidification. However, their applicability is still relatively limited due to requirement of energy intensive compressor. On the other hand, membrane-based heat and mass exchangers have been proposed for pre-cooling and pre-dehumidification of air.

Selection criteria for solid desiccant materials are largely based on their sorption isotherm characteristics, which presents the affinity of water vapour in respect to different water vapour pressure and temperature. Advance in desiccant material development focus on achieving the most ideal sorption isotherm. Different approach has been investigated, with the most common being developing composite desiccant, such as confining salt to porous host adsorbent. By combining two different material properties, composite materials with superior adsorption capacity which require low regeneration heat can be obtained.

Solid desiccant dehumidifier can generally be divided into two types: fixed desiccant bed and rotating desiccant wheel. While fixed desiccant beds have simpler structure with less moving parts, rotary desiccant systems are widely adopted with the main advantages of continuous dehumidification process, as adsorption and desorption process can be performed together in one wheel. To form an air conditioning system, desiccant wheel(s) can be connected to cooling unit such as evaporative cooler to sensibly cool the dehumidified air. In addition, heat exchangers can also be employed to pre-cool the process air either prior or post dehumidification process.

The performance of solid desiccant dehumidifier depends on various factors, including the materials used, the geometry of the air passage, operating parameters, etc. Honeycomb type channels have high contact area between the desiccant and process air stream, with triangular and sinusoidal shaped channels among the most effective geometries for air dehumidification. Alternatively, air passages with packed desiccant beds which maximise contact between air stream and adsorbent have also been proposed. However, both honeycomb type and packed desiccant channels suffer from high pressure drop, which could lead to important energy

consumption for the fan. To overcome this issue, alternatives such as radial blades desiccant wheel and radial flow bed have been proposed, however further optimisations are required.

Among various operating parameters, regeneration air temperature and flow rates are the most frequently investigated. When choosing the optimum regeneration temperature, a trade-off between required thermal energy for regeneration and effective dehumidification energy should be considered. Higher air flow rates usually lead to higher amount of adsorbed moisture for every completed cycle. On the other hand, when lower humidity output is desired, smaller air flow is recommended. However, the most crucial factor that often limits the dehumidification performance is the heat released by the desiccant during adsorption. As well as adsorption heat, residual heat from previous regeneration process causes air temperature to increase considerably and reduce the adsorption rate.

Desiccant dehumidifiers with internal heat exchangers have been investigated with the main focus on effectively remove adsorption heat during dehumidification in order to approach isothermal air dehumidification. Air and water are commonly adopted as secondary fluid in this type of system, with configuration such as cross-flow and fin-tube heat exchanger adopted as the basis of the dehumidifier. If secondary fluid at much lower temperature than the process air is used, the air dehumidification system can treat both sensible and latent load simultaneously.

Last but not least, different types of mathematical modelling for solid desiccant systems were presented. The governing equations describing the adsorption and desorption process usually assume uniform air distribution, thus in case of desiccant wheel or bed with multiple channels, the heat and mass balance for one channel could represent the overall system. Temperature and humidity gradient of the air stream usually assumed to be only in direction of travel, while heat and moisture distribution in the desiccant layer along its thickness can also be considered. For desiccant with internal heat exchanger, a supplementary heat balance representing the secondary air and adjustments to boundary conditions of the desiccant heat and mass balance would be required.

Chapter 3: Design and computer modelling

3.1 Introduction

From the literature review in the previous chapter, it was shown that many types of adsorption beds/wheels geometries have been studied. Internally cooled desiccant configurations for removal of adsorption heat have been proposed to increase dehumidification performance. With better heat transfer potential, water as the secondary heat transfer fluid has been investigated and promising results have been reported, however with the expense increased complexity due to required water circulating system. Moreover, most of proposed configuration focused on heat removal during air dehumidification, while regeneration heat provided only by either the primary or secondary fluid. On the other hand, desiccant integration onto the air channels was mostly done by coating or using adhesive, which could limit heat transfer to/from the desiccant to the working fluid.

In this work the proposed design configuration was considered by taking into account the following aspect:

- i) Use of air as secondary fluid for flexibility of choosing a source (ambient air, return air from building, etc.)
- ii) Utilization of secondary air stream to help remove heat during air dehumidification, while also to enhance heating of primary air channels from both inside and outside during desiccant regeneration
- iii) Channels arrangement to provide abundant heat transfer area while limiting pressure loss
- iv) Solution to hold desiccant in place using low thermal resistance medium

The proposed system with the above considerations will be presented in the following section.

3.2 Outline configuration of the shell-tube solid desiccant heat and mass exchanger

The design combines solid desiccant bed in the form of hollow tubes within tubes of a shell-tube heat exchanger configuration. The solid desiccant hollow tubes forms air channels for air dehumidification or desiccant regeneration. The shell-tube heat exchanger is composed of a bundle of tubes onto which a thin layer of solid desiccant is held inside the tubes by forming rolled fine wire copper mesh, and the annular gap between the mesh and the tube is filled with the desiccant material. The tubes are placed in a cylinder with baffle plates, forming a shell-tube heat and mass exchanger (HMX). Fig 3-1 shows the arrangement of the embedded solid desiccant material and shell-tube heat and mass exchanger.

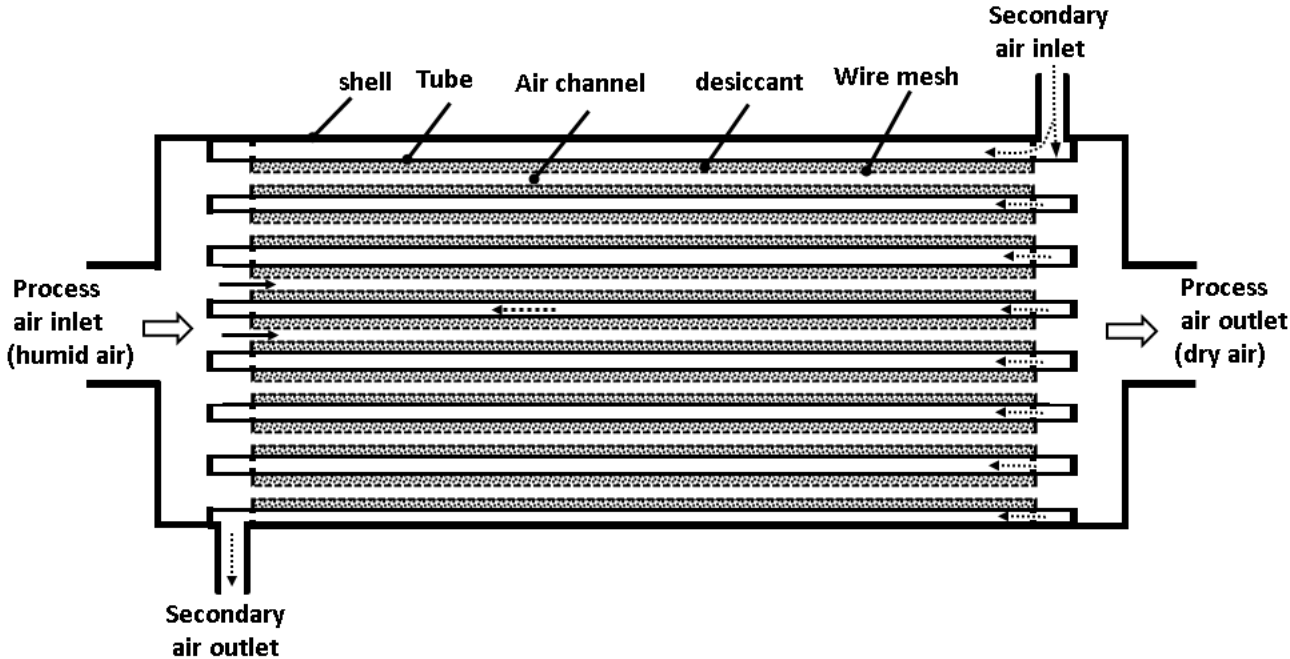


Fig 3-1 Arrangement of the proposed shell-tube HMX (adsorption mode)

Chapter 3: Design and computer modelling

Like existing solid desiccant systems, the proposed air dehumidification arrangement undergoes processes of adsorption (moisture uptake) and regeneration (desorption). During the adsorption process, humid, hot process air from ambient goes through the desiccant tubes, and the desiccant adsorbs moisture from the process air and releases heat of adsorption. On the shell side, secondary air which also from ambient (or other sources such as return air from air conditioned building, etc.) is circulated to remove heat from the desiccant tubes and cool the adsorbent beds. In regeneration mode, both process and secondary air streams are heated and deployed for regeneration only. On the tube side the regeneration (heated process air) air heats the desiccant directly and removes moisture. The secondary air on the other hand, is circulated through the shell side, heating the desiccant tubes indirectly, causing faster regeneration process.

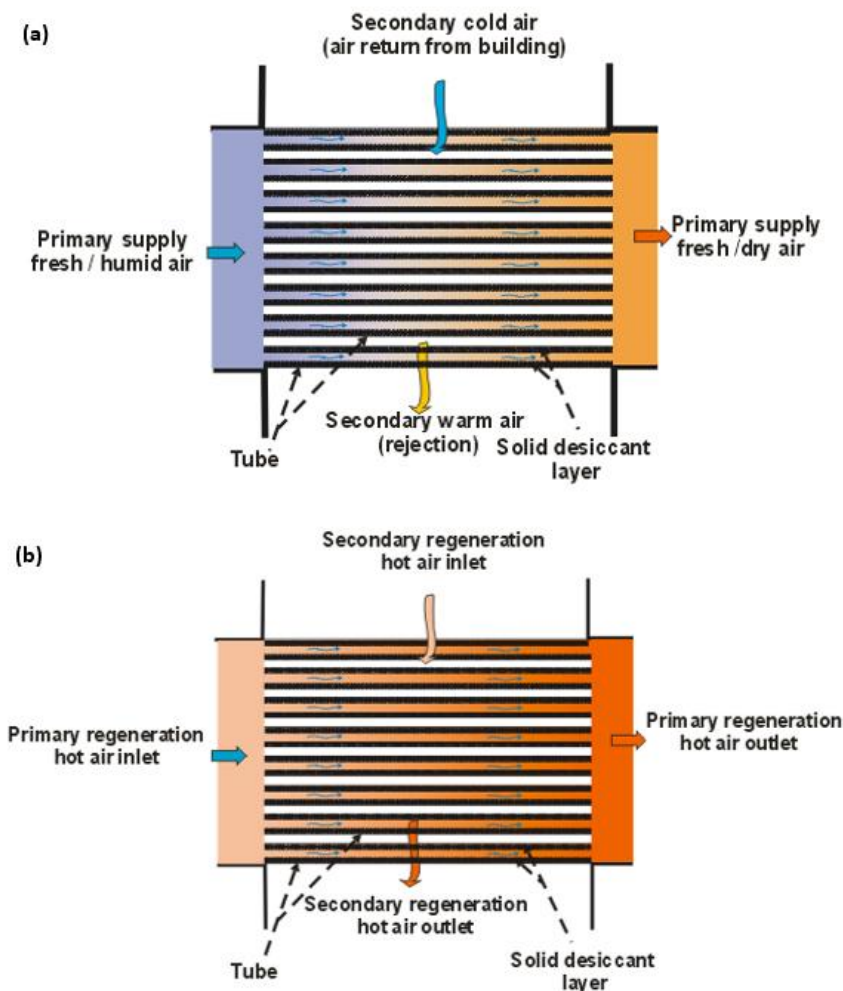


Fig 3-2 Schematics for (a) adsorption and (b) regeneration process

Chapter 3: Design and computer modelling

The shell-tube arrangement enables heat transfer between the two air streams and the desiccant, while mass transfer only occurs in the desiccant tubes. In regeneration process, the desiccant is heated both from within the desiccant tubes and from outside (helped by the secondary airstream in the shell side), as illustrated in Fig 3-2 (b). This enables the desiccant to reach the temperature required for regeneration and increases the desorption rate. During dehumidification process (Fig 3-2 (a)), secondary air stream helps evacuate heat from the desiccant as it releases adsorption heat (due to adsorbing moisture from the process air stream) and sensible heat from preceding regeneration process. This accelerates cooling of the desiccant, which improve adsorption rate, while limiting the amount of heat transferred from the desiccant to the process air stream. By limiting the mass transfer to only occur in the tube side, the system has flexibility in term of usage of cooling air during dehumidification process, in expense of limited desorption rate potential.

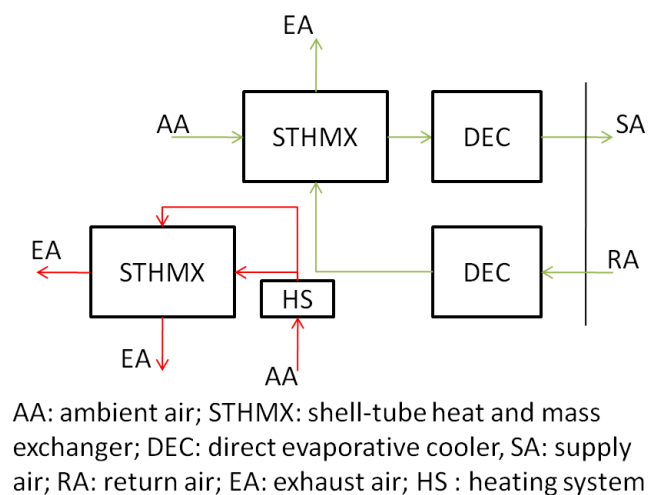


Fig 3-3 Shell-tube desiccant heat and mass exchanger replacing the desiccant wheel and heat exchanger in Pennington cycle configuration

When compared to common desiccant air conditioning systems such as the Pennington cycle, the shell-tube configuration proposed in this study eliminates the need for auxiliary external heat exchanger post dehumidification. Fig 3-3 shows the positioning of the Shell-tube desiccant heat and mass exchanger (STHMX) in Pennington cycle, replacing the desiccant wheel and heat exchanger unit.

By combining the desiccant dehumidifier and heat exchanger into a single unit, the dehumidifier ambient air can go directly to subsequent cooling system such as a direct evaporative cooling (DEC) before supplied to building. On the other hand, the return air can be directed back to the shell-side of the STHMX to help remove heat of desiccant and consequently the process air. As the STHMX is a fixed bed type dehumidifier, two units are required to work in tandem in order to allow continuous dehumidification-regeneration cycle.

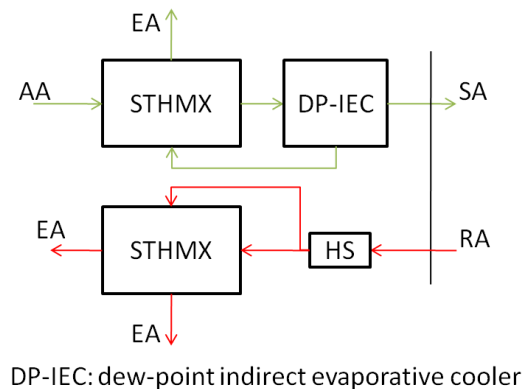


Fig 3-4 STHMX combined with a dew-point indirect evaporative cooler

The overall size of the system can be further reduced by replacing the DEC with a dew-point indirect evaporative cooler (DP-IEC) as shown in Fig 3-4. The indirect evaporative cooler, which commonly consists of a dry channel and a wet channel (where the water evaporation takes place) for two separate airstream to pass through, provides a very interesting potential for integration with STHMX. While air from the dry channel can be directly supplied to building, the air from the wet channel is usually rejected to ambient. By integrating it to the STHMX, the “wet air” from the cooler can be used as cooling air for the dehumidifier. Thus, by adopting a DP-IEC, one cooling unit would be sufficient to provide both supply air and cooling air to diverted back to the STHMX. Furthermore, the return air from building can be directed to the second dehumidifier unit to perform regeneration process. This can reduce the number of component required and thus make the overall system more compact.

3.3 Mathematical formulation

Modelling of solid desiccant systems are based on applying the principles of heat and mass transfer processes between the air stream and desiccant material and solving the heat transfer and mass conservation governing laws. Mathematical modelling of different dehumidification systems is however specific to the configuration of a particular system and the accuracy of the model mainly depends on the soundness of assumptions used in solving the governing equations.

The main difference between the general models for desiccant dehumidifiers and the model for internally cooled desiccant is that the temperature of desiccant layer is also affected by a secondary fluid. For example, Weixing et al. [44] adopted a GSR model for a cross-cooled desiccant channels with additional heat balance equations for the secondary air flow and the separator plate between the primary and the secondary channel. Narayanan et al. [49] opted for a 1-D GSSR model for a non-adiabatic wheel to include the heat and moisture transport resistance, however to simplify the model, the heat resistance between the desiccant layer and secondary air was assumed to be negligible while constant temperature was assumed for the secondary air thus no heat balance for the cooling air. Goldsworthy et al. [50] proposed a simplified model for a water-cooled desiccant wheel, which consists of 1-D GSR model for the air flow coupled with a 2-D SSR model for the desiccant layer. Additionally, a 1-D SSR model was proposed for the metal tube used as primary air channel which also holds the desiccant. To simplify the model, constant water temperature was assumed for the secondary channel.

The mathematical model for the proposed system in this study is derived from the application of energy and mass conservation laws in the solid desiccant layer and airflow in both the tube and shell site to simulate the air moisture removal potential of the dehumidifier as well parametric studies to investigate different operation conditions of the system. Several GSSR models were taken into consideration [32,35,37,56,57] and several modifications were made to conform to the system configuration proposed in this study.

Chapter 3: Design and computer modelling

The transient heat and mass transfer between the desiccant and the airflow in the desiccant channel is considered both in longitudinal and radial direction (2-dimensional model). On the shell side channel, the heat transfer model is considered in the airflow direction only (1-dimensional model). Fig 3-5 shows a control volume associated with the infinitesimal length dx . It is divided into three regions: secondary air (1), desiccant (2) and process air (3).

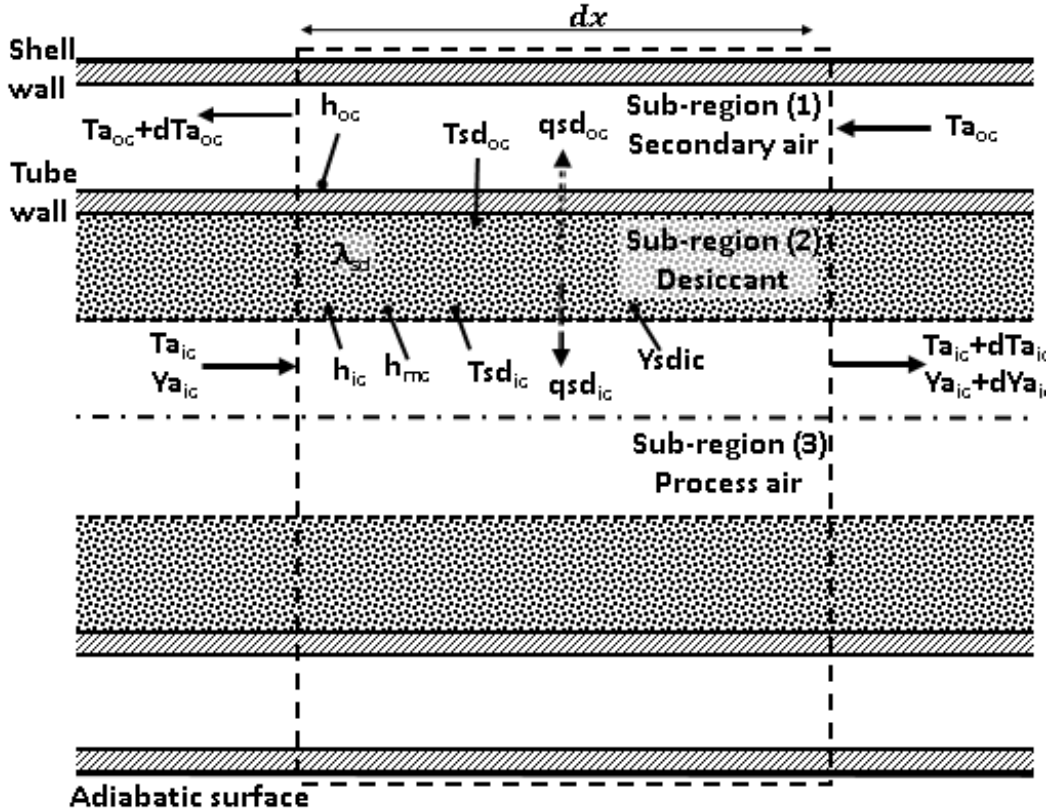


Fig 3-5 Control volume for mathematical modelling

The main assumptions applied to the control region are as follows:

- i. Air mass flow rates and inlet thermal properties are uniformly distributed in a plane perpendicular to the direction of flow
- ii. Pressure loss throughout the channels are negligible
- iii. Change of air temperature and moisture content are assumed to be dominated by heat and mass transfer between air stream and desiccant, thus

- iv. Only air temperature and water vapour distribution along the direction of the flow are considered
- v. Diffusion and heat conduction in the air stream are negligible
- vi. Convective heat and mass transfer coefficients are constant
- vii. Adsorption heat occurs mainly due to convective mass transfer between process air stream and desiccant layer
- viii. Tube wall is assumed to be very thin and its thermal resistance is negligible
- ix. Thermo-physical properties of the desiccant material are stable
- x. The wall of the shell side is assumed to not affect the temperature of secondary air
- xi. The outer boundary of the system is adiabatic

Compared to other models for desiccant dehumidifier with internal heat exchanger, one of the advantages of the proposed model for this study is that the proposed model offers 2-D heat and moisture balance for the desiccant layer which takes into account the moisture transport resistance through the thickness of desiccant layer. Additionally, heat balance for the secondary flow is also proposed to describe temperature change during both dehumidification and regeneration process. On the other hand, to avoid over-complication, the separator between the primary and secondary channel could be assumed to be sufficiently conductive thus the heat resistance could be neglected. The model proposed in this study thus combines the advantages of the other models considered.

The energy and mass balance equations for the three sub-regions of the system are formulated as follows:

3.3.1. Energy balance of secondary air in the shell side

The secondary air in sub-region 1 flows through the shell side (outer channel) and exchanges heat with the adsorbent layer in sub-region 2 both during the adsorption cycle (as cooling air)

and desorption cycle (as heating air). No mass transfer occurs in the shell side thus mass balance is not applied here. The heat balance of the secondary air is written as:

$$\rho_a c_a A_{oc} \left(\frac{\partial T_{aoc}}{\partial t} + u_{aoc} \frac{\partial T_{aoc}}{\partial x} \right) = h_{oc} p_{od} (T_{sd_{oc}} - T_{aoc}) \quad (3.1)$$

The term on the left hand side of the equation above represents the heat storage term in the secondary air stream and the temperature change along the outer channel's length. The right hand side of the equation is the convective heat transfer between the secondary air stream and the desiccant. ρ_a is density of air [kg m^{-3}], A_{oc} is cross section area for air flow in shell side [m^2], u_{aoc} is velocity of secondary air [m s^{-1}], c_{pa} is specific heat of air [$\text{J kg}^{-1} \text{K}^{-1}$], T_{aoc} is temperature of secondary air [K], h_{oc} is the convective heat transfer coefficient in shell side [$\text{W m}^{-2} \text{K}^{-1}$], $T_{sd_{oc}}$ is temperature of desiccant surface [K] at the interface with the tube wall with a contact perimeter p_{od} [m].

3.3.2. Heat and mass balance of process air

The air in sub region 3 or the inner channel (process air in adsorption mode or regeneration air in desorption mode) flows over the solid desiccant layer (sub-region 2), resulting in both exchange of sensible heat and moisture. The dynamic mass conservation of the primary air stream is described as follow:

$$\rho_a A_{ic} \left(\frac{\partial Y_{aic}}{\partial t} + u_{aic} \frac{\partial Y_{aic}}{\partial x} \right) = h_m p_{id} (Y_{sd_{ic}} - Y_{aic}) \quad (3.2)$$

The terms on left hand side of the above equations explains the moisture storage in the primary air and the change of air moisture constant along the channel's length. The term on the right hand side of the equations describes the convective mass transfer between the airstream in the inner channel and the desiccant wall. A_{ic} is the inner channel cross section area for air flow [m^2], Y_{aic} is humidity ratio of primary air [kg kg^{-1}], u_{aic} is velocity of primary air [m s^{-1}], $Y_{sd_{ic}}$ is the gas phase equilibrium moisture content at the surface in contact with primary air [kg kg^{-1}], and h_m is mass transfer coefficient [$\text{kg m}^{-2} \text{s}^{-1}$], p_{id} is the perimeter of inner channel (desiccant layer) [m].

Similarly, change of temperature in sub region 3 is expressed by the energy conservation balance written as:

$$\rho_a c_a A_{ic} \left(\frac{\partial T_{a_{ic}}}{\partial t} + u_{a_{ic}} \frac{\partial T_{a_{ic}}}{\partial x} \right) = h_{ic} p_{id} (T_{sd_{ic}} - T_{a_{ic}}) + h_m c_v p_{id} (Y_{sd_{ic}} - Y_{a_{ic}}) (T_{sd_{ic}} - T_{a_{ic}}) \quad (3.3)$$

Similar to the heat balance of the airflow in the shell side channel, the left hand side of the above equation represents the heat storage of the primary air flow and air temperature change along the direction of travel, while the first term on the right hand side of the equations is the convective heat transfer between the primary air and the desiccant wall. In addition, the second term on the right hand side of the equation describes the sensible heat transfer between the air and the desiccant due to the convective mass transfer. $T_{a_{ic}}$ is temperature of primary air [K], h_{ic} is heat transfer coefficient for inner channel [$\text{W m}^{-2} \text{K}^{-1}$], c_v is specific heat of water vapour [$\text{J kg}^{-1} \text{K}^{-1}$], and $T_{sd_{ic}}$ is temperature of desiccant surface in contact with the primary air stream [K].

The convective heat and mass transfer coefficients are calculated using the following relation:

Nusselt and Sherwood number

$$Nu = \frac{h D_h}{\lambda_a} \quad (3.4)$$

$$Sh = \frac{h_m D_h}{\rho_a D_{va}} \quad (3.5)$$

Where λ_a is the air heat conductivity [$\text{W m}^{-1} \text{K}^{-1}$], D_h is hydraulic diameter [m], D_{va} is moisture diffusivity in air [$\text{m}^2 \text{s}^{-1}$]. Nusselt and Sherwood numbers are calculated based on the Reynold number of our system, which below 2300. As the system use a fully developed laminar flow, Nu and Sh are constants.

3.3.3. Heat and energy balance of the desiccant layer

The desiccant layer exchanges heat with air streams in both tube side and shell side. It is assumed that the desiccant and adsorbed moisture within are at the same temperature and there is no heat transfer between the two. Similarly, it is assumed that heat is distributed along the desiccant layer as homogenous material. Therefore, heat transfer in the desiccant

layer is modelled as a 2-D thermal diffusion process. The conservation of energy of the desiccant layer can be expressed as:

$$(\rho c)_m \frac{\partial T_d}{\partial t} = \lambda_m \left(\frac{\partial^2 T_d}{\partial x^2} + \frac{\partial^2 T_d}{\partial y^2} \right) \quad (3.6)$$

The left hand side of the equation gives the heat storage if the desiccant material, while the right hand side of the equation describe the heat conduction in desiccant material along the two directions and heat of adsorption. The equivalent specific heat $(\rho c)_m$ and thermal conductive λ_m of the loaded adsorbent layer with moisture are expressed as [60]:

$$(\rho c)_m = \rho_v c_{pv} \varepsilon + (1 - \varepsilon) \rho_d c_d \quad (3.7)$$

$$\lambda_m = \varepsilon \lambda_v + (1 - \varepsilon) \lambda_d \quad (3.8)$$

Where ρ_d is the desiccant density [kg m^{-3}], c_d is specific heat of desiccant [$\text{J kg}^{-1} \text{K}^{-1}$], T_d is the desiccant temperature (K), λ_d is the desiccant thermal conductivity [$\text{W m}^{-1} \text{K}^{-1}$], and q_{st} is latent heat of adsorption of the desiccant layer [J kg^{-1}]. In this study, porosity of the desiccant layer ε is assumed to be very small thus can be neglected.

The distribution of water content along the desiccant layer is expressed as moisture diffusion through the porous desiccant layer along the airflow direction (x-axis) and thickness (radial direction). The moisture diffusion is a combination of ordinary, Knudsen gas diffusion and surface diffusion. For regular density silica gel adsorbents, the ordinary diffusion can be omitted as pores in the materials particulates are very small ($<100\text{\AA}$) and surface diffusion is more dominant than Knudsen diffusion in ordinary density silica gel by a factor of 16 to 43 [32,58]. Therefore, the mass balance of the desiccant layer is expressed as:

$$\frac{\partial W}{\partial t} = D_s \left(\frac{\partial^2 W}{\partial x^2} + \frac{\partial^2 W}{\partial y^2} \right) \quad (3.9)$$

Where D_s [$\text{m}^2 \text{s}^{-1}$] is the effective diffusion coefficient which is assumed constant over the desiccant layer control volume for a given desiccant temperature. This is given by the following [32,61]:

$$D_s = D_0 e^{-0.45(q_{st}/RT_{sd})} \quad (3.10)$$

With R is the gas constant of water vapour [$\text{J kg}^{-1} \text{K}^{-1}$] and the coefficient of diffusivity at equilibrium $D_0 = 1.6 \times 10^{-6} \text{ m}^2/\text{s}$ [32,61].

To relate the equations of heat and mass transfer between sub-region 2 and sub-region 3, equilibrium adsorption isotherm can be used. The equilibrium isotherm describes moisture content of desiccant layer surface in function of relative humidity (RH) of air in contact with the surface.

For regular density silica gel, the isotherm equation can be expressed as follow [58]:

$$RH = 0.0078 - 0.05759W + 24.16554W - 124.78W^3 + 204.226W^4 \quad (3.11)$$

The relation between humidity ratio and relative humidity can be expressed using Clapeyron equation (assuming a standard atmospheric pressure of 101325 Pa) as follow [37]:

$$\frac{RH}{Y} = 10^{-6} e^{5294/T} - 1.61RH \quad (3.12)$$

The main properties of the selected desiccant materials are summarised in Table 3-1.

Table 3-1 Properties of solid desiccant material [32]

Properties	Unit	Value
Material	-	Silica Gel RD
Density	kg m^{-3}	800
Thermal conductivity	$\text{W m}^{-1} \text{K}^{-1}$	0.2
Specific heat capacity	$\text{J kg}^{-1} \text{K}^{-1}$	921
Adsorption heat	kJ kg^{-1}	2370

3.3.4. Boundary conditions

To solve equation (3.1) – (3.12), following boundary conditions are assumed:

Chapter 3: Design and computer modelling

For dehumidification mode, process air at temperature equal to $T_{p,inlet}$ and at humidity equal to $Y_{p,inlet}$ is supplied to the inlet of the tube side. For the shell side, cooling air at temperature of $T_{c,inlet}$ is assumed at the inlet of the shell side, as written below:

$$T_{aic}(x = 0, t) = T_{inlet} \quad (3.13)$$

$$T_{aoc}(x = L, t) = T_{c,inlet} \quad (3.14)$$

$$Y_{aic}(x = 0, t) = Y_{inlet} \quad (3.15)$$

For the regeneration process, regeneration air temperature ($T_{r,inlet}$) and humidity ($Y_{r,inlet}$) were assumed at the inlet of each channel:

$$T_{aic}(x = 0, t) = T_{r,inlet} \quad (3.16)$$

$$T_{aoc}(x = L, t) = T_{r,inlet} \quad (3.17)$$

$$Y_{aic}(x = 0, t) = Y_{r,inlet} \quad (3.18)$$

For the adsorbent layer, following boundary conditions are applied:

It is assumed that the desiccant is perfectly insulated and impermeable at the inlet and outlet of the channels, and the outer surface or the tube wall is impermeable (Neumann boundary conditions):

$$\left. \frac{\partial T}{\partial x} \right|_{x=0} = \left. \frac{\partial T}{\partial x} \right|_{x=L} = 0 \quad (3.19)$$

$$\left. \frac{\partial W}{\partial x} \right|_{x=0} = \left. \frac{\partial W}{\partial x} \right|_{x=L} = \left. \frac{\partial W}{\partial y} \right|_{y=0} = 0 \quad (3.20)$$

The heat flux in radial direction at the outer surface was assumed to be described by the convective heat transfer between the air in the shell side channel and the desiccant layer surface:

$$-\lambda_d \left. \frac{\partial T}{\partial y} \right|_{y=0} = h_{oc}(T_{aoc} - T_{sd_{oc}}) \quad (3.21)$$

The heat flux in radial direction at the inner surface was assumed to be described by the convective heat transfer between the air in the desiccant channel and the desiccant layer surface, the sensible heat transfer due to mass exchange between the airstream and the desiccant surface, and the latent heat of moisture adsorption of the airstream at the surface of the desiccant:

$$-\lambda_d \frac{\partial T}{\partial y} \Big|_{y=\delta} = h_{ic}(T_{sdic} - T_{aic}) + h_m C_v (Y_{sdic} - Y_{aic})(T_{sdic} - T_{aic}) + h_m q_{st}(Y_{sdic} - Y_{aic}) \quad (3.22)$$

The mass flux in radial direction at the inner surface was assumed to be described by the convective mass transfer between the inner surface of the desiccant layer and the airstream in the desiccant channel:

$$-\rho_d D \frac{\partial W}{\partial y} \Big|_{y=\delta} = h_m (Y_{sdic} - Y_{aic}) \quad (3.23)$$

3.4. Numerical solutions and computer model

The mathematical formulations of the proposed system involve complex and nested heat and mass transfer equations, which cannot be solved analytically. Hence, numerical method is employed to find an approximation solution that reflects the heat and mass transfer processes occurring in the system. Fig 3-6 shows a discretised control volume model and the operating parameters on an infinitesimal scale.

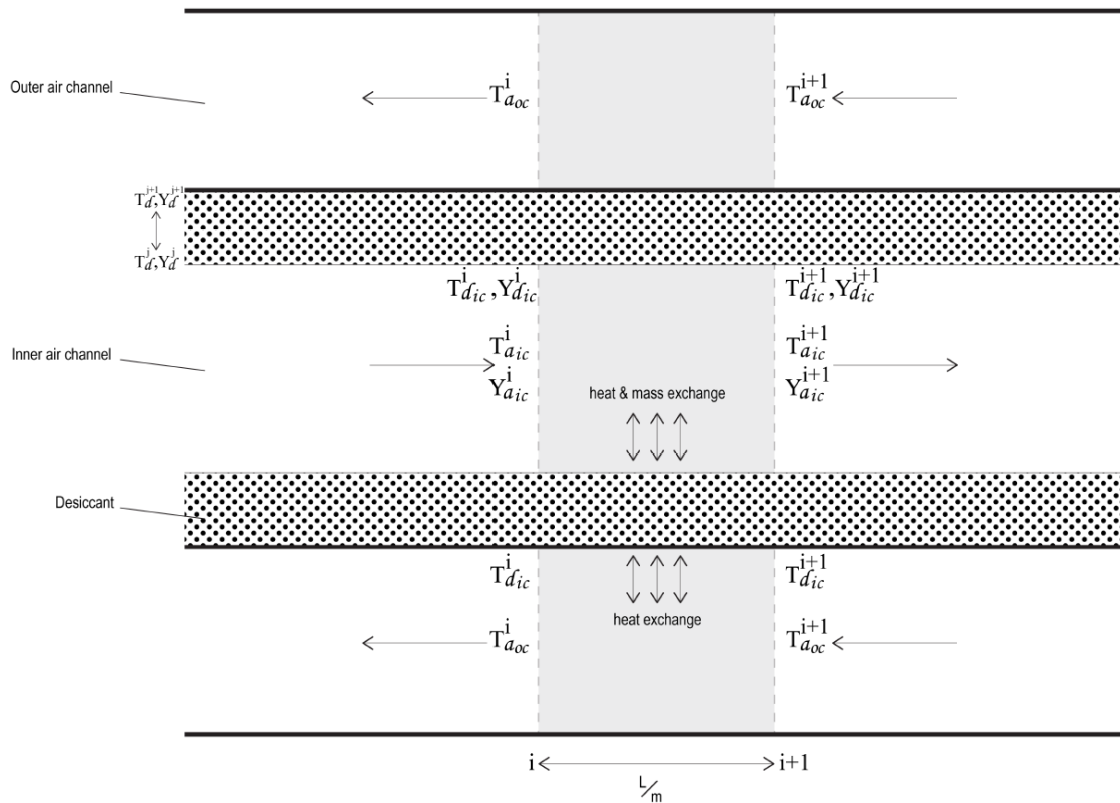


Fig 3-6 Control volume of the model

In discretising the governing equations, the derivatives in axial direction (∂x) are discretized into nodes i ($i=1, 2, 3\dots, m$) with the distance of each node equal to Δx , and derivatives in radial direction (∂y) are discretized into nodes j ($j=1, 2, 3\dots, n$) with Δy as the distance between the nodes. The numerical method employed to solve the equations is the implicit scheme finite difference method. While explicit schemes are generally simpler, they have strict stability criterion in order to reach convergent results. Implicit techniques offers alternatives that guarantee stability [62].

3.4.1. Discretisation of equations in sub-region 1 and sub-region 3 (air channels)

Partial derivatives in equation (3.1) – (3.3) are substituted with finite-difference representations by treating the air channels as a grid of discrete points along the direction of airflow. By doing so, change of air temperature and humidity can be calculated over certain step size (Δx). On the other hand, the amount of heat and moisture stored in the airstream over a unit time period Δt is also taken into account.

For equation (3.1) – (3.3), the derivatives in respect to x are substituted by the backward-implicit finite-divided-difference formulas, while the derivatives in respect to t are approximated by the forward finite-difference formulas. In implicit methods, the spatial derivative is approximated at an advanced time level ($k + 1$), instead of current time level (k) in explicit scheme.

The discretised derivatives are as follows:

$$\frac{\partial T_{a_{oc}}}{\partial t} = \frac{T_{a_{oc}i}^{k+1} - T_{a_{oc}i}^k}{\Delta t} \quad (3.24)$$

$$\frac{\partial T_{a_{oc}}}{\partial x} \cong \frac{T_{a_{oc}i}^{k+1} - T_{a_{oc}i-1}^{k+1}}{\Delta x} \quad (3.25)$$

$$\frac{\partial Y_{a_{ic}}}{\partial t} = \frac{Y_{a_{ic}i}^{k+1} - Y_{a_{ic}i}^k}{\Delta t} \quad (3.26)$$

$$\frac{\partial Y_{a_{ic}}}{\partial x} \cong \frac{Y_{a_{ic}i}^{k+1} - Y_{a_{ic}i-1}^{k+1}}{\Delta x} \quad (3.27)$$

$$\frac{\partial T_{a_{ic}}}{\partial t} = \frac{T_{a_{(ic)}_i^{k+1}} - T_{a_{(ic)}_i^k}}{\Delta t} \quad (3.28)$$

$$\frac{\partial T_{a_{ic}}}{\partial x} \cong \frac{T_{a_{(ic)}_i^{k+1}} - T_{a_{(ic)}_{i-1}^{k+1}}}{\Delta x} \quad (3.29)$$

Then, by substituting equation (3.24) – (3.29) into equation (3.1) – (3.3), the partial differential equations are transformed into algebraic difference equations.

The discretisation of equation (3.1) yields

$$\rho_a c_{pa} A_{oc} \left(\frac{T_{a_{(oc)}_i^{k+1}} - T_{a_{(oc)}_i^k}}{\Delta t} + u_{aoc} \frac{T_{a_{(oc)}_i^{k+1}} - T_{a_{(oc)}_{i-1}^{k+1}}}{\Delta x} \right) = h_{oc} p_{od} \left(T_{sd_{(oc)}_i^k} - T_{a_{(oc)}_i^k} \right) \quad (3.30)$$

Which can be solved for (along the inlet boundary conditions)

$$T_{a_{(oc)}_i^{k+1}} = \frac{1}{1 + \alpha_{oc}} \left(T_{a_{(oc)}_i^k} + \alpha_{oc} T_{a_{(oc)}_{i-1}^{k+1}} + \beta_{oc} \left(T_{sd_{(oc)}_i^k} - T_{a_{(oc)}_i^k} \right) \right) \quad (3.31)$$

Where $\alpha_{oc} = \frac{u_{aoc} \Delta t}{\Delta x}$ and $\beta_{oc} = \frac{h_{oc} p_{od} \Delta t}{\rho_a c_{pa} A_{oc}}$

Equation (3.2) is transformed into the following equation

$$\rho_a A_{ic} \left(\frac{Y_{a_{(ic)}_i^{k+1}} - Y_{a_{(ic)}_i^k}}{\Delta t} + u_{aic} \frac{Y_{a_{(ic)}_i^{k+1}} - Y_{a_{(ic)}_{i-1}^{k+1}}}{\Delta x} \right) = h_m p_{id} \left(Y_{sd_{(ic)}_i^k} - Y_{a_{(ic)}_i^k} \right) \quad (3.32)$$

Which can be substituted into

$$Y_{a_{(ic)}_i^{k+1}} = \frac{1}{1 + \alpha_{ic}} \left(Y_{a_{(ic)}_i^k} + \alpha_{ic} Y_{a_{(ic)}_{i-1}^{k+1}} + \gamma \left(Y_{sd_{(ic)}_i^k} - Y_{a_{(ic)}_i^k} \right) \right) \quad (3.33)$$

Where $\alpha_{ic} = \frac{u_{aic} \Delta t}{\Delta x}$ and $\gamma = \frac{h_m p_{id} \Delta t}{\rho_a A_{ic}}$

The finite-difference representation of equation (3.3) is as follows

$$\rho_a C_a A_{ic} \left(\frac{T_{a_{(ic)}_i^{k+1}} - T_{a_{(ic)}_i^k}}{\Delta t} + u_{aic} \frac{T_{a_{(ic)}_i^{k+1}} - T_{a_{(ic)}_{i-1}^{k+1}}}{\Delta x} \right) = h_{ic} p_{id} \left(T_{sd_{(ic)}_i^k} - T_{a_{(ic)}_i^k} \right) + h_m C_v p_{id} \left(Y_{sd_{(ic)}_i^k} - Y_{a_{(ic)}_i^k} \right) \left(T_{sd_{(ic)}_i^k} - T_{a_{(ic)}_i^k} \right) \quad (3.34)$$

Thus

$$T_{a_{(ic)}_i^{k+1}} = \frac{1}{1 + \alpha_{ic}} \left(T_{a_{(ic)}_i^k} + \alpha_{ic} T_{a_{(ic)}_{i-1}^{k+1}} + \beta_{ic} \left(T_{sd_{(ic)}_i^k} - T_{a_{(ic)}_i^k} \right) + \gamma_h \left(Y_{sd_{(ic)}_i^k} - Y_{a_{(ic)}_i^k} \right) \left(T_{sd_{(ic)}_i^k} - T_{a_{(ic)}_i^k} \right) \right) \quad (3.35)$$

With $\beta_{ic} = \frac{h_{ic} p_{ia} \Delta t}{\rho_a c_{pa} A_{ic}}$ and $\gamma_h = \gamma \frac{C_v}{C_a}$

3.4.2. Discretization of equations in sub-region 2 (desiccant layer)

Since equation (3.6) and (3.9) are parabolic equations in two spatial dimensions (in x-direction as well as y-direction), application of standard implicit finite-difference schemes can lead to exorbitantly large computation time [62]. To solve this problem, the alternating-direction implicit, or ADI, can be employed. In this scheme, calculation for every time-step is divided by half, where each increment (Δx and Δy) is executed in two steps. This means that for the first half-step, the approximations of derivatives in x-direction are expressed explicitly, while approximations of derivatives in y-directions are expressed implicitly. For the second half-step, approximations are done the other way around.

For the first-half time step, the derivatives in equation (3.6) and (3.9) are substituted by the following formulas:

$$\frac{\partial T_d}{\partial t} = \frac{T_{d,i,j}^{k+\frac{1}{2}} - T_{d,i,j}^k}{\Delta t/2} \tag{3.36}$$

$$\frac{\partial^2 T_d}{\partial x^2} = \frac{T_{d,i-1,j}^k - 2T_{d,i,j}^k + T_{d,i+1,j}^k}{(\Delta x)^2} \tag{3.37}$$

$$\frac{\partial^2 T_d}{\partial y^2} \cong \frac{T_{d,i,j-1}^{k+\frac{1}{2}} - 2T_{d,i,j}^{k+\frac{1}{2}} + T_{d,i,j+1}^{k+\frac{1}{2}}}{(\Delta y)^2} \tag{3.38}$$

$$\frac{\partial W}{\partial t} = \frac{W_{i,j}^{k+\frac{1}{2}} - W_{i,j}^k}{\Delta t/2} \tag{3.39}$$

$$\frac{\partial^2 W}{\partial x^2} = \frac{W_{i-1,j}^k - 2W_{i,j}^k + W_{i+1,j}^k}{(\Delta x)^2} \tag{3.40}$$

$$\frac{\partial^2 W}{\partial y^2} \cong \frac{W_{i,j-1}^{k+\frac{1}{2}} - 2W_{i,j}^{k+\frac{1}{2}} + W_{i,j+1}^{k+\frac{1}{2}}}{(\Delta y)^2} \tag{3.41}$$

Hence, by substituting the above equations to equation(3.6) and (3.9), following equations are obtained (assuming $\varepsilon=0$):

$$\rho_d c_d \frac{T_{d_{i,j}}^{k+\frac{1}{2}} - T_{d_{i,j}}^k}{\Delta t/2} = \lambda_d \left(\frac{T_{d_{i-1,j}}^k - 2T_{d_{i,j}}^k + T_{d_{i+1,j}}^k}{(\Delta x)^2} + \frac{T_{d_{i,j-1}}^{k+\frac{1}{2}} - 2T_{d_{i,j}}^{k+\frac{1}{2}} + T_{d_{i,j+1}}^{k+\frac{1}{2}}}{(\Delta y)^2} \right) \quad (3.42)$$

$$\frac{W_{i,j}^{k+\frac{1}{2}} - W_{i,j}^k}{\Delta t/2} = D_s \left(\frac{W_{i-1,j}^k - 2W_{i,j}^k + W_{i+1,j}^k}{(\Delta x)^2} + \frac{W_{i,j-1}^{k+\frac{1}{2}} - 2W_{i,j}^{k+\frac{1}{2}} + W_{i,j+1}^{k+\frac{1}{2}}}{(\Delta y)^2} \right) \quad (3.43)$$

Thus

$$-\lambda_y T_{d_{i,j-1}}^{k+\frac{1}{2}} + (1 + 2\lambda_y) T_{d_{i,j}}^{k+\frac{1}{2}} - \lambda_y T_{d_{i,j+1}}^{k+\frac{1}{2}} = \lambda_x T_{d_{i-1,j}}^k + (1 - 2\lambda_x) T_{d_{i,j}}^k + \lambda_x T_{d_{i+1,j}}^k \quad (3.44)$$

With $\lambda_y = \frac{\lambda_d(\Delta t/2)}{\rho_d c_d(\Delta y)^2}$ and $\lambda_x = \frac{\lambda_d(\Delta t/2)}{\rho_d c_d(\Delta x)^2}$

$$-D_y W_{i,j-1}^{k+\frac{1}{2}} + (1 + 2D_y) W_{i,j}^{k+\frac{1}{2}} - D_y W_{i,j+1}^{k+\frac{1}{2}} = D_x W_{i-1,j}^k + (1 - 2D_x) W_{i,j}^k + D_x W_{i+1,j}^k \quad (3.45)$$

With $D_y = \frac{D_s(\Delta t/2)}{(\Delta y)^2}$ and $D_x = \frac{D_s(\Delta t/2)}{(\Delta x)^2}$

Equation (3.44) and (3.45) contain several unknowns at time level $(k + \frac{1}{2})$, thus they cannot be solved by simple algebraic rearrangement as in equation (3.31), (3.33), and (3.35). Thus, they must be solved simultaneously along with the boundary conditions. Equation (3.44) and (3.45) applies for interior nodes of $1 < i < m$ and $1 < j < n$. Modification for the boundary nodes for equation (3.44) are as follows:

For $i = 1, 1 < j < n$ and $i = m, 1 < j < n$ the boundary condition equation (3.19) is applied and discretised with the following centre finite-divided-difference formulas:

$$\left. \frac{\partial T_d}{\partial x} \right|_{i=1}^k = \frac{T_{d_{2,j}}^k - T_{d_{0,j}}^k}{2\Delta x} \quad (3.46)$$

$$\left. \frac{\partial T_d}{\partial x} \right|_{i=m}^k = \frac{T_{d_{m+1,j}}^k - T_{d_{m-1,j}}^k}{2\Delta x} \quad (3.47)$$

Hence

$$T_{d_{0,j}}^k = T_{d_{2,j}}^k - 2\Delta x \left. \frac{\partial T_d}{\partial x} \right|_{i=1}^k \quad (3.48)$$

$$T_{d_{m+1,j}}^k = T_{d_{m-1,j}}^k + 2\Delta x \left. \frac{\partial T_d}{\partial x} \right|_{i=m}^k \quad (3.49)$$

Chapter 3: Design and computer modelling

By substituting equation (3.48) and (3.49) to equation (3.44) the following formulas are

obtained ($\frac{\partial T_d}{\partial x}\bigg|_{i=1}^k = \frac{\partial T_d}{\partial x}\bigg|_{i=m}^k = 0$):

$$-\lambda_y T_{d_{1,j-1}}^{k+\frac{1}{2}} + (1 + 2\lambda_y) T_{d_{1,j}}^{k+\frac{1}{2}} - \lambda_y T_{d_{1,j+1}}^{k+\frac{1}{2}} = (1 - 2\lambda_x) T_{d_{1,j}}^k + \lambda_x T_{d_{2+1,j}}^k \quad (3.50)$$

$$-\lambda_y T_{d_{m,j-1}}^{k+\frac{1}{2}} + (1 + 2\lambda_y) T_{d_{m,j}}^{k+\frac{1}{2}} - \lambda_y T_{d_{m,j+1}}^{k+\frac{1}{2}} = 2\lambda_x T_{d_{m-1,j}}^k + (1 - 2\lambda_x) T_{d_{m,j}}^k \quad (3.51)$$

For $j = 1$, boundary equation (3.21) is applicable:

$$\lambda_d \frac{\partial T}{\partial y}\bigg|_{j=1}^{k+\frac{1}{2}} \cong \lambda_d \frac{T_{d_{i,2}}^{k+\frac{1}{2}} - T_{d_{i,0}}^{k+\frac{1}{2}}}{2\Delta y} = h_{oc} (T_{d_{i,1}}^k - T_{a_{(oc)i}}^k) \quad (3.52)$$

Hence

$$T_{d_{i,0}}^{k+\frac{1}{2}} = T_{d_{i,2}}^{k+\frac{1}{2}} - NTU_{oc} (T_{d_{i,1}}^k - T_{a_{(oc)i}}^k) \quad (3.53)$$

With $T_{d_{i,1}}^k = T_{sd_{(oc)i}}^k$ and $NTU_{oc} = \frac{2\Delta y h_{oc}}{\lambda_d}$

Thus, for $1 < i < m$, $j = 1$, equation (3.53) is substituted to equation (3.44) resulting in following equation:

$$(1 + 2\lambda_y) T_{d_{i,1}}^{k+\frac{1}{2}} - 2\lambda_y T_{d_{i,2}}^{k+\frac{1}{2}} = \lambda_x T_{d_{i-1,1}}^k + (1 - 2\lambda_x) T_{d_{i,1}}^k + \lambda_x T_{d_{i+1,1}}^k - \lambda_y \left(NTU_{oc} (T_{d_{i,1}}^k - T_{a_{(oc)i}}^k) \right) \quad (3.54)$$

Furthermore, for $i = 1$, $j = 1$

$$(1 + 2\lambda_y) T_{d_{1,1}}^{k+\frac{1}{2}} - 2\lambda_y T_{d_{1,2}}^{k+\frac{1}{2}} = (1 - 2\lambda_x) T_{d_{1,1}}^k + 2\lambda_x T_{d_{2,1}}^k - \lambda_y \left(NTU_{oc} (T_{d_{1,1}}^k - T_{a_{(oc)1}}^k) \right) \quad (3.55)$$

For $i = m$, $j = 1$, following equation is applied:

$$(1 + 2\lambda_y) T_{d_{m,1}}^{k+\frac{1}{2}} - 2\lambda_y T_{d_{m,2}}^{k+\frac{1}{2}} = 2\lambda_x T_{d_{m-1,1}}^k + (1 - 2\lambda_x) T_{d_{m,1}}^k - \lambda_y \left(NTU_{oc} (T_{d_{m,1}}^k - T_{a_{(oc)m}}^k) \right) \quad (3.56)$$

Chapter 3: Design and computer modelling

For $j = n$, boundary condition equation (3.22) is applied as follows:

$$-\lambda_d \frac{\partial T}{\partial y} \Big|_{j=n}^{k+\frac{1}{2}} \cong -\lambda_d \frac{T_{d_{i,n+1}}^{k+\frac{1}{2}} - T_{d_{i,n-1}}^{k+\frac{1}{2}}}{2\Delta y} = h_{ic} (T_{d_{i,n}}^k - T_{a_{(ic)_i}}^k) + h_m C_v (Y_{sd_{(ic)_i}}^k - Y_{a_{(ic)_i}}^k) (T_{d_{i,n}}^k - T_{a_{(ic)_i}}^k) + h_m q_{st} (Y_{sd_{(ic)_i}}^k - Y_{a_{(ic)_i}}^k) \quad (3.57)$$

Hence

$$T_{d_{i,n+1}}^{k+\frac{1}{2}} = T_{d_{i,n-1}}^{k+\frac{1}{2}} - NTU_{ic} (T_{d_{i,n}}^k - T_{a_{(ic)_i}}^k) - NTU_{hmic} (Y_{sd_{(ic)_i}}^k - Y_{a_{(ic)_i}}^k) (T_{d_{i,n}}^k - T_{a_{(ic)_i}}^k) - NTU_{hmic} q_{st} (Y_{sd_{(ic)_i}}^k - Y_{a_{(ic)_i}}^k) \quad (3.58)$$

With $T_{d_{i,n}}^k = T_{sd_{(ic)_i}}^k$, $NTU_{ic} = \frac{2\Delta y h_{ic}}{\lambda_d}$, and $NTU_{hmic} = \frac{2\Delta y h_m C_v}{\lambda_d}$

For $1 < i < m$, $j = n$, substituting equation (3.58) to equation (3.44) holds:

$$-2\lambda_y T_{d_{i,n-1}}^{k+\frac{1}{2}} + (1 + 2\lambda_y) T_{d_{i,n}}^{k+\frac{1}{2}} = \lambda_x T_{d_{i-1,n}}^k + (1 - 2\lambda_x) T_{d_{i,n}}^k + \lambda_x T_{d_{i+1,n}}^k - \lambda_y \left(NTU_{ic} (T_{d_{i,n}}^k - T_{a_{(ic)_i}}^k) - NTU_{hmic} (Y_{sd_{(ic)_i}}^k - Y_{a_{(ic)_i}}^k) (T_{d_{i,n}}^k - T_{a_{(ic)_i}}^k) - NTU_{hmic} q_{st} (Y_{sd_{(ic)_i}}^k - Y_{a_{(ic)_i}}^k) \right) \quad (3.59)$$

As for $i = 1$ and $j = n$, equation (3.59) becomes

$$-2\lambda_y T_{d_{1,n-1}}^{k+\frac{1}{2}} + (1 + 2\lambda_y) T_{d_{1,n}}^{k+\frac{1}{2}} = (1 - 2\lambda_x) T_{d_{1,n}}^k + 2\lambda_x T_{d_{2,n}}^k - \lambda_y \left(NTU_{ic} (T_{d_{1,n}}^k - T_{a_{(ic)_1}}^k) - NTU_{hmic} (Y_{sd_{(ic)_1}}^k - Y_{a_{(ic)_1}}^k) (T_{d_{1,n}}^k - T_{a_{(ic)_1}}^k) - NTU_{hmic} q_{st} (Y_{sd_{(ic)_1}}^k - Y_{a_{(ic)_1}}^k) \right) \quad (3.60)$$

For $i = m$ and $j = n$, following equation is applied

$$-2\lambda_y T_{d_{m,n-1}}^{k+\frac{1}{2}} + (1 + 2\lambda_y) T_{d_{m,n}}^{k+\frac{1}{2}} = 2\lambda_x T_{d_{m-1,n}}^k + (1 - 2\lambda_x) T_{d_{m,n}}^k - \lambda_y \left(NTU_{ic} (T_{d_{m,n}}^k - T_{a_{(ic)_m}}^k) - NTU_{hmic} (Y_{sd_{(ic)_m}}^k - Y_{a_{(ic)_m}}^k) (T_{d_{m,n}}^k - T_{a_{(ic)_m}}^k) - NTU_{hmic} q_{st} (Y_{sd_{(ic)_m}}^k - Y_{a_{(ic)_m}}^k) \right) \quad (3.61)$$

Similar to equation (3.44), modifications for the boundary nodes for equation (3.45) are as follow:

For $i = 1$ and $1 < j < n$ (boundary condition (3.20)):

$$-D_y W_{1,j-1}^{k+\frac{1}{2}} + (1 + 2D_y)W_{1,j}^{k+\frac{1}{2}} - D_y W_{1,j+1}^{k+\frac{1}{2}} = (1 - 2D_x)W_{1,j}^k + 2D_x W_{2,j}^k \quad (3.62)$$

For $i = m$ and $1 < j < n$ (boundary condition (3.20)):

$$-D_y W_{n,j-1}^{k+\frac{1}{2}} + (1 + 2D_y)W_{n,j}^{k+\frac{1}{2}} - D_y W_{n,j+1}^{k+\frac{1}{2}} = 2D_x W_{n-1,j}^k + (1 - 2D_x)W_{n,j}^k \quad (3.63)$$

For $1 < i < m$ and $j = 1$ (boundary condition (3.20)):

$$(1 + 2D_y)W_{i,1}^{k+\frac{1}{2}} - 2D_y W_{i,2}^{k+\frac{1}{2}} = D_x W_{i-1,1}^k + (1 - 2D_x)W_{i,1}^k + D_x W_{i+1,1}^k \quad (3.64)$$

Then, for $i = 1$ and $j = 1$:

$$(1 + 2D_y)W_{1,1}^{k+\frac{1}{2}} - 2D_y W_{1,2}^{k+\frac{1}{2}} = (1 - 2D_x)W_{1,1}^k + 2D_x W_{2,1}^k \quad (3.65)$$

And for $i = m$ and $j = 1$:

$$(1 + 2D_y)W_{m,1}^{k+\frac{1}{2}} - 2D_y W_{m,2}^{k+\frac{1}{2}} = 2D_x W_{m-1,1}^k + (1 - 2D_x)W_{m,1}^k \quad (3.66)$$

For $1 < i < m$ and $j = n$ (boundary condition equation (3.23)):

$$-2D_y W_{i,n-1}^{k+\frac{1}{2}} + (1 + 2D_y)W_{i,n}^{k+\frac{1}{2}} = -D_y \left(NTU_m \left(Y_{sd(i)c_i}^k - Y_{a(i)c_i}^k \right) \right) + D_x W_{i-1,n}^k + (1 - 2D_x)W_{i,n}^k + D_x W_{i+1,n}^k \quad (3.67)$$

With $NTU_m = \frac{2h_m \Delta y}{\rho_a D}$ and $Y_{sd(i)c_i}^k$ is calculated using (3.11) and (3.12), using variables $W_{i,n}^k$ and $T_{d,i,n}^k$.

Additionally, for $i = 1$ and $= n$:

$$-2D_y W_{1,n-1}^{k+\frac{1}{2}} + (1 + 2D_y) W_{1,n}^{k+\frac{1}{2}} = -D_y \left(NTU_m \left(Y_{sd(ic)_1}^k - Y_{a(ic)_1}^k \right) \right) + (1 - 2D_x) W_{1,n}^k + 2D_x W_{2,n}^k \quad (3.68)$$

Also, for $i = m$ and $= n$:

$$-2D_y W_{m,n-1}^{k+\frac{1}{2}} + (1 + 2D_y) W_{m,n}^{k+\frac{1}{2}} = -D_y \left(NTU_m \left(Y_{sd(ic)_m}^k - Y_{a(ic)_m}^k \right) \right) + 2D_x W_{m-1,n}^k + (1 - 2D_x) W_{m,n}^k \quad (3.69)$$

When equation (3.44) and its modification are written for all the nodes, the variables $T_{d_{i,j}}^{k+\frac{1}{2}}$ can then be solved simultaneously by arranging them as linear algebraic equations per nodes i . The same approach can be used to solve equation (3.45) and its modification for every node.

For example, for nodes $i = 1, 1 \leq j \leq n$, the equation (3.50), (3.55), (3.60) are arranged as follow:

$$\begin{vmatrix} (1 + 2\lambda_y) & -2\lambda_y & & & & & \\ -\lambda_y & (1 + 2\lambda_y) & -\lambda_y & & & & \\ & -\lambda_y & (1 + 2\lambda_y) & -\lambda_y & & & \\ & & -\lambda_y & (1 + 2\lambda_y) & -\lambda_y & & \\ & & & -\lambda_y & (1 + 2\lambda_y) & -\lambda_y & \\ & & & & -2\lambda_y & (1 + 2\lambda_y) & \end{vmatrix} \begin{Bmatrix} T_{d_{(i=1,j=1,k+1/2)}} \\ T_{d_{(i=1,j=2,k+1/2)}} \\ T_{d_{(i=1,j,k+1/2)}} \\ T_{d_{(i=1,j=n-1,k+1/2)}} \\ T_{d_{(i=1,j=n,k+1/2)}} \end{Bmatrix} = \begin{Bmatrix} r_{eq_{(i=1,j=1)}} \\ r_{eq_{(i=1,j=2)}} \\ r_{eq_{(i=1,j)}} \\ r_{eq_{(i=1,j=n-1)}} \\ r_{eq_{(i=1,j=n)}} \end{Bmatrix} \quad (3.70)$$

With r_{eq} is the right hand side of the equations (3.50), (3.55), (3.60) for the respective nodes i, j .

For the second-half time step, the derivatives in x-direction are now approximated implicitly, while derivatives in y-direction are approximated explicitly. Thus, the bias introduced by the approximations in the first-half step will be partially corrected. The approximations in the second-half step are as follows ($\varepsilon = 1$):

$$\rho_d c_d \frac{T_{d_{i,j}}^{k+1} - T_{d_{i,j}}^{k+\frac{1}{2}}}{\Delta t/2} = \lambda_d \left(\frac{T_{d_{i-1,j}}^{k+1} - 2T_{d_{i,j}}^{k+1} + T_{d_{i+1,j}}^{k+1}}{(\Delta x)^2} + \frac{T_{d_{i,j-1}}^{k+\frac{1}{2}} - 2T_{d_{i,j}}^{k+\frac{1}{2}} + T_{d_{i,j+1}}^{k+\frac{1}{2}}}{(\Delta y)^2} \right) \quad (3.71)$$

$$\frac{W_{i,j}^{k+1} - W_{i,j}^{k+\frac{1}{2}}}{\Delta t/2} = D_s \left(\frac{W_{i-1,j}^{k+1} - 2W_{i,j}^{k+1} + W_{i+1,j}^{k+1}}{(\Delta x)^2} + \frac{W_{i,j-1}^{k+\frac{1}{2}} - 2W_{i,j}^{k+\frac{1}{2}} + W_{i,j+1}^{k+\frac{1}{2}}}{(\Delta y)^2} \right) \quad (3.72)$$

Which, for $1 < i < m$, $1 < j < n$ can be written as:

$$-\lambda_x T_{d_{i-1,j}}^{k+1} + (1 + 2\lambda_x) T_{d_{i,j}}^{k+1} - \lambda_x T_{d_{i+1,j}}^{k+1} = \lambda_y T_{d_{i,j-1}}^{k+\frac{1}{2}} + (1 - 2\lambda_y) T_{d_{i,j}}^{k+\frac{1}{2}} + \lambda_y T_{d_{i,j+1}}^{k+\frac{1}{2}} \quad (3.73)$$

$$-D_x W_{i-1,j}^{k+1} + (1 + 2D_x) W_{i,j}^{k+1} - D_x W_{i+1,j}^{k+1} = D_y W_{i,j-1}^{k+\frac{1}{2}} + (1 - 2D_y) W_{i,j}^{k+\frac{1}{2}} + D_y W_{i,j+1}^{k+\frac{1}{2}} \quad (3.74)$$

Again, when written for every node, the resulting equations can be arranged as linear algebraic equations and solved as in equation (3.70).

3.4.3. Computer model algorithm

Following the discretization of the governing equations and their boundary conditions using the chosen numerical method, a computer model was developed to perform the iteration process and determine values of the required variables at each assigned grid points. Fig 3-7 shows the computer model flow chart which illustrates the subroutines and iterative steps. For the computer model, the physical system is divided into a fixed number of grid points, and fixed time step for each iteration (0.025 s).

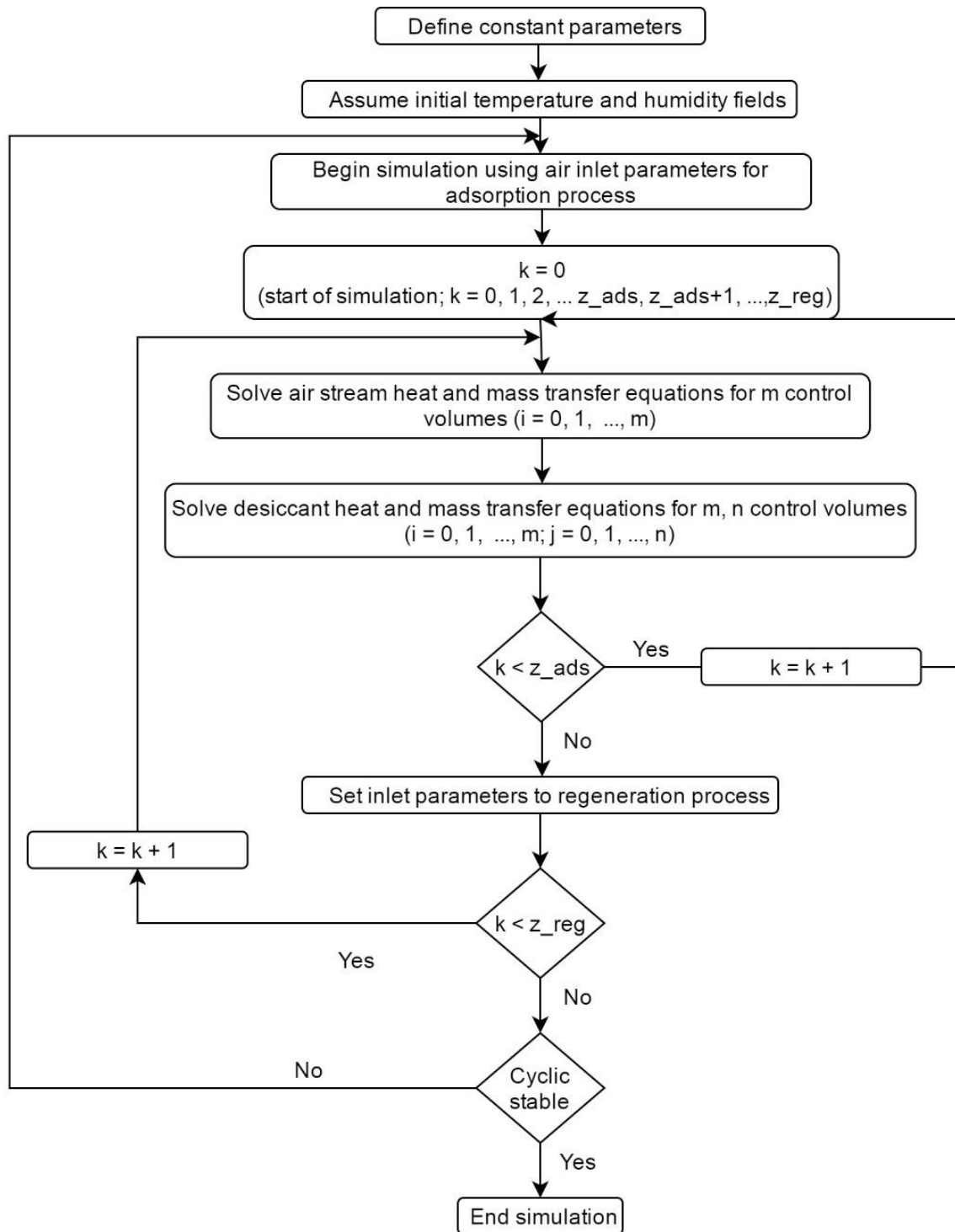


Fig 3-7 Computer model flow chart

Chapter 3: Design and computer modelling

The resulting algorithm is then implemented using MATLAB programming language to run the simulation. The complete MATLAB codes can be found in Appendices A, B, and C. The algorithm and the iteration process are explained as follows:

- i) Determine system specification, desiccant material properties and operating conditions such as inlet air velocity, temperature and humidity for dehumidification and regeneration process, cycle times;
- ii) Calculate convective heat and mass transfer coefficient, moisture diffusivity, etc. at $T_{ave} = 1/2(T_{p,inlet} + T_{r,inlet})$ and assume constant thermos-physical parameters;
- iii) Assume initial temperature ($k = 1$) and humidity fields of both air streams and desiccant layer for every grid points i and j ;
 - Based on assumed initial values of $W_{i,j=n}^{k=1}$, calculate initial values of $RH_{d,i,j=n}^{k=1}$
 - Using calculated $RH_{d,i,j=n}^{k=1}$ and assumed $T_{d,i,j=n}^{k=1}$, calculate $Y_{sd(ic)_i}^{k=1}$
- iv) Start iteration using inlet air velocity, temperature and moisture ratio for dehumidification process;
- v) For the first half step,
 - Employ equation (3.31), (3.33), (3.35) to calculate air temperature and humidity of air ($T_{a(oc)_i}^{k+1/2}, Y_{a(ic)_i}^{k+1/2}, T_{a(ic)_i}^{k+1/2}$) at every grid points i
 - Solve simultaneously $W_{i=1,j}^{k+1/2}$ for every grid points j , then simultaneously solve all variables $W_{i,j}^{k+1/2}$ for every grid points j at the next grid points $i = 2, 3, \dots, m$
 - Solve simultaneously $T_{d,i=1,j}^{k+1/2}$ for every grid points j (equation (3.70)), then simultaneously solve all variables $T_{d,i,j}^{k+1/2}$ for every grid points j at the next grid points $i = 2, 3, \dots, m$

- Using calculated values $W_{i,j=n}^{k+1/2}$, $T_{d,i,j=n}^{k+1/2}$, calculate new values

$$RH_{d,i,j=n}^{k+1/2} \text{ and } Y_{sd(ic)_i}^{k+1/2}$$

vi) For the second half step,

- Employ equation (3.31), (3.33), (3.35) to calculate air temperature and humidity of air ($T_{a(oc)_i}^{k+1}$, $Y_{a(ic)_i}^{k+1}$, $T_{a(ic)_i}^{k+1}$) at every grid points i
- Solve simultaneously $W_{i,j=1}^{k+1}$ for every grid points i , then simultaneously solve all variables $W_{i,j}^{k+1}$ for every grid points i at the next grid points $j = 2, 3, \dots, n$
- Solve simultaneously $T_{d,i,j=1}^{k+1}$ for every grid points i , then simultaneously solve all variables $T_{d,i,j}^{k+1}$ for every grid points i at the next grid points $j = 2, 3, \dots, n$
- Using calculated values $W_{i,j=n}^{k+1}$, $T_{d,i,j=n}^{k+1}$, calculate new values

$$RH_{d,i,j=n}^{k+1} \text{ and } Y_{sd(ic)_i}^{k+1}$$

vii) Repeat step v and vi until the end of adsorption cycle ($k = z_{ads}$);

viii) Change inlet air conditions to that of regeneration process;

ix) Repeat step v and vi until the end of regeneration cycle ($k = z_{reg}$);

x) Redo step iv to ix until the results convergence or reach cyclical steady state, regardless of initial conditions;

- The cyclical steady state condition is assumed when the calculated air humidity and temperature of the last cycle was within 0.1% of the previous cycle

xi) End simulation.

3.4.4. Validation of the computer model

The validation of the computer model was performed using available data from literature on desiccant systems. In validating the model, known design specification and empirical operating parameters of a desiccant wheel air dehumidification system were used [32,63].

Table 3-2 Desiccant wheel parameters used for validation [32,63]

Wheel parameter	Value
Rotation speed	30 RPH
Primary air stream face area fraction	0.5
Length	10-40 cm
Hydraulic diameter of each channel	1.50 mm
Air velocity	2.86 m/s
Process air inlet temperature	305.5 K
Regeneration air inlet temperature	353.2 K
Process air inlet humidity	19.5 g/kg
Regeneration air inlet humidity	11.9 g/kg
Nusselt number	2.4

Three different lengths (or wheel thickness) were chosen for the validation process: 10 cm, 20 cm, and 40 cm, while the rotational speed of the wheel was set to 30 RPH. Other parameters and conditions used for the validation are given in Table 3-2. Properties of the desiccant material are given in Table 3-1. Results of the computer model and published experimental tests are shown in Fig 3-8. It can be seen that there is a good agreement between the computer model and experimental results. Varying the desiccant wheel thickness from 10 to 40 cm improved the wheel's air dehumidification performance (i.e., outlet average humidity ratio decreased from 11.66 g/kg to 9.67 g/kg) as shown in Fig 3-8(a), at the same time the dehumidified air temperature increased from 56.86°C to 70.95°C (Fig 3-8(b)). The discrepancy between the computer model and experimental results of air

humidity ratio and temperature is as low as 3%, giving high confidence of the simulation results.

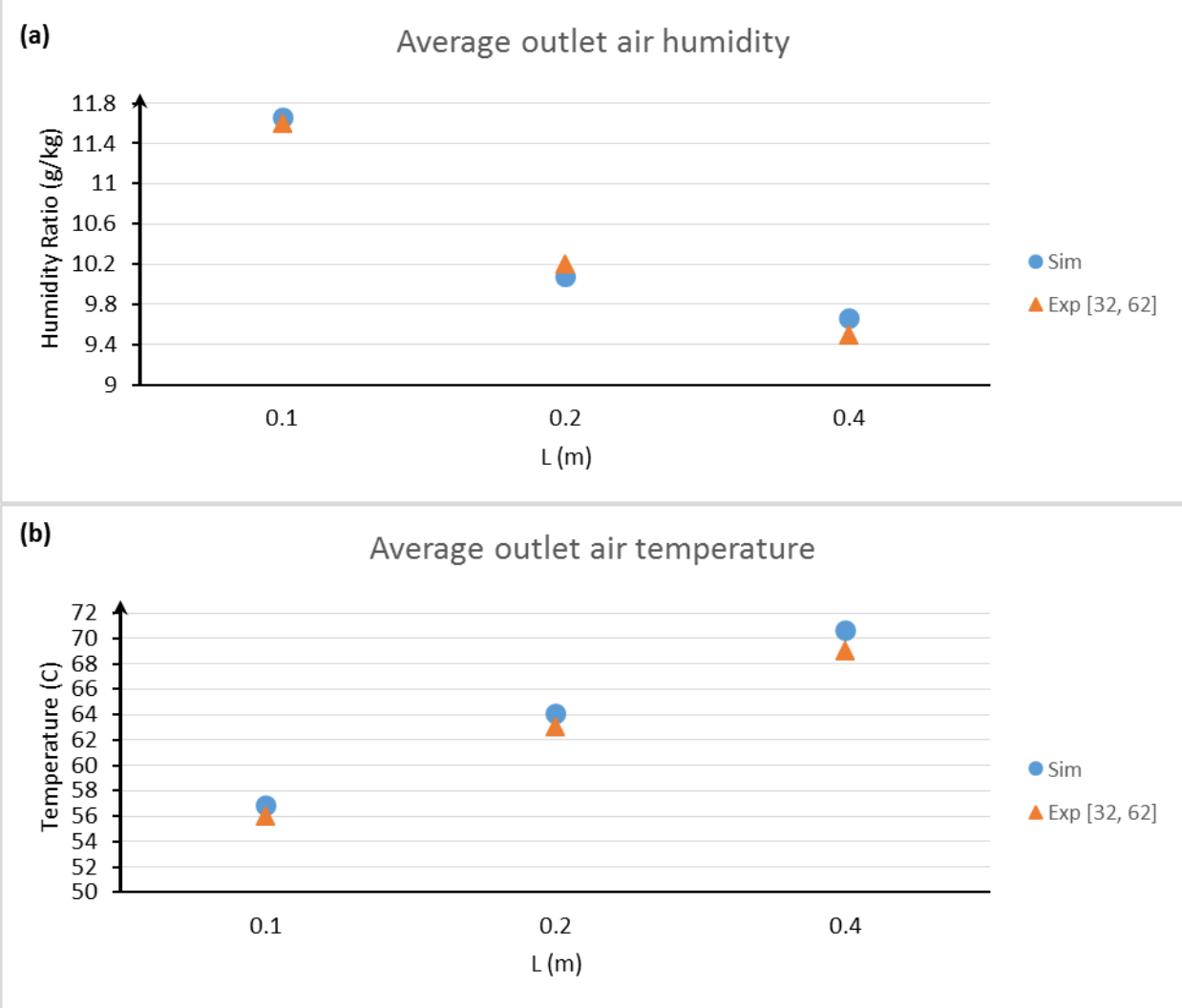


Fig 3-8 Validation of computer model: (a) Process air average outlet humidity ratio; and (b) Process air average outlet temperature.

3.5. Performance indices

The performance of air dehumidification systems is usually indicated by three main parameters or indices, defined as follows:

3.5.1. Dehumidification Coefficient of Performance (DCOP)

The dehumidification coefficient of performance (DCOP) of the system defines its energy performance. This is given as the ratio of latent heat removed from air to energy required for desiccant regeneration. It can be expressed by:

$$DCOP = \frac{\dot{m}_{p,ic} L_v (Y_{p,ic,inlet} - \bar{Y}_{p,ic,outlet})}{\dot{m}_{r,ic} (h_{r,ic,inlet} - \bar{h}_{r,ic,outlet}) + \dot{m}_{r,oc} C_a (T_{r,oc,inlet} - \bar{T}_{r,oc,outlet})} \quad (3.75)$$

Where $\dot{m}_{p,ic}$ is the mass flow rate of dehumidified process air [kg s^{-1}], L_v is latent heat of vaporization [J kg^{-1}], $\bar{Y}_{p,ic,outlet}$ is the mean outlet humidity of process air during adsorption cycle [kg kg^{-1}], $\dot{m}_{r,ic}$ and $\dot{m}_{r,oc}$ is mass flow rate of regeneration air in inner and outer channel, respectively [kg s^{-1}], $h_{r,ic,inlet}$ and $\bar{h}_{r,ic,outlet}$ are the inlet enthalpy and the mean outlet enthalpy of regeneration air in the inner channel, respectively [J kg^{-1}], $\bar{T}_{r,oc,outlet}$ is mean outlet temperature of regeneration air in the outer channel [K].

3.5.2. Dehumidification Capacity (DC)

The dehumidification capacity (DC) is defined as the amount of water vapour removed over one complete cycle [kg h^{-1}]. This is expressed by the following:

$$DC = \frac{\dot{m}_{p,ic} (Y_{p,ic,inlet} - \bar{Y}_{p,ic,outlet}) t_{ad} 3600}{t_{cyc}} \quad (3.76)$$

With t_{ad} and t_{cyc} are the adsorption process time and total cycle time (adsorption + regeneration), respectively [s].

3.5.3. Overall relative moisture removal efficiency

The overall relative moisture removal efficiency (η) represents the ratio of overall moisture removal to inlet moisture ratio of process air:

$$\eta = \frac{Y_{p,ic,inlet} - \bar{Y}_{p,ic,outlet}}{Y_{p,ic,inlet}} \quad (3.77)$$

3.6. Computer model results of a single shell-tube heat and mass exchanger configuration modelling

The model was used to analyse the performance of the concentric channels (shell-tube) dehumidification system. Initially, outlet air temperature and humidity at different cycles were compared to evaluate the convergence of the computer model. Then temperature and humidity profile of the system was analysed to understand the behaviour of the dehumidifier. Furthermore, the performance between concentric channels system with single adiabatic channel system was compared to demonstrate the performance gain of enhanced heating/cooling. The base parameters used for the simulations are listed in Table 3-3.

Table 3-3 Base operating parameters of the computer model

Parameter	Unit	Value
Length of channel, L	m	0.1
Desiccant thickness, δ	mm	0.125
Hydraulic diameter outer channel, Dh_{oc}	mm	3.38
Hydraulic diameter inner channel, Dh_{ic}	mm	3.08
Air velocity, u	m/s	2.5
Inlet moisture ratio of air, $Y_{p,inlet}, Y_{r,inlet}$	kg/kg _{da}	0.020
Process/cooling Inlet air temperature, $T_{p,inlet}, T_{c,inlet}$	°C	32
Inlet air temperature (regeneration), $T_{r,inlet}, T_{h,inlet}$	°C	80
Adsorption time, t_{ad}	s	60
Regeneration time, t_{reg}	s	60

3.6.1. Cyclical steady state

As previously mentioned in section 3.4.3, initial temperature and humidity throughout the system were assumed. For both the tube-side and shell-side air stream, uniform temperature equal to $T_{r,inlet}$ was assumed as initial temperature along the length of the channels, while initial air humidity was assumed to be equal to $Y_{r,inlet}$ spread uniformly.

Chapter 3: Design and computer modelling

Similarly, identical temperature and humidity initial conditions were assumed to be uniform throughout the desiccant layer. Then, as iterations were done with inlet air for dehumidification process, the heat and mass transfer between the air stream and the desiccant layer caused reduction of the temperature at every grid points (compared to the initial temperatures – with the exception of the inlet air), and humidity of air stream decreased while water content of desiccant increased. This was followed by calculations during regeneration process where inlet air temperature switched to that of respective cycle. This time, the air stream transfers its heat to the desiccant thus the temperature of every grid points increased (relatively to that of the previous cycle). At the same time, the water content of desiccant decreased while the air stream was humidified.

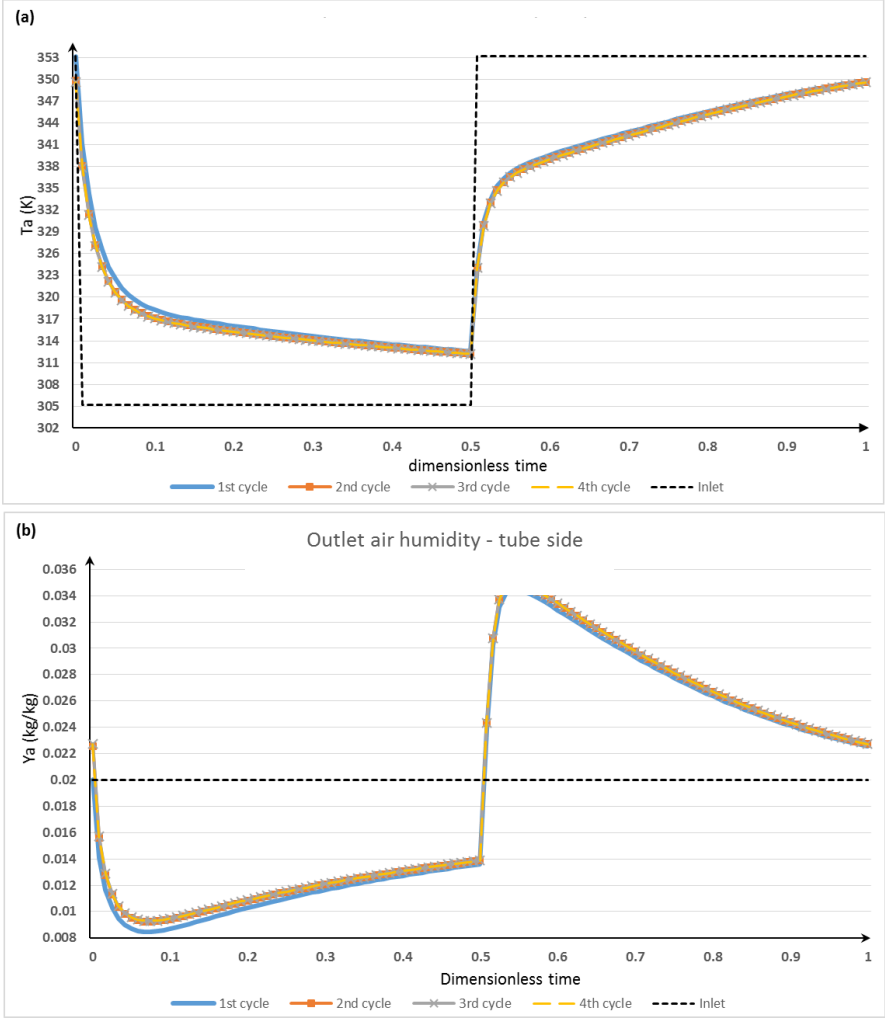


Fig 3-9 Outlet air (a) temperature and (b) humidity over multiple cycles

By continuously switching the dehumidification and regeneration cycles, the change of temperature and humidity over time of one complete cycle would be more or less identical with the previous or subsequent complete cycles after numerous iterations. In that case, cyclical steady state – or convergence – could be assumed to be reached. Fig 3-9 shows that between the 1st and 2nd complete cycle (dehumidification + regeneration), there were still considerable discrepancies of calculated outlet air temperature and humidity over time. After the 2nd cycle, however, the gap decreased and after the 4th cycle, it could be assumed that the cyclical steady state was reached. The number of required iterations of complete cycles to reach the steady state could be affected by the geometries / operating parameters used. For example, if longer channels were assumed, cyclical steady state could be reached after the 6th or 7th cycle. Simulations with lower air velocities would take more than 4 cycles to reach convergence, while higher air velocities had less significant impact on the convergence rate. Similar behaviour was also observed with varied cycle times.

3.6.2. Temperature and humidity distribution along the air channels

During dehumidification process, primary air at T_{inlet} and Y_{inlet} enters the tube-side channel to be dehumidified, while secondary air at $T_{c,inlet}$ enters the shell-side channel to help remove heat from the desiccant. Since the desiccant was previously regenerated, its surface was significantly higher than the air streams. Thus, along the air streams' direction of travel, increase of air temperature could be observed. It can also be observed that after half-length of the channel, the air stream reached its maximum temperature before decreased again as it reached the outlet. This was due to the secondary/cooling air stream in counter-flow direction. As time progress, the increase of temperature became less significant since the temperature of the desiccant got closer to that of the air stream. Fig 3-10 shows the primary air temperature distribution for every 10 s. Note that there was significant difference between the air temperature along the channel after 1 s of adsorption and 10 s of adsorption. In the beginning of dehumidification process, the desiccant temperature dropped quickly and there was little adsorption. This was reflected by the quick drop of the temperature distribution in

Chapter 3: Design and computer modelling

the air channels. Then, as adsorption rate increased, more adsorption heat was released by the desiccant, hence the cooling rate decreased. On the other hand, this was also due to less temperature difference between the air stream and the desiccant layer as time progress, which affects the heat transfer rate. Conversely, when air inlet temperature was switched to $T_{r,inlet}$ the air transfer its heat to the desiccant, thus air temperature reduction could be observed along the direction of travel. However, near the outlet the temperature rose again, due to the counter-flow nature of the secondary/heating air in the shell-side. Again, the gap between the temperature after 1 s and that after 10 s was bigger than the others. At the beginning of the regeneration cycle, the desiccant temperature rose quickly while there was little desorption.

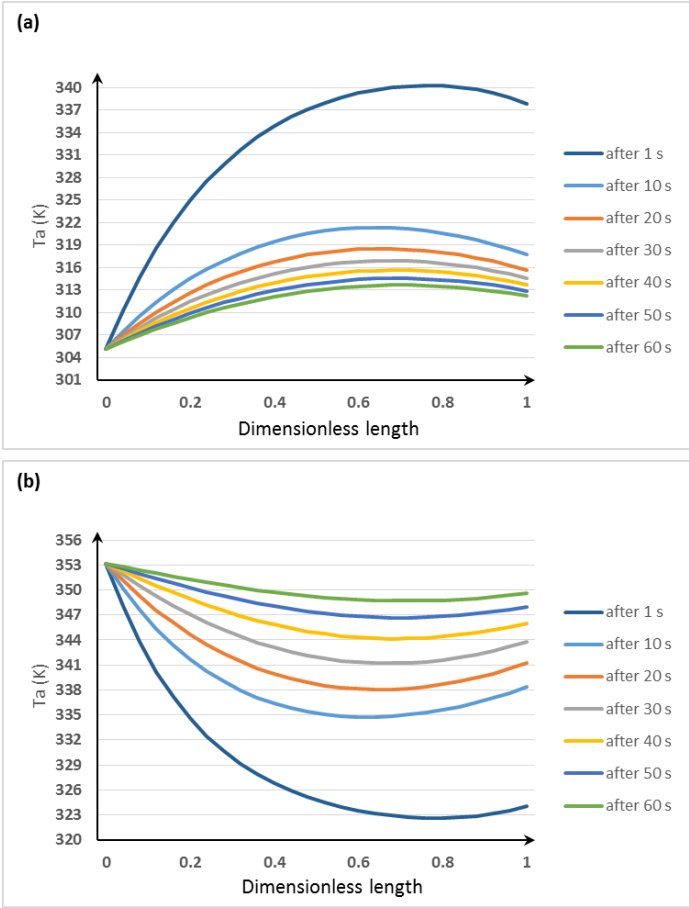


Fig 3-10 Primary air temperature profile along the channel for (a) dehumidification and (b) regeneration process

As more moisture was desorbed, as well as less difference between desiccant temperature and that of air stream, the heating rate decreased. Fig 3-11 shows the temperature profile of the secondary air, which travels in counter-flow direction. Due to the channels geometries, identical inlet conditions and thin desiccant layer, the temperature profile of the secondary air almost resembles that of the primary air.

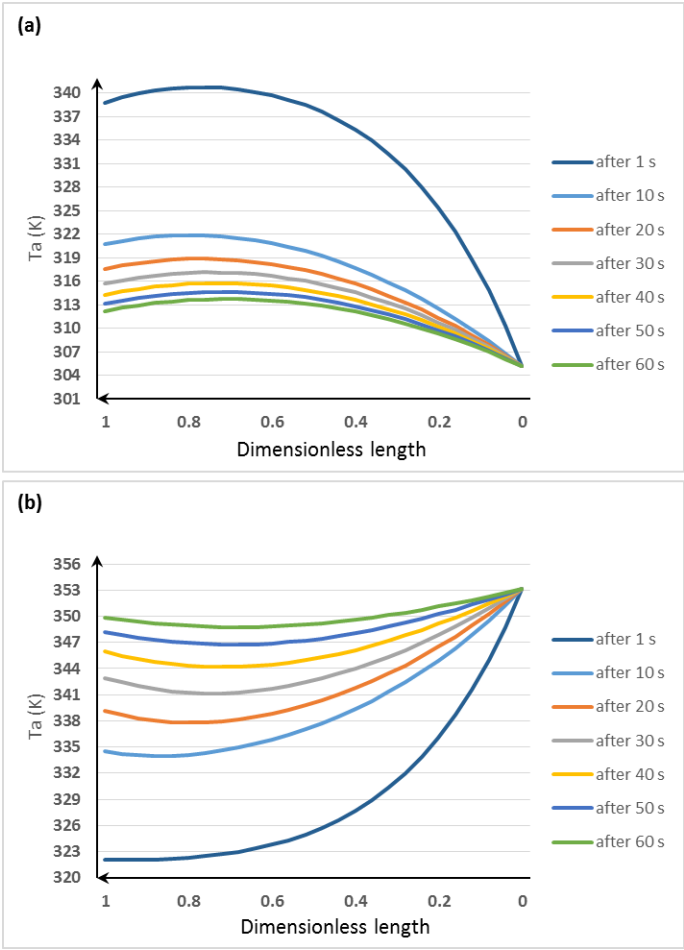


Fig 3-11 Secondary air temperature profile along the channel for (a) dehumidification and (b) regeneration process

With the desiccant layer adsorbing moisture from the primary air stream, reduction of humidity along the channel could be observed in Fig 3-12. Note that at the beginning of dehumidification process, small reduction of humidity followed by slight re-increase was observed. This was due to high temperature of the desiccant. As the desiccant cooled down,

Chapter 3: Design and computer modelling

more moisture was absorbed, as reflected by the air humidity profile after 10 s of dehumidification process. After that, the desiccant got closer to saturation, thus adsorption rate decreased. At beginning of regeneration process, it was observed that the air humidity increased but decreased again as it travelled along the channel. This was because the desiccant temperature was just slightly increased, and the desorbed moisture was re-adsorbed again at the part where the water content was lower. Shortly after, desorption rate significantly increased, reflected by the sharp increase of humidity of air along the channel. Then, with less moisture left in the desiccant, less moisture was desorbed by the airstream, thus increase of moisture in the air stream became less significant over time.

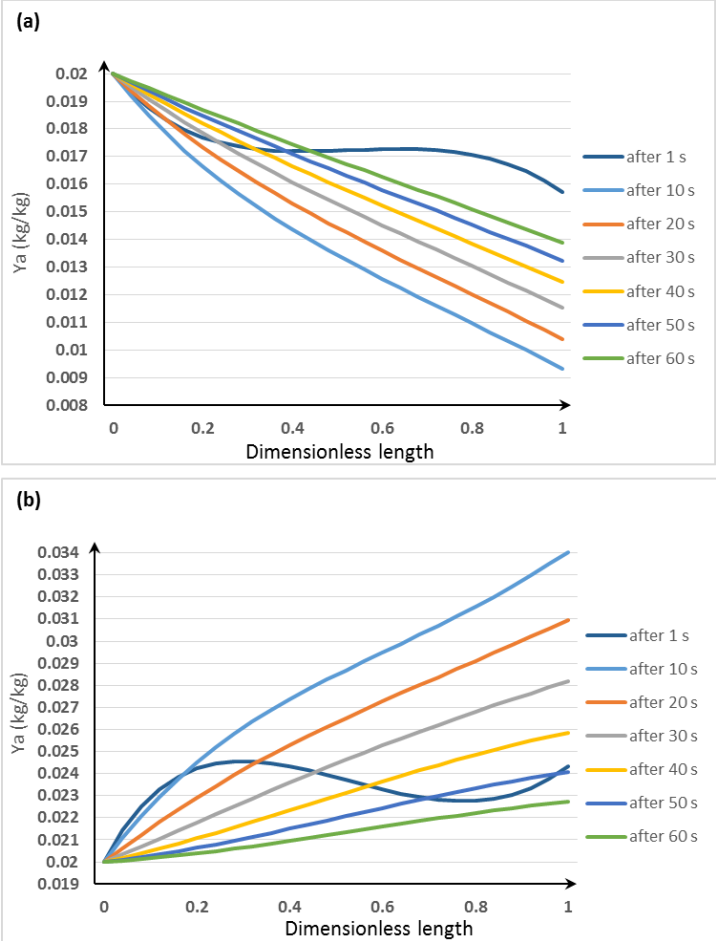


Fig 3-12 Primary air humidity profile along the channel for (a) dehumidification and (b) regeneration process

3.6.3. Temperature and humidity distribution in the desiccant layer

Fig 3-13 shows the temperature distribution at the desiccant surface which is in contact with primary air stream. Note that significant gap could be observed between the temperature range after 60 s of adsorption and that of after 10 s of desorption, with only 10 s difference between the two. Conversely, significant difference of temperature was observed between “after 60 s” of regeneration and “after 10 s” of adsorption. Moreover, during early phase (10 s) adsorption process, the desiccant temperature near the outlet of primary air dropped more significantly. This was due do the secondary/cooling air in counter-flow direction, as well as the adsorption heat which was more significant near the inlet of primary air as reflected in Fig 3-12 and Fig 3-12. Then, when reaching the end of adsorption cycle, with reduced adsorption rate, the temperature near the inlet became closer to that of near the outlet.

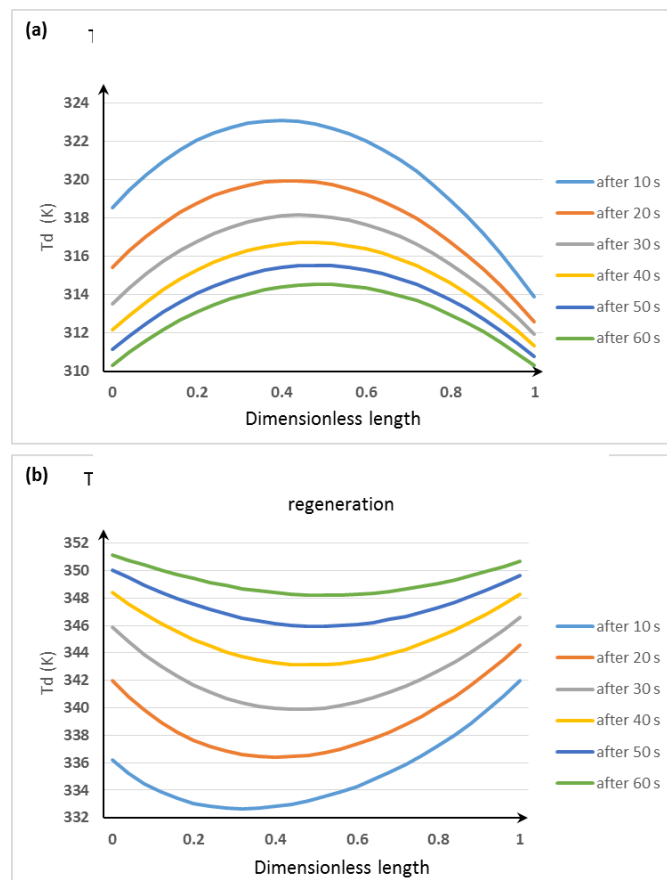


Fig 3-13 Temperature profile of desiccant surface in contact with primary air for (a) dehumidification and (b) regeneration process

Chapter 3: Design and computer modelling

Conversely, the temperature increase was more significant near the outlet during the beginning of regeneration process, and the temperature distribution became more uniform at the end of regeneration cycle. As the desiccant layer was very thin, there was little discrepancy of temperature along the thickness of the layer. Thus, the temperature profile of the desiccant surface in contact with secondary air was nearly identical with that shown in Fig 3-13. However, since mass transfer between air stream and desiccant layer only occurred in the tube-side channel, considerable difference of moisture distribution along the layer thickness was observed. Fig 3-14 shows water content distribution of the desiccant layer for different thickness level.

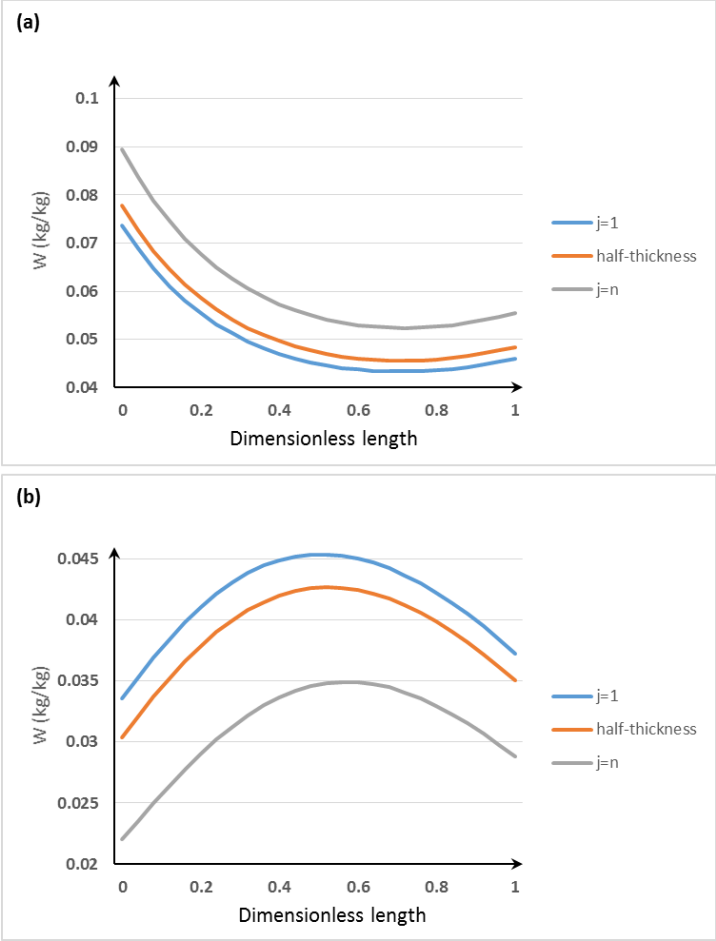


Fig 3-14 Moisture profile of desiccant layer for (a) adsorption and (b) desorption process

During dehumidification process, the desiccant layer adsorbed moisture from the primary air stream which caused its water content increased over time. However, due the mass resistance of the layer, the increase of water content at the outer layer ($j = n$) was more significant than the deeper layers. Additionally, it was also observed that adsorbed moisture concentrated near the inlet of primary air. This means that most of adsorption occurred near the inlet where the air humidity was at highest value. Along its travel, the air stream lost some of its moisture, which reduced the mass transfer driving force. Similarly, during the regeneration process, highest desorption rate was found near the inlet. It was also found that the water content drop during regeneration near the outlet was more significant than at half-length of the layer. This was due to heated air passed through in counter-flow direction, thus higher temperature at both ends of the channel length, which facilitated the desorption rate.

3.6.4. Performance improvement of the shell-tube configuration

Compared to simple single channel configuration, the concentric channel (shell-tube) configuration was able to achieve higher adsorption rate, with average humidity outlet 15% lower than the other configuration. As shown in Fig 3-15, the air humidity decreased faster in the improved configuration by concentric channel (CC) and was lower than the simple single channel configuration (SC) during the entire dehumidification period. This was due to the faster cooling of the desiccant, as reflected by the lower air temperature output (15% difference). The lower outlet air temperature could have significant impact on subsequent cooling system performance (either conventional or passive cooling systems) since the sensible load of the dehumidified air was reduced. The faster cooling was made possible with the help of the cooling air at the outer channel. On the other hand, the CC configuration also gained from better heating of desiccant during the regeneration process, thus more moisture could be desorbed, as shown by higher outlet air temperature and humidity.

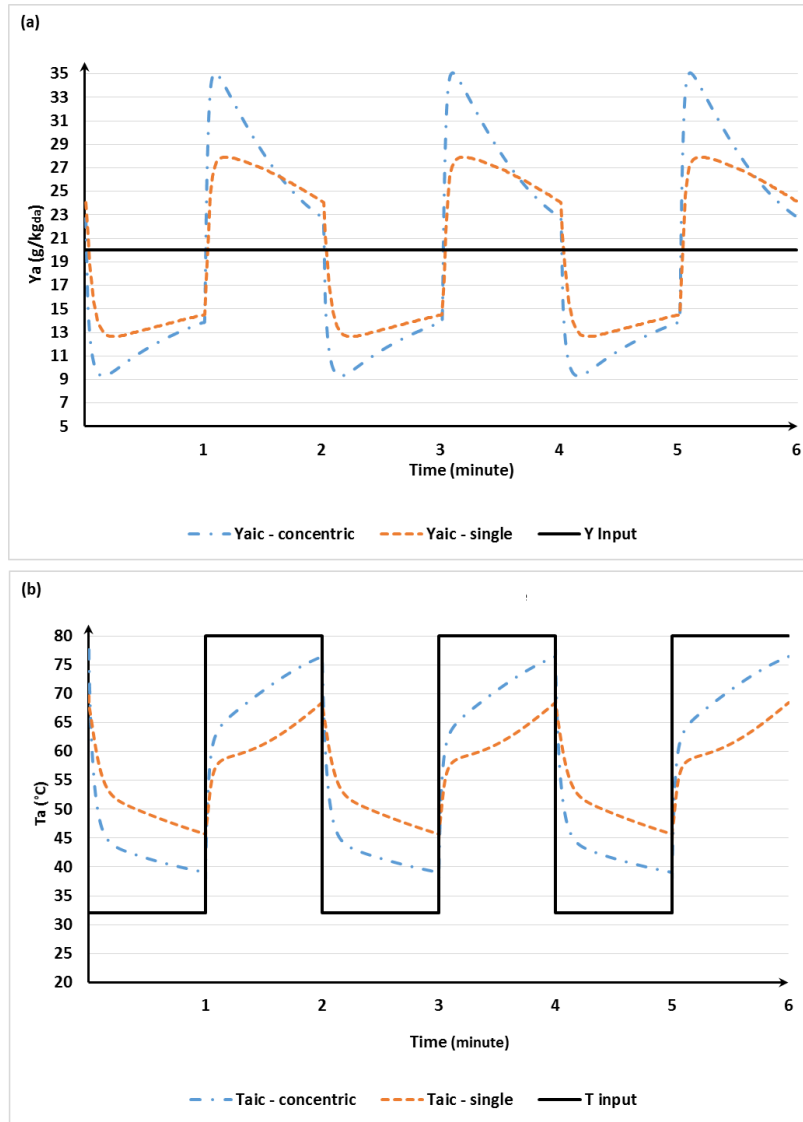


Fig 3-15 Variation of outlet (a) air humidity ratio and (b) temperature

For identical air velocity and cycle time, lower mean outlet air humidity of the concentric channels configuration during the adsorption period lead to higher DC and η (increased by 15%) as shown in Fig 3-16. DCOP was also significantly increased by 35%, despite the extra effort for providing hot air used in regeneration process. The extra effort to heat the regeneration air stream was compensated by better dehumidification performance. Moreover, as desiccant was heated faster, $(h_{r,ic,inlet} - \bar{h}_{r,ic,outlet})$ and $(T_{r,oc,inlet} - \bar{T}_{r,oc,outlet})$ became smaller, which contributed to higher COP (see equation (3.76)).

Chapter 3: Design and computer modelling

The enhanced heat transfer with the CC configuration also provided the possibility of using shorter regeneration cycle length. By using only half cycle length for desorption period, the CC was able to achieve similar dehumidification performance to SC, with overall output air humidity ratio (during dehumidification period) on both case was within 3% to each other. With shorter regeneration time, CC efficiency was still 7% higher than SC. Less time used for desorption also means that more adsorption can be achieved in continuous cycles, as shown by significant increase of DC (up to 42%). However, DCOP was also reduced by 42%. This was due extra heating required by CC for regeneration to achieve similar performance (DCOP did not take into account the shortened cycle time), and the slightly higher efficiency was not enough to compensate the additional required heating energy. However, it can be said that the lower DCOP is balanced with gains on dehumidification amount.

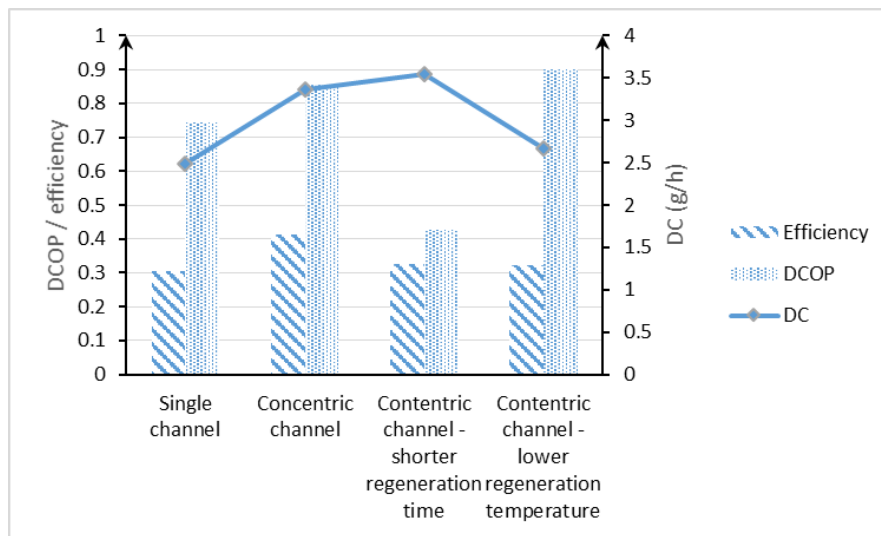


Fig 3-16 Performance comparison of different working scenario

By using external heating to help the desorption process, the CC configuration could also allow lower regeneration temperature. This means energy consumption for heating the regeneration air could be substantially reduced. Even with lower temperature (65°C instead of 80°C), when compared to SC, CC could still achieve similar DC and efficiency. Its DCOP, meanwhile, was 20% higher due to similar adsorption capability was achieved with lower

regeneration temperature. Of the four different cases (SC, CC, CC with shortened regeneration cycle or CC30R, and CC with lower temperature or CCTR65), the CC provided the highest overall performance, with the highest efficiency (26% higher than CC30R) and second-highest DCOP (15% gain compared to SC and less than 5% lower than CCTR65), while its dehumidification capacity was only around 5% lower than CC30R (Fig 3-16).

3.6.5. Effect of channel length

For this parametric study, various channel lengths were simulated, from 8 cm to 28 cm length. The other parameters from Table 3-3 were unchanged. Longer channel means more desiccant is added along the channel. This could lead to better dehumidification performance, as the channel can adsorb more water vapour from the air stream before the desiccant reach saturation. Fig 3-17 shows that from 8 cm channel to 20 cm channel, DC and efficiency increased as more desiccant was added. They decreased again, however, for 24 cm and 28 cm channel length. With higher amount desiccant is used, more heat is required to regenerate the material. As regeneration temperature, mass flow rate and cycle time were unchanged, the longer channels were not as well heated as the shorter channels. Moreover, during adsorption cycle, longer channels also took more time to cool down the desiccant layer, which also affected the dehumidification performance. The impact of adding more desiccant to required amount of heating was shown in decreasing DCOP on longer channels.

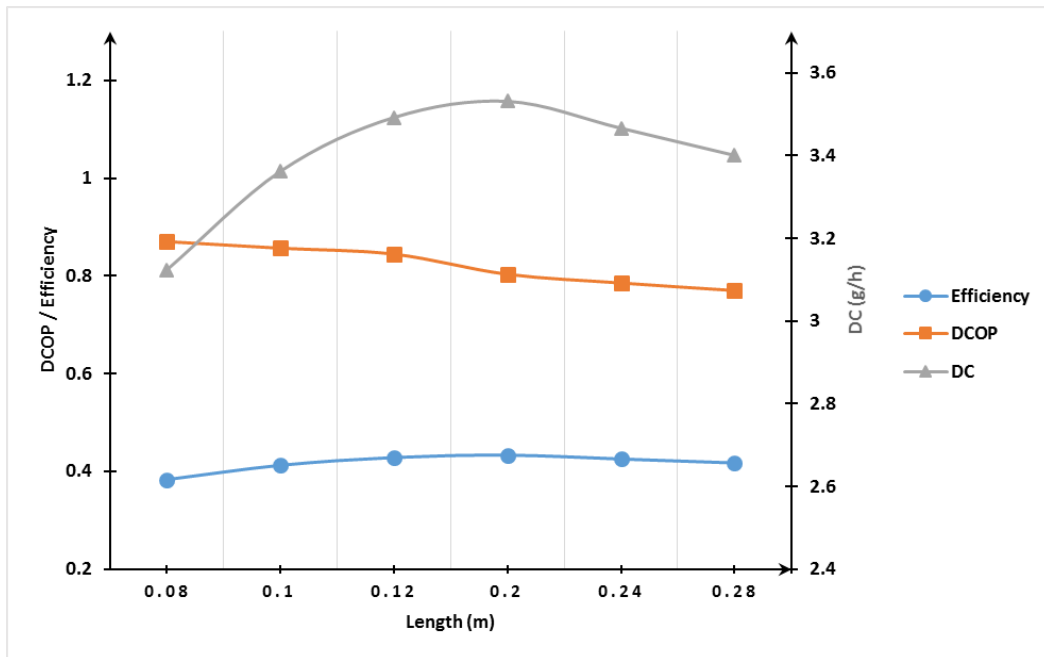


Fig 3-17 Dehumidification performance for different air channel length

Therefore, when determining the optimum length, the balance between the gain on DC and efficiency and lowered DCOP should be considered. For instance, with 10 cm channels as base, by increasing the length to 12 cm, DC increased by 4%, while DCOP decreased by 1.4%. Adding the length to 20 cm gained 5% of DC, while DCOP became 6% lower. DCOP could be increased by 1.5% with shorter length, however DC was lowered by 7%.

3.6.6. Effect of air velocity

The air velocity for both adsorption and regeneration cycles were varied from 1 m/s to 3 m/s. The air velocity for both channels is identical. Other parameters from Table 3-3 were unchanged. Generally, higher air velocity (thus higher airflow) means higher amount of air passed through the channel during the cycle time. This can lead to higher amount of water vapour removed from the process air during every adsorption cycle. In this study, biggest impact of varying the air velocity was on dehumidification amount.

Fig 3-18 shows that by increasing the air velocity from 1 m/s to 3 m/s, the dehumidification capacity was multiplied. The DCOP was also considerably increased by 10%. This was due to increased heat transfer rate, thus the desiccant was heated more effectively during the regeneration process, while during the adsorption process, the desiccant temperature dropped faster. However, the system's efficiency decreased with bigger airflow. As the desiccant cooled down faster, higher adsorption rate was achieved at the beginning of the cycle. However, this also caused the desiccant surface to reach saturation faster. With increase of air velocity from 1 m/s to 3 m/s, the system efficiency dropped by 13% (higher outlet average of process air humidity for every adsorption cycle).

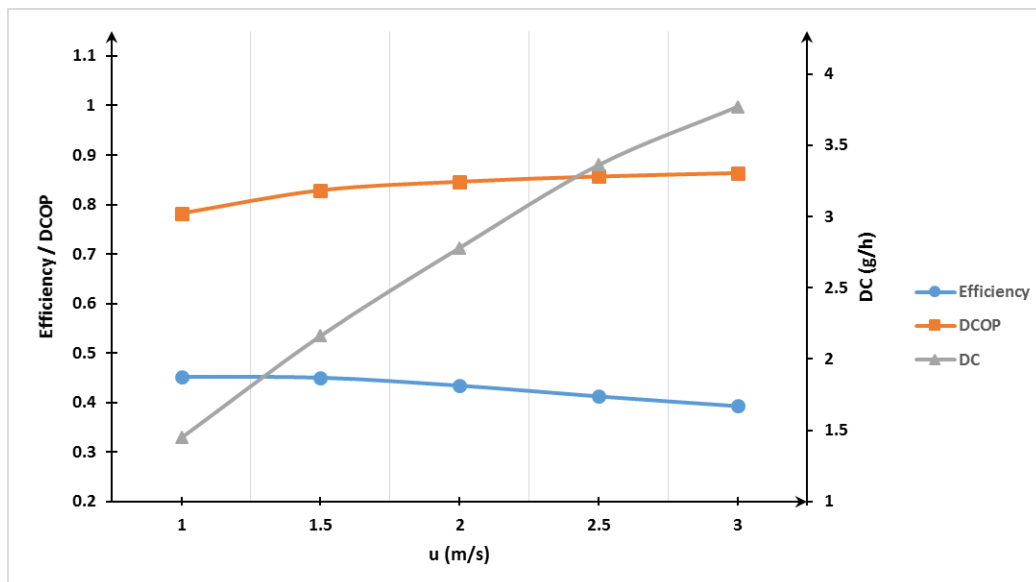


Fig 3-18 Dehumidification performance for different air velocities

The biggest improvement can be seen when increasing the air velocity from 1 m/s to 1.5 m/s, where DC increased by almost 50%, and DCOP increased by 5.9%. The reduction of dehumidification efficiency was also rather negligible (less than 0.5%). With further rise of air velocity, however, the improvement of DC and DCOP became less significant, while reduction of efficiency was more considerable.

3.6.7. Effect of cycle time

This time, total cycle length was varied. Total cycle length was varied from 60 s each to 360 s, with 50-50 proportion for adsorption and regeneration process. Others parameters were taken from Table 3-3. Varying the cycle length will affect the amount of water vapour adsorbed from air for every cycle. Moreover, longer cycle time allows more water to be desorbed from the desiccant, thus better regeneration process. This can be seen on the increasing DCOP with longer cycle time (Fig 3-19). This particularly applies to small-sized channels as short regeneration cycle length would be sufficient to remove most of adsorbed water from the desiccant. By adding the cycle length from 60 s to 360 s, the DCOP was increased by 13%. Further additional cycle time, however, has less significant effect on DCOP.

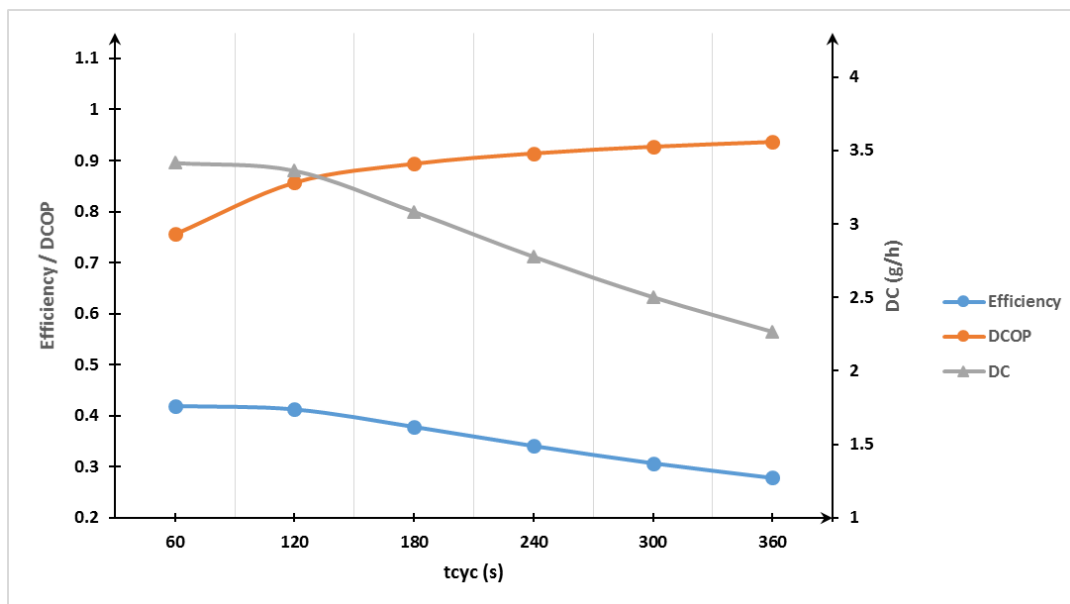


Fig 3-19 Dehumidification performance for various cycle time

The longer adsorption cycle time, however, had negative impact on DC of the system. This can be seen particularly on cycles longer than 120 s, with DC reduced by at least 8% for every addition of 60 s to the cycle length. In this small-sized channels, longer adsorption cycles allowed the desiccant to reach saturation faster, thus less moisture adsorbed over time. The longer regeneration cycles made small impact on DC, as shorter cycle length was already

sufficient. Thus, the outlet mean humidity ratio of process air increased (which was also reflected by reduced efficiency on longer cycles). Moreover, longer cycles time reduced the number of cycles over a certain period of operating times, which also contributed to lower DC. Thus, shorter cycle length seemed more preferable. If higher DCOP is desired, increasing the cycle length from 60 s to 120 s gave the most favourable improvement, as DCOP increased by 13%, while DC and efficiency reduced by only 1.5%.

3.7. Summary

In this chapter, the shell-tube solid desiccant air dehumidification system was introduced. The system configuration and working principles were also described. Then, mathematical model was developed, based on existing models for solid desiccant dehumidification systems. Certain modifications on general governing equations and boundary conditions were considered to represent the effect of secondary air stream on improving cooling and heating of desiccant layer. With the main goal of investigating and better understanding the improvement potential of the proposed configuration, assumptions were made to avoid over-complicating the mathematical model. As such, the shell-tube heat and mass exchanger configurations were represented with mathematical model of two concentric air channels with counter-flow configuration.

Transient, partial differential equations of heat and mass transfer between air and desiccant layer were solved using finite difference method. The resulting algebraic equations were then written as MATLAB codes, and computer algorithm was developed to perform iterative process and determine values of required variables at each assigned grid points. The developed model was validated by applying it to a desiccant wheel and comparing the predicted values to published experimental data. Three performance indices were determined to assess the overall performance of the proposed system: the energy performance defined by the dehumidification coefficient of performance (DCOP), the dehumidification capacity (DC) to describe amount of water vapour removed over one complete cycle, and the dehumidification efficiency.

It was demonstrated that, by performing continuous iterations of moisture adsorption and desorption process, the outlet air temperature and humidity ratio variations would reach stable conditions between each cycles, thus approaching cyclical steady state, regardless of assumed initial conditions. However, operating parameters such as channel lengths, air velocity, etc. affected the number of iterations required to achieve cyclical steady state.

As dehumidification process resumed by changing the inlet air temperature, it was observed that air temperature throughout the channel dropped immediately when moisture adsorption was very small due to high temperature of the desiccant layer. However, as adsorption rate increased over time, decrease of air temperature became less significant, which was contributed by adsorption heat released from the desiccant layer. The inverse phenomena were observed during regeneration process.

It was observed that air humidity ratio fluctuated throughout the channel at the start of both dehumidification and regeneration process. At this point, the desiccant temperature and moisture distribution throughout the channel caused the desiccant to adsorb moisture at one point while desorb moisture at another. The fluctuations only occurred at the start of each process, after which air humidity consistently decreased / increased as it travelled the air channel. It was also observed that over time, the decrease / increase of air humidity ratio became less significant following the change of moisture adsorption /desorption rate.

Throughout the dehumidification process, it was observed that desiccant surface temperature at both ends of the channel dropped faster than the mid-point. This was due to the counter flow air arrangement, with air temperature was lowest at the inlet points. On the other hand, the desiccant temperature around the inlet of secondary air channel decreased faster than the other side. Since moisture adsorption was most significant around the inlet of primary air channel, the heat adsorption released was also more important, affecting the cooling rate of the desiccant layer. Similar observation was found during regeneration process.

When compared to simple singular channel configuration, the concentric channel configuration was able to improve the dehumidification performance considerably. Particular improvement on DCOP was noted, signifying that improvement on dehumidification capacity

was more important the extra energy required for regeneration. It was also demonstrated the concentric channel configuration allowed shorter regeneration time or lower regeneration temperature while maintaining reasonable performance.

Several parametric studies were conducted to further analyse system performance under various working conditions. It was observed longer channel length could be considered to achieve higher dehumidification, however required energy to desorb moisture would also increase, as reflected by lower DCOP for longer channel. Heat removal / addition of desiccant layer could be improved with higher airflow, thus higher dehumidification capacity. However, efficiency decreased as airflow increased, indicating air dehumidification would be more efficient at lower air velocity. On the other hand, as desiccant layer moisture adsorption rate decreased as it adsorbed more water vapour, it was observed that short cycle time would be preferable for more efficient dehumidification.

Chapter 4: Small scale laboratory prototype construction

4.1. Earlier design prototype

Prior to the design and construction of the shell-tube solid desiccant dehumidifier, a simpler dehumidification unit was fabricated and tested. The simplified configuration consists of single desiccant-adhered tube enclosed in a larger air passage to form a concentric channels arrangement. The single-tube was built as early prototype to verify several design features of the later shell-tube configuration, such as the solid desiccant integration to the tube-side channels, air flow arrangement, and heating for regeneration process. The schematic of the first prototype configuration is shown in Fig 4-1. As desiccant powder was held on the inner surface of the inner tube using a rolled mesh, it should be verified that 1) with the mesh between the desiccant and air stream, the adsorption could still take place, and 2) the mesh could properly hold the desiccant inside the tube.

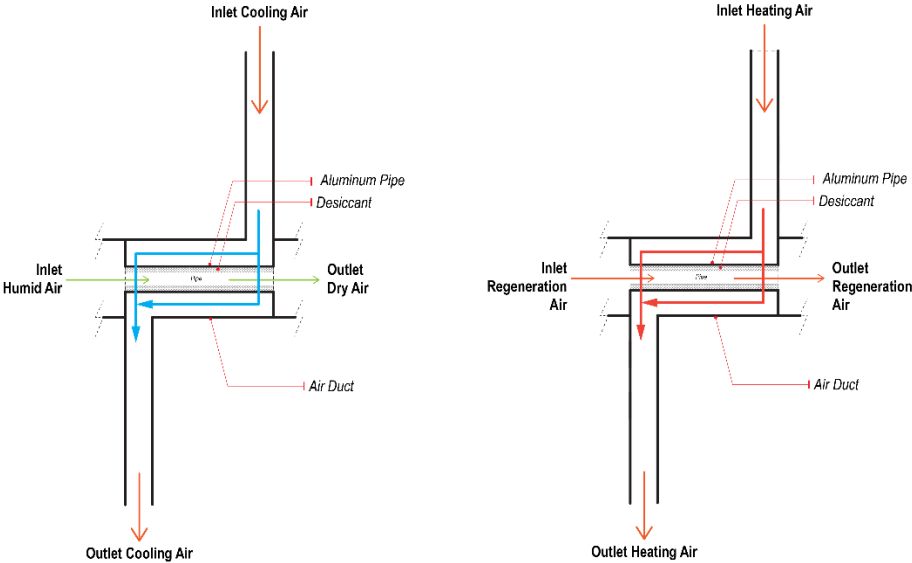


Fig 4-1 Schematic of earlier prototype with single tube-side channel

Chapter 4: Small scale laboratory prototype construction

In this early prototype, it was anticipated that the dehumidification unit can be integrated to an existing indirect evaporative cooler and the cooling air for the shell-side of the dehumidifier could be sourced from the cooler as shown in Fig 4-2. With the unit integrated, the humid air from the ambient could be drawn to the desiccant unit by the fan of the cooling unit. Then, dried air exiting the tube-side of the dehumidifier, would pass through the evaporative cooler and be directed back to the shell-side as cooling air (Fig 4-2). Air heating for regeneration process was achieved using tape heaters wrapped onto the inlets of the dehumidifier unit.

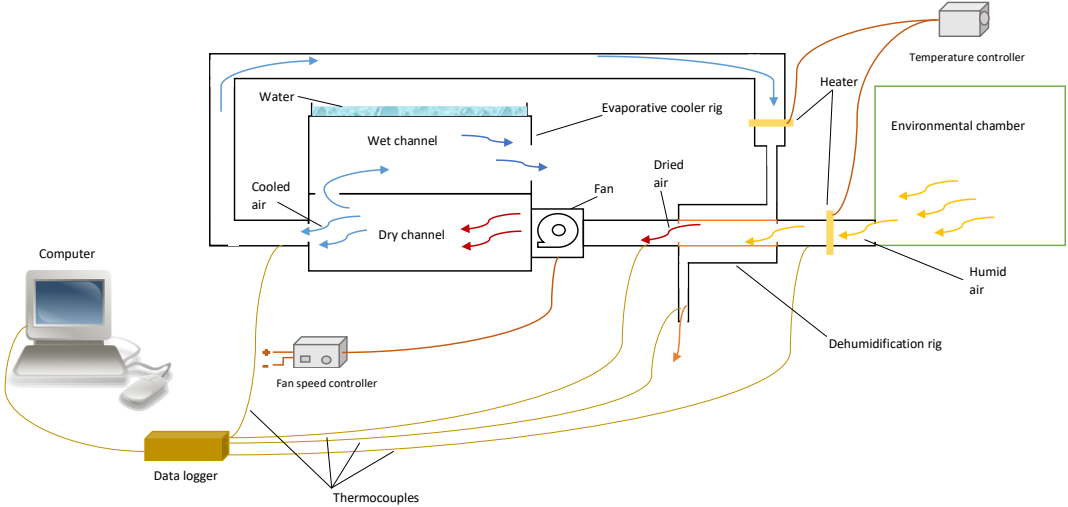


Fig 4-2 Constructed early prototype rig and the flow diagram

Chapter 4: Small scale laboratory prototype construction

Fig 4-3 shows the testing results for both dehumidification and regeneration process of the first prototype. It can be seen that during regeneration process, the outlet air humidity ratio was higher compared to the inlet, and vice-versa, the outlet air humidity was lower than the inlet during the dehumidification process. This confirmed that air moisture can pass through the mesh to allow adsorption and desorption.

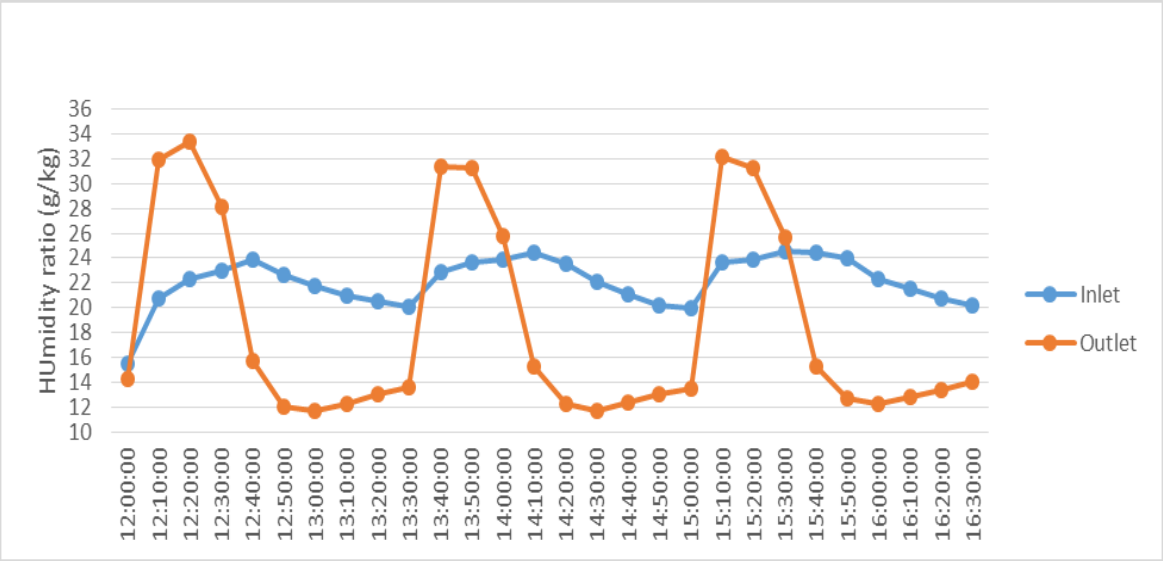


Fig 4-3 Test results of the first prototype: Primary air humidity profile over time for both adsorption and desorption process

The testing with the first prototype also provided feedbacks for the shell-tube prototype:

- i) The copper mesh could properly hold the desiccant powder inside the tube. It was observed that there wasn't any desiccant loss due to air stream passing through the tube
- ii) The mesh did not hinder proper contact between the air and the desiccant, allowing adsorption/desorption process to take place
- iii) While the dehumidifier was anticipated to work in tandem with a cooling unit (such as the evaporative cooler used during the test), the desiccant unit should be able to work independently for the following reasons

- a. Using this arrangement, the secondary air could only be sourced from the cooler, limiting the possibility of using different source such as ambient air
 - b. As the fan was positioned between the dehumidifier and the evaporative cooler, the air has to pass through the cooling unit before be directed to the shell-side channel. This meant that during regeneration process, hot air from the desiccant tube would be cooled down by the cooler before being re-heated prior entering the shell-side channel. Not only that it would be inefficient, the evaporative cooler would be unnecessarily heated during the desiccant regeneration process
- iv) Therefore, an additional fan would be required so that hot air could enter the shell-side channel without having to go through the evaporative cooler
- v) Ducting arrangement of the test rig should take into account the possibility of different air flow scenarios. For instance, the air should be able to go through only the shell-side. This would allow heat removal form the desiccant tube post-regeneration process without adding moisture to the desiccant, which would ensure dehumidification process to take place with the desiccant at low temperature and low moisture content.

The feedback from the early prototype were taken into consideration during the design and construction of the shell-tube desiccant dehumidifier rig explained in the following sections.

4.2. Design and construction of the shell-tube desiccant rig

A proof of concept prototype shell-tube solid desiccant heat and mass exchanger for air dehumidification was built and tested under controlled laboratory conditions of air temperature, humidity and flow rate. As described in chapter 3, the prototype consists of multiple tubes onto which a solid desiccant (silica gel) layer was adhered onto the inner surface of the tubes using a fine rolled copper wire mesh. The desiccant-filled tubes are arranged equidistantly along the inner passage of the shell-side air duct, as shown in Fig 4-4.

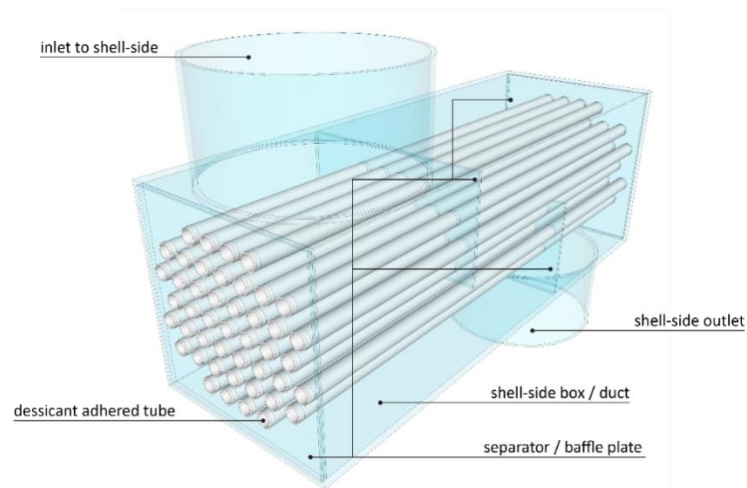


Fig 4-4 3D sketch of the tubes and shell arrangement

The tubes arrangement was considered to achieve maximum heat and mass transfer area between the desiccant layer and the process air while minimising pressure loss. The process/regeneration air flow through the desiccant tubes and cooling/heating airflow through the shell side are shown in Fig 4-5.

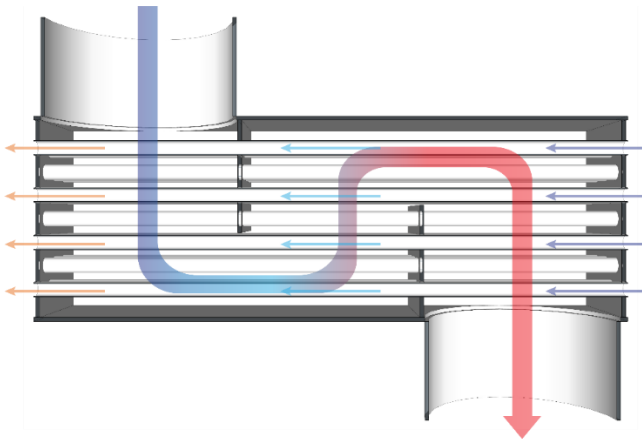


Fig 4-5 Air flow paths through the heat exchanger

The physical dimension of the heat exchanger tubes, outer shell and inlet and outlet ducts are given in Table 4-1.

Table 4-1 Dehumidifier prototype specification

Component	Specification	Unit	Value
Outer shell	Material	-	Al
	Overall length	mm	300
	Overall width	mm	104
	Overall height	mm	200
	Inlet-outlet OD	mm	100
Tubes	Material	-	Al
	Desiccant tube OD	mm	8
	Tube wall thickness	mm	0.45
	Number of tubes	-	45
Wire mesh	Material	-	Cu
	Mesh count	in	250
Desiccant	Material	-	Silica Gel
	Desiccant layer thickness	mm	±1

Chapter 4: Small scale laboratory prototype construction

Additionally, the CAD drawings detailing some of the dimensions of the prototype are shown in Fig 4-6.

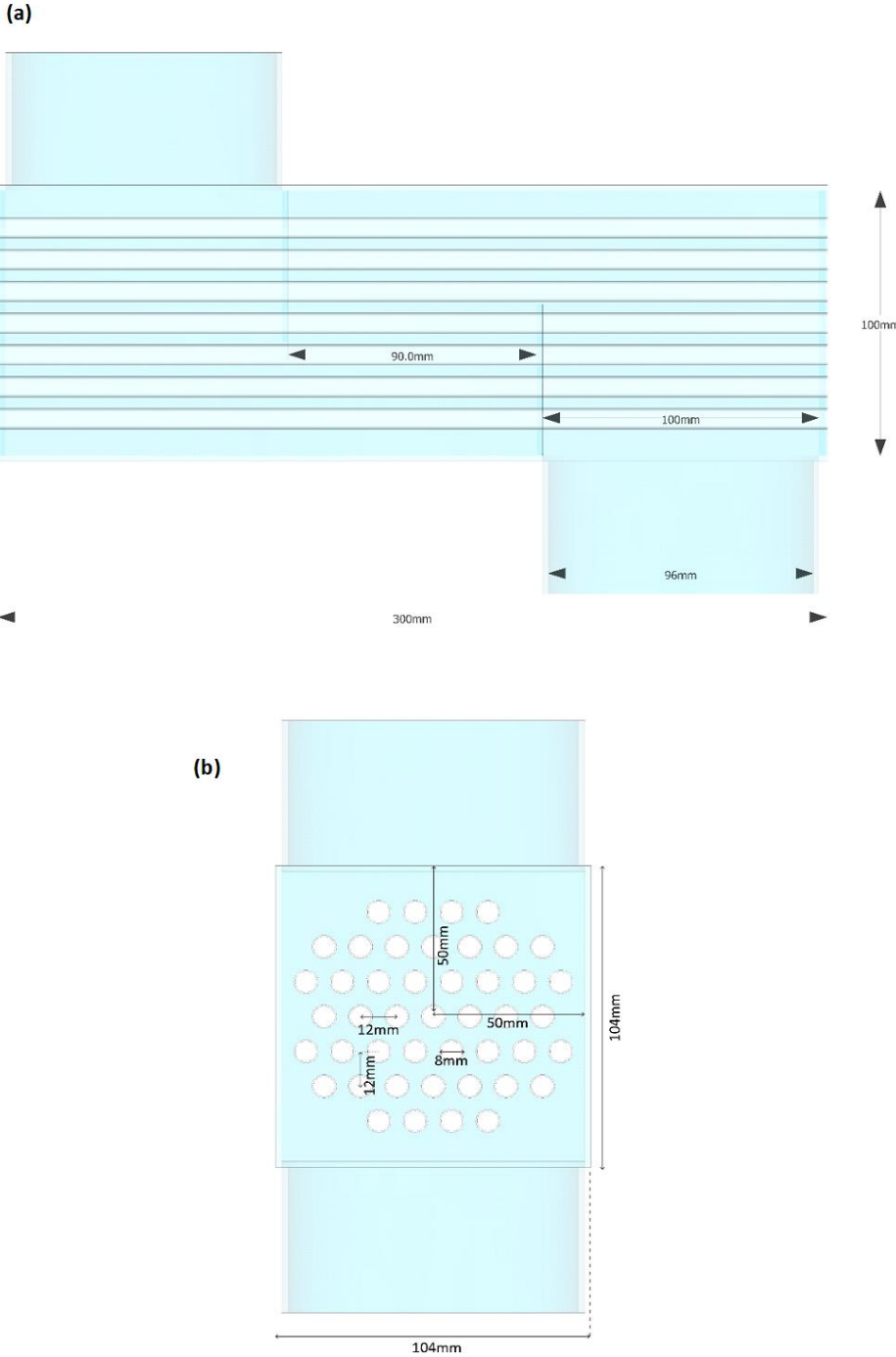


Fig 4-6 CAD drawing of the prototype: (a) front view and (b) side view

Chapter 4: Small scale laboratory prototype construction

The heat and mass exchanger tubes were bundled together through perforated end plates. Two further baffle plates were inserted in between to direct the air flow over the tubes on the shell side, as shown in Fig 4-7.

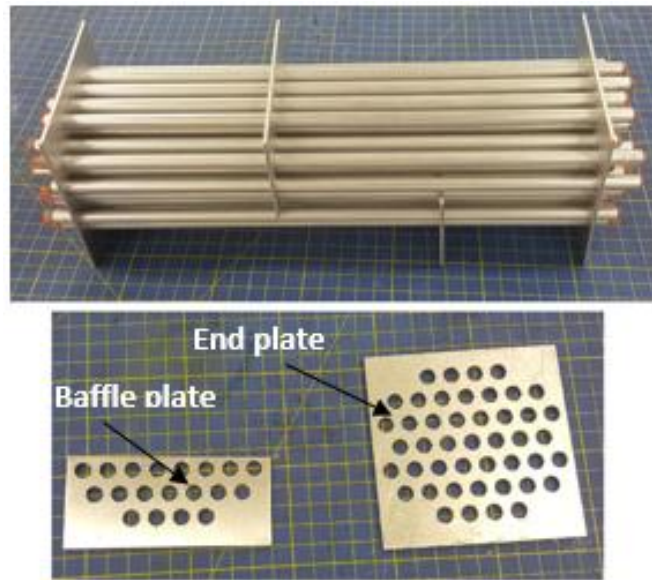


Fig 4-7 Construction shell-tube heat and mass exchanger

The shell was then completed by inserting the side plates and forming a sealed enclosure around the tubes. Two of the opposite side plates were fitted with opening for air circulation through the shell side as shown in Fig 4-8.

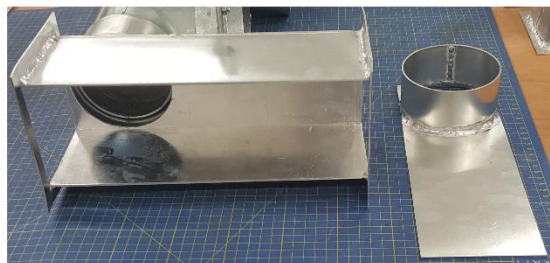


Fig 4-8 Shell-side casing

To ensure the blown air goes through both tube-side and shell-side of the prototype, an “air box / flow separator” was fabricated as shown in Fig 4-9. As the air enters the box, the baffle plates inside the box will divide the airflow and direct them to the inlets of both tube-side and shell-side of the prototype.

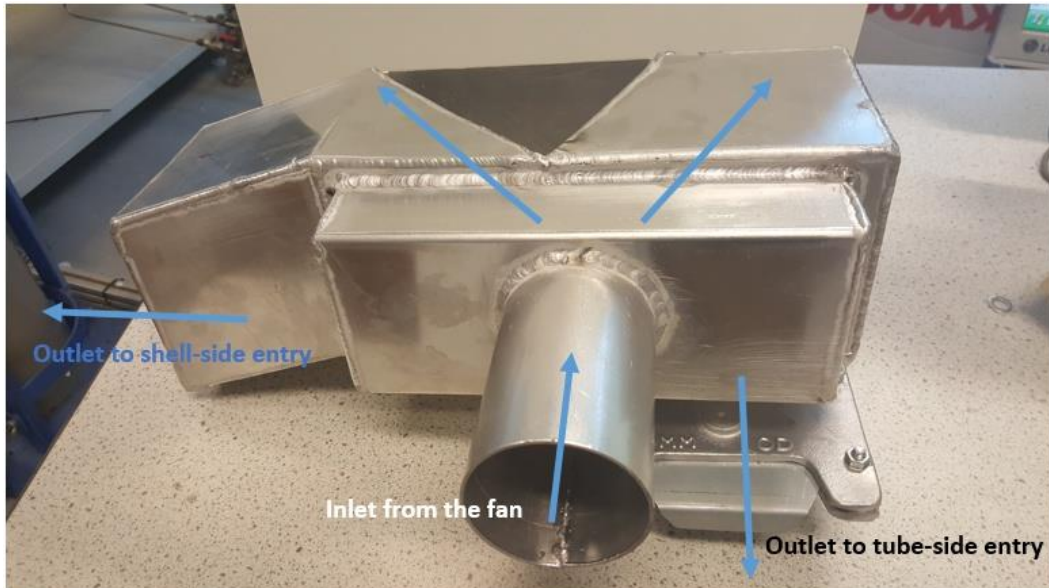


Fig 4-9 Air flow separator

4.3. Desiccant filling

Fig 4-10 shows the aluminium tube-wire mesh annulus. Fig 4-10 (a) and (b) show cut wire meshes into 35 cm length and width of 1.8 cm. The copper mesh were rolled with help of a solid metal rod – forming a rolled mesh tube with diameter of around 5 mm, taking into account the overlapping to prevent powder leakage – and inserted in the aluminium tubes the heat exchanger aluminium tubes concentrically as shown in Fig 4-10 (c) and (d). This created a 1 mm annulus gap between the copper mesh and the internal surface of aluminium tube. Sealing one end of the annular gap, the aluminium tube was put in standing position, and silica gel powder was poured into the open side of the annulus gap until filled, as shown in Fig 4-10 (e) and (f). As the tube was filled with desiccant, both ends were sealed to prevent leaking.

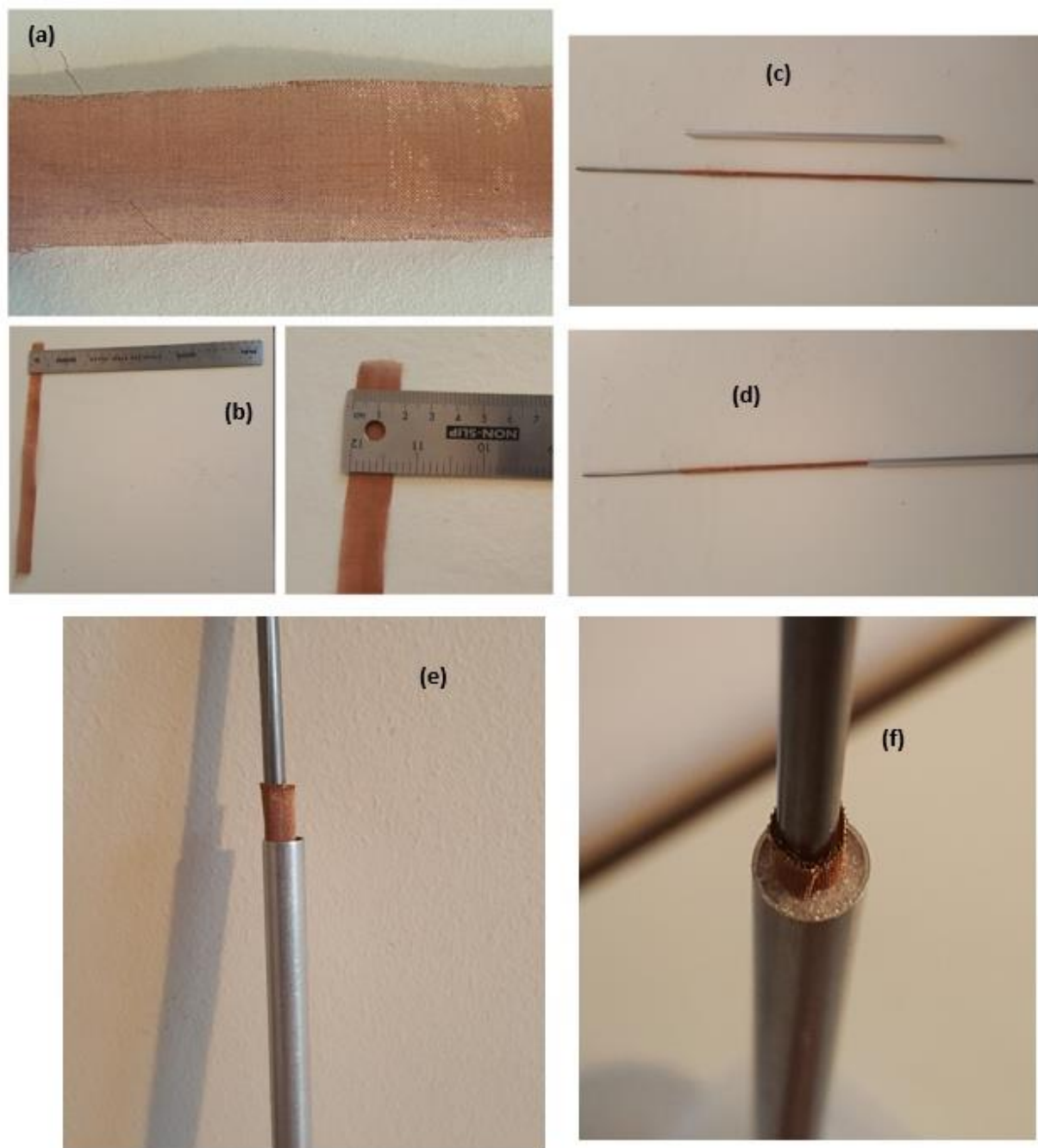


Fig 4-10 Desiccant tube filling process: (a) wire copper mesh, (b) cutting wire mesh into small sections, (c) Rolling mesh with help of metal rod, (d) insertion of rolled mesh into the tube, (e) desiccant tube ready for filling, (f) aluminium tube filled with desiccant powder

Chapter 4: Small scale laboratory prototype construction

An industrial grade Silica gel powder was acquired with powder particles size ranging from 75-650 μm . The desiccant material properties are shown in Table 4-2.

Table 4-2 Silica gel properties (Sigma Aldrich 214396)

Properties	Unit	Value
Grade	-	High-purity grade (Davisil Grade 12)
Form	-	Powder
Particle size	mesh	28-200
	μm	75-650
Pore size	cm^3/g pore volume	0.23
	\AA	22
Surface area	m^2/g	800
Melting point	$^{\circ}\text{C}$	>1600
Boiling point	$^{\circ}\text{C}$	2230

The silica gel particles varies in size and to achieve consistency of powder particles size, the powder was passed through a sieve to separate fine particles that may fall from the mesh tube and leak into the air side, as shown in Fig 4-11.

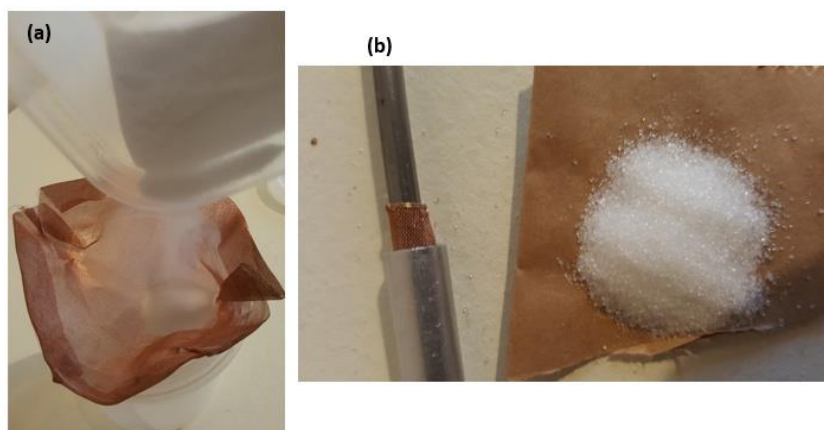


Fig 4-11(a) desiccant powder sieving, (b) sieved powder to be poured inside the tube

4.4. Auxiliary components

To perform different working cycle (e.g. dehumidification and regeneration process), the prototype needs to be connected to other components, such as the climate chamber, the heater, etc. The connections between these components are mainly achieved by attaching solid / flexible tubes to the prototype. To provide the heating for regeneration air, the HOTWIND SYSTEM hot air blower is attached to experimental setup (Fig 4-12).



Fig 4-12 Hot air blower

The heater fan is used to draw air from the climate chamber then heat it directly to desired temperature before blowing the hot air through the prototype. The air temperature at the outlet of the heater fan can be directly adjusted, while air flow rate can also be adjusted with the fan power knob. The fan can also act solely as air blower by turning of the heating feature. The specification of the hot air fan is shown in Table 4-3.

Table 4-3 Hot air blower specification

Attributes	Unit	Value
Voltage	V	230
Power	W	3700
Max air outlet temperature	°C	650
Air volume (20 °C)	l/m	200-900
Size (L x W x H)	mm	332 x 106 x 179

4.5. Test rig

A fully instrumented test rig was built. The rig was built so that the all operating parameters including inlet air dry bulb temperature, humidity, airflow rate, regeneration air temperature, and outlet air conditions can be measured and the dehumidification performance investigated. The controlled properties of ambient air from the environmental chamber can be diverted through an air gate dampers and diverters to the test prototype desiccant tubes for air dehumidification and desiccant regeneration, as well as through the outer shell for cooling and heating of the tubes. Fig 4-13 shows the fully assembled experimental setup.

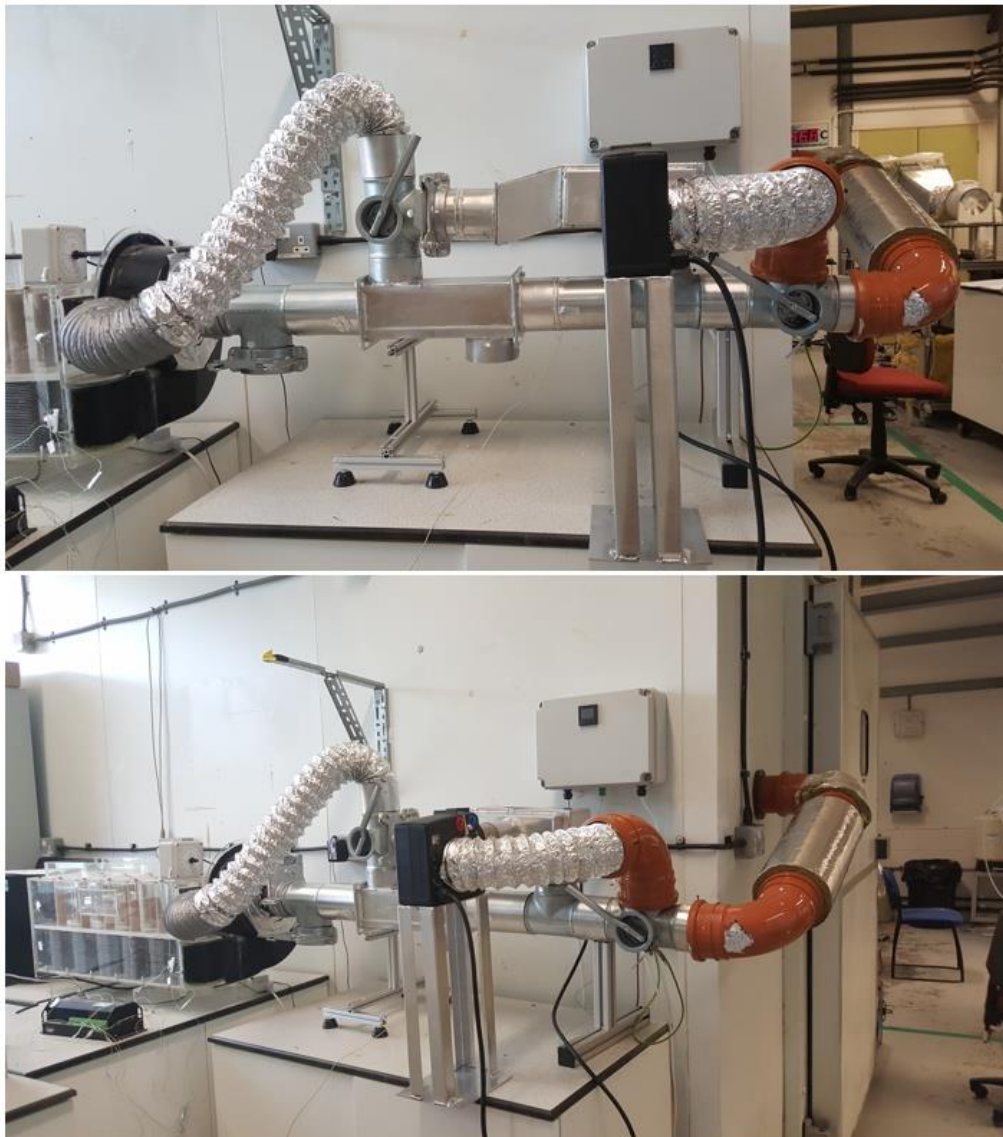


Fig 4-13 Assembled test rig

4.6. Measuring instruments

The thermal performance of the prototype was evaluated experimentally by measuring and recording the main operating parameters of the rig using data acquisition. This include process and regeneration air temperatures, relative humidity, and flow rates.

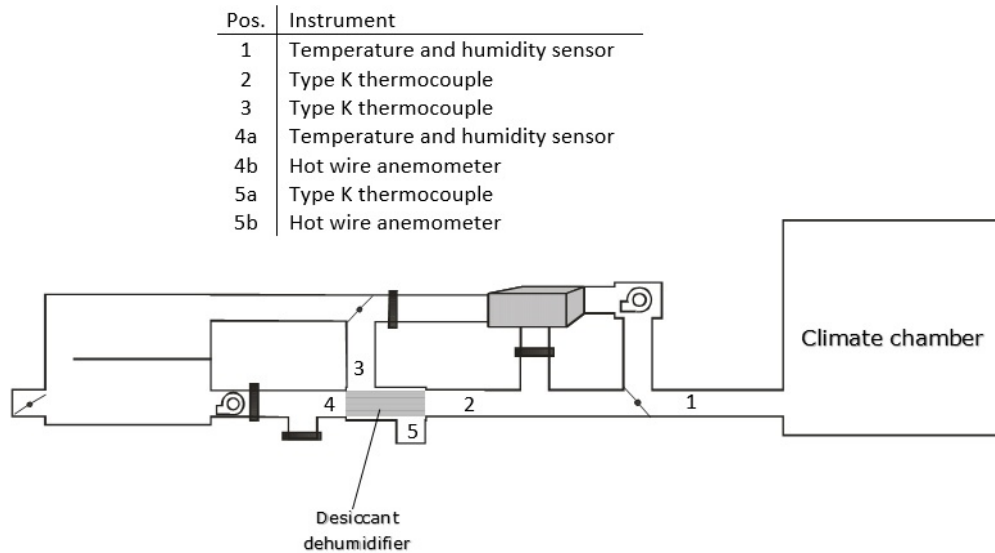


Fig 4-14 Positioning of measurement instrument

The following devices are used to measure and save testing data (Fig 4-14):

- Humidity and temperature meters: RS-1365 humidity and temperature meter is located at the inlet pipe near the climate chamber to measure humidity and temperature of inlet air to the dehumidifier, while RS-232 humidity and temperature meter is used to measure humidity and temperature of process/regeneration air at the outlet of the dehumidifier. The humidity and temperature meters also have data-logging capability and store data to and be monitored in desktop computer.
- Thermocouples: K-type thermocouples are placed in several points (middle of air flow passage), such as near the inlet of dehumidifier (after heater/fan), inlet of shell-side box, and outlet of shell-side box.

Chapter 4: Small scale laboratory prototype construction

- Data taker DT500 series 2 is used to store measured temperature by the thermocouples. The data taker is connected to a desktop computer and ran by DeLogger 4 program, which can read data sent from the data taker and display it on the monitor.
- Anemometer: a portable hotwire anemometer (Testo 405-V1) is used to measure air flow velocity at the outlet of the dehumidifier (both tube-side and shell-side).

The type and specification of the instruments were used in this work are summarised in Table 4-4. Fig 4-15 shows the measuring instruments used in the testing.

Table 4-4 Measurement summary

No.	Instrument	Variable	range	Accuracy of reading
1	Temperature/Humidity sensor	Inlet air humidity and temperature	-20 to 60 °C, 10% - 95% RH	± 1% RH ± 0.5 °C
2	Type K thermocouple	Inlet air temperature (tube-side)	-50 to +250°C	±0.4%
3	Type K thermocouple	Inlet air temperature (shell-side)	-50 to +250°C	±0.4%
4a	Temperature/Humidity sensor	Outlet air humidity and temperature (tube-side)	-20 to 60 °C, 10% - 95% RH	± 1% RH ± 0.5 °C
4b	Hotwire anemometer	Outlet air velocity (tube-side)	0 to 10 m/s	±5 %
5a	Type K thermocouple	Outlet air temperature (shell-side)	-50 to +250°C	±0.4%
5b	Hotwire anemometer	Outlet air velocity (shell-side)	0 to 10 m/s	± 5%

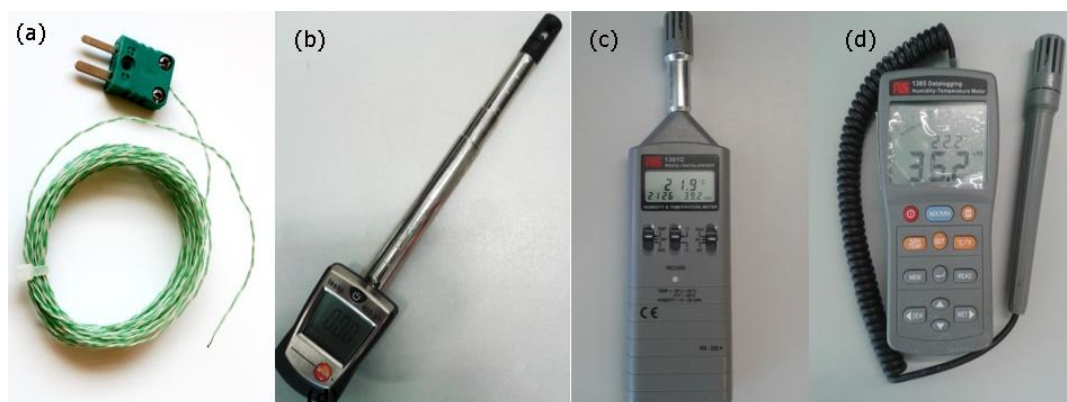


Fig 4-15 Measurement instruments (a) thermocouple,(b) hot wire anemometer,(c) temperature and humidity sensor, and(d) hand held temperature and humidity meter

4.7. Experimental setup and operating modes

The experimental testing of the dehumidifier prototype was conducted under controlled laboratory temperature and humidity conditions. Fig 4-16 shows the general layout of the test rig and associated components. The air dehumidification heat test prototype is connected to a multiple duct arrangement, which links the rig to the environmental chamber. The air temperature and relative humidity inside the chamber can be adjusted and maintained via the chamber's control panel.

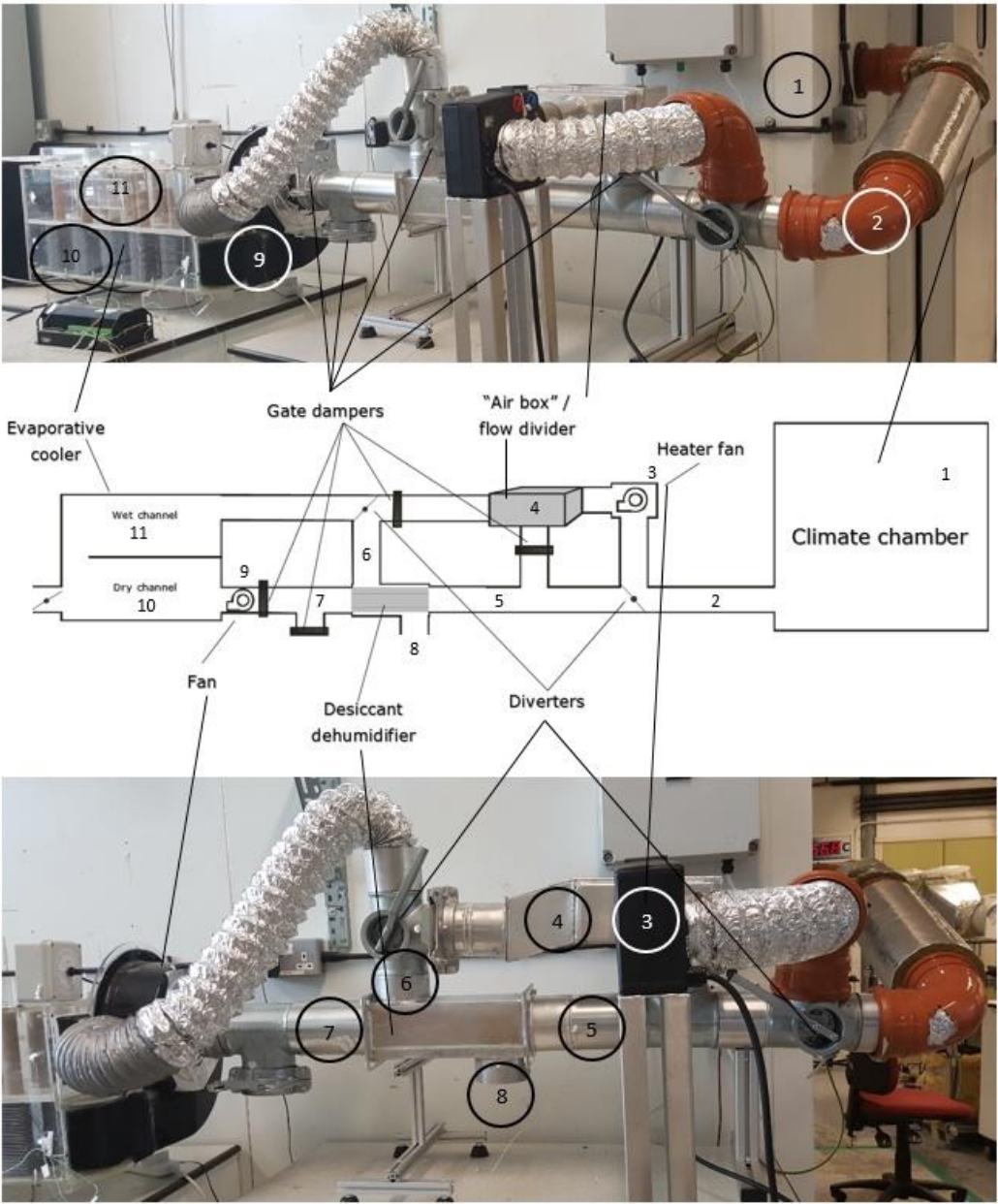


Fig 4-16 Experimental setup

Chapter 4: Small scale laboratory prototype construction

In the experiment tests, ambient air is drawn from the climate chamber (point 1) through a duct (point 2) by a variable-speed, adjustable temperature heater fan (point 3). During dehumidification process, the heater is turned off thus the fan only serves to circulate air through the rig.

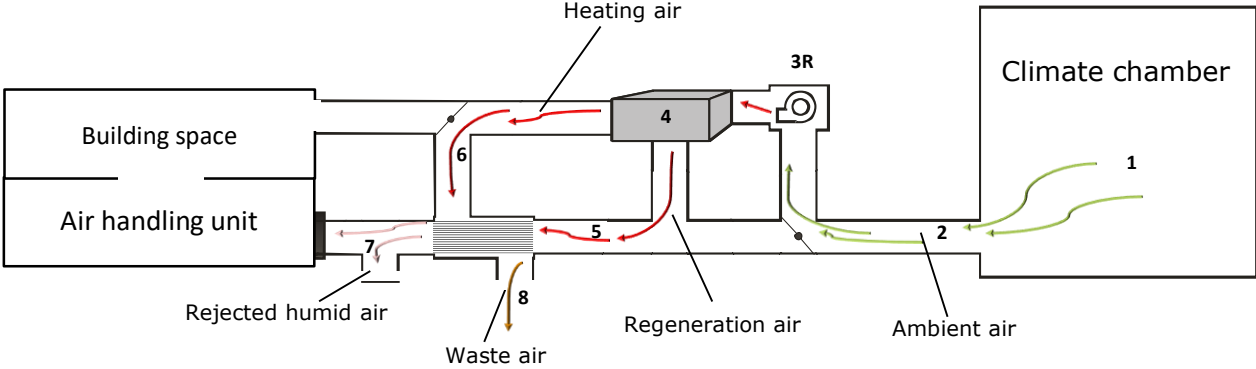


Fig 4-17 Airflow schematics for regeneration process

During regeneration process, the heater is set to regeneration temperature and heat the air from the chamber to state 3R, as illustrated in Fig 4-17. From there, the airflow is divided using an "air box" (point 4) into two passageways, the tube-side inlet duct (point 5) and the shell side inlet duct (point 6). The flow through these passages can be regulated using the gate valves and slide gates. During regeneration process, the air from point 5 transfer its heat to the desiccant tubes and desorb moisture from the desiccant, then exit at lower temperature and increased humidity ratio (point 7). On the other hand, air from point 6 also transfer its heat to the outer surface of the desiccant tubes and exit at lower temperature and constant humidity ratio (point 8).

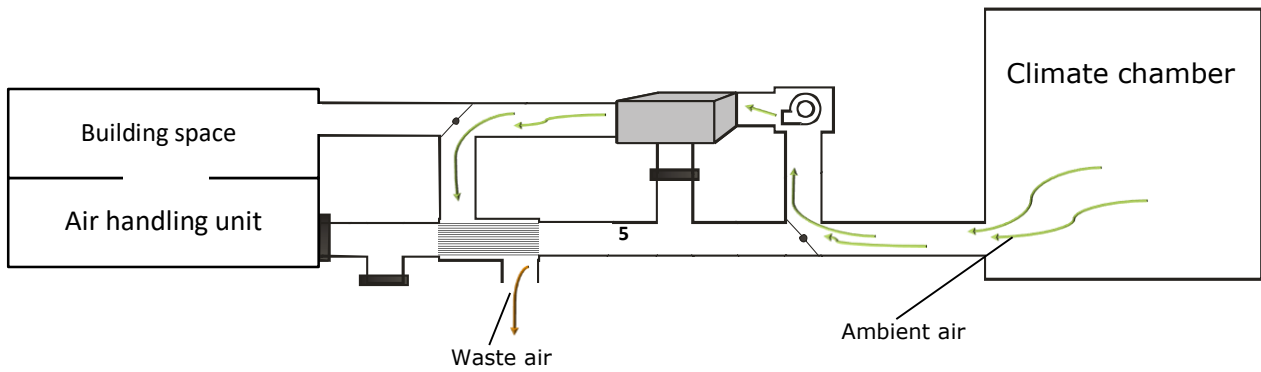


Fig 4-18 Airflow schematic during cool down period

After regeneration is completed, heater is turned off while keeping the fan on, and passage to point 5 is closed. Thus, air at "ambient" temperature passed through the shell-side only, removing heat from the dehumidifier (Fig 4-18).

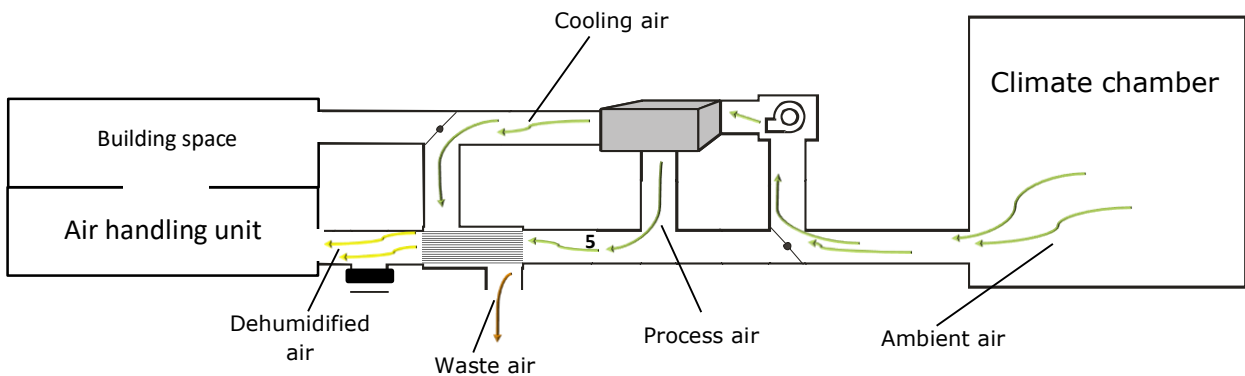


Fig 4-19 Airflow schematics during dehumidification period

Then, dehumidification process is started by opening passage to point 5, allowing air from the chamber passed through the tubes (Fig 4-19). The desiccant will adsorb moisture from the air and release its heat to the process air stream. The process air will exit at lower humidity ratio, while secondary air removes heat from the tubes and exit the shell-side at higher temperature.

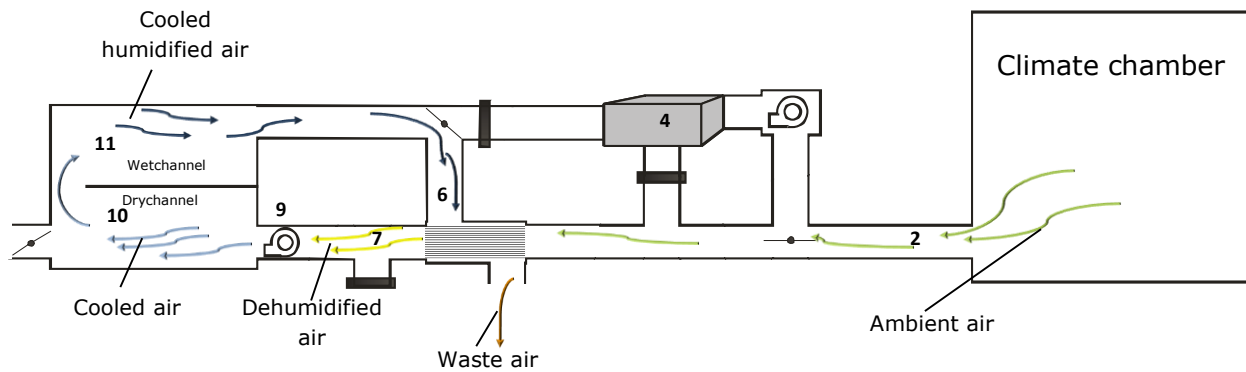


Fig 4-20 Integration of dew point evaporative cooler

It is worth mentioning that the proposed air dehumidification systems lend itself well for integration with dew-point (sub-wet bulb) evaporative cooler (Fig 4-20). In this case, dehumidification process can be performed using the fan of an evaporative cooler (point 9) attached to the outlet of the dehumidifier tube (point 7), drawing the air directly from point 2 through the desiccant tube, then flowing the dehumidified air through the dry channel of the evaporative cooler (point 10). Some of the air is then diverted to the wet channel of the evaporative cooler (point 11) before directed back to the dehumidifier through the shell-side duct (point 6). In such arrangement, cool and humid air rejected from the evaporative cooler is circulated through the shell side of the heat exchanger to remove effectively heat of adsorption generated in the desiccant layer during the adsorption process. In this alternative mode, the heater fan is completely turned off and the passageway through point 4 is closed.

4.8. Test conditions

The experimental tests of the built prototype dehumidification system were conducted under controlled inlet air temperature and humidity that represent the hot and humid climate. The tests conducted include comparing the performance of three scenarios:

- i) Continuous Operation cycle of dehumidification and regeneration.
- ii) Continuous dehumidification-regeneration cycle without secondary airflow (no shell side heat removal or addition air stream)

Chapter 4: Small scale laboratory prototype construction

- iii) Supplementary cooling period between the end of regeneration cycles and the start of dehumidification process.

The three different cyclic scenarios were tested under the default operating parameters (air flow, inlet air temperature and humidity, and regeneration temperature). Then, the adsorption and desorption process of the prototype were evaluated by varying the default operating parameters, with the exception of inlet air temperature. For this parametric tests, three airflow rate scenarios were selected: a) the default airflow rate for both dehumidification and regeneration cycles, b) variable airflow rate for the dehumidification and regeneration process, and c) variable airflow for regeneration process. The air flow rate of secondary air during cooling period was held constant for all three scenarios to maximise heat removal. Three regeneration temperature set values were selected for the fan heater: 120°C, 130°C, and 140°C. Lastly, three different humidity set value for inlet air from the climate chamber were tested: 60%, 70%, and 80%. When one operating parameters was changed, the other were unchanged from the default settings. The testing scenarios are summarised in Fig 4-21.

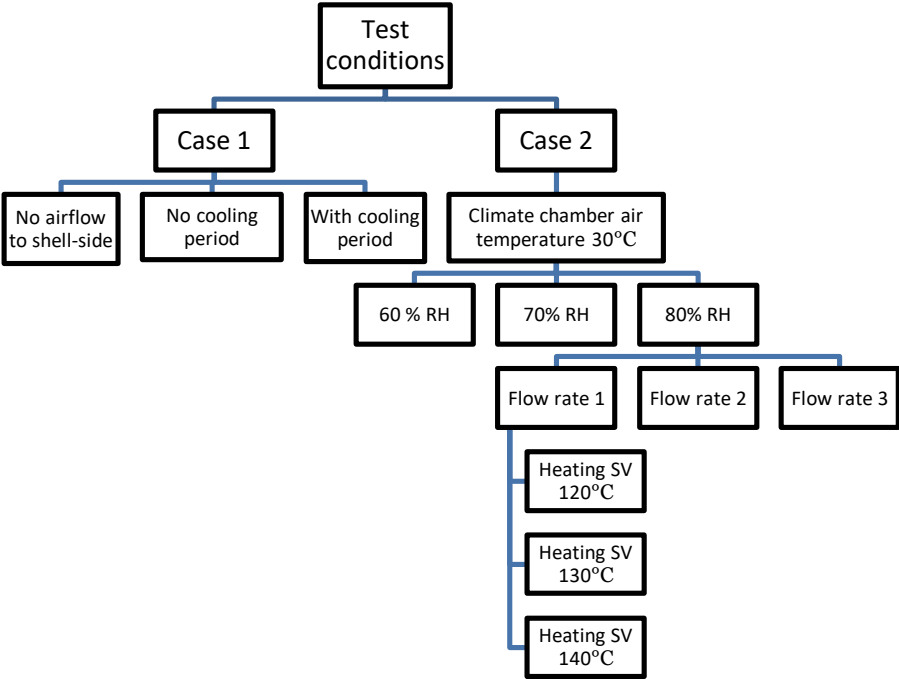


Fig 4-21 Testing scenarios

4.9. Test procedure and health and safety checks

The experiment was conducted in the following steps:

- i. Check all electric connection and sockets of the PC, data logger, fan heater, and connection of humidity sensors to the PC.
- ii. Check if the duct is connected from the environmental chamber and the rig.
- iii. Check all thermocouple that they are all connected to the rig and in the right order.
- iv. Check if all the gates and diverters are in correct position. At this point, access from the chamber through the heater fan and shell-side of the dehumidifier is left open, while access to the tube-side is closed.
- v. Check the environmental chamber and make sure that there is no one inside, before switching it on.
- vi. Switching the environmental chamber on and set it to required temperature and humidity.
- vii. Switching the computer, humidity sensors and data logger on to check if the sensors and thermocouples are giving readings.
- viii. Switching the heater fan on when the temperature and humidity inside the chamber reaches the desire values to start drawing air through the shell-side (without turning on the heater).
- ix. Open new file on the computer and start monitoring the reading of temperature and humidity.
- x. When temperature and humidity at the inlet duct stabilizes, the experiment can be started by desorbing the moisture from the desiccant tubes.
- xi. Turn on the heater to increase temperature of airflow coming from the climate chamber.
- xii. Open the air passage to the tube-side of the dehumidifier.

- xiii. Once regeneration cycle is completed, close access to the tube-side and turn off the heater.
- xiv. Start cooling period by adjusting the airflow rate.
- xv. After cooling period is completed, start the dehumidification cycle by re-opening the access through the tube-side.
- xvi. At the end of the dehumidification cycle, repeat from point 8 to approach theoretical cyclical steady state.
- xvii. After recording for required period, you can start switching off all equipment:
- xviii. Switch off the environmental chamber.
- xix. Switch off the fan.
- xx. Save all data files and then switch off the data logger and then the PC.
- xxi. Double check that all switches are off.
- xxii. The experiment ended.

4.10. Experimental observations and limitations

4.10.1. Desiccant tubes handling

Since desiccant powder is held inside the tubes by rolled copper mesh, some of the powder could still leak through the mesh. This was anticipated by two approach. The first was the sieving process of the powder prior to insertion to the tubes. However, even after several sieving, it was difficult to guarantee that the very fine powder was totally separated from the rest of the particles. The second approach was to create slight overlap when rolling the mesh. The overlap was intended to limit the gap created during the rolling process. However, it was observed during the construction that the powder was still leaking if the tubes were shaken vigorously, even if both ends of the tubes were already sealed. Since the tube was filled with the powder, the powder could cause pressure to the rolled mesh and filled through the

overlap. To avoid excessive leaking, the tubes should be handled with care during construction and assembly. It was observed that during testing, the airflow did not cause further leaking of the powder, thus it was assumed that low vibration should not cause leaking, as long as the dehumidifier unit is fixed in place.

4.10.2. Heating of regeneration air

During preliminary design process of the prototype, a heating tape was chosen as heating device for the regeneration process. Initially, heating tape would be wrapped around the outside surface of inlet of both tube-side and shell side ducting. The tape would heat the metal surface, and subsequently the hot surface would heat the passing air. Thermocouple was used to control the heating power based on temperature measurement of passing airflow. This worked quite well in the initial prototype (similar design but only single desiccant tube) with smaller ducting diameter. However, in the main prototype, the heating of the ducting surface was deemed insufficient, especially with higher airflow, as the diameter of the tube was bigger than the initial prototype. It was then decided to replace the heater with a heater fan, which could suck air from any source and heat it directly before blowing it through the dehumidifier inlets. This heater worked very well and was able to reach set temperature easily. However, two issues were encountered with the heater. The first issue was temperature control. Since the heater was positioned to be able to supply hot air both to tube-side and shell-side inlets, the heated air had to travel some distance before reaching the inlets. Thus, drop of temperature between the heater outlet and the dehumidifier inlets was significant. Insulation could have prevented this, but since the air passage was used in both regeneration and dehumidification process, heat loss was actually preferable during “cooling period” of the system. Moreover, since temperature of the heated air was not controlled by thermocouple near the inlets, the heater fan had to be adjusted manually to reach desirable inlet air temperature during regeneration process. Thus, constant inlets regeneration air temperature was not achievable, and the testing results should be analysed using average inlets temperature. Additionally, due to different passages, it was very difficult to reach equal

temperature between the inlets in tube-side and shell-side. In this case, the temperature of regeneration air at the inlet of tube-side was prioritised when adjusting the heater fan.

4.10.3. Measurement limits

The humidity and temperature sensors used at both inlet and outlet of the system have maximum operating temperature of 60°C, which limit the possibility of choosing regeneration air temperature. While the sensor for the inlet is positioned before the heater to address this issue (the air temperature and humidity is measured near the climate chamber, while air temperature post-heating is measured again with thermocouple), measurement of air temperature and humidity at the outlet of the desiccant tubes is also limited to 60°C. Hence, regeneration cycle time should also be limited to avoid reaching outlet temperature outside the measurement range of the sensor.

4.10.4. Heat storage of system's structure

Since the main structure of the prototype is made of aluminium (chosen for availability and ease of manufacturing), heat storage becomes an issue when performing testing of continuous cycles of adsorption and regeneration processes. This is notably observed when the desiccant is regenerated and adsorption cycle follows. Since the air passages (mainly aluminium ducts) is still at high temperature, ambient air from the climate chamber will be heated even before reaching the inlet of desiccant tubes. The same case also applies to the shell-side box, limiting the cooling process of desiccant, hence dehumidification performance is very limited. To overcome this, a third cycle, namely "cooling period" is employed between the end of regeneration cycle and the beginning of dehumidification cycle. During this period, air will go through only the shell side, taking away heat stored inside the prototype as well as the passage ducts, while access through the desiccant tubes is blocked. This will allow the rig structure to cool down before dehumidification process is resumed with very limited change to water content of the desiccant. Hence, high airflow is preferable during this period, however

it should be adjusted with consideration that after certain fan power level, the heat produced by the fans will be significant and cause considerable increase of air temperature. On the other hand, relatively low temperature can cause heat loss of regeneration air along the passage between the heater and the dehumidifier inlet. As previously mentioned, insulating the passage was not preferable since the rig structure should be cooled as soon as possible before resuming dehumidification cycle. Thus, for regeneration cycle, the heater fan is set to a very high temperature (above 100°C) to achieve temperature around 60-90°C near the inlets of the dehumidifier.

4.11. Preliminary results

The performance parameters of the dehumidifier prototype are presented in Table 4-5 for “ambient” air conditioned at 30°C, 80% RH, fan adjusted at airflow level 1 for dehumidification and regeneration process, and heating at set value 120°C for regeneration air. Prior to the testing, the desiccant tubes were completely regenerated, and then cooled down using only secondary air stream to approach ambient temperature (by monitoring air temperature at the inlet and outlet of shell-side duct. Therefore, at the dehumidification process of the first cycle, the dehumidifier was at relatively low temperature and low water content. Successive cycles were tested until cyclical steady state condition was reach. It was observed that with the chosen testing conditions, the steady state condition was reached after 6 cycles.

Chapter 4: Small scale laboratory prototype construction

Table 4-5 Testing results for inlet air at 30°C, 80% RH, heating set value 120°C, airflow level 1

Parameter	Comp. Cycle 1		Comp. Cycle 6	
	D	R	D	R
Tube-side average inlet air temperature (°C)	28.71	53.14	35.61	58.67
Tube-side average outlet air temperature (°C)	32.84	47.27	39.12	48.24
Tube-side average inlet air humidity (g/kg)	22.30	22.40	22.32	22.66
Tube-side average outlet air humidity (g/kg)	5.13	22.74	14.06	28.56
Shell-side average inlet air temperature (°C)	29.11	73.65	35.07	77.85
Shell-side average outlet air temperature (°C)	34.07	45.88	40.11	48.26
Tube-side volumetric flow rate (m ³ /h)		4.07		
Shell-side volumetric flow rate (m ³ /h)		12.09		
DCOP		0.44		0.2
Dehumidification capacity (g/h)		24.97		12.60
Efficiency		0.77		0.37

The performance indices of the two cycles indicate that the dehumidification performance of the prototype was much higher at the first cycle. As shown in Table 4-5, the DCOP, DC, and efficiency of the first cycle were about twice compared to the 6th cycle. However, even though the dehumidification effect was more significant at the first cycle, the performance indices were formulated with the assumption of stable outputs between different cycles, and they did not reflect the poor desorption process of the first cycle. Thus, the performance indices of the 6th cycle were more appropriate for the tested operating conditions.

4.12. Summary

This chapter provided the construction process of the dehumidifier prototype. The dehumidifier components and specification were also described, including the desiccant materials, auxiliary components and measurement instruments. Preparation of desiccant tubes were also presented, showing the filling process of desiccant powder into the tubes as well as the sieving process of the desiccant powder. Then, operating modes of the constructed rig were presented, explaining various working scenarios possible. The different working conditions tested was briefly explained, followed by step-by-step testing procedures for all testing conditions.

Several limitations were observed during fabrication and testing of the experimental rig. As desiccant powder was held inside the tubes using rolled wire mesh, some of the fine powders could leak through the mesh if the tubes are forcefully. The measurement limitations of the humidity sensors limited the choice of regeneration temperature and regeneration process time to avoid trespassing the upper limit of temperature measurement. On the other hand, the aluminium rig channels caused significant heat loss during regeneration process. However, in spite of the heat loss problem, it was decided to avoid covering the whole rig with thermal insulation, due to residual heat stored in the rig structures after regeneration, which could severely affect dehumidification performance. Preliminary results of the experiments were presented, while detailed analysis of the testing results will be discussed in the next chapter.

Chapter 5: Results analysis and discussion

The laboratory prototype shell-tube desiccant dehumidifier was tested to assess its air dehumidification performance. The system was tested over a period of time (i.e., several cycles of successive adsorption/regeneration) to achieve consistent outlet air conditions that approach cyclical steady state. A cooling period between each cycle was also introduced for some tests to help remove residual heat from the regenerated desiccant layer. The air temperature and humidity ratio variation were measured to determine the dehumidification capacity of the heat and mass exchanger and associated desiccant layers.

5.1. Uncertainty of experimental data

The dehumidification performance of the dehumidifier prototype depends mainly of two variables: the primary air temperature and its humidity ratio. While air temperature and its relative humidity (depends on temperature) were directly measured by the temperature and humidity sensor during testing, the humidity ratio of air (independent to temperature) could be calculated based on the measured variables. As previously mentioned in section 3.3.3, the humidity ratio can be calculated using the following equation:

$$\frac{RH}{Y} = 10^{-6} e^{5294/T} - 1.61RH \quad (5.1)$$

Since the air temperature (T) and relative humidity (RH) values were measured with some uncertainty (depends on measuring instruments as presented on Table 4-4), the calculated humidity ratio (Y) would also have uncertainty due to the two measured variables. In general, the relative uncertainty in the result (R) due to uncertainty in x_i can be estimated using the following expression [64]:

$$u_{R_i} = \frac{x_i}{R} \frac{\partial R}{\partial x_i} u_{x_i} \quad (5.2)$$

With u_{x_i} is the relative uncertainty in measurement of variable x_i . From above equation, the relative uncertainty in air humidity ratio due to relative humidity can be written as:

$$u_{Y,RH} = \frac{10^{-6} e^{5294/T}}{10^{-6} e^{5294/T} - 1.61RH} u_{RH} \quad (5.3)$$

With u_{RH} is the relative uncertainty in air relative humidity measurement. On the other hand, the relative uncertainty of air humidity ratio due to temperature is expressed as follow:

$$u_{Y,T} = \frac{10^{-6} e^{5294/T}}{10^{-6} e^{5294/T} - 1.61RH} \frac{5294}{T} u_T \quad (5.4)$$

With u_T is the relative uncertainty in air temperature measurement. Thus, the relative uncertainty in humidity ratio is written as follows:

$$u_Y = \left[(u_{Y,RH})^2 + (u_{Y,T})^2 \right]^{1/2} \quad (5.5)$$

From the above equations, it can be deduced that the uncertainty in humidity ratio is a variable that depends on measured temperature and relative humidity, and that it would depend mainly on its uncertainty due to air temperature measurement. Furthermore, even with relative uncertainty in air temperature and relative humidity measurement between 1-2%, the nature of equation (5.1) could lead to relatively large uncertainty in humidity ratio. The variation of relative uncertainty in humidity ratio based on measurements during one of the experimental tests is presented in Table 5-1.

Chapter 5: Results analysis and discussion

Table 5-1 Estimated relative uncertainty in air humidity ratio

Process	Time	T inlet (°C)	RH inlet	Y inlet (g/kg)	u_Y inlet	T outlet (°C)	RH outlet	Y outlet (g/kg)	u_Y outlet
Adsorption	12:10	29.90	84.30%	22.49	±30.30%	39.80	28.40%	12.95	±21.99%
	12:11	29.70	84.20%	22.19	±30.51%	39.90	30.40%	13.96	±21.93%
	12:12	29.70	84.60%	22.30	±30.52%	39.60	31.60%	14.29	±22.11%
	12:13	29.70	85.10%	22.44	±30.52%	39.00	32.50%	14.23	±22.47%
	12:14	29.70	84.90%	22.38	±30.52%	38.40	33.30%	14.11	±22.84%
Regeneration	12:15	29.70	85.20%	22.47	±30.52%	37.80	34.00%	13.94	±23.22%
	12:16	29.70	85.30%	22.49	±30.53%	42.10	40.00%	20.87	±20.78%
	12:17	29.90	85.80%	22.90	±30.32%	47.30	41.30%	28.53	±18.45%
	12:18	29.60	85.70%	22.47	±30.64%	50.80	39.00%	32.29	±17.15%
	12:19	29.90	85.90%	22.93	±30.32%	53.30	36.90%	34.66	±16.33%
	12:20	29.90	86.00%	22.96	±30.32%	55.30	35.10%	36.40	±15.74%

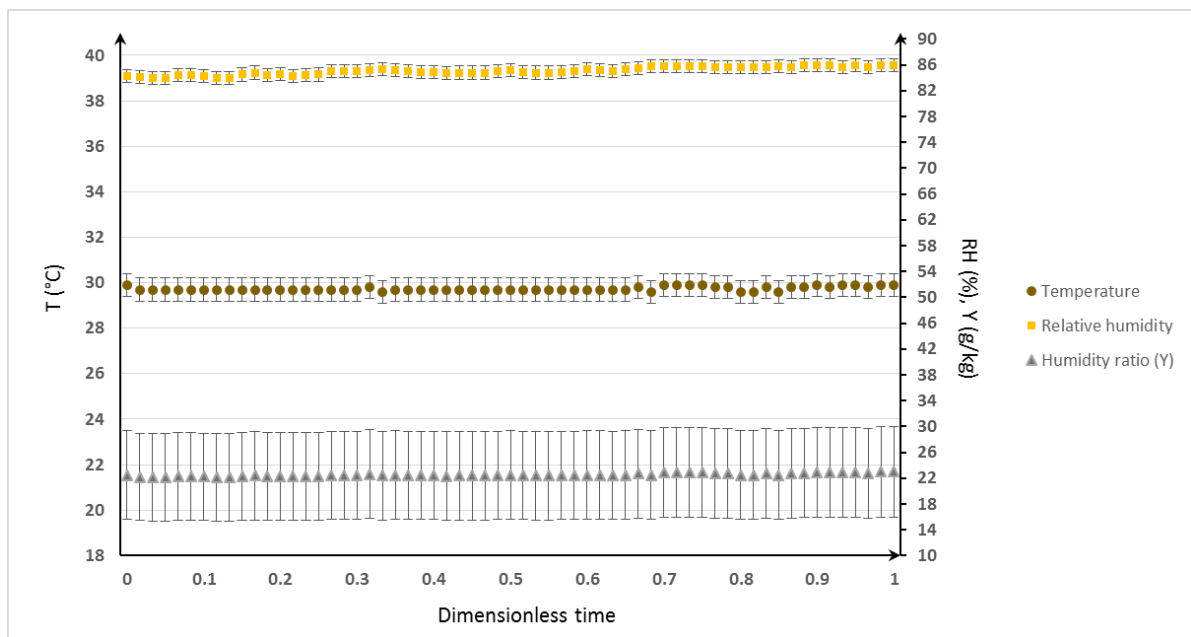


Fig 5-1 Uncertainty in inlet air temperature and humidity

As the temperature and relative humidity of inlet air from the climate chamber were relatively constant at around 29°C and 85% RH, the relative uncertainty in calculated humidity ratio didn't vary much during both adsorption and regeneration process. However, the estimated relative uncertainty for the inlet air were relatively large at around ±30%, or between ±6-7 g/kg of the calculated values, as represented by the error bars shown in Fig 5-1).

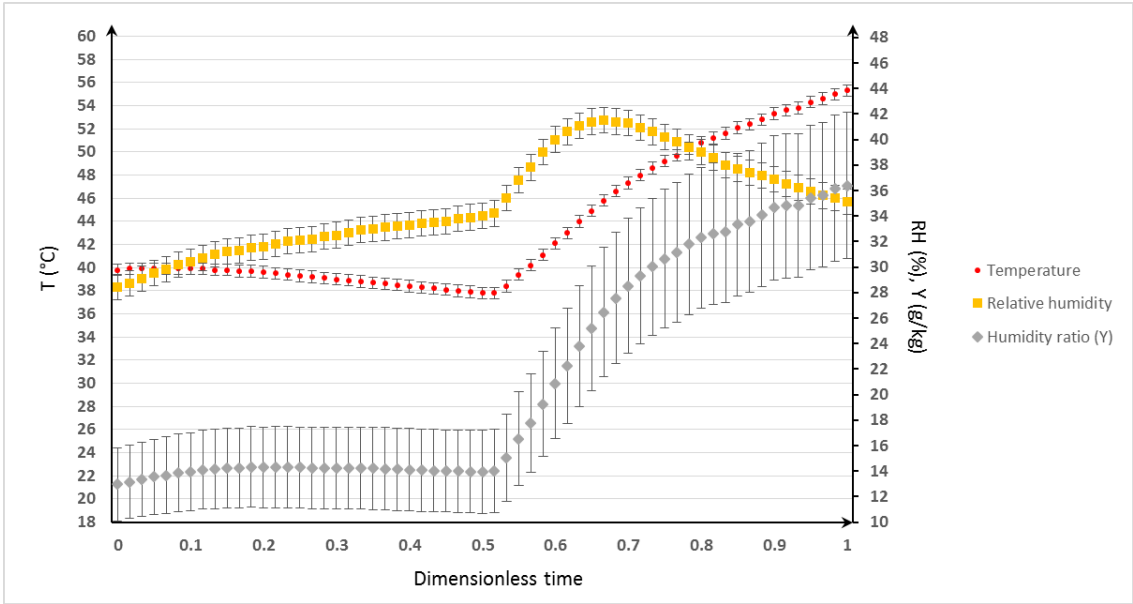


Fig 5-2 Uncertainty in outlet air temperature and humidity

When compared to the outlet air, it can be seen that the relative uncertainty in humidity ratio decreased with higher air temperature. This confirmed the large dependency of the relative uncertainty to measured temperature. During adsorption process, the outlet air temperature decreased as the desiccant cooled down, while the uncertainty in outlet humidity ratio increased. Conversely, the relative uncertainty in outlet air humidity ratio decreased when outlet air temperature increased during regeneration process. However, since outlet humidity ratio increased during regeneration process, its uncertainty (around ± 5 g/kg) was higher compared to the adsorption process (around ± 3 g/kg), as shown in Fig 5-2. On the other hand, it was also observed the relative uncertainty in humidity ratio depended less on relative humidity. Since the experimental testing of the dehumidifier was performed with multiple successive cycles until cyclical steady state was approached i.e. with temperature and humidity readings consistent between each cycle, it could be assumed that the calculated humidity ratio would be consistent as well. In this case, considering also the small uncertainty in temperature and relative humidity measurement, the relative uncertainty in humidity ratio would be acceptable. For the following sections, it would be assumed that the relative

uncertainty in humidity ratio is constant at around $\pm 30\%$ for inlet air and around $\pm 20\%$ for outlet air, and the error bars would be omitted for clearer representation.

5.2. Effect of secondary air stream on dehumidification performance

The importance of secondary air stream to maximise dehumidification performance is investigated. The test rig was built and set up so that different operating case scenarios can be considered and a comparative analysis drawn.

5.2.1. Case a – air dehumidification with no secondary (shell side) air flow and no cooling period

In this test case, the air flow passage of the shell-side of the heat exchanger was blocked and the only process air from the environmental chamber was drawn through desiccant tubes (tube side of the heat exchanger). The process air was supplied from climate chamber at condition of high temperature and humidity (as found in tropical climates). For the adsorption cycle, the air temperature was set at 30°C and humidity ratio at 22.90 g/kg while the temperature of air for the regeneration cycle of the adsorbent was set at 120°C . Fig 5-3 shows the process air temperatures and humidity ratio at the inlet and outlet of the dehumidification system after a number of adsorption and regeneration cycles. It can be seen in Fig 5-3 that at the start of the adsorption cycle, following immediately from a regeneration cycle, the process air temperature was set to 30°C (T_{inlet} of the environmental chamber) and the humidity ratio (Y_{inlet}) at 22.90 g/kg . However, because of the residual heat stored in the air ducts and the heat exchanger, the air temperature at the inlet of the dehumidification system is increased to 84.5°C while its lowest temperature at the end of the adsorption cycle decreased to 41°C , which is still about 10°C above the ambient temperature.

Moreover, the outlet air temperature at the start of the cycle was about 58°C and decreased slowly reaching 48°C at the end of the cycle. This high inlet temperature of process air led to poor dehumidification effect, as can be seen from Fig 5-3. By the end of the adsorption cycle, the process air humidity ratio decreased to 19 g/kg, a mere 3.5 g/kg lower than the ambient air.

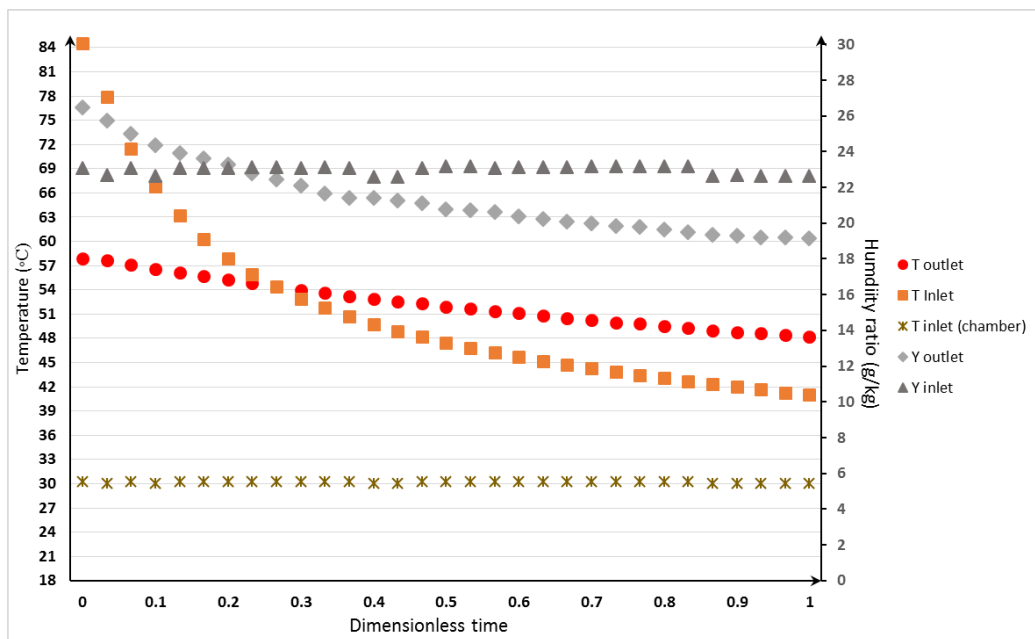


Fig 5-3 Case a - Primary air temperature and humidity ratio variation for dehumidification process ($T_{cyc}/2=5$ min, $v_p=11.02$ m³/h, $T_{inlet}=30^\circ\text{C}$, $Y_{inlet}=22$ g/kg)

Similarly, the regeneration cycle was performed using an electric heat source with temperature set to 120°C. However, due to heat losses along the air ducts, the initial regeneration air temperature was only about 64°C, increasing to 84°C by the end of the regeneration cycle to as the rig structure heated up, as shown in Fig 5-4. However, since the heat was only provided by the primary air, the heating of desiccant layer wasn't very effective, as reflected by the modest increase of outlet air temperature (around 11°C increase over the regeneration process). It was also observed that although desorption began soon after the start of the regeneration process, the outlet air humidity ratio only increased slightly during the process. The outlet air humidity ratio was only 3 g/kg higher compared to the inlet,

suggesting a low desorption effect, although this was also affected by the low adsorption during preceding process.

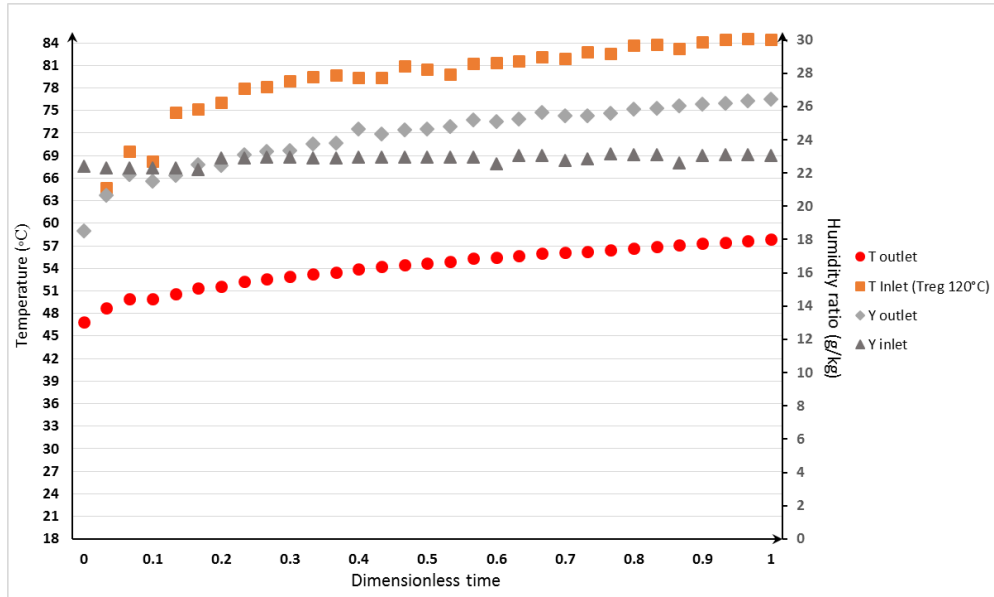


Fig 5-4 Case a - Primary air temperature and humidity ratio variation for regeneration process ($T_{Cyc}/2=5$ min, $v_p=11.02$ m³/h, $T_{inlet}=30^\circ\text{C}$, $Y_{inlet}=22$ g/kg)

5.2.2. Case b – air dehumidification with secondary (shell side) air flow and no cooling period

In this case, the effect of secondary air in the shell side was considered. The air valves (gates) for circulating secondary air through the shell side of the heat exchanger were opened. With similar operating conditions of temperature and humidity ratio as in Case a, Fig 5-5 show measured performance results. Likewise, in this test, there is no cooling down period between the dehumidification and regeneration process as the shown by high inlet air temperature ($T_{inlet}= 69^\circ\text{C}$) at the beginning of the process. Moreover, even though the inlet air temperature gradually decreased over time to around 42°C , the residual heat left inside the rig structure resulted in high outlet air temperature. The heat removal, aided by the secondary airstream, reduced the outlet air temperature to 49°C at the end of the dehumidification process.

Chapter 5: Results analysis and discussion

However, this still significantly higher than the ambient temperature and comparable in magnitude to that recorded in case a. Importantly, the introduction of secondary air, caused significant improvement in air dehumidification with process air outlet humidity ratio dropping to 15 g/kg, a decrease of 7 g/kg.

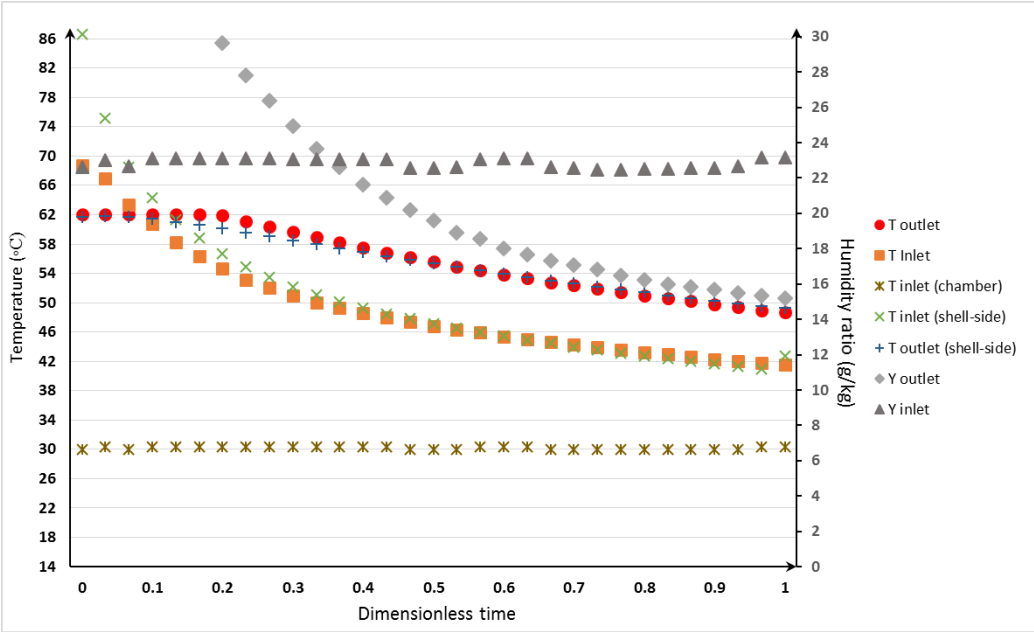


Fig 5-5 Case b - Primary air temperature and humidity ratio variation for dehumidification process ($T_{cyc}/2=5$ min, $v_p=4.07$ m³/h, $V_{secondary}=12.09$ m³/h, $T_{inlet}=30$ °C, $Y_{inlet}=22$ g/kg)

It can be observed from in Fig 5-6Fig 5-6 that the regeneration process in this case yields higher rate of moisture desorption. The outlet air humidity ratio increased considerably during the regeneration process, reaching 37 g/kg, which is 12 g/kg higher than the ambient. The secondary air cooling also contributed to faster start of desorption cycle. It is also shown that the outlet air temperature gradually increased from 48°C to over 60°C during the regeneration process while the desiccant tubes were heated by the secondary air stream.

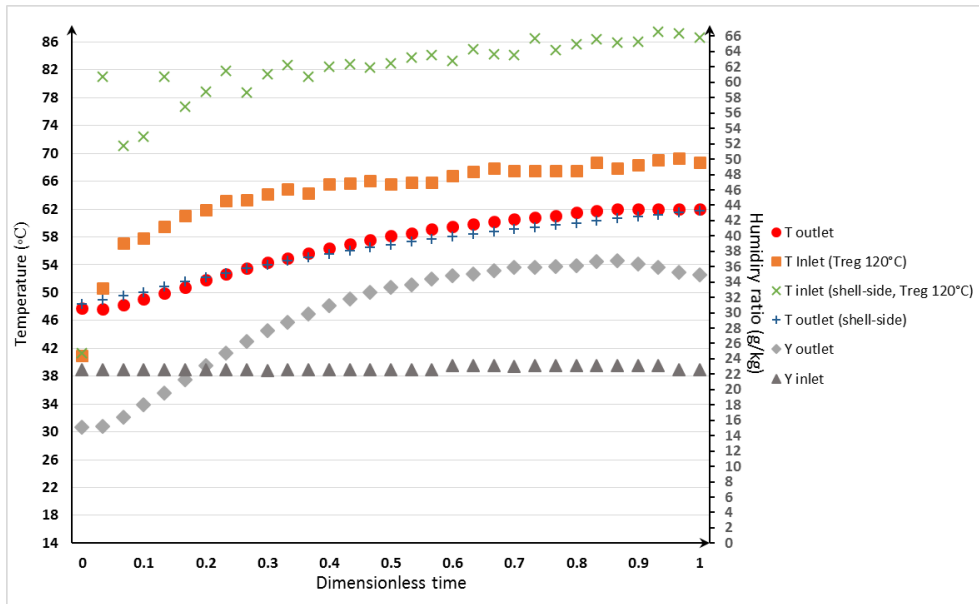


Fig 5-6 Case b - Primary air temperature and humidity ratio variation for regeneration process ($T_{cyc}/2=5$ min, $v_p=4.07$ m³/h, $V_{secondary}=12.09$ m³/h, $T_{inlet}=30$ °C, $Y_{inlet}=22$ g/kg)

5.2.3. Case c – air dehumidification with secondary (shell side) air flow and a cooling period

In this case, the regeneration cycle is followed immediately with a cooling down period, where the desiccant temperature is restored to its initial conditions before the start of the dehumidification cycle. With similar initial operating parameters as in previous cases (i.e., process air temperature T_{inlet} of 30 °C (from the environmental chamber) and humidity ratio, Y_{inlet} of 22 g/kg). The cooling period of the adsorbent was realised from the shell side only with ambient air at high flow rate (22 m³/h). The inlet gates for the tube side of the heat exchanger were blocked so that no moisture adsorption takes place during this period. The cooling of the system from the shell side also allows removing residual heat stored in the system ducts and tubes, cooling the solid desiccant after each regeneration cycle. The improved dehumidification performance is shown in Fig 5-7.

It can be seen that the temperature of the process air during dehumidification cycle continued to decrease until it reached 38°C at the end of the dehumidification process, which indicates that the heat of adsorption generated in the desiccant was effectively removed by the shell

side air flow. Similarly, the moisture adsorption is strong during the dehumidification period. At the start of the cycle, outlet air humidity ratio was as low as 13 g/kg, which is 9.5 g/kg lower than the ambient inlet. This rate of dehumidification was largely maintained with the air humidity ratio at the end of the process stabilising at 14 g/kg.

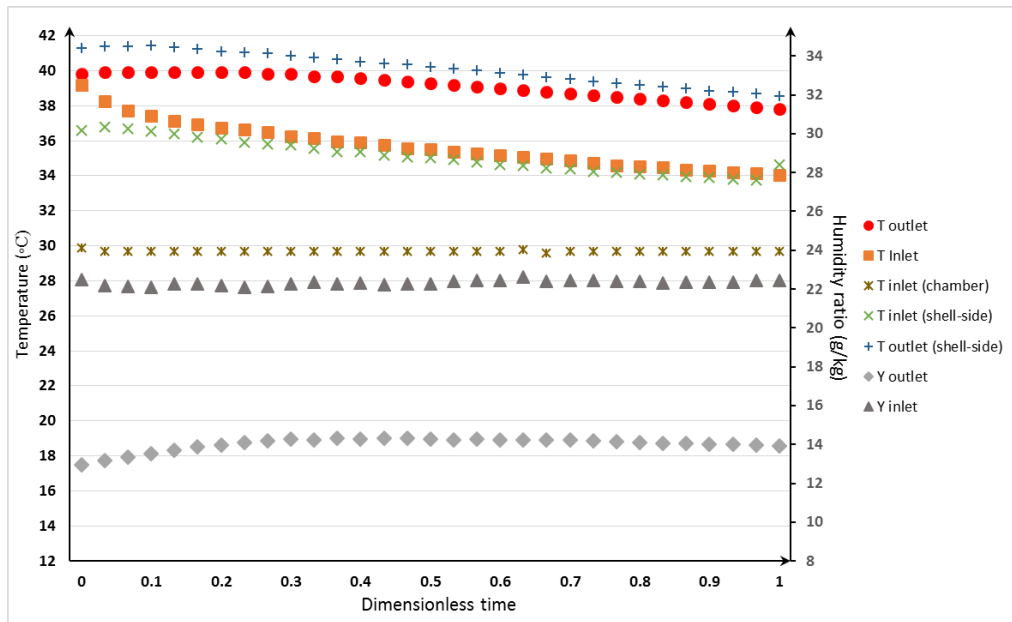


Fig 5-7 Case c - Primary air temperature and humidity ratio variation for dehumidification process

$$(T_{cyc}/2=5 \text{ min}, v_p=4.07 \text{ m}^3/\text{h}, v_{secondary}=12.09 \text{ m}^3/\text{h}, T_{inlet}=30^\circ\text{C}, Y_{inlet}=22 \text{ g/kg})$$

With regeneration process initiated immediately after the end of the dehumidification cycle, the system's ducts and metal parts were at a lower temperature than in Case (a) and Case (b). This means that regeneration air temperature at the inlet of the heat and mass exchanger is lower due to heat losses along the air ducts and heat storage in the metal parts.

As can be seen in Fig 5-8, the initial regeneration air temperature decreased from the set value of 120°C to 45°C at the inlet of the heat exchanger before climbing up again to 64.5°C as the system heat up. The heating of the desiccant tubes was also helped by the secondary air stream which inlet temperature increased from about 60°C to up to 84°C at the end of the regeneration cycle. As a result, the process air outlet temperature increased consistently over the duration of the regeneration process, increasing from 38°C to 55°C. it is interesting

Chapter 5: Results analysis and discussion

to see that as the air is introduced into the desiccant tube for regeneration there is some moisture adsorption process taking place before this reversed. It was also observed that the rate of regeneration of the desiccant increased throughout the regeneration process; reaching 36 g/kg at the end of the cycle that is 13 g/kg higher compared to the inlet.

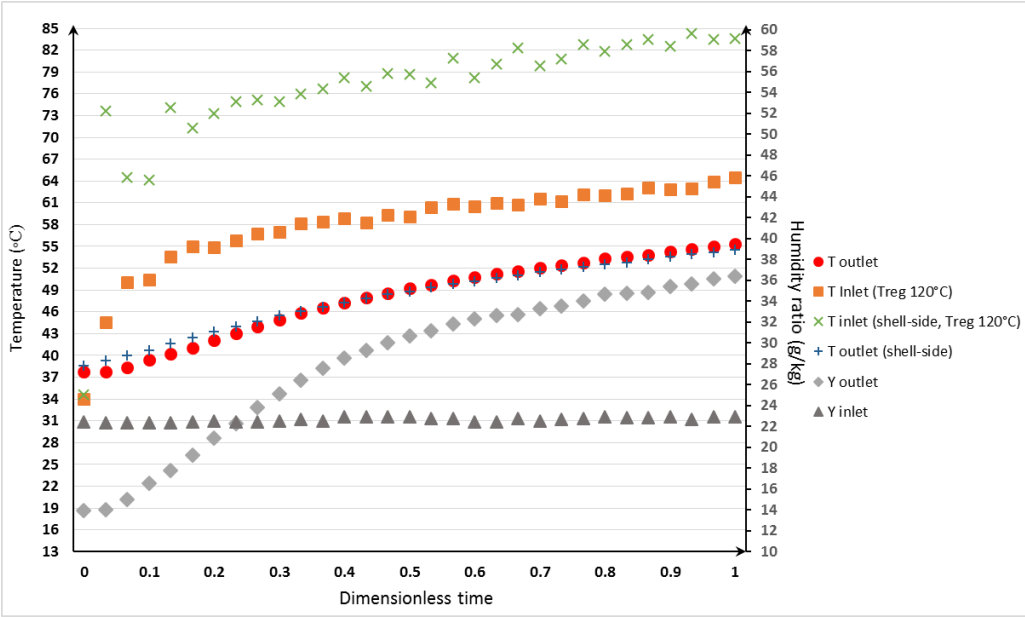


Fig 5-8 Case c - Primary air temperature and humidity ratio variation for regeneration process ($T_{cyc}/2=5$ min, $v_p=4.07$ m³/h, $v_{secondary}=12.09$ m³/h, $T_{inlet}=30^{\circ}C$, $Y_{inlet}=22$ g/kg)

5.2.4. Comparative analysis

The tested three design scenarios were compared and a summary of the performance data is presented in Fig 5-9. The figure shows that under the same ambient conditions of temperature ($T_{inlet}=30^{\circ}C$ and humidity ratio ($Y_{inlet}=22$ g/kg) the performance of the three cases is greatly affected by the way the adsorbent is regenerated and cooled. It can be seen for example that Case (b) had the worst performance. This can be explained by increased heat storage in the shell of the heat exchanger compared for example to case (a) where the shell void was closed. For example, the Dehumidification Coefficient of Performance (DCOP) in Case (b) is very poor (0.03) compared to case (a) of 0.15. Likewise, the dehumidification capacity (DC) of Case (b)

is lower than that of Case (a) standing at 2.5 and 10 g/h respectively. On the other hand, significant performance improvement was observed in Case (c). The introduction of the cooling period at the end of each regeneration process helped improve all performance indices. For example, the DCOP, DC and efficiency increased fourfold.

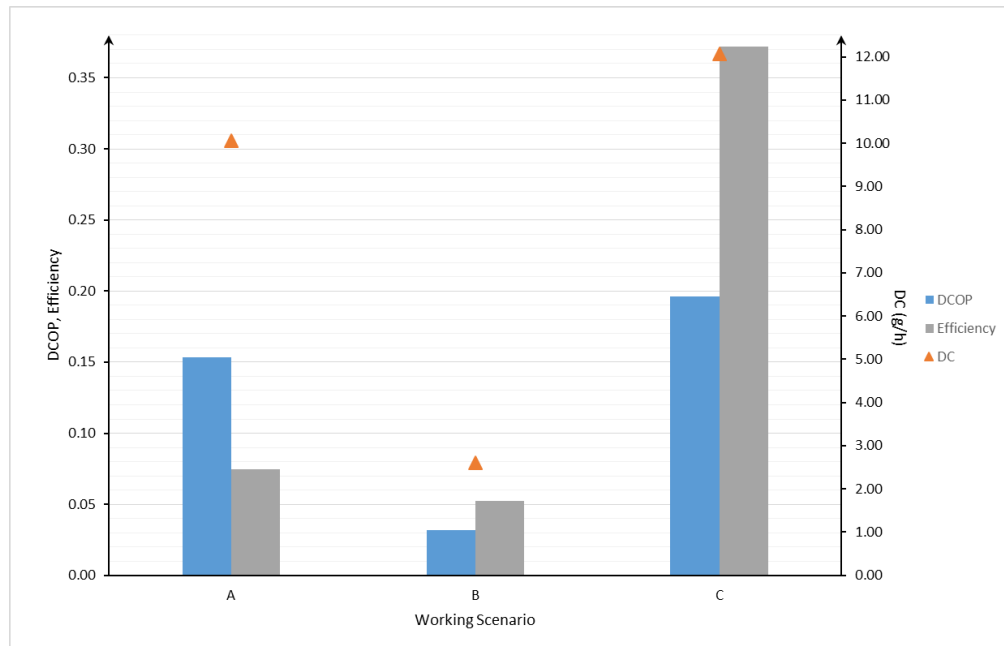


Fig 5-9 Dehumidification performance for different types of working cycle

5.3. Parametric analysis

Form the test results presented in the previous section, it is apparent that a cooling period between the dehumidification and regeneration cycle is required for high performance. A parametric analysis was conducted to evaluate the effect of airflow rate, regeneration temperature, and inlet air humidity ratio.

5.3.1. Effect of airflow rate

For this study, three different airflow settings were compared by adjusting the airflow rate through the desiccant tubes while maintaining the shell side flow rate roughly constant. Three

Chapter 5: Results analysis and discussion

flow rates were considered both for dehumidification and regeneration cycle. In all tests the inlet process air temperature and humidity ratio were held constant at about 30°C and 22 g/kg respectively while the regeneration temperature set to 120°C. The resulting airflow rate as well as temperature and humidity profile is presented in Table 5-2 for each case.

Table 5-2 Measured air conditions for different airflow settings

Parameter	Flow rate 1		Flow rate 2		Flow rate 3	
	D	R	D	R	D	R
Process air flow rate (m ³ /h)	4.07	4.07	5.77	5.77	4.07	5.77
Shell-side flow rate (m ³ /h)	12.01	12.01	13.85	13.85	12.01	13.85
Process air inlet temperature (°C)	35.61	58.67	36.17	64.62	36.84	65.32
Process air outlet temperature (°C)	39.12	48.24	40.25	51.62	40.70	51.03
Process air inlet humidity (g/kg)	22.32	22.66	22.57	22.67	22.53	22.48
Process air outlet humidity (g/kg)	14.06	28.56	13.42	29.41	13.08	27.99
Shell-side inlet air temperature (°C)	35.07	77.85	35.43	78.79	36.03	79.12
Shell-side outlet air temperature (°C)	40.11	48.26	40.87	50.91	41.76	51.53

It can be seen from Table 5-2 that the lowest outlet air humidity and biggest humidity ratio drop during dehumidification was found in flow rate 3. This indicates that, even with slightly higher temperature, moisture adsorption was more effective in lower process air velocity. With higher airflow rate, regeneration was more effective as the rig structure was heated faster and is reflected with higher regeneration inlet air temperature), resulting in better dehumidification. Fig 5-10 shows that the highest DCOP and DC or 0.26 and 19 g/h respectively were obtained with flow rate case 2, while the highest efficiency of 0.42 was achieved in case of flow rate case 3.

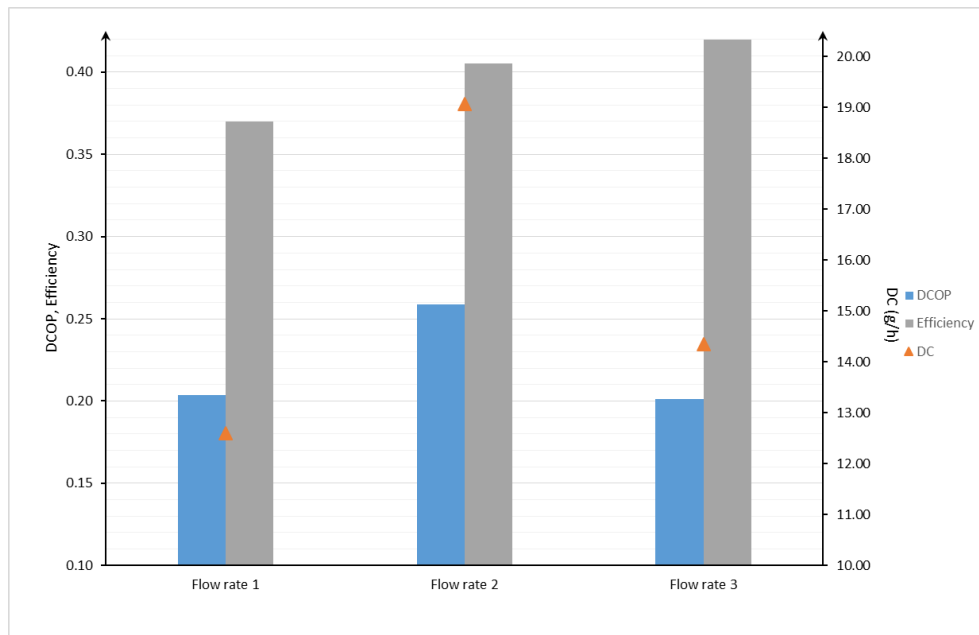


Fig 5-10 Dehumidification performance with different flow rates

5.3.2. Effect of regeneration temperature

The effect of moisture desorption during regeneration on dehumidification performance was further analysed by varying the regeneration temperature set value of the heater from 120°C to 140°C, while airflow rate and climate chamber setting were kept identical to that of flow rate 1 in the previous study. Table 5-3 presents the average air temperature and humidity entering and exiting the rig for three different heater set values.

Table 5-3 Air temperature and humidity profile for different regeneration temperature set values

Parameter (average)	Treg=120°C		Treg=130°C		Treg=140°C	
	D	R	D	R	D	R
Process air inlet temperature (°C)	35.61	58.67	35.79	58.88	35.31	87.32
Process air outlet temperature (°C)	39.12	48.24	39.76	51.19	41.28	50.99
Process air inlet humidity (g/kg)	22.32	22.66	22.19	22.13	22.27	22.33
Process air outlet humidity (g/kg)	14.06	28.56	12.11	29.17	11.64	30.11
Shell-side inlet air temperature (°C)	35.07	77.85	35.08	81.70	35.31	87.32
Shell-side outlet air temperature (°C)	40.11	48.26	40.59	49.57	41.28	50.99

Chapter 5: Results analysis and discussion

As expected, desorption effect increased with higher regeneration temperature. Consequently, the lowest process air outlet humidity (up to 17% lower than in the other cases) was achieved with highest regeneration temperature. On the other hand, process air temperature during dehumidification process was kept low thanks to the cooling period. In all three cases, inlet air temperature was maintained at round 35°C, with slight increase at the outlet (less than 6°C). This indicated that higher dehumidification performance could be achieved with higher regeneration temperature, allowing more moisture to be desorbed, thus higher moisture removal during dehumidification process. This was also confirmed with improved DC and efficiency as regeneration temperature increased (Fig 5-11).

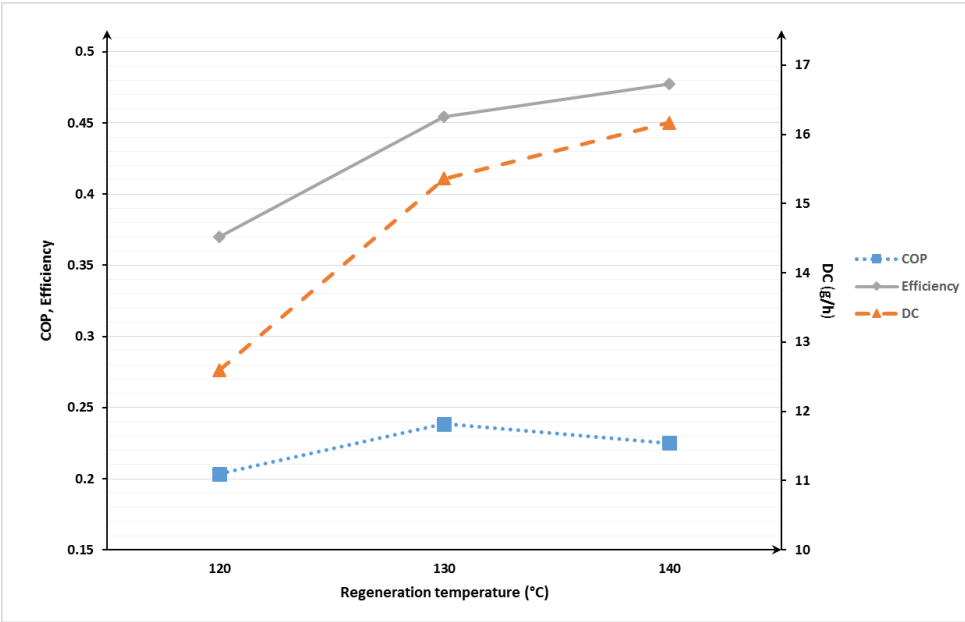


Fig 5-11 Dehumidification performance with varied regeneration temperature

When regeneration temperature was increased from 120°C to 140°C, DC and efficiency was improved by about 28%. Less significant effect was found on DCOP (around 10% increase). However, it was also observed that as temperature was increased from 130°C to 140°C, DCOP actually lowered by 5.62%. On the other hand, improvement on DC and efficiency by about 5% was also less significant compared to when regeneration temperature was increased from 120°C to 130°C (up to about 22% improvement in dehumidification performance). This

indicated that increase of energy required for heating and regeneration was more significant than the gain in dehumidification power, as reflected by the lowered DCOP.

5.3.3. Effect of inlet air humidity

In this study, effect of inlet air humidity was analysed by comparing 3 air humidity setting of the climate chamber from 60% RH to 80% RH. Temperature was kept at 30°C while airflow rate and regeneration temperature settings from the previous study were adopted. Table 5-4 shows the temperature and humidity profile for different inlet air humidity set values.

Table 5-4 Measured air conditions for different inlet humidity set values

Parameter (average)	60% RH		70% RH		80% RH	
	D	R	D	R	D	R
Process air inlet temperature (°C)	35.01	59.97	35.26	57.53	35.61	58.67
Process air outlet temperature (°C)	38.34	48.55	38.76	48.23	39.12	48.24
Process air inlet humidity (g/kg)	17.50	17.66	19.90	19.86	22.32	22.66
Process air outlet humidity (g/kg)	10.31	23.12	11.75	24.99	14.06	28.56
Shell-side inlet air temperature (°C)	34.63	77.42	34.83	76.50	35.07	77.85
Shell-side outlet air temperature (°C)	38.91	47.78	39.46	47.62	40.11	48.26

During dehumidification process, the lowest outlet air humidity at 10.31 g/kg was found with the climate chamber setting of 60% RH, while higher value at the outlet was observed for higher RH set values. The outlet humidity of 14.06 g/kg achieved with 80% RH set value was about 36% higher than in the first case. This indicated the dehumidifier worked best at lower inlet humidity if outlet air humidity was required to be as low as possible. This is also shown with the highest efficiency achieved with the lowest inlet air humidity (Fig 5-12). However, higher DC was actually achieved with higher RH set value.

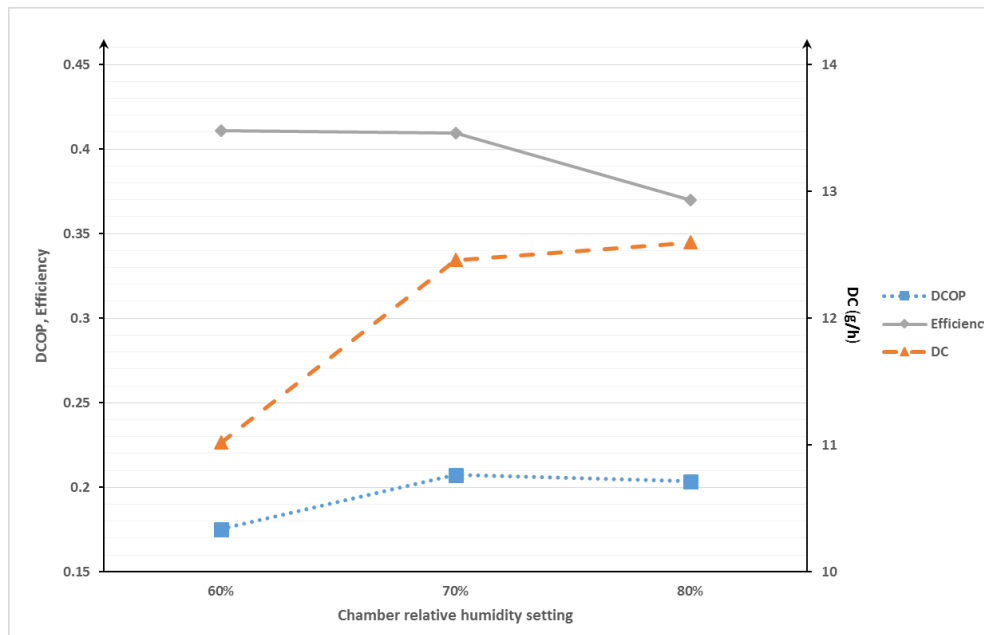


Fig 5-12 Effect on inlet air humidity on dehumidification performance

The calculation of DC put more emphasis on humidity drop rather than the value at the outlet. The humidity drop was higher as the driving force was stronger with higher inlet air humidity. In this case, DC was found to be highest with 80% RH set value. This was also reflected on the DCOP, even though DCOP dropped a little when inlet set value was increased from 70% RH to 80% RH, indicating that moisture desorption was more effective with the lower air humidity. The reduction, however, was less than 2%. With the performance indices concerned, the 70% RH test conditions gave the best overall results with considerable improvement on DC and DCOP over the lower inlet set value, while the efficiency on both cases was more or less equal.

5.4. Simplified energy assessment

The energy saving potential of the dehumidifier compared to common air dehumidification technology such as vapour compression (thermal condensation) system could be evaluated. For this purpose, the heating energy for desiccant regeneration of the shell-tube dehumidifier was compared with electrical energy required by the vapour compression system to achieve the same amount of moisture removal. While the regeneration heating energy of the

Chapter 5: Results analysis and discussion

dehumidifier can be calculated based on the experimental results (for example from Table 5-3), the electrical energy of the vapour compression system can be estimated using assumed COP value while also taking into account that air dehumidification is achieved by over-cooling the air below its dew-point followed by re-heating. Assuming electrical COP of 2 for a traditional vapour compression system in hot climate [65], the simplified energy assessment under similar working condition is presented in Table 5-5.

Table 5-5 Simplified energy assessment of the dehumidifier prototype

	Vapour compression	Shell-tube desiccant	Shell-tube desiccant (60% solar assisted)
Ambient air temperature (°C)	35.61	35.61	35.61
Ambient air humidity (g/kg)	22.32	22.32	22.32
Supply air humidity (g/kg)	14.06	14.06	14.06
Air flow (kg/h)	4.07	4.07	4.07
Energy consumption (kWh)	248.09	419.01	167.60
Energy saving/loss	-	40.79% (loss)	32.45% (saving)

It can be seen that under similar working condition, the dehumidifier would consume more energy than vapour compression system. This was due to its low COP, which was mainly affected by the heat storage issues of the dehumidifier rig, limiting its adsorption and desorption rate. Also, the higher energy consumption compared to vapour compression air conditioning systems is a common case for electricity driven desiccant systems [16]. On the other hand, one of the interests of desiccant-based dehumidification systems is the possibility of various heat sources for desiccant regeneration. For example, if regeneration heat can be provided by solar energy, the dehumidifier energy efficiency could be considerably increased. With the assumption that solar energy can provide up to 60% of regeneration heat, the dehumidifier could achieve around 30% energy saving compared to traditional systems. It can also be noted that by addressing the heat storage problem, dehumidification performance would be substantially improved, thus even higher energy saving potential.

5.5. Mathematical model refinement

The results and experience gained from testing the prototype rig could be used to improve the mathematical model. One significant finding was the thermal mass of the rig structure, which greatly affect the dehumidification performance, especially if the desiccant tubes weren't sensibly cooled after regeneration process. If it takes considerable amount of times to bring down the rig to optimal working temperature, the moisture adsorption may not begin immediately after the start of dehumidification process (i.e. desiccant still desorb moisture).

Although the adsorption/desorption process described in the developed mathematical model has been validated, the model considered a simpler concentric channel configuration, with the assumption that heat transfer takes place only between the air stream and the desiccant layer. Thus, improvement could be made to better represent the heat transfer especially in the secondary channel, as the air exchanges heat not only with the desiccant, but also the shell structure. The following equations were modified / added as the first step to make the mathematical model more relevant to the prototype:

5.5.1. New energy balance for secondary air stream

The updated heat transfer equation for the secondary air stream will also consider the convective heat exchange between the air and shell-side surface, presented as follow:

$$\rho_a c_{pa} A_{oc} \left(\frac{\partial T_{aoc}}{\partial t} + u_{aoc} \frac{\partial T_{aoc}}{\partial x} \right) = h_{oc} p_{od} (T_{sd_{oc}} - T_{aoc}) + h_{oc} p_{sh} (T_{sh} - T_{aoc}) \quad (5.6)$$

Where p_{sh} is the perimeter of shell-side channel [m], and T_{sh} is the surface temperature of the channel [K].

5.5.2. Energy balance for the shell-side surface

The temperature change over time of the outer channel surface is described by the following equation:

$$\rho_{sh} c_{psh} V_{sh} \frac{\partial T_{sh}}{\partial t} = h_{oc} p_{sh} L (T_{a_{oc}} - T_{sh}) \quad (5.7)$$

Where ρ_{sh} is the density of the shell-side channel [kg m⁻³], c_{psh} is specific heat of air [J kg⁻¹ K⁻¹], V_{sh} is the volume [m³], and L is the channel's length [m]. It is assumed that convection is the dominant heat transfer mode, thus heat conduction is neglected. The temperature change of the surface along air flow can be reflected by coupling with equation (5.6). Boundary conditions from the previous model were attained.

5.5.3. Discretization of the new equations

The updated energy balance for the secondary air stream (equation (5.6)) is discretised with the same numerical method applied to equation (3.1), resulting the following equations:

$$T_{a_{(oc)_i}^{k+1}} = \frac{1}{1+\alpha_{oc}} \left(T_{a_{(oc)_i}^k} + \alpha_{oc} T_{a_{(oc)_{i-1}}^{k+1}} + \beta_{oc} (T_{sd_{(oc)_i}^k} - T_{a_{(oc)_i}^k}) + \beta_{ocsh} (T_{sh_i}^k - T_{a_{(oc)_i}^k}) \right) \quad (5.8)$$

Where $\beta_{ocsh} = \frac{h_{oc} p_{sh} \Delta t}{\rho_a c_{pa} A_{oc}}$.

The energy balance for the outer channel surface equation (5.7) is discretised as follows:

$$\rho_{sh} c_{psh} V_{sh} \frac{(T_{sh_i}^{k+1} - T_{sh_i}^k)}{\Delta t} = h_{oc} p_{sh} L (T_{a_{(oc)_i}^k} - T_{sh_i}^k) \quad (5.9)$$

Thus

$$T_{sh_i}^{k+1} = T_{sh_i}^k + \beta_{sh} (T_{a_{(oc)_i}^k} - T_{sh_i}^k) \quad (5.10)$$

Where $\beta_{sh} = \frac{h_{oc} p_{sh} L \Delta t}{\rho_{sh} c_{psh} V_{sh}}$.

5.5.4. Results of updated model

Operating parameters of the computer model were updated based on the feedback from the test rig and are presented in Table 5-6. The shell material was assumed to be aluminium.

Table 5-6 Operating parameters for the updated computer model

Parameter	Unit	Value
Length of channel, L	m	0.3
Desiccant thickness, δ	mm	1
Hydraulic diameter outer channel, Dh_{oc}	mm	5
Hydraulic diameter inner channel, Dh_{ic}	mm	5.1
Shell-side channel's thickness	mm	1
Air velocity (both channels), u_{ic}, u_{oc}	m/s	1.2
Inlet moisture ratio of air, $Y_{p,inlet}, Y_{r,inlet}$	kg/kg _{da}	0.020
Process & cooling air inlet temperature, $T_{p,inlet}, T_{c,inlet}$	°C	30
Regeneration & heating air temperature, $T_{r,inlet}, T_{h,inlet}$	°C	80
Adsorption time, t_{ad}	s	300
Regeneration time, t_{reg}	s	300

Fig 5-13 shows that at the beginning of dehumidification process, the desiccant was still desorbing moisture, as reflected by the higher outlet air humidity compared to the inlet. After the preceding regeneration process, desiccant was at high temperature and slowly cooled down during the dehumidification process (Fig 5-14 and Fig 5-15). The moisture desorption continued for around 30 seconds after the beginning of dehumidification, during which outlet air humidity gradually lowered as temperature decreased, and after which the desiccant along the channel began adsorbing moisture from the air. This was significantly different from the previous model, where dehumidification began almost immediately after the end of regeneration process (Fig 3-15). Other important difference can be observed on how outlet air temperature change over time. With the previous model, outlet air temperature dropped to 45°C during one minute of dehumidification process (Fig 3-15), while it took longer in the updated model to reach the same temperature (Fig 5-14).

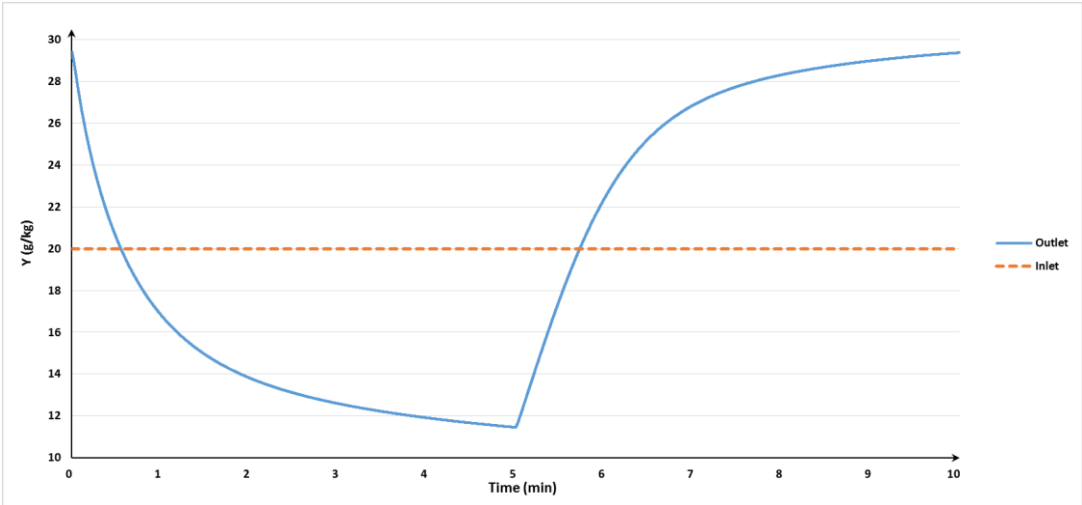


Fig 5-13 Humidity ratio of primary air stream (dehumidification and regeneration process)

While desiccant amount in the current model was significantly higher, the slower cooling rate of the desiccant during dehumidification was also affected by the heat transferred from the shell-side surface to the secondary air. As shown in Fig 5-15, the secondary air outlet temperature was always higher than the outlet temperature of the primary air, indicating that the secondary air gained more heat across the outer channel compared to the primary air. This affected the heat removal from the desiccant, which consequently also affected the dehumidification rate. Fig 5-13 and Fig 5-14 also show that outlet air humidity continued to decrease with time as outlet temperature decreased. It was observed that the decrease of outlet air temperature was more important at the beginning of dehumidification process, and became less significant as more moisture removed from the air stream. The lowest outlet air humidity and temperature at 11.45 g/kg and 41.96°C was actually achieved at the end of dehumidification process, indicating more moisture can be adsorbed if the heat from the desiccant can be removed more effectively.

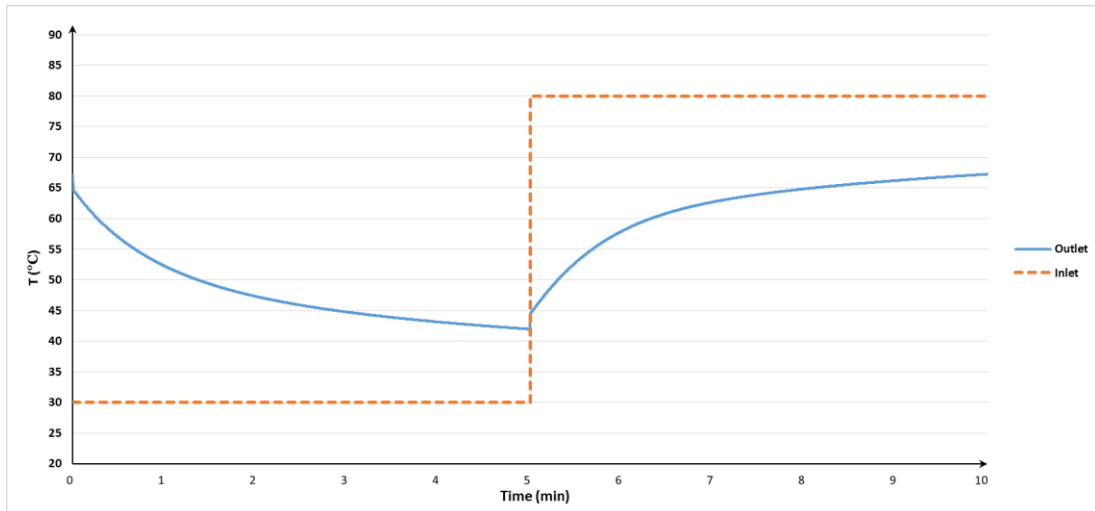


Fig 5-14 Temperature of primary air stream (dehumidification and regeneration process)

Similar to the dehumidification process, the desiccant was still adsorbing moisture from the air at the beginning of the regeneration process. It can also be observed that dehumidification effect decreased significantly as desiccant temperature increased (reflected with increase of outlet air temperature). After around 40 seconds, adsorption could be considered negligible as air exit at higher humidity compared to its inlet condition. As time progress, more moisture was desorbed with increase of temperature. Highest outlet air temperature and humidity at 67.24°C and 29.37 g/kg was achieved at the end of regeneration cycle. The DCOP, DC, and efficiency achieved with the operating parameters was 0.11, 0.17 g/h, and 0.27 respectively. Overall, the results of the updated mathematical and computer model indicated the importance of cooling/heating of the desiccant on dehumidification performance. The new model also reflected the findings from the test rig, especially related to the heat storage of rig structure. More update can be considered to further improve the model, and will be explained in the next chapter.

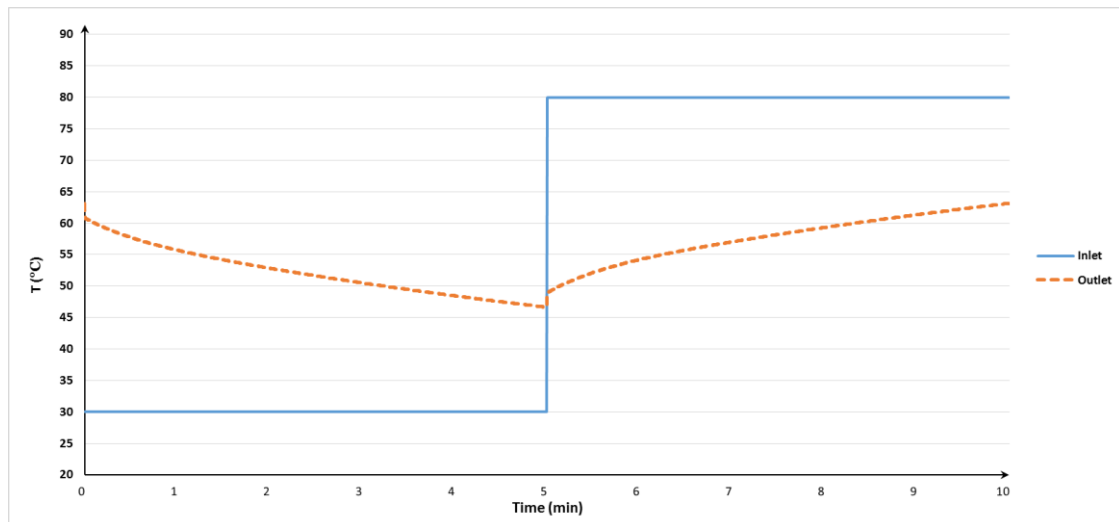


Fig 5-15 Temperature of secondary air stream (dehumidification and regeneration process)

Although the updated model results can't be directly compared with the experimental result since their operating conditions differs (especially the inlet air temperature), the observed behaviour is still comparable. Fig 5-16 shows comparison of the process air humidity ratio between the simulation results with experimental results of Case B from the previous section. It can be seen the outlet air humidity variation over the dehumidification period are comparable between the simulation and experimental results. In both cases, outlet air humidity was still higher than the inlet at the beginning of the dehumidification process. Then, as desiccant temperature decreased, outlet air humidity ratio also decreased and became lower than the inlet after a while. Moreover, it is also shown that the lowest outlet humidity ratio was achieved at the end of dehumidification. Therefore, it can be assumed that the refined mathematical model was able to predict the heat storage problem in the rig structure and its effect on dehumidification effectiveness. The discrepancy between the experimental data and the simulated results were between 14-32%. It should also be noted that the simulation assumed constant inlet air conditions and did not replicate the inconsistent inlet air temperature throughout dehumidification and regeneration process (due to the thermal mass of the rig structure).

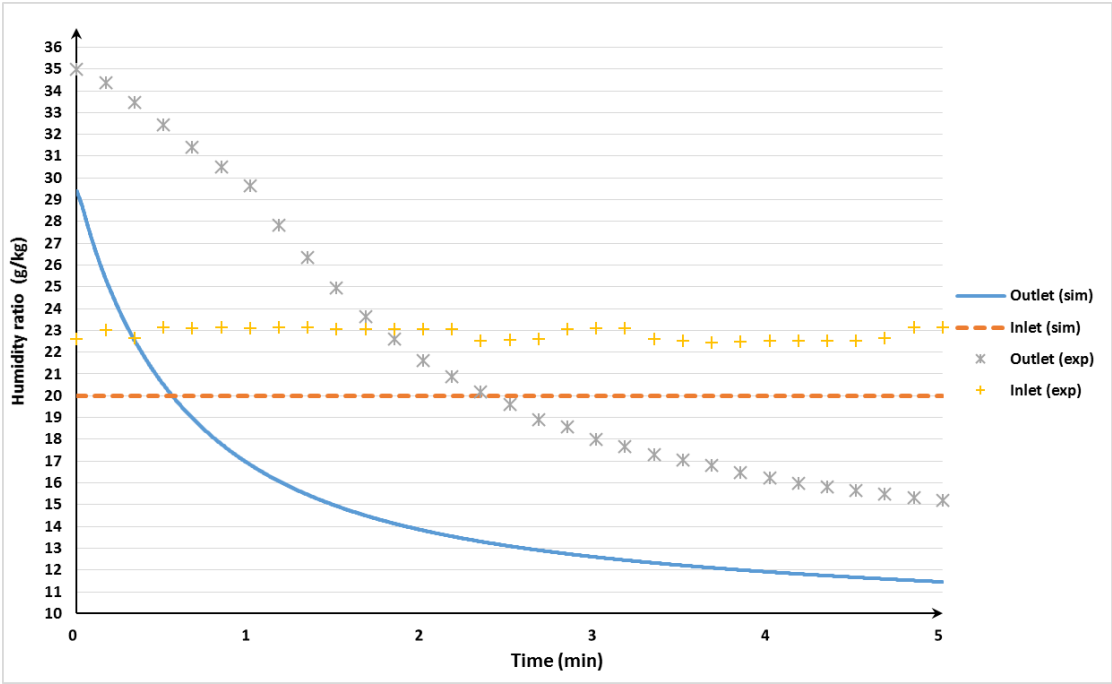


Fig 5-16 Air humidity ratio - comparison between simulation and experimental results

5.6. Summary

The experimental results of a laboratory prototype air dehumidification system were evaluated and analysis. This include presenting measured performance data of temperature, humidity ratio and flow rate variation for the dehumidification and regeneration cycle. In addition, results of three case design scenarios were presented in which it was demonstrated the importance of the secondary airflow to improving the dehumidification performance of the system.

Commonly, a solid desiccant air dehumidification consists of continuously switching between dehumidification and regeneration process. In this work, a secondary air flow was used to introduce a cooling period to help remove heat stored in the system components as well as heat of adsorption of the desiccant. It was shown that the proposed configuration could effectively reduce the process air humidity ratio significantly when kept at near ambient temperature during the adsorption process.

The effect of secondary airstream was further confirmed when different working scenarios was tested (cycles without secondary air and cycles with secondary air but without cooling period). It was shown that the working cycles without proper heat removal suffered from low dehumidification effect, mainly due to high temperature which limit desiccant layer moisture adsorption rate. It was also observed that working cycle with both secondary air stream (Case c) and cooling period achieved the highest performance number, and significantly higher than other tested working scenarios. For example, the efficiency achieved in case C was over 4 times higher than the two other cases.

The air dehumidification arrangement was also tested in various operating conditions for system optimisation. When comparing different airflow rate settings, it was observed that highest coefficient of performance (DCOP) and dehumidification capacity (DC) was achieved with higher airflow. Increase on DC with higher airflow was particularly observed, with improvement up to 50% compared to other cases with lower airflow during dehumidification process. This indicate more effective heating during regeneration and better heat removal was advantageous for system performance. However, highest dehumidification efficiency was achieved with mixed air flow setting, indicating moisture adsorption rate was more efficient under lower process air velocity. When tested under identical ambient air conditions and air flow, the dehumidifier achieved higher DC and efficiency (over 20% improvement) with higher regeneration temperature set value. However, it was also observed that effect on DCOP was less significant, as improvement achieved during air dehumidification was balanced by the higher heating energy for desiccant regeneration. Last but not least, different inlet air humidity ratios were also tested to evaluate system performance under various climate conditions. It was shown that DCOP and DC increased as inlet air humidity increased, as driving force for mass transfer between air stream and desiccant layer also increased. However, lower outlet air humidity ratio was actually achieved with lower inlet air humidity. This was also reflected by decrease in dehumidification efficiency with higher inlet air humidity.

One of the feedback gained from the test rig was heat storage in the rig structure, causing delay in moisture adsorption during dehumidification process, and inversely, delay in moisture

desorption during regeneration process. This was particularly true when cooling period wasn't included in the working cycles. This finding was considered for mathematical model refinement. Heat balance of shell-side casing was added to better represent the experimental conditions, while secondary air heat balance was updated to include heat exchange with the shell-side surface. The new simulation results showed that the updated model was able to predict the delay in moisture adsorption and desorption in respective process. Moreover, the increase of dehumidification over time as desiccant temperature decreased as shown in the updated simulation results also confirmed the finding from the experimental rig. Although the testing conditions of the dehumidifier rig weren't fully recreated with the new model, it was demonstrated that the system behaviour represented by the simulation agrees well with measured testing results. Thus, it can be assumed that the update was able to increase the model relevancy with the prototype, while further improvement could be considered in future works.

Chapter 6: Conclusion and future work

6.1. Conclusions

In this research project, a new air dehumidification arrangement was designed, modelled and a laboratory scale prototype was tested. The solid desiccant air dehumidification system used a shell-tube heat and mass exchanger configuration that allows indirect cooling/heating of the adsorbent through the shell side of the heat exchanger. The design offered an effective solution to the problem of removing heat of adsorption and residual heat of the regeneration process. The main results and achievements of this research project can be summarised as follows:

6.1.1. Contribution

The key contributions of this research work can be summarised as follow:

- i. The novel design of solid desiccant air dehumidification with air-to-air, shell-tube heat and mass exchanger configuration. This arrangement allows removal of adsorption heat as well as residual heat commonly encountered in common configuration such as honeycomb rotary desiccant wheel. When compared to other internally cooled solid desiccant systems, the use of air as secondary wheel reduces the complexity of the system, while use of both primary and secondary air to provide heat during regeneration exploits the full capabilities of the shell-tube arrangement. Another novel feature proposed in this work is the way the desiccant adhered onto the inner surface of the primary air channels. By using wired mesh to hold the desiccant particles in place instead of using adhesives commonly used in other works, heat transfer resistance between the secondary air and the desiccant can be minimised. This

- arrangement can ensure effective adsorption and desorption processes, thus improve system performance.
- ii. Complex mathematical formulation of the governing heat and mass transfer balance equation and MATLAB computer model were developed for system optimisation. The mathematical model was based on various model previously introduced by other researchers. The model combined the advantages of other models it based on, such as 2-D consideration for heat and mass transport phenomena inside the desiccant layer, while temperature and moisture gradient of the air stream was considered in the flow direction only to avoid over complication. Moreover, the heat balance of the secondary air was also considered, which was an improvement compared to other works where the temperature in the secondary channels were assumed to be constant. With proper adjustment on the secondary air heat balance, this model could provide a good basis for various internally cooled desiccant systems.
 - iii. A laboratory scale prototype was built and tested in order to demonstrate the viability of the proposed concept. The constructed rig also confirmed the feasibility of using wire mesh to adhere desiccant particles inside an air passage. The copper mesh used in this study was able to properly hold the desiccant in place while also allowed moisture to pass through to achieve air dehumidification and desiccant regeneration. Furthermore, the rig arrangement allowed the introduction of an intermediary period between the end of regeneration and the resume of dehumidification process. In this "cooling period", air is pass through only the shell-side channel. This allows removal of residual heat from regeneration process without using primary air stream. As the secondary air does not have direct contact with desiccant particles, the desiccant heat can be removed effectively without adding moisture. Thus, dehumidification process can be performed with the desiccant at low temperature and water content, allowing higher adsorption rate and dehumidification performance.

6.1.2. The main findings

The main findings of the experimental and computer modelling can be summarized as follows:

- i. Mathematical model was specifically developed for solid desiccant air dehumidifier with concentric channels and counter flow configuration. The complex heat and mass transfer equations were solved using implicit scheme finite difference method, and computer algorithm was developed as MATLAB codes to conduct simulations.
- ii. The computer model was applied to a desiccant wheel for validation using published experimental data. The low discrepancy (3%) between the computer model and experimental results of air temperature and humidity ratio gave high confidence that the computer model was able to predict the heat and mass transfer inside the desiccant filled air channel.
- iii. Theoretical results were obtained by performing simulations using developed computer model to assess system performance. With ambient air temperature of 32°C and humidity of 20 g/kg, regeneration temperature of 80°C, and air velocity of 2.5 m/s, the air dehumidification performance of the concentric channel (CC) configuration was compared to adiabatic single channel (SC) configuration. The resulting COP ranged from 0.41 to 0.9, while DC ranged between 0.61 – 0.9 g/h and efficiency range of 0.3 - 0.4. It was found that, when compared to the SC system, the CC configuration was able to achieve: 15% lower outlet average air temperature and humidity ratio during dehumidification process, 15% improvement on DC and dehumidification efficiency, and 35% increase in COP. It was also found that improved heating would allow shorter regeneration time or lower regeneration temperature while maintaining reasonable performance.
- iv. Several parametric studies were also performed using the computer model. Three main parameters were varied: channel length, air velocity, and cycle time.
 - o Simulations with various channel length ranging from 8 to 28 cm were conducted, and it was found that DC ranged between 3.12 and 3.53 g/h,

efficiency ranged from 0.38 to 0.43, while COP ranged from 0.77 to 0.87. It was also observed that 20 cm was the optimum length for DC and efficiency, while COP decreased as length increased.

- With air velocity varied between 1 to 3 m/s, it was found that DC ranged between 1.45 and 4.51 g/h, efficiency ranged from 0.35 to 0.45, and COP ranged from 0.78 to 0.87. It was also reported that DC increased significantly with higher airflow, while impact on COP was less important. However, efficiency dropped with higher air velocity.
 - With total cycle length varied from 60 s each to 360 s, it was found that DC ranged between 2.27 and 3.41 g/h, while efficiency ranged from 0.28 to 0.42 and COP ranged from 0.76 to 0.94. It was also observed while higher COP was achieved for longer cycle time, shorter cycle time was preferable for higher DC and efficiency.
- v. Experimental test rig was designed and fabricated. The desiccant tubes were prepared by inserting rolled copper mesh and filling the gap between the mesh and tube's internal surface with desiccant powder. To minimise powder leakage, sieving process was performed to separate the very fine desiccant particulate. The assembled test rig was tested under various operating conditions. Several limitations were observed during testing, such as desiccant leakage risk, heat loss during regeneration, temperature measurement limits, and residual heat from preceding regeneration process.
- vi. With ambient air temperature of 29.74°C and humidity ratio of 22.5 g/kg supplied from climate chamber under constant flow rate of 4.07 m³/h through the tube-side channel and 12.09 m³/h through the shell-side, and regeneration temperature set value of 120°C, the dehumidifier was able to achieve, process air average outlet humidity ratio of 14.06 g/kg and average outlet temperature of 39.12°C, COP of 0.2, DC of 12.6 g/h, and efficiency of 0.37.

- vii. The importance of heat removal by secondary air stream was demonstrated. Compared to other cases without using secondary air stream, the properly cooled dehumidifier was able to achieve COP, DC and efficiency more than 4 times higher.
- viii. Several operating parameters were tested for parametric studies of the dehumidifier prototype:
 - With three different airflow settings (Setting 1, 2, and 3), the DC varied from 12.6 to 14.35 g/h, COP ranged 0.2 to 0.26, while efficiency ranged from 0.37 to 0.42. It was particularly noted that compared to setting 1, DC improved by 50% with setting 2. It was also indicated that moisture adsorption was more efficient under lower air velocity.
 - When regeneration temperature set value was increased from 120°C to 140°C, it was reported that DC increased from 12.6 to 16.17 g/h, COP increased from 0.2 to 0.22, and efficiency improved from 0.37 to 0.48. However, COP decreased as regeneration temperature set value was increased from 130°C to 140°C, indicating that improved dehumidification effect was balanced by higher required energy for regeneration.
 - When comparing three different climate chamber air RH set value (60%, 70%, 80%), it was found that DC increased from 11.02 to 12.6 g/h as inlet humidity increased, while impact on COP was less important. However, average outlet air humidity ratio also increased, thus efficiency decreased from 0.41 to 0.37.
- ix. Feedback from experimental testing results was used to refine the mathematical model. The updated model now includes heat balance for shell-side casing, while heat balance of secondary air now takes into account convective heat exchange with shell-side surface. Simulation results of the refined model were compared with experimental results with similar working conditions, and it was indicated that the new model was able to replicate the heat storage issue encountered with the test rig.

6.2. Future work

In this research, the potential of using the shell-tube configuration to achieve better dehumidification has been investigated. However, further studies can be considered to explore further opportunities to improve the dehumidifier performance as well as its applicability for air conditioning systems.

6.2.1. Further refinement on mathematical model

As the developed mathematical model in this project assumed concentric channel condition, several updates can be considered to make the model more relevant to the dehumidifier prototype and the experimental testing conditions. The first one would be further rework of heat balance equation of secondary air stream. The following secondary air heat balance can be adopted, based on ref. [50]:

$$T_{a_{oc},out} = T_{a_{oc},in} + \frac{\pi D_t N_t}{\dot{V}_{a_{oc}}} \frac{1}{\rho_a c_{pa}} \int_0^L h_{oc} (T_t - T_{a_{oc}}) dz$$

With D_t is outer diameter of the desiccant tube, is N_t number of tubes, and T_t is tube temperature. Further investigations is required to determine the value of heat transfer coefficient h_{oc} in above equation. The second update would consider the heat and mass transfer between the stagnant air inside the desiccant tube and adsorbent layer surface during the post-regeneration cooling period. In particular, convective heat and mass transfer should be determined under such consideration.

6.2.2. Heat storage and further testing possibilities

It was observed that the performance potential of the dehumidifier prototype was limited by the heat storage of the rig structure made mainly of aluminium. During regeneration process, heat loss throughout the passageways between the heater fan and the dehumidifier inlets caused significant drop the regeneration air temperature even before entering the rig, causing

delay in moisture desorption. On the other hand, residual heat stored after regeneration process increased process air inlet temperature, and subsequently limit moisture adsorption rate. Even though the implementation of cooling period considerably helped improve dehumidification, it remains interesting to consider materials with low heat capacity for the shell-side casing and connecting tubes, which would allow faster heat removal during cooling period, thus limiting temperature increase of ambient air supplied from the chamber during dehumidification period. Additionally, use of thermal insulation would also help minimize heat loss during regeneration process.

In this work the dehumidification and regeneration cycle time were limited by the heat stored in the system's structure. Addressing the heat storage problem would allow shorter cooling period and/or longer regeneration process to ensure higher dehumidification capacity of the system. It would be useful to consider various cycle duration and the impact on the overall performance of the system. Also, higher regeneration temperature can also be considered if the residual heat could be removed easily, which also mean the cooling period can be shortened to achieve higher moisture removal per cycle time. Furthermore, once heat removal problem is addressed, possibilities for higher amount and/or length of the desiccant tubes could be explored to achieve higher airflows while maintaining optimum air velocity for better dehumidification performance. On the other hand, further design in which continuous dehumidification can be achieved through a dual heat and mass exchangers operating out of phase.

6.2.3. Integration with cooling systems for building application

During the experimental investigations, the chosen testing conditions put more focus on the prototype behaviour under various working cycle and system performance without exploiting feasibility of cooling system post air dehumidification. By integrating the dehumidifier with an indirect evaporative cooler, it would be interesting to explore the use of cool humid air normally rejected from the "wet channel" of the cooler for heat removal of the desiccant unit. This would allow the dehumidifier to supply dry air to the evaporative cooling system and

extend its usefulness into high humid regions of the world, while also improve its cooling performance by recovering 'coolth' from the rejected cold and humid air and improve the dehumidification capacity of the shell-tube desiccant system. Furthermore, the combination of the shell-tube dehumidifier and the indirect evaporative cooler can provide an alternative to the common vapour compression systems. One of the main advantages of this alternative solution is that it doesn't require the energy intensive compressor (thus high electricity demands and carbon emission) used in traditional air conditioning systems for air cooling and dehumidification. Also, controlled air humidity would improve the health of building's occupant. Another benefit is that this solid desiccant – evaporative cooling system does not require dangerous refrigerant such as CFCs, HCFCs, and HFCs which cause environmental concerns such as greenhouse gases emissions and the ozone-layer depletion.

The potential of the dehumidifier rig for application in air conditioning systems can be evaluated by assessing its compatibility with the evaporative cooler, which require inlet air to be dry enough for optimum cooling capacity. For this purpose, the outlet temperature and humidity of the process air was compared to the inlet air condition used in a sub-wet-bulb temperature indirect evaporative cooler [66]. It was reported that the cooler would be able to supply air within the comfort zone for inlet condition of 30-42°C and 15-30%RH. This is not far from the outlet air conditions achieved by the dehumidifier rig with operating conditions presented on Table 5-3, with temperature ranging from around 39-41°C and humidity around 23-27%. This indicated that the dehumidifier rig would be capable to provide dry air for the evaporative cooler.

The integration of the shell-tube desiccant dehumidifier and the sub-wet-bulb temperature evaporative cooler to form an air conditioning system will provide the opportunity to investigate the energy saving potential compared to the common vapour compression air conditioning system in hot and humid climate. For example, for a typical domestic building in a hot and dry region, the evaporative cooler was able to achieve annual electrical energy savings amounting to 3.172 MWh compared to traditional air conditioning systems, which suffer from low COP under hot conditions [66].

In hot and humid conditions, the integrated desiccant dehumidifier – evaporative cooling system could also achieve considerable energy saving, especially with the abundance of solar energy available that can be used as regeneration heat source. Therefore, feasibility of using solar energy systems to provide regeneration air for the shell-tube dehumidifier can also be considered in future studies. On the other hand, the dehumidifier performance under required airflow for building application (around 30-40 m³/h) should be investigated. Based on the tested working conditions, the current shell-tube desiccant prototype would be equivalent to about 1/9 scale compared to the required airflow for a domestic building application. To achieve the required supply air flow rate, the dehumidifier prototype should either use higher air velocities, or be increased in size. For consideration, it was also observed from the theoretical studies as well as the testing results that low air velocities would be preferable for better dehumidification process. Therefore, longer tube channels / higher number of tubes might achieve higher airflow while maintaining dehumidification performance, or by employing multiple stages of dehumidification. Therefore, further investigations can be conducted to address the scaling challenge for building applications.

References

- [1] M. Frontczak, P. Wargocki, Literature survey on how different factors influence human comfort in indoor environments, *Build. Environ.* 46 (2011) 922–937. doi:10.1016/j.buildenv.2010.10.021.
- [2] A. Costa, M.M. Keane, J.I. Torrens, E. Corry, Building operation and energy performance: Monitoring, analysis and optimisation toolkit, *Appl. Energy*. 101 (2013) 310–316. doi:10.1016/j.apenergy.2011.10.037.
- [3] X. Cao, X. Dai, J. Liu, Building energy-consumption status worldwide and the state-of-the-art technologies for zero-energy buildings during the past decade, *Energy Build.* 128 (2016) 198–213. doi:10.1016/j.enbuild.2016.06.089.
- [4] A. Dadoo, L. Gustavsson, R. Sathre, Building energy-efficiency standards in a life cycle primary energy perspective, *Energy Build.* 43 (2011) 1589–1597. doi:10.1016/j.enbuild.2011.03.002.
- [5] Q.J. Kwong, N.M. Adam, B.B. Sahari, Thermal comfort assessment and potential for energy efficiency enhancement in modern tropical buildings: A review, *Energy Build.* 68 (2014) 547–557. doi:10.1016/j.enbuild.2013.09.034.
- [6] D. Setyawan, Formulating revolving fund scheme to support energy efficiency projects in Indonesia, *Energy Procedia*. 47 (2014) 37–46. doi:10.1016/j.egypro.2014.01.194.
- [7] A.R. Katili, R. Boukhanouf, R. Wilson, Space Cooling in Buildings in Hot and Humid Climates – a Review of the Effect of Humidity on the Applicability of Existing Cooling Techniques, in: 14th International Conference on Sustainable Energy Technologies – SET 2015, Nottingham, 2015. doi:10.13140/RG.2.1.3011.5287.
- [8] Z. Li, W. Chen, S. Deng, Z. Lin, The characteristics of space cooling load and indoor humidity control for residences in the subtropics, *Build. Environ.* 41 (2006) 1137–1147. doi:10.1016/j.buildenv.2005.05.016.
- [9] R. Boukhanouf, H.G. Ibrahim, A. Alharbi, M. Kanzari, Investigation of an Evaporative Cooler for Buildings in Hot and Dry Climates, *J. Clean Energy Technol.* 2 (2014) 221–225.
- [10] B. Ford, R. Schiano-Phan, E. Francis, *The Architecture & Engineering of Draught Cooling - A Design Sourcebook*, PHDC Press, 2010.
- [11] A.R. Katili, A. Trabelsi, J. Virgone, Cooling System by Evaporation of Water in a Fibrous Wall, in: 2014 ASHRAE/IBPSA-USA Building Simulation Conference, Atlanta, 2014: pp. 497–504.
- [12] J.M. Seo, D. Song, K.H. Lee, Possibility of coupling outdoor air cooling and radiant floor cooling under hot and humid climate conditions, *Energy Build.* 81 (2014) 219–226. doi:10.1016/j.enbuild.2014.06.023.

References

- [13] A.N.Z. Sanusi, L. Shao, N. Ibrahim, Passive ground cooling system for low energy buildings in Malaysia (hot and humid climates), *Renew. Energy*. 49 (2013) 193–196. doi:10.1016/j.renene.2012.01.033.
- [14] D. La, Y. Dai, Y. Li, T. Ge, R. Wang, Case study and theoretical analysis of a solar driven two-stage rotary desiccant cooling system assisted by vapor compression air-conditioning, *Sol. Energy*. 85 (2011) 2997–3009. doi:10.1016/j.solener.2011.08.039.
- [15] N. Enteria, H. Yoshino, A. Mochida, A. Satake, R. Yoshie, R. Takaki, H. Yonekura, T. Mitamura, Y. Tanaka, Performance of solar-desiccant cooling system with Silica-Gel (SiO₂) and Titanium Dioxide (TiO₂) desiccant wheel applied in East Asian climates, *Sol. Energy*. 86 (2012) 1261–1279. doi:10.1016/j.solener.2012.01.018.
- [16] R. Qi, L. Lu, H. Yang, Investigation on air-conditioning load profile and energy consumption of desiccant cooling system for commercial buildings in Hong Kong, *Energy Build.* 49 (2012) 509–518. doi:10.1016/j.enbuild.2012.02.051.
- [17] O. Labban, T. Chen, A.F. Ghoniem, J.H. Lienhard, L.K. Norford, Next-generation HVAC: Prospects for and limitations of desiccant and membrane-based dehumidification and cooling, *Appl. Energy*. 200 (2017) 330–346. doi:10.1016/j.apenergy.2017.05.051.
- [18] N. Enteria, K. Mizutani, The role of the thermally activated desiccant cooling technologies in the issue of energy and environment, *Renew. Sustain. Energy Rev.* 15 (2011) 2095–2122. doi:10.1016/j.rser.2011.01.013.
- [19] K. Daou, R.Z. Wang, Z.Z. Xia, Desiccant cooling air conditioning: A review, *Renew. Sustain. Energy Rev.* 10 (2006) 55–77. doi:10.1016/j.rser.2004.09.010.
- [20] L.Z. Zhang, Progress on heat and moisture recovery with membranes: From fundamentals to engineering applications, *Energy Convers. Manag.* 63 (2012) 173–195. doi:10.1016/j.enconman.2011.11.033.
- [21] S.M. Huang, L.Z. Zhang, Researches and trends in membrane-based liquid desiccant air dehumidification, *Renew. Sustain. Energy Rev.* 28 (2013) 425–440. doi:10.1016/j.rser.2013.08.005.
- [22] J. Woods, Membrane processes for heating, ventilation, and air conditioning, *Renew. Sustain. Energy Rev.* 33 (2014) 290–304. doi:10.1016/j.rser.2014.01.092.
- [23] X. Zheng, T.S. Ge, R.Z. Wang, Recent progress on desiccant materials for solid desiccant cooling systems, *Energy*. 74 (2014) 280–294. doi:10.1016/j.energy.2014.07.027.
- [24] F. Rouquerol, J. Rouquerol, K. Sing, Adsorption by Powders and Porous Solids: Principles, Methodology and Applications, Academic Press, San Diego, 1999.

References

- [25] D. La, Y.J. Dai, Y. Li, R.Z. Wang, T.S. Ge, Technical development of rotary desiccant dehumidification and air conditioning: A review, *Renew. Sustain. Energy Rev.* 14 (2010) 130–147. doi:10.1016/j.rser.2009.07.016.
- [26] E.P. Ng, S. Mintova, Nanoporous materials with enhanced hydrophilicity and high water sorption capacity, *Microporous Mesoporous Mater.* 114 (2008) 1–26. doi:10.1016/j.micromeso.2007.12.022.
- [27] C.X. Jia, Y.J. Dai, J.Y. Wu, R.Z. Wang, Experimental comparison of two honeycombed desiccant wheels fabricated with silica gel and composite desiccant material, *Energy Convers. Manag.* 47 (2006) 2523–2534. doi:10.1016/j.enconman.2005.10.034.
- [28] C.X. Jia, Y.J. Dai, J.Y. Wu, R.Z. Wang, Use of compound desiccant to develop high performance desiccant cooling system, *Int. J. Refrig.* 30 (2007) 345–353. doi:10.1016/j.ijrefrig.2006.04.001.
- [29] N.A. Pennington, *Humidity Changer for Air-Conditioning*, 2700537, 1955.
- [30] A. Yadav, V.K. Bajpai, Optimization of Operating Parameters of Desiccant Wheel for Rotation Speed, *Int. Journal Adv. Sci. Technol.* 32 (2011) 109–116.
- [31] L.Z. Zhang, Transient and conjugate heat and mass transfer in hexagonal ducts with adsorbent walls, *Int. J. Heat Mass Transf.* 84 (2015) 271–281. doi:10.1016/j.ijheatmasstransfer.2015.01.029.
- [32] M. Goldsworthy, S. White, Optimisation of a desiccant cooling system design with indirect evaporative cooler, *Int. J. Refrig.* 34 (2011) 148–158. doi:10.1016/j.ijrefrig.2010.07.005.
- [33] H.S. Al-Sharqawi, N. Lior, Effect of Flow-Duct Geometry on Solid Desiccant Dehumidification, *Ind. Eng. Chem. Res.* 47 (2008) 1569–1585. doi:10.1021/ie0707319.
- [34] R. Narayanan, Investigation of Geometry Effects of Channels of a Silica-gel Desiccant Wheel, *Energy Procedia.* 110 (2017) 20–25. doi:10.1016/j.egypro.2017.03.099.
- [35] T.S. Ge, F. Ziegler, R.Z. Wang, A mathematical model for predicting the performance of a compound desiccant wheel (A model of compound desiccant wheel), *Appl. Therm. Eng.* 30 (2010) 1005–1015. doi:10.1016/j.applthermaleng.2010.01.012.
- [36] D. O'Connor, J.K. Calautit, B.R. Hughes, A novel design of a desiccant rotary wheel for passive ventilation applications, *Appl. Energy.* 179 (2016) 99–109. doi:10.1016/j.apenergy.2016.06.029.
- [37] L.Z. Zhang, H.X. Fu, Q.R. Yang, J.C. Xu, Performance comparisons of honeycomb-type adsorbent beds (wheels) for air dehumidification with various desiccant wall materials, *Energy.* 65 (2014) 430–440. doi:10.1016/j.energy.2013.11.042.
- [38] A. Ramzy K, T.P. Ashok Babu, R. Kadoli, Semi-analytical method for heat and moisture transfer in packed

References

- bed of silica gel, *Int. J. Heat Mass Transf.* 54 (2011) 983–993.
doi:10.1016/j.ijheatmasstransfer.2010.09.007.
- [39] A.K. Ramzy, R. Kadoli, T.P. Ashok Babu, Experimental and theoretical investigations on the cyclic operation of TSA cycle for air dehumidification using packed beds of silica gel particles, *Energy*. 56 (2013) 8–24.
doi:10.1016/j.energy.2013.03.048.
- [40] M.M. Awad, A. Ramzy K, A.M. Hamed, M.M. Bekheit, Theoretical and experimental investigation on the radial flow desiccant dehumidification bed, *Appl. Therm. Eng.* 28 (2008) 75–85.
doi:10.1016/j.applthermaleng.2006.12.018.
- [41] F. Fernández-Hernández, J.M. Cejudo-López, F. Domínguez-Muñoz, A. Carrillo-Andrés, A new desiccant channel to be integrated in building facades, *Energy Build.* 86 (2015) 318–327.
doi:10.1016/j.enbuild.2014.10.009.
- [42] S. Shimooka, K. Oshima, H. Hidaka, T. Takewaki, H. Kakiuchi, A. Kodama, M. Kubota, H. Matsuda, The evaluation of direct cooling and heating desiccant device coated with FAM, *J. Chem. Eng. Japan.* 40 (2007) 1330–1334. doi:10.1252/jcej.07WE193.
- [43] K. Fathalah, S.E. Aly, Study of a waste heat driven modified packed desiccant bed dehumidifier, *Energy Convers. Manag.* 37 (1996) 457–471. doi:10.1016/0196-8904(95)00201-4.
- [44] Y. Weixing, Z. Yi, L. Xiaoru, Y. Xiugan, Study of a new modified cross-cooled compact solid desiccant dehumidifier, *Appl. Therm. Eng.* 28 (2008) 2257–2266. doi:10.1016/j.applthermaleng.2008.01.006.
- [45] M. Kubota, N. Hanaoka, H. Matsuda, A. Kodama, Dehumidification behavior of cross-flow heat exchanger type adsorber coated with aluminophosphate zeolite for desiccant humidity control system, *Appl. Therm. Eng.* 122 (2017) 618–625. doi:10.1016/j.applthermaleng.2017.05.047.
- [46] T.S. Ge, Y.J. Dai, R.Z. Wang, Z.Z. Peng, Experimental comparison and analysis on silica gel and polymer coated fin-tube heat exchangers, *Energy*. 35 (2010) 2893–2900. doi:10.1016/j.energy.2010.03.020.
- [47] A. Kumar, A. Yadav, Étude Expérimentale De Système De Conditionnement D’Air Solaire À Déshydratant Basée Sur Un Échangeur De Chaleur Enrobé De Gel De Silice, *Int. J. Refrig.* 69 (2016) 51–63.
doi:10.1016/j.ijrefrig.2016.05.008.
- [48] A. Kodama, N. Watanabe, T. Hirose, M. Goto, H. Okano, Performance of a multipass honeycomb adsorber regenerated by a direct hot water heating, *Adsorption*. 11 (2005) 603–608. doi:10.1007/s10450-005-5992-6.
- [49] R. Narayanan, W.Y. Saman, S.D. White, A non-adiabatic desiccant wheel: Modeling and experimental validation, *Appl. Therm. Eng.* 61 (2013) 178–185. doi:10.1016/j.applthermaleng.2013.07.007.

References

- [50] M.J. Goldsworthy, S. White, Design and performance of an internal heat exchange desiccant wheel, *Int. J. Refrig.* 39 (2014) 152–159. doi:10.1016/j.ijrefrig.2013.10.009.
- [51] T.S. Ge, Y. Li, R.Z. Wang, Y.J. Dai, A review of the mathematical models for predicting rotary desiccant wheel, *Renew. Sustain. Energy Rev.* 12 (2008) 1485–1528. doi:10.1016/j.rser.2007.01.012.
- [52] T. Kravchik, E. Korin, I. Borde, Influence of material properties and heat removal on mass and heat transfer in a solid desiccant dehumidifier, *Chem. Eng. Process. Process Intensif.* 27 (1990) 19–25. doi:10.1016/0255-2701(90)85003-M.
- [53] F.E. Nia, D. van Paassen, M.H. Saidi, Modeling and simulation of desiccant wheel for air conditioning, *Energy Build.* 38 (2006) 1230–1239. doi:10.1016/j.enbuild.2006.03.020.
- [54] S. Yamaguchi, K. Saito, Numerical and experimental performance analysis of rotary desiccant wheels, *Int. J. Heat Mass Transf.* 60 (2013) 51–60. doi:10.1016/j.ijheatmasstransfer.2012.12.036.
- [55] K.J. Chua, Heat and mass transfer of composite desiccants for energy efficient air dehumidification: Modelling and experiment, *Appl. Therm. Eng.* 89 (2015) 703–716. doi:10.1016/j.applthermaleng.2015.06.061.
- [56] M. Intini, M. Goldsworthy, S. White, C.M. Joppolo, Experimental analysis and numerical modelling of an AQSOA zeolite desiccant wheel, *Appl. Therm. Eng.* 80 (2015) 20–30. doi:10.1016/j.applthermaleng.2015.01.036.
- [57] X.J. Zhang, Y.J. Dai, R.Z. Wang, A simulation study of heat and mass transfer in a honeycombed rotary desiccant dehumidifier, *Appl. Therm. Eng.* 23 (2003) 989–1003. doi:10.1016/S1359-4311(03)00047-4.
- [58] A.A. Pesaran, A.F. Mills, Moisture transport in silica gel packed beds-I. Theoretical study, *Int. J. Heat Mass Transf.* 30 (1987) 1037–1049.
- [59] L.Z. Zhang, J.L. Niu, Performance comparisons of desiccant wheels for air dehumidification and enthalpy recovery, *Appl. Therm. Eng.* (2002). doi:10.1016/S1359-4311(02)00050-9.
- [60] A. Bejan, A.D. Kraus, *Heat Transfer Handbook*, Mech. Eng. (2003) 1480. doi:10.1021/ja1097622.
- [61] K.J. Sladek, E.R. Gilliland, R.F. Baddour, Diffusion on Surfaces. II. Correlation of Diffusivities of Physically and Chemically Adsorbed Species, *Ind. Eng. Chem. Fundam.* 13 (1974) 100–105. doi:10.1021/i160050a002.
- [62] S. Chapra, R. Canale, *Numerical methods for engineers*, McGrawHill, 2010.
- [63] K. Tsutsui, S. Yamaguchi, K. Saito, et al., Effect of design and operating conditions on performance of desiccant wheels, in: 2008.

References

- [64] R.W. Fox, P.J. Pritchard, A.T. McDonald, Fox and McDonald's introduction to fluid mechanics., John Wiley & Sons, Inc. ; John Wiley [distributor], Hoboken, NJ; Chichester, 2011.
- [65] Z. Duan, C. Zhan, X. Zhang, M. Mustafa, X. Zhao, B. Alimohammadisagvand, A. Hasan, Indirect evaporative cooling: Past, present and future potentials, *Renew. Sustain. Energy Rev.* (2012). doi:10.1016/j.rser.2012.07.007.
- [66] O. Amer, A heat pipe and porous ceramic based sub wet-bulb temperature evaporative cooler: a theoretical and experimental study, (2017). <http://eprints.nottingham.ac.uk/43343/>.

Appendices

Appendix A – Computer Algorithm written in MATLAB script file

```
%constant properties

%specification of desiccant material

Cpd = 921; %specific heat of dehumidifier, J/kgK
kd = 0.2; %thermal conductivity of dehumidifier, W/mK
rod = 800; %dehumidifier density, kg/m^3
qst = 2370*1000; %heat of adsorption of desiccant, J/kg

%construct parameter of dehumidifier
c = 1/1000; %thickness of des, m
csh = 1/1000; %thickness of shell, m
Aic = 2.04179E-05; %area of cross section NET, inner channel m^2
Aoc = 0.000082425; %area of cross section NET, inner channel m^2
pic = 0.016014; %perimeter of air flow passage, m TUBE
poc = 0.02512; %perimeter of air flow passage, m TUBE
psh = 0.04082; %perimeter of air flow passage, m SHELL
L = 0.3; %thickness of wheel, m
Dh = 0.00510; % hydraulic diameter of inner channel, m
Dho = 0.005; %outer

%operating parameters

%primary air
Tp = (30+273.15); %process air inlet temperature, K
Yp = (20/1000); %inlet humidity ratio of process air, kg/kg
upa = 1.2; %air velocity of process air, dehumidification process, m/s
ureg = 2.5; %air velocity of regeneration air, dehumidification process, m/s
Treg = (80+273.15); %regeneration air temperature (inlet), K
Yreg = (20/1000); %humidity ratio of regeneration air (inlet), kg/kg

%secondary air
Tc = (30+273.15); %cooling air inlet temperature, K
Th = (80+273.15); %heating air inlet temperature, K
usa = 1.2; %velocity of cooling air, m/s
%uh = 2.5; %velocity of heating air, m/s

%simulation parameter
deltat = 0.025/2; %half time step,
deltax = 0.004; %space step along length,
nx = (L/deltax)+1;
deltay = c/8; %space step along thickness (8 segments)
ct = 300; %cycle time, s
n = ct/deltat; %number of time step

%other properties

Tave=(Tp+Treg+Tc+Th)/4; %average inlet temperature, K
roa = 1.076; %air density at (Tave=(Tamb+Treg)/2), kg/m^3 T AVERAGE
Cpa = 1006.3; %specific heat of air, J/kgK Tave
Cpv = 1872;%specific heat of water vapor, J/kgK
```

Appendices

```
Dva = 2.82*10^-5; %moisture diffusivity in air, m^2/s
ka = 0.028246; %air thermal conductivity, W/mK; 0.0263;
rosh = 2712; %density of shell, kg/m3
Cpsh = 0.91*1000; %specific heat of shell, J/kgK
D0 = 1.6*10^(-6);
R = 461; %J/kgK
D = D0*exp(-0.45*(qst/(R*Tave)));
Nu = 3.020700893; %Nusselt number for inner channel (average)
Nuo = 2.981084429; %outer
Sh = 3.020700893; %Sherwood number (average)
h = (Nu*ka)/Dh; %heat transfer coefficient, inner channel, W/m^2K
ho = (Nuo*ka)/Dho; %inner channel
hm = (roa*Sh*Dva)/Dh; %mass transfer coefficient, kg/m^2.s

%summarised coeff for air mass balance
XK1 = deltat*upa/(deltax);
XK1o = deltat*usa/(deltax);
XK2 = hm*pic*deltat/(roa*Aic);

%summarised coeff for air heat balance
XK3 = h*pic*deltat/(roa*Cpa*Aic);
XK3o = ho*poc*deltat/(roa*Cpa*Aoc);
XK2h = XK2*Cpv/Cpa;
XK3sh = ho*psh*deltat/(roa*Cpa*Aoc);

%summarised coeff for desiccant mass balance
XKa = D*(deltat/2)/(deltax^2);
XKb = D*(deltat/2)/(deltay^2);
Bim = 2*hm*deltay/(rod*D);

%summarised coeff for desiccant heat balance
XKc = kd*(deltat/2)/(rod*Cpd*(deltax^2));
XKd = kd*(deltat/2)/(rod*Cpd*(deltay^2));
Bi1 = 2*h*deltay/kd;
Bi1o = 2*ho*deltay/kd;
Bi2 = 2*hm*Cpv*deltay/kd;
Bi3 = 2*hm*qst*deltay/kd;

%summarised coeff for shell heat balance
XKsh = ho*psh*deltat/(rosh*Cpsh*psh*csh);

%dependent variables of the system

Ya=1:nx; %process air humidity ratio, kg/kg

Yd=1:nx; %desiccant surface humidity ratio, kg/kg
W=1:nx; %dehumidifier water content, kg/kg

Ta=1:nx; %process air temperature, K
Tao=1:nx; %outer channel

Td=1:nx; %desiccant surface temperature, K
Tsh=1:nx; %shell temperature, K

RH = 1:nx; %relative humidity
RHa = 1:nx; %relative humidity of air

%Matrix component for Tridiagonal Matrix solver for heat balance
e=rand(1,nx, 9);
```

Appendices

```
ep=1:(nx-2);

f=rand(1,nx, 9);
fp=1:nx;

g=rand(1,nx, 9);
gp=1:(nx-2);

r=rand(1,nx, 9);
rp=1:nx;

%Matrix component for Tridiagonal Matrix solver for mass balance
em=rand(1,nx, 9);
emp=1:(nx-1);

fm=rand(1,nx, 9);
fmp=1:nx;

gm=rand(1,nx, 9);
gmp=1:(nx-1);

rm=rand(1,nx, 9);
rmp=1:(nx-2);

%adsorption cycle
Yinlet = Yp;
Tinlet = Tp;
Taoilet = Tc;

for t = 1:2:n %time step
%initial condition

for x=1:nx

    Ya(1, :) =
[0.0200000000000000,0.0201936204589559,0.0203830494533427,0.0205683549762402,
0.0207496610781503,0.0209270992658737,0.0211008003176031,0.0212708930061347,0
.0214375039369868,0.0216007575475760,0.0217607761246966,0.0219176798220875,0.
0220715866765783,0.0222226126229994,0.0223708715080542,0.0225164751032837,0.0
226595331172139,0.0228001532067536,0.0229384409878906,0.0230745000457164,0.02
32084319437983,0.0233403362328986,0.0234703104590348,0.0235984501708578,0.023
7248489263197,0.0238495982985915,0.0239727878811841,0.0240945052922196,0.0242
148361777937,0.0243338642143650,0.0244516711101028,0.0245683366051202,0.02468
39384705196,0.0247985525061700,0.0249122525371382,0.0250251104086925,0.025137
1959797942,0.0252485771149957,0.0253593196746595,0.0254694875034139,0.0255791
424167606,0.0256883441857497,0.0257971505196370,0.0259056170464416,0.02601379
72913175,0.0261217426526596,0.0262295023758607,0.0263371235246392,0.026444650
9498576,0.0265521272557553,0.0266595927635167,0.0267670854721001,0.0268746410
162554,0.0269822926216565,0.0270900710570808,0.0271980045835680,0.02730611890
04924,0.0274144370884893,0.0275229795491729,0.0276317639415937,0.027740805115
3810,0.0278501150405234,0.0279597027337447,0.0280695741814363,0.0281797322591
141,0.0282901766473732,0.0284009037442966,0.0285119065740651,0.02862317468987
77,0.0287346940583129,0.0288464468455613,0.0289584106552713,0.029070554893887
4,0.0291828235129656,0.0292950617593310,0.0294067674341901];
    Ta(1, :) =
[353.150000000000,352.563875114745,351.996277269803,351.446541306408,350.9141
92519485,350.398799139258,349.899946057061,349.417229981493,348.950258390164,
348.498649170921,348.062030395552,347.640040121711,347.232326202264,346.83854
6097570,346.458366689626,346.091464097826,345.737523496224,345.396238932280,3
45.067313147084,344.750457397057,344.445391277147,344.151842545539,343.869546
```

Appendices

949909, 343.598248055265, 343.337697073393, 343.087652693974, 342.847880917397, 342.618154889322, 342.398254737037, 342.187967407658, 341.987086508208, 341.795412147637, 341.612750780807, 341.438915054499, 341.273723655476, 341.117001160640, 340.968577889322, 340.828289757732, 340.695978135613, 340.571489705118, 340.454676321933, 340.345394878691, 340.243507170671, 340.148879763828, 340.061383865149, 339.980895195373, 339.907293864066, 339.840464247079, 339.780294866386, 339.726678272322, 339.679510928207, 339.638693097378, 339.604128732616, 339.575725367972, 339.553394012979, 339.537049049262, 339.526608129510, 339.521992078819, 339.523124798379, 339.529933171486, 339.542346971863, 339.560298774245, 339.583723867216, 339.612560168241, 339.646748140847, 339.686230713865, 339.730953202518, 339.780863230408, 339.835910647241, 339.896047411366, 339.961227248524, 340.031403956419, 340.106521810912, 340.186461889550, 340.270755019509, 340.357135540781];

Tao(1, :) =

[336.298740593812, 336.389313541626, 336.483510613564, 336.581789207247, 336.684218365060, 336.790798827363, 336.901520129108, 337.016370584488, 337.135338967357, 337.258414728118, 337.385587947123, 337.516849238255, 337.652189642200, 337.791600517160, 337.935073428581, 338.082600038214, 338.234171992523, 338.389780810419, 338.549417770243, 338.713073795947, 338.880739342389, 339.052404279693, 339.228057776590, 339.407688182668, 339.591282909462, 339.778828310311, 339.970309558896, 340.165710526403, 340.365013657212, 340.568199843058, 340.775248295576, 340.986136417156, 341.200839670044, 341.419331443602, 341.641582919666, 341.867562935926, 342.097237847263, 342.330571384967, 342.567524513786, 342.808055286722, 343.052118697537, 343.299666530887, 343.550647210044, 343.805005642150, 344.062683060946, 344.323616866942, 344.587740464978, 344.854983099134, 345.125269684964, 345.398520639027, 345.674651705670, 345.953573781077, 346.235192734535, 346.519409226948, 346.806118526564, 347.095210321948, 347.386568532211, 347.680071114507, 347.975589868854, 348.272990240301, 348.572131118516, 348.872864634848, 349.175035956948, 349.478483081048, 349.783036621999, 350.088519601209, 350.394747232620, 350.701526706984, 351.008656974952, 351.315928531369, 351.623123214099, 351.930014097811, 352.236365962649, 352.541939105064, 352.846511716502, 353.150000000000];

Tsh(1, :) =

[331.693503240336, 331.744644507831, 331.798521774014, 331.855479433791, 331.915596329265, 331.978910511530, 332.045455029169, 332.115263669826, 332.188371886202, 332.264816920833, 332.344637787709, 332.427875226165, 332.514571649379, 332.604771092146, 332.698519158922, 332.795862972260, 332.896851121527, 333.001533611791, 333.109961812719, 333.222188407330, 333.338267340484, 333.458253766928, 333.582203998776, 333.710175452293, 333.842226593799, 333.978416884604, 334.118806724776, 334.263457395658, 334.412431000949, 334.565790406205, 334.723599176670, 334.885921513196, 335.052822186206, 335.224366467484, 335.400620059659, 335.581649023242, 335.767519701043, 335.958298639824, 336.154052509013, 336.354848016324, 336.560751820123, 336.771830438347, 336.988150153812, 337.209776915742, 337.436776237312, 337.669213089038, 337.907151787795, 338.150655881303, 338.399788027824, 338.654609870898, 338.915181908892, 339.181563359129, 339.453812016367, 339.731984105393, 340.016134127492, 340.306314700503, 340.602576392252, 340.904967547029, 341.213534104877, 341.528319413362, 341.849364031528, 342.176705525758, 342.510378257152, 342.850413160131, 343.196837511907, 343.549674692441, 343.908943934541, 344.274660063728, 344.646833227650, 345.025468615397, 345.410566171180, 345.802120334311, 346.200120028748, 346.604550422747, 347.015406415458, 347.432780028999];

RHa(1, x) = Ya(1, x) * (10^-6 * exp(5294/Ta(1, x))) / (1 + 1.61 * Ya(1, x));

for y=1:9

W(1, :, 1) =

[0.134133925463011, 0.133993010866491, 0.133862272911138, 0.133744501591512, 0.133636088953433, 0.133535430747546, 0.133441648965227, 0.133354095291077, 0.133272206418876, 0.133195463300774, 0.133123379096977, 0.133055494823287, 0.132991377051888, 0.132930616190081, 0.132872824958952, 0.132817636975506, 0.132764705412578, 0.132713701728065, 0.132664314459130, 0.132616248077972, 0.132569221905916, 0.132522969082512, 0.132477235586519, 0.132431779305452, 0.132386369150611, 0.132340784214443, 0.132294812967195, 0.132248252489907, 0.132200907740856, 0.13215259085262];

Appendices

0, 0.132103120457099, 0.132052321035798, 0.13200022292891, 0.131946058548515, 0.131890268150008, 0.131832492898678, 0.131772577489936, 0.131710368964591, 0.131645716169163, 0.131578469223264, 0.131508478991918, 0.131435596560996, 0.131359672713803, 0.131280557406952, 0.131198099243788, 0.131112144943474, 0.131022538804086, 0.130929122157917, 0.130831732817374, 0.130730204509724, 0.130624366299059, 0.130514041993895, 0.130399049538709, 0.130279200387871, 0.130154298860343, 0.130024141473640, 0.129888516255405, 0.129747202031162, 0.129599967686640, 0.129446571403253, 0.129286759865217, 0.129120267436918, 0.128946815309192, 0.128766110613335, 0.128577845502397, 0.128381696201824, 0.128177322042169, 0.127964364531236, 0.127742446716983, 0.127511173965446, 0.127270141415927, 0.127018974093786, 0.126757534337411, 0.126487018112711, 0.126215924334757, 0.125996251967687];

W(1, :, 2) =

[0.133841621940737, 0.133712820028793, 0.133594764551757, 0.133489264436739, 0.133392632688488, 0.133303272742509, 0.133220321815097, 0.133143146506722, 0.133071197696653, 0.133003969891713, 0.132940989236254, 0.132881809190674, 0.132826008253697, 0.132773188259640, 0.132722972874347, 0.132675006193749, 0.132628951419466, 0.132584489603070, 0.132541318454695, 0.132499151212607, 0.132457715570557, 0.132416752659604, 0.132376016081334, 0.132335270989187, 0.132294293214826, 0.132252868436432, 0.132210791385922, 0.132167865092144, 0.132123900157199, 0.132078714063083, 0.132032130506000, 0.131983978755690, 0.131934093037293, 0.131882311933240, 0.131828477802899, 0.131772436217580, 0.131714035408764, 0.131653125727365, 0.131589559111932, 0.131523188563804, 0.131453867627198, 0.131381449872346, 0.131305788379799, 0.131226735224044, 0.131144140954703, 0.131057854073494, 0.130967720505287, 0.130873583061532, 0.130775280894420, 0.130672648940123, 0.130565517349482, 0.130453710904609, 0.130337048419747, 0.130215342124883, 0.130088397030539, 0.129956010272278, 0.129817970433328, 0.129674056843938, 0.129524038855940, 0.129367675091119, 0.129204712661984, 0.129034886363588, 0.128857917835148, 0.128673514690352, 0.128481369615997, 0.128281159441062, 0.128072544188967, 0.127855166169950, 0.127628649362774, 0.127392600202167, 0.127146615022798, 0.126890320300606, 0.126623582657534, 0.126347631223023, 0.126071234701661, 0.125848279951196];

W(1, :, 3) =

[0.132919383998001, 0.132827502820383, 0.132748140414055, 0.132680102526071, 0.132619450328477, 0.132564607071698, 0.132514754834103, 0.132469304627142, 0.132427749659093, 0.132389624919186, 0.132354495357313, 0.132321951652518, 0.132291607998026, 0.132263100452617, 0.132236085486972, 0.132210238630206, 0.132185253191353, 0.132160839047600, 0.132136721495068, 0.132112640158870, 0.132088347959359, 0.132063610131360, 0.132038203293401, 0.132011914563741, 0.131984540720222, 0.131955887400909, 0.131925768342583, 0.131894004654239, 0.131860424122788, 0.131824860548254, 0.131787153105859, 0.131747145732426, 0.131704686534692, 0.131659627217072, 0.131611822526673, 0.131561129713238, 0.131507408001945, 0.131450518076925, 0.131390321573489, 0.131326680577142, 0.131259457127425, 0.131188512724781, 0.131113707838639, 0.131034901414931, 0.130951950381387, 0.130864709148895, 0.130773029107313, 0.130676758114121, 0.130575739974364, 0.130469813910340, 0.130358814019482, 0.130242568719045, 0.130120900176038, 0.129993623721022, 0.129860547244349, 0.129721470573475, 0.129576184829957, 0.129424471764865, 0.129266103071240, 0.129100839672418, 0.128928430984961, 0.128748614155052, 0.128561113267326, 0.128365638525218, 0.128161885402711, 0.127949533769781, 0.127728247004238, 0.127497671145791, 0.127257434335754, 0.127007147639488, 0.126746412494541, 0.126474861555587, 0.126192377568468, 0.125900298928926, 0.125608236440867, 0.125375801665518];

W(1, :, 4) =

[0.131238575623412, 0.131209883738296, 0.131196859308058, 0.131193126409607, 0.131194279815685, 0.131198765038853, 0.131205835955268, 0.131214976186093, 0.131225748451847, 0.131237754339994, 0.131250622730095, 0.131264005702141, 0.131277576420209, 0.131291027568859, 0.131304069978687, 0.131316431348304, 0.131327855038089, 0.131338098927774, 0.131346934333889, 0.131354144983934, 0.131359526044373, 0.131362883199407, 0.131364031777668, 0.131362795923808, 0.131359007812118, 0.131352506899291, 0.131343139213519, 0.131330756677191, 0.131315216460513, 0.131296380363472, 0.131274114223605, 0.131248287347176, 0.131218771961399, 0.131185442685395, 0.131148176017769, 0.131106849838599, 0.131061342923867, 0.131011534470295, 0.130957303628698, 0.130898529044027, 0.130835088400269, 0.130766857968494, 0.130693712156397, 0.130615523057625, 0.130532159999412, 0.130443489086898, 0.130349372742680, 0.130249669240128, 0.130144232229061, 0.130032910252379, 0.129915546252314, 0.129

Appendices

791977065035, 0.129662032902253, 0.129525536818651, 0.129382304163900, 0.129232142018130, 0.129074848609667, 0.128910212714040, 0.128738013033121, 0.128558017553498, 0.128369982883093, 0.128173653565197, 0.127968761369188, 0.127755024557367, 0.127532147128088, 0.127299818037793, 0.127057710414556, 0.126805480817326, 0.126542768776767, 0.126269197696745, 0.125984382433209, 0.125687971849682, 0.125379886065318, 0.125061676110452, 0.124744452897237, 0.124497506485694];

W(1, :, 5) =

[0.128608406640301, 0.128670712638710, 0.128753451892051, 0.128842702369663, 0.128933315998121, 0.129023747091554, 0.129113342992700, 0.129201685120364, 0.129288430461829, 0.129373271167516, 0.129455923240505, 0.129536122618741, 0.129613623183806, 0.129688195305069, 0.129759624565584, 0.129827710579743, 0.129892265878838, 0.129953114856988, 0.130010092773687, 0.130063044810120, 0.130111825176523, 0.130156296267782, 0.130196327864608, 0.130231796377440, 0.130262584130426, 0.130288578682738, 0.130309672184602, 0.130325760765465, 0.130336743951775, 0.130342524111947, 0.130343005926128, 0.130338095878500, 0.130327701769904, 0.130311732248609, 0.130290096357256, 0.130262703093897, 0.130229460985299, 0.130190277670625, 0.130145059493720, 0.130093711102352, 0.130036135052674, 0.129972231417404, 0.129901897396160, 0.129825026926460, 0.129741510294019, 0.129651233740926, 0.129554079070420, 0.129449923246958, 0.129338637990387, 0.129220089363016, 0.129094137348439, 0.128960635421090, 0.128819430105390, 0.128670360523564, 0.128513257931124, 0.128347945239178, 0.128174236522645, 0.127991936513659, 0.127800840079361, 0.127600731683472, 0.127391384831022, 0.127172561495747, 0.126944011529781, 0.126705472055472, 0.126456666839890, 0.126197305654888, 0.125927083635271, 0.125645680687446, 0.125352761178442, 0.125047974988877, 0.124730965525892, 0.124401416071117, 0.124059319606170, 0.123706581768358, 0.123356574508331, 0.123092210758673];

W(1, :, 6) =

[0.124808210114249, 0.124989815976664, 0.125198476861726, 0.125410243798682, 0.125618878689688, 0.125822809756451, 0.126021490867891, 0.126214620771084, 0.126401970656334, 0.126583342817151, 0.126758559543815, 0.126927459390799, 0.127089895323746, 0.127245733382446, 0.127394851517179, 0.127537138511742, 0.127672492970328, 0.127800822361198, 0.127922042113746, 0.128036074766382, 0.128142849162800, 0.128242299694085, 0.128334365584240, 0.128418990216537, 0.128496120498232, 0.128565706261166, 0.128627699695772, 0.128682054816162, 0.128728726953910, 0.128767672278307, 0.128798847340863, 0.128822208641961, 0.128837712217610, 0.128845313244281, 0.128844965659999, 0.128836621799804, 0.128820232043851, 0.128795744476461, 0.128763104554502, 0.128722254783576, 0.128673134400492, 0.128615679060637, 0.128549820528886, 0.128475486372724, 0.128392599656389, 0.128301078634804, 0.128200836446220, 0.128091780802448, 0.127973813675719, 0.127846830981156, 0.127710722253965, 0.127565370320532, 0.127410650962549, 0.127246432573486, 0.127072575806687, 0.126888933214499, 0.126695348877833, 0.126491658025698, 0.126277686644259, 0.126053251075101, 0.125818157602413, 0.125572202028961, 0.125315169240819, 0.125046832761055, 0.124766954293263, 0.124475283258109, 0.124171556335230, 0.123855497061662, 0.123526815716829, 0.123185210633636, 0.122830377175329, 0.122462061144956, 0.122080380585034, 0.121687777653927, 0.121300712883341, 0.121019278351715];

W(1, :, 7) =

[0.119626364052930, 0.119953835405406, 0.120316988823073, 0.120679435477782, 0.121033435469695, 0.121377330657288, 0.121710682102655, 0.122033316405251, 0.122345130962180, 0.122646050452975, 0.122936015778251, 0.123214980495322, 0.123482909100200, 0.123739775806319, 0.123985563487930, 0.124220262705107, 0.124443870788788, 0.124656390979384, 0.124857831615961, 0.125048205373811, 0.125227528548300, 0.125395820382777, 0.125553102438424, 0.125699398003724, 0.125834731541353, 0.125959128170271, 0.126072613180750, 0.126175211580244, 0.126266947667893, 0.126347844635674, 0.126417924194110, 0.126477206220652, 0.126525708428833, 0.126563446056341, 0.126590431570353, 0.126606674388380, 0.126612180613071, 0.126606952779412, 0.126590989612876, 0.126564285797139, 0.126526831749992, 0.126478613406235, 0.126419612006330, 0.126349803889672, 0.126269160291419, 0.126177647141875, 0.126075224867450, 0.125961848192331, 0.125837465940018, 0.125702020833972, 0.125555449296615, 0.125397681246109, 0.125228639890250, 0.125048241516994, 0.124856395281118, 0.124653002986675, 0.124437958864848, 0.124211149347016, 0.123972452832807, 0.123721739453075, 0.123458870827805, 0.123183699819012, 0.122896070278925, 0.122595816793879, 0.122282764425033, 0.121956728449240, 0.121617514112253, 0.121264916445632, 0.12089

Appendices

8720389863, 0.120518702505296, 0.120124641692143, 0.119716384129848, 0.1192942407
85915, 0.118861400474037, 0.118438208511605, 0.118144475407947];

W(1, :, 8) =

[0.112899891049681, 0.113394895192568, 0.113936175930231, 0.114472854039220, 0.11
4995235376583, 0.115501488687377, 0.115991267054131, 0.116464523040516, 0.1169212
81072410, 0.117361589997160, 0.117785511797217, 0.118193118145984, 0.118584488805
163, 0.118959710502080, 0.119318875963021, 0.119662083023270, 0.119989433793705, 0
.120301033878241, 0.120596991639677, 0.120877417512211, 0.121142423358957, 0.1213
92121872660, 0.121626626017808, 0.121846048512222, 0.122050501346195, 0.122240095
337240, 0.122414939718482, 0.122575141758785, 0.122720806412680, 0.12285203599826
3, 0.122968929901188, 0.123071584303034, 0.123160091932288, 0.123234541836286, 0.1
23295019172533, 0.123341605017845, 0.123374376193839, 0.123393405107380, 0.123398
759604612, 0.123390502837337, 0.123368693140481, 0.123333383919539, 0.12328462354
6898, 0.123222455266006, 0.123146917102452, 0.123058041781053, 0.122955856648097,
0.122840383598001, 0.122711639003648, 0.122569633649763, 0.122414372668728, 0.122
245855478345, 0.122064075721029, 0.121869021204081, 0.121660673840661, 0.12143900
9591243, 0.121203998405301, 0.120955604163139, 0.120693784617787, 0.1204184913370
05, 0.120129669645497, 0.119827258567549, 0.119511190770429, 0.119181392509078, 0.
118837783573263, 0.118480277240449, 0.118108780246634, 0.117723192829286, 0.11732
3409116887, 0.116909319411422, 0.116480823663778, 0.116037913357315, 0.1155811703
68517, 0.115114742381630, 0.114663470403849, 0.114367615039863];

W(1, :, 9) =

[0.104548103779705, 0.105223844105889, 0.105958102671931, 0.106684200153377, 0.10
7390038192712, 0.108073502383851, 0.108734304796788, 0.109372507144771, 0.1099882
48015660, 0.110581689273435, 0.111153004164229, 0.111702373916051, 0.112229986219
476, 0.112736034176415, 0.113220715396156, 0.113684231162889, 0.114126785656243, 0
.114548585220066, 0.114949837677770, 0.115330751693127, 0.115691536175402, 0.1160
32399727601, 0.116353550136448, 0.116655193902649, 0.116937535809876, 0.117200778
530888, 0.117445122269138, 0.117670764434221, 0.117877899349479, 0.11806671799014
9, 0.118237407750367, 0.118390152237454, 0.118525131091909, 0.118642519831537, 0.1
18742489718275, 0.118825207646220, 0.118890836049511, 0.118939532828710, 0.118971
451294389, 0.118986740126735, 0.118985543349971, 0.118968000320506, 0.11893424572
7772, 0.118884409606730, 0.118818617361143, 0.118736989796737, 0.118639643163422,
0.118526689205831, 0.118398235221474, 0.118254384125867, 0.118095234524041, 0.117
920880787935, 0.117731413139163, 0.117526917736787, 0.117307476769705, 0.11707316
8553409, 0.116824067630834, 0.116560244877172, 0.116281767608527, 0.1159886996943
77, 0.115681101673882, 0.115359030876159, 0.115022541544735, 0.114671684966591, 0.
114306509606763, 0.113927061251599, 0.113533383173272, 0.113125516376610, 0.11270
3500261723, 0.112267375669013, 0.111817202288992, 0.111353163290143, 0.1108761890
98233, 0.110391561383173, 0.109928854297985, 0.109646920676001];

Td(1, :, 1) =

[338.055546763667, 337.980855497630, 337.882281843690, 337.785047058670, 337.6935
27510991, 337.608372571038, 337.529578298876, 337.457029971036, 337.390597631688,
337.330153138600, 337.275573224966, 337.226739973316, 337.183540781624, 337.14586
8223390, 337.113619885086, 337.086698199507, 337.065010279556, 337.048467753677, 3
37.036986603407, 337.030487003267, 337.028893163222, 337.032133173821, 337.040138
854180, 337.052845602914, 337.070192252098, 337.092120924354, 337.118576893109, 33
7.149508446069, 337.184866751943, 337.224605730435, 337.268681925505, 337.3170543
81892, 337.369684524901, 337.426536043416, 337.487574776124, 337.552768600912, 337
.622087327406, 337.695502592605, 337.772987759571, 337.854517819134, 337.94006929
4548, 338.029620149078, 338.123149696438, 338.220638514051, 338.322068359072, 338.
427422087122, 338.536683573689, 338.649837638130, 338.766869970234, 338.887767059
288, 339.012516125588, 339.141105054335, 339.273522331863, 339.409756984134, 339.5
49798517423, 339.693636861138, 339.841262312675, 339.992665484245, 340.1478372515
59, 340.306768704275, 340.469451098093, 340.635875808354, 340.806034285004, 340.97
9918008699, 341.157518447748, 341.338827014999, 341.523835021060, 341.71253360475
5, 341.904913528194, 342.100964146374, 342.300667333603, 342.503961238418, 342.710
529994926, 342.918635725552, 343.118970017051, 343.264272133999];

Appendices

Td(1, :, 2) =

[338.075183392265, 337.998691848241, 337.898076231494, 337.798780518714, 337.705218420971, 337.618044732237, 337.537255334864, 337.462734373178, 337.394350627355, 337.331974708225, 337.275482146948, 337.224753874099, 337.179676186424, 337.140140606622, 337.106043720282, 337.077287008687, 337.053776682072, 337.035423514542, 337.022142681133, 337.013853597255, 337.010479760721, 337.011948596507, 337.018191304383, 337.029142709531, 337.044741116248, 337.064928164804, 337.089648691522, 337.118850592124, 337.152484688372, 337.190504598025, 337.232866608116, 337.279529551545, 337.330454686986, 337.385605582066, 337.444947999823, 337.508449788374, 337.576080773788, 337.647812656107, 337.723618908478, 337.803474679347, 337.887356697678, 337.975243181131, 338.067113747167, 338.162949327027, 338.262732082517, 338.366445325578, 338.474073440558, 338.585601809154, 338.701016737970, 338.820305388620, 338.943455710340, 339.070456375039, 339.201296714732, 339.335966661291, 339.474456688445, 339.616757755955, 339.762861255886, 339.912758960893, 340.066442974408, 340.223905682654, 340.385139708323, 340.550137865827, 340.718893117936, 340.891398533603, 341.067647246659, 341.247632414464, 341.431347172895, 341.618784568379, 341.809937353371, 342.004796949197, 342.203347321880, 342.405528423066, 342.611024057177, 342.818083539875, 343.017318113270, 343.161048950706];

Td(1, :, 3) =

[338.097106171828, 338.018689416457, 337.916005619521, 337.814642747141, 337.719035719953, 337.629841924100, 337.547056567402, 337.470562566092, 337.400227407836, 337.335920438279, 337.277515968755, 337.224893758866, 337.177938983653, 337.136542093123, 337.100598648746, 337.070009155820, 337.044678896264, 337.024517763112, 337.009440097145, 336.999364525949, 336.994213805576, 336.993914664963, 336.998397653264, 337.007596990203, 337.021450419536, 337.039899065732, 337.062887293897, 337.090362573016, 337.122275342539, 337.158578882320, 337.199229185932, 337.244184837341, 337.293406890949, 337.346858754956, 337.404506078048, 337.466316639360, 337.532260241683, 337.602308607876, 337.676435280443, 337.754615524232, 337.836826232195, 337.923045834182, 338.013254208701, 338.107432597609, 338.205563523676, 338.307630710962, 338.413619007978, 338.523514313556, 338.637303505387, 338.754974371165, 338.876515542292, 339.001916430070, 339.131167164333, 339.264258534441, 339.401181932586, 339.541929299311, 339.686493071184, 339.834866130529, 339.987041757107, 340.143013581667, 340.302775541214, 340.466321835877, 340.633646887211, 340.804745297730, 340.979611811328, 341.158241273693, 341.340628589053, 341.526768653868, 341.716656153282, 341.910284520877, 342.107639786515, 342.308663837241, 342.513041195185, 342.719014346142, 342.917145045730, 343.059489085458];

Td(1, :, 4) =

[338.121302164220, 338.040831523841, 337.936053037913, 337.832616601011, 337.734962117370, 337.643746721429, 337.558964447945, 337.480496889286, 337.408210212488, 337.341972480221, 337.281656766641, 337.227141641791, 337.178311138957, 337.135054613962, 337.097266581328, 337.064846546275, 337.037698837147, 337.015732439541, 336.998860832600, 336.987001827732, 336.980077409966, 336.978013582085, 336.980740211701, 336.988190881380, 337.000302741915, 337.017016368846, 337.038275622267, 337.064027509990, 337.094222054095, 337.128812160874, 337.167753494200, 337.211004352303, 337.258525547952, 337.310280292018, 337.366234080405, 337.426354584306, 337.490611543754, 337.558976664434, 337.631423517706, 337.707927443804, 337.788465458149, 337.873016160749, 337.961559648618, 338.054077431178, 338.150552348586, 338.250968492933, 338.355311132272, 338.463566637413, 338.575722411438, 338.691766821875, 338.811689135484, 338.935479455580, 339.063128661851, 339.194628352593, 339.329970789291, 339.469148843480, 339.612155945802, 339.758986037161, 339.909633521894, 340.064093222827, 340.222360338116, 340.384430399721, 340.550299233351, 340.719962919674, 340.893417756456, 341.070660220715, 341.251686927225, 341.436494563932, 341.625079689959, 341.817437695938, 342.013556646593, 342.213380496225, 342.416595536235, 342.621443430805, 342.818467476693, 342.959607388839];

Td(1, :, 5) =

[338.147761838255, 338.065104586282, 337.958204732328, 337.852688211013, 337.752983639185, 337.659745052848, 337.572964815014, 337.492523098708, 337.418284722609, 337.350116449003, 337.287890097911, 337.231483031603, 337.180778121918, 337.135663609366, 337.096032939035, 337.061784592316, 337.032821919044, 337.009052971348, 336.990390339658, 336.976750991169, 336.968056110933, 336.964230945767, 336.965204651114, 336.970910140982, 336.981283941064, 336.996266045132, 337.015799774758, 337.039831642422, 337.068311218049, 337.101190998984, 337.138426283428, 337.1799750

Appendices

47328, 337.225797824717, 337.275857591488, 337.330119652570, 337.388551532493, 337.451122869284, 337.517805311684, 337.588572419617, 337.663399567893, 337.742263853076, 337.825144003483, 337.912020292263, 338.002874453507, 338.097689601330, 338.196450151889, 338.299141748269, 338.405751188200, 338.516266354530, 338.630676148430, 338.748970425239, 338.871139932916, 338.997176253028, 339.127071744201, 339.260819487975, 339.398413236985, 339.539847365381, 339.685116821397, 339.834217081973, 339.987144109322, 340.143894309309, 340.304464491505, 340.468851830759, 340.637053830067, 340.809068284398, 340.984893244573, 341.164526977513, 341.347967903461, 341.535214396096, 341.726263747121, 341.921106026334, 342.119687386481, 342.321696940629, 342.525381551168, 342.721297151877, 342.861413995377];

Td(1, :, 6) =

[338.176475429735, 338.091494432220, 337.982446450019, 337.874843231146, 337.773085842928, 337.677822383711, 337.589043047722, 337.506626493797, 337.430436164998, 337.360337506253, 337.296201066899, 337.237902983631, 337.185324947545, 337.138354063090, 337.096882683810, 337.060808243882, 337.030033090062, 337.004464315324, 336.984013594667, 336.968597023370, 336.958134957896, 336.952551859612, 336.951776141490, 336.955740017902, 336.964379357622, 336.977633540132, 336.995445315275, 337.017760666348, 337.044528676641, 337.075701399463, 337.111233731659, 337.151083290639, 337.195210294880, 337.243577447922, 337.296149825804, 337.352894767934, 337.413781771346, 337.478782388314, 337.547870127283, 337.621020357065, 337.698210214261, 337.779418513867, 337.864625662998, 337.953813577708, 338.046965602823, 338.144066434762, 338.245102047284, 338.350059620105, 338.458927470337, 338.571694986689, 338.688352566381, 338.808891554697, 338.933304187127, 339.061583534030, 339.193723447740, 339.329718512042, 339.469563993942, 339.613255797630, 339.760790420536, 339.912164911373, 340.067376830038, 340.226424209229, 340.389305517607, 340.556019624305, 340.726565764416, 340.900943504575, 341.079152704937, 341.261193458280, 341.447065892778, 341.636769144522, 341.830295257740, 342.027592713524, 342.228354495989, 342.430838676853, 342.625644895205, 342.764918599503];

Td(1, :, 7) =

[338.207432953407, 338.119986301873, 338.008763443475, 337.899066842561, 337.795253821734, 337.697963720337, 337.607184070207, 337.522791922110, 337.444649316774, 337.372620365267, 337.306574330150, 337.246386105169, 337.191936181807, 337.143110508119, 337.099800324398, 337.061901994619, 337.029316838273, 337.001950963875, 336.979715104648, 336.962524456622, 336.950298519417, 336.942960939825, 336.940439358398, 336.942665259143, 336.949573822440, 336.961103781293, 336.977197280955, 336.997799742015, 337.022859726977, 337.052328810344, 337.086161452251, 337.124314875626, 337.166748946882, 337.213426060139, 337.264311024926, 337.319370957369, 337.378575174809, 337.441895093816, 337.509304131581, 337.580777610610, 337.656292666696, 337.735828160126, 337.819364590056, 337.906884012017, 337.998369958512, 338.093807362620, 338.193182484598, 338.296482841389, 338.403697139009, 338.514815207744, 338.629827940106, 338.748727231475, 338.871505923387, 338.998157749381, 339.128677283338, 339.263059890240, 339.401301679266, 339.543399459117, 339.689350695495, 339.839153470594, 339.992806444496, 340.150308818323, 340.311660298972, 340.476861065221, 340.645911734867, 340.818813331973, 340.995567250576, 341.176175195722, 341.360638989467, 341.548959554950, 341.741130879310, 341.937103899963, 342.136576514605, 342.337823986456, 342.531520606709, 342.670130450049];

Td(1, :, 8) =

[338.240624215866, 338.150564846250, 338.037140474365, 337.925343757639, 337.819472208598, 337.720153614453, 337.627372356267, 337.541003784142, 337.460908510381, 337.386949296207, 337.318994101787, 337.256916561017, 337.200595947348, 337.149917032551, 337.104769922395, 337.065049888086, 337.030657198078, 337.001496951540, 336.977478913962, 336.958517355195, 336.944530890147, 336.935442322295, 336.931178490204, 336.931670117155, 336.936851664033, 336.946661185542, 336.961040189841, 336.979933501652, 337.003289128888, 337.031058132838, 337.063194501908, 337.099655028946, 337.140399192133, 337.185389039430, 337.234589076572, 337.287966158562, 337.345489384662, 337.407129996816, 337.472861281489, 337.542658474869, 337.616498671385, 337.694360735509, 337.776225216772, 337.862074267968, 337.951891566480, 338.045662238685, 338.143372787378, 338.245011022179, 338.350565992840, 338.460027925433, 338.573388161325, 338.690639098905, 338.811774137985, 338.936787626821, 339.065674811664, 339.198431788780, 339.335055458842, 339.475543483611, 339.619894244790, 339.768106804952, 339.920180870401, 340.076116755829, 340.235915350592, 340.399578086395, 340.567106906034, 340.738504232294, 340.913772933366, 341.09291626587

Appendices

```
4, 341.275937684654, 341.462839841975, 341.653618635436, 341.848227584232, 342.046
370531498, 342.246345865013, 342.438933260577, 342.577058346321];
```

```
Td(1, :, 9) =
[338.276033945433, 338.183209226373, 338.067556889181, 337.953653267961, 337.8457
20197947, 337.744371159212, 337.649586900641, 337.561240980823, 337.479192558416,
337.403303029525, 337.333439036980, 337.269472938576, 337.211282771952, 337.15875
2113325, 337.111769913273, 337.070230328266, 337.034032552537, 337.003080651583, 3
36.977283397782, 336.956554108426, 336.940810486397, 336.929974463658, 336.923972
047750, 336.922733171408, 336.926191545438, 336.934284514950, 336.946952919018, 33
6.964140953842, 336.985796039458, 337.011868690023, 337.042312387700, 337.0770834
60152, 337.116140961640, 337.159446557722, 337.206964413519, 337.258661085548, 337
.314505417073, 337.374468436939, 337.438523261867, 337.506645002155, 337.57881067
0743, 337.654999095598, 337.735190835379, 337.819368098313, 337.907514664262, 337.
999615809897, 338.095658236953, 338.195630003502, 338.299520458189, 338.407320177
369, 338.519020905108, 338.634615495959, 338.754097860470, 338.877462913349, 339.0
04706524206, 339.135825470813, 339.270817394768, 339.409680759500, 339.5524148104
78, 339.699019537544, 339.849495639209, 340.003844488782, 340.162068102161, 340.32
4169107060, 340.490150713331, 340.660016683470, 340.833771299733, 341.01141930921
6, 341.192965737938, 341.378414908752, 341.567764596221, 341.760971023519, 341.957
744996374, 342.156413889133, 342.347893172786, 342.485713081402];
```

```
RH(1, x, y) = 0.0078-(0.05759*W(1, x, y))+(24.16554*(W(1, x, y)^2))-
(124.78*(W(1, x, y)^3))+(204.226*W(1, x, y)^4);
```

```
end
```

```
Yd(1, x, 9) = RH(1, x, 9)/((10^-6*exp(5294/Td(1, x, 9)))-(1.61*RH(1,
x, 9)));
```

```
end
```

```
%air stream heat and mass transfer at first half of time step
```

```
%inlet
```

```
for x = 1
```

```
Ya(t+1, x) = Yinlet;
```

```
Ta(t+1, x) = Tinlet;
```

```
Tao(t+1, (nx+1)-x) = Taoinlet;
```

```
end
```

```
%after inlet
```

```
for x = 2:nx
```

```
Ya(t+1, x) = (1/(1+XK1))*(Ya(t, x) + (XK2*(Yd(t, x, 9) - Ya(t, x))) +
(XK1*(Ya(t+1, (x-1))))); %backward implicit
```

```
Ta(t+1, x) = (1/(1+XK1))*(Ta(t, x) + XK1*Ta(t+1, x-1) + XK3*(Td(t, x, 9) -
Ta(t, x)) + XK2h*(Yd(t, x, 9) - Ya(t, x))*(Td(t, x, 9) - Ta(t, x)));
%Backward imp
```

```
Tao(t+1, (nx+1)-x) = (1/(1+XK1o))*(Tao(t, (nx+1)-x) + XK1o*Tao(t+1, (nx+1)-
(x-1)) + XK3o*(Td(t, (nx+1)-x, 1) -Tao(t, (nx+1)-x)) + XK3sh*(Tsh(t, (nx+1)-
x) -Tao(t, (nx+1)-x))); %Backward imp
```

Appendices

```
end

%shell heat balance 1st half step

for x = 1:nx

    Tsh(t+1, x) = Tsh(t, x) + XKsh*(Tao(t, x) - Tsh(t, x));

end

%DESICCANT heat and mass balance 1ST HALF

%HEAT

% input:
%     e = subdiagonal vector
%     f = diagonal vector
%     g = superdiagonal vector
%     r = right hand side vector
% output:
%     Td = solution vector

%for every segment along x
for x=1:nx

for y=1:9

fp(t, x, y) = 1+2*XKd;

end

for y=1:7

    ep(t, x, y) = (-XKd);

    gp(t, x, y) = (-XKd);

end

end

%for left hand boundary
for x=1
for y=1:7
    rp(t, 1, y+1) = (1-2*XKc)*Td(t, 1, y+1)+2*XKc*Td(t, 2, y+1);
end
end

for x=1

for y = 1:9
```

Appendices

```
e(t, 1, :) = [0; ep(t, 1, 1); ep(t, 1, 2); ep(t, 1, 3); ep(t, 1, 4); ep(t, 1, 5); ep(t, 1, 6); ep(t, 1, 7); (-2*XKd)];
f(t, 1, :) = fp(t, 1, :);
g(t, 1, :) = [(-2*XKd); gp(t, 1, 1); gp(t, 1, 2); gp(t, 1, 3); gp(t, 1, 4); gp(t, 1, 5); gp(t, 1, 6); gp(t, 1, 7); 0];
r(t, 1, :) = [(1-2*XKc)*Td(t, 1, 1)+2*XKc*Td(t, 2, 1) - XKd*(Bilo*(Td(t, 1, 1)-Tao(t, 1))); rp(t, 1, 2); rp(t, 1, 3); rp(t, 1, 4); rp(t, 1, 5); rp(t, 1, 6); rp(t, 1, 7); rp(t, 1, 8); (1-2*XKc)*Td(t, 1, 9)+2*XKc*Td(t, 2, 9) - XKd*(Bi1*(Td(t, 1, 9)-Ta(t, 1))+Bi2*(Yd(t, 1, 9)-Ya(t, 1)))*(Td(t, 1, 9)-Ta(t, 1))+Bi3*(Yd(t, 1, 9)-Ya(t, 1)))];
```

```
% TridiagHEAT: Tridiagonal equation solver banded system
% Td = TridiagHEAT(e,f,g,r): Tridiagonal system solver.
```

```
Td(t+1, 1, :) = TridiagHEAT (e(t, 1, :),f(t, 1, :),g(t, 1, :),r(t, 1, :));
%Call other function from other script
```

```
end
```

```
end
```

```
%for between left and right boundaries
for x=2:(nx-1)
```

```
for y=1:7
```

```
rp(t, x, y+1) = XKc*Td(t, x-1, y+1)+(1-2*XKc)*Td(t, x, y+1)+XKc*Td(t, x+1, y+1);
```

```
end
```

```
e(t, x, :) = [0; ep(t, x, 1); ep(t, x, 2); ep(t, x, 3); ep(t, x, 4); ep(t, x, 5); ep(t, x, 6); ep(t, x, 7); (-2*XKd)];
f(t, x, :) = fp(t, x, :);
g(t, x, :) = [(-2*XKd); gp(t, x, 1); gp(t, x, 2); gp(t, x, 3); gp(t, x, 4); gp(t, x, 5); gp(t, x, 6); gp(t, x, 7); 0];
r(t, x, :) = [XKc*Td(t, x-1, 1)+(1-2*XKc)*Td(t, x, 1)+XKc*Td(t, x+1, 1) - XKd*(Bilo*(Td(t, x, 1)-Tao(t, x))); rp(t, x, 2); rp(t, x, 3); rp(t, x, 4); rp(t, x, 5); rp(t, x, 6); rp(t, x, 7); rp(t, x, 8); XKc*Td(t, x-1, 9)+(1-2*XKc)*Td(t, x, 9)+XKc*Td(t, x+1, 9)-XKd*(Bi1*(Td(t, x, 9)-Ta(t, x))+Bi2*(Yd(t, x, 9)-Ya(t, x)))*(Td(t, x, 9)-Ta(t, x))+Bi3*(Yd(t, x, 9)-Ya(t, x)))];
```

```
% TridiagHEAT: Tridiagonal equation solver banded system
% Td = TridiagHEAT(e,f,g,r): Tridiagonal system solver.
```

```
Td(t+1, x, :) = TridiagHEAT (e(t, x, :),f(t, x, :),g(t, x, :),r(t, x, :));
%Call other function from other script
```

```
end
```

```
%for right hand boundary
for x=nx
```

```
for y=1:7
```

Appendices

```
rp(t, nx, y+1) = 2*XKc*Td(t, (nx-1), y+1)+(1-2*XKc)*Td(t, nx, y+1);

end

e(t, nx, :) = [0; ep(t, nx, 1); ep(t, nx, 2); ep(t, nx, 3); ep(t, nx, 4);
ep(t, nx, 5); ep(t, nx, 6); ep(t, nx, 7); (-2*XKd)];
f(t, nx, :) = fp(t, nx, :);
g(t, nx, :) = [(-2*XKd); gp(t, nx, 1); gp(t, nx, 2); gp(t, nx, 3); gp(t, nx,
4); gp(t, nx, 5); gp(t, nx, 6); gp(t, nx, 7); 0];
r(t, nx, :) = [2*XKc*Td(t, (nx-1), 1)+(1-2*XKc)*Td(t, nx, 1) -
XKd*(Bilo*(Td(t, nx, 1)-Tao(t, nx))); rp(t, nx, 2); rp(t, nx, 3); rp(t, nx,
4); rp(t, nx, 5); rp(t, nx, 6); rp(t, nx, 7); rp(t, nx, 8); 2*XKc*Td(t, (nx-
1), 9)+(1-2*XKc)*Td(t, nx, 9)-XKd*(Bi1*(Td(t, nx, 9)-Ta(t, nx))+Bi2*(Yd(t,
nx, 9)-Ya(t, nx))*(Td(t, nx, 9)-Ta(t, nx))+Bi3*(Yd(t, nx, 9)-Ya(t, nx)))]];

% TridiagHEAT: Tridiagonal equation solver banded system
% Td = TridiagHEAT(e,f,g,r): Tridiagonal system solver.

Td(t+1, nx, :) = TridiagHEAT (e(t, nx, :),f(t, nx, :),g(t, nx, :),r(t, nx,
:)); %Call other function from other script

end

%MASS 1st HALF

% input:
% em = subdiagonal vector
% fm = diagonal vector
% gm = superdiagonal vector
% rm = right hand side vector
% output:
% W = solution vector

%for every segment along x
for x=1:nx

for y=1:9

fmp(t, x, y) = 1+2*XKb;

end

for y=1:7

emp(t, x, y) = (-XKb);

gmp(t, x, y) = (-XKb);

end

end

%left hand boundary
for x=1
```

Appendices

```
for y=1:8

    rmp(t, 1, y) = (1-2*XKa)*W(t, 1, y)+2*XKa*W(t, 2, y);

end

em(t, 1, :) = [0; emp(t, 1, 1); emp(t, 1, 2); emp(t, 1, 3); emp(t, 1, 4);
emp(t, 1, 5); emp(t, 1, 6); emp(t, 1, 7); (-2*XKb)];
fm(t, 1, :) = fmp(t, 1, :);
gm(t, 1, :) = [(-2*XKb); gmp(t, 1, 1); gmp(t, 1, 2); gmp(t, 1, 3); gmp(t, 1,
4); gmp(t, 1, 5); gmp(t, 1, 6); gmp(t, 1, 7); 0];
rm(t, 1, :) = [rmp(t, 1, 1); rmp(t, 1, 2); rmp(t, 1, 3); rmp(t, 1, 4); rmp(t,
1, 5); rmp(t, 1, 6); rmp(t, 1, 7); rmp(t, 1, 8); (1-2*XKa)*W(t, 1,
9)+2*XKa*W(t, 2, 9)-XKb*Bim*(Yd(t, 1, 9)-Ya(t, 1))];

% TridiagMASS: Tridiagonal equation solver banded system
% W = TridiagMASS(e,f,g,r): Tridiagonal system solver.

W(t+1, 1, :) = TridiagMASS (em(t, 1, :),fm(t, 1, :),gm(t, 1, :),rm(t, 1, :));
%Call other function from other script

end

%between left and right boundaries
for x=2:(nx-1)

for y=1:8

rmp(t, x, y) = XKa*W(t, x-1, y)+(1-2*XKa)*W(t, x, y)+XKa*W(t, x+1, y);

end

em(t, x, :) = [0; emp(t, x, 1); emp(t, x, 2); emp(t, x, 3); emp(t, x, 4);
emp(t, x, 5); emp(t, x, 6); emp(t, x, 7); (-2*XKb)];
fm(t, x, :) = fmp(t, x, :);
gm(t, x, :) = [(-2*XKb); gmp(t, x, 1); gmp(t, x, 2); gmp(t, x, 3); gmp(t, x,
4); gmp(t, x, 5); gmp(t, x, 6); gmp(t, x, 7); 0];
rm(t, x, :) = [rmp(t, x, 1); rmp(t, x, 2); rmp(t, x, 3); rmp(t, x, 4); rmp(t,
x, 5); rmp(t, x, 6); rmp(t, x, 7); rmp(t, x, 8); XKa*W(t, x-1, 9)+(1-
2*XKa)*W(t, x, 9)+XKa*W(t, x+1, 9)-XKb*Bim*(Yd(t, x, 9)-Ya(t, x))];

% TridiagMASS: Tridiagonal equation solver banded system
% W = TridiagMASS(e,f,g,r): Tridiagonal system solver.

W(t+1, x, :) = TridiagMASS (em(t, x, :),fm(t, x, :),gm(t, x, :),rm(t, x, :));
%Call other function from other script

End

%right hand boundary
for x=nx
```

Appendices

```
for y=1:8

rmp(t, nx, y) = 2*XKa*W(t, (nx-1), y)+(1-2*XKa)*W(t, nx, y);

end

em(t, nx, :) = [0; emp(t, nx, 1); emp(t, nx, 2); emp(t, nx, 3); emp(t, nx,
4); emp(t, nx, 5); emp(t, nx, 6); emp(t, nx, 7); (-2*XKb)];
fm(t, nx, :) = fmp(t, nx, :);
gm(t, nx, :) = [(-2*XKb); gmp(t, nx, 1); gmp(t, nx, 2); gmp(t, nx, 3); gmp(t,
nx, 4); gmp(t, nx, 5); gmp(t, nx, 6); gmp(t, nx, 7); 0];
rm(t, nx, :) = [rmp(t, nx, 1); rmp(t, nx, 2); rmp(t, nx, 3); rmp(t, nx, 4);
rmp(t, nx, 5); rmp(t, nx, 6); rmp(t, nx, 7); rmp(t, nx, 8); 2*XKa*W(t, (nx-
1), 9)+(1-2*XKa)*W(t, nx, 9)-XKb*Bim*(Yd(t, nx, 9)-Ya(t, nx))];

% TridiagMASS: Tridiagonal equation solver banded system
% W = TridiagMASS(e,f,g,r): Tridiagonal system solver.

W(t+1, nx, :) = TridiagMASS (em(t, nx, :),fm(t, nx, :),gm(t, nx, :),rm(t, nx,
:)); %Call other function from other script

end

%Updating the other variables
for x=1:nx %space step

RHa(t+1, x) = Ya(t+1, x)*(10^-6*exp(5294/Ta(t+1, x)))/(1+1.61*Ya(t+1, x));
if RHa (t+1, x) > 1

    RHa(t+1, x) = 1;
    Ya(t+1, x)=RHa(t+1, x)/((10^-6*exp(5294/Ta(t+1, x)))-(1.61*RHa(t+1,
x)));

end

for y=1:9

    RH(t+1, x, y)= 0.0078-(0.05759*W(t+1, x, y))+(24.16554*(W(t+1, x, y)^2))-
(124.78*(W(t+1, x, y)^3))+204.226*W(t+1, x, y)^4;%C/(C-1+(Wmax/W(t+1, x,
y))); %RH after each t

if RH (t+1, x, y) > 1

    RH(t+1, x, y) = 1;

end

end

Yd(t+1, x, 9)=RH(t+1, x, 9)/((10^-6*exp(5294/Td(t+1, x, 9)))-(1.61*RH(t+1,
x, 9)));

end
```

Appendices

```
%SECOND STEP
%air stream heat and mass transfer at 2nd half of time step
%inlet
for x = 1

    Ya(t+2, x) = Yinlet;

Ta(t+2, x) = Tinlet;

    Tao(t+2, (nx+1)-x) = Taoinlet;

end

%after inlet

for x = 2:nx

Ya(t+2, x) = (1/(1+XK1))*(Ya(t+1, x) + (XK2*(Yd(t+1, x, 9) - Ya(t+1, x))) +
(XK1*(Ya(t+2, (x-1))))); %backward implicit

    Ta(t+2, x) = (1/(1+XK1))*(Ta(t+1, x) + XK1*Ta(t+2, x-1) + XK3*(Td(t+1, x, 9)
-Ta(t+1, x)) + XK2h*(Yd(t+1, x, 9) - Ya(t+1, x))*(Td(t+1, x, 9) - Ta(t+1,
x))); %Backward imp

    Tao(t+2, (nx+1)-x) = (1/(1+XK1o))*(Tao(t+1, (nx+1)-x) + XK1o*Tao(t+2,
(nx+1)-(x-1)) + XK3o*(Td(t+1, (nx+1)-x, 1) -Tao(t+1, (nx+1)-x)) +
XK3sh*(Tsh(t+1, (nx+1)-x) -Tao(t+1, (nx+1)-x))); %Backward imp

end

%shell heat balance 2ND half step

for x = 1:nx

    Tsh(t+2, x) = Tsh(t+1, x) + XKsh*(Tao(t+1, x) - Tsh(t+1, x));

end

%MASS 2ND HALF

% input:
%     em = subdiagonal vector
%     fm = diagonal vector
%     gm = superdiagonal vector
%     rm = right hand side vector
% output:
%     W = solution vector

%for lower boundary
for x=1:nx

for y=1

fmp(t+1, x, y) = 1+2*XKa;
    rmp(t+1, x, y) = (1-2*XKb)*W(t+1, x, 1)+2*XKb*W(t+1, x, 2);
```

Appendices

```
end

end

for x=1:(nx-2)

for y=1

    emp(t+1, x, y) = (-XKa);

    gmp(t+1, x, y) = (-XKa);

end

end

for x=1:nx

for y=1

em(t+1, :, 1) = [0 emp(t+1, 1:(nx-2), 1) (-2*XKa)];
fm(t+1, :, 1) = fmp(t+1, :, 1);
gm(t+1, :, 1) = [(-2*XKa) gmp(t+1, 1:(nx-2), 1) 0];
rm(t+1, :, 1) = rmp(t+1, :, 1);

% TridiagMASS: Tridiagonal equation solver banded system
% W = TridiagMASS(e,f,g,r): Tridiagonal system solver.

W(t+2, :, 1) = TridiagMASS (em(t+1, :, 1),fm(t+1, :, 1),gm(t+1, :, 1),rm(t+1,
:, 1)); %Call other function from other script

end

end

%for between upper and lower boundaries
for x=1:nx

for y=2:8

fmp(t+1, x, y) = 1+2*XKa;
    rmp(t+1, x, y) = XKb*W(t+1, x, y-1)+(1-2*XKb)*W(t+1, x, y)+XKb*W(t+1,
x, y+1);

end

end

for x=1:(nx-2)

for y=2:8

    emp(t+1, x, y) = (-XKa);

    gmp(t+1, x, y) = (-XKa);
```

Appendices

```
end

end

for x=1:nx

for y=2:8

em(t+1, :, y) = [0 emp(t+1, 1:(nx-2), y) (-2*XKa)];
fm(t+1, :, y) = fmp(t+1, :, y);
gm(t+1, :, y) = [(-2*XKa) gmp(t+1, 1:(nx-2), y) 0];
rm(t+1, :, y) = rmp(t+1, :, y);

% TridiagMASS: Tridiagonal equation solver banded system
% W = TridiagMASS(e,f,g,r): Tridiagonal system solver.

W(t+2, :, y) = TridiagMASS (em(t+1, :, y),fm(t+1, :, y),gm(t+1, :, y),rm(t+1,
:, y)); %Call other function from other script

end

end

%for upper boundary
for x=1:nx

for y=9

fmp(t+1, x, y) = 1+2*XKa;
rmp(t+1, x, y) = 2*XKb*W(t+1, x, 8)+(1-2*XKb)*W(t+1, x, 9)-
XKb*(Bim*(Yd(t+1, x, 9)-Ya(t+1, x)));

end

end

for x=1:(nx-2)

for y=9

emp(t+1, x, y) = (-XKa);

gmp(t+1, x, y) = (-XKa);

end

end

for x=1:nx

for y=9

em(t+1, :, 9) = [0 emp(t+1, 1:(nx-2), 9) (-2*XKa)];
fm(t+1, :, 9) = fmp(t+1, :, 9);
gm(t+1, :, 9) = [(-2*XKa) gmp(t+1, 1:(nx-2), 9) 0];
rm(t+1, :, 9) = rmp(t+1, :, 9);
```

Appendices

```
% TridiagMASS: Tridiagonal equation solver banded system
%      W = TridiagMASS(e,f,g,r): Tridiagonal system solver.

W(t+2, :, 9) = TridiagMASS (em(t+1, :, 9),fm(t+1, :, 9),gm(t+1, :, 9),rm(t+1,
:, 9)); %Call other function from other script

end

end

%HEAT 2ND STEP

%  input:
%      e = subdiagonal vector
%      f = diagonal vector
%      g = superdiagonal vector
%      r = right hand side vector
%  output:
%      Td = solution vector

%lower boundary
for x=1:nx

for y=1

fp(t+1, x, y) = 1+2*XKc;
rp(t+1, x, y) = (1-2*XKd)*Td(t+1, x, 1)+2*XKd*Td(t+1, x, 2) -
XKd*(Bilo*(Td(t+1, x, 1)-Tao(t+1, x)));

end

end

for x=1:(nx-2)

for y=1

ep(t+1, x, y) = (-XKc);

gp(t+1, x, y) = (-XKc);

end

end

for x=1:nx

for y=1

e(t+1, :, 1) = [0 ep(t+1, 1:(nx-2), 1) (-2*XKc)];
f(t+1, :, 1) = fp(t+1, :, 1);
g(t+1, :, 1) = [(-2*XKc) gp(t+1, 1:(nx-2), 1) 0];
```

Appendices

```
r(t+1, :, 1) = rp(t+1, :, 1);

% TridiagHEAT: Tridiagonal equation solver banded system
% Td = TridiagHEAT(e,f,g,r): Tridiagonal system solver.

Td(t+2, :, 1) = TridiagHEAT (e(t+1, :, 1),f(t+1, :, 1),g(t+1, :, 1),r(t+1, :,
1)); %Call other function from other script

end

end

%between lower and upper boundaries
for x=1:nx

for y=2:8

fp(t+1, x, y) = 1+2*XKc;
rp(t+1, x, y) = XKd*Td(t+1, x, y-1)+(1-2*XKd)*Td(t+1, x,
y)+XKd*Td(t+1, x, y+1);

end

end

for x=1:(nx-2)

for y=2:8

ep(t+1, x, y) = (-XKc);

gp(t+1, x, y) = (-XKc);

end

end

for x=1:nx

for y=2:8

e(t+1, :, y) = [0 ep(t+1, 1:(nx-2), y) (-2*XKc)];
f(t+1, :, y) = fp(t+1, :, y);
g(t+1, :, y) = [(-2*XKc) gp(t+1, 1:(nx-2), y) 0];
r(t+1, :, y) = rp(t+1, :, y);

% TridiagHEAT: Tridiagonal equation solver banded system
% Td = TridiagHEAT(e,f,g,r): Tridiagonal system solver.

Td(t+2, :, y) = TridiagHEAT (e(t+1, :, y),f(t+1, :, y),g(t+1, :, y),r(t+1, :,
y)); %Call other function from other script

end

end
```

Appendices

```
%upper boundary
for x=1:nx

for y=9

fp(t+1, x, y) = 1+2*XKc;
rp(t+1, x, y) = 2*XKd*Td(t+1, x, 8)+(1-2*XKd)*Td(t+1, x, 9)-
XKd*(Bi1*(Td(t+1, x, 9)-Ta(t+1, x))+Bi2*(Yd(t+1, x, 9)-Ya(t+1, x))*(Td(t+1,
x, 9)-Ta(t+1, x))+Bi3*(Yd(t+1, x, 9)-Ya(t+1, x)));

end

end

for x=1:(nx-2)

for y=9

ep(t+1, x, y) = (-XKc);

gp(t+1, x, y) = (-XKc);

end

end

for x=1:nx

for y=9

e(t+1, :, 9) = [0 ep(t+1, 1:(nx-2), 9) (-2*XKc)];
f(t+1, :, 9) = fp(t+1, :, 9);
g(t+1, :, 9) = [(-2*XKc) gp(t+1, 1:(nx-2), 9) 0];
r(t+1, :, 9) = rp(t+1, :, 9);

% TridiagHEAT: Tridiagonal equation solver banded system
% Td = TridiagHEAT(e,f,g,r): Tridiagonal system solver.

Td(t+2, :, 9) = TridiagHEAT (e(t+1, :, 9),f(t+1, :, 9),g(t+1, :, 9),r(t+1, :,
9)); %Call other function from other script

end

end

%Updating the other variables after 2nd step
for x=1:nx %space step

RHa(t+2, x) = Ya(t+2, x)*(10^-6*exp(5294/Ta(t+2, x)))/(1+1.61*Ya(t+2, x));
if RHa (t+2, x) > 1

RHa(t+2, x) = 1;
```

Appendices

```
Ya(t+2, x)=RHa(t+2, x)/((10^-6*exp(5294/Ta(t+2, x)))-(1.61*RHa(t+2,
x)));

end

for y=1:9

    RH(t+2, x, y)= 0.0078-(0.05759*W(t+2, x, y))+(24.16554*(W(t+2, x, y)^2))-
(124.78*(W(t+2, x, y)^3))+(204.226*W(t+2, x, y)^4); %C/(C-1+(Wmax/W(t+2, x,
y))); %RH after each t

if RH (t+2, x, y) > 1

    RH(t+2, x, y) = 1;

end

end

Yd(t+2, x, 9)=RH(t+2, x, 9)/((10^-6*exp(5294/Td(t+2, x, 9)))-(1.61*RH(t+2,
x, 9)));

end

end

%%%%%%%%%%%%%%%%%%%%%%%%%%%%%%%%%%%%%%%%%%%%%%%%%%%%%%%%%%%%%%%%%%%%%%%%

%REGENERATION CYCLE
Yinlet = Yreg;
Tinlet = Treg;
Taoilet = Th;

for t = n+1:2:2*n %time step

%air stream heat and mass transfer at first half of time step
%inlet
for x = 1

    Ya(t+1, x) = Yinlet;

Ta(t+1, x) = Tinlet;

    Tao(t+1, (nx+1)-x) = Taoilet;

end

%after inlet

for x = 2:nx
```

Appendices

```
Ya(t+1, x) = (1/(1+XK1))*(Ya(t, x) + (XK2*(Yd(t, x, 9) - Ya(t, x))) +
(XK1*(Ya(t+1, (x-1))))); %backward implicit

Ta(t+1, x) = (1/(1+XK1))*(Ta(t, x) + XK1*Ta(t+1, x-1) + XK3*(Td(t, x, 9) -
Ta(t, x)) + XK2h*(Yd(t, x, 9) - Ya(t, x))*(Td(t, x, 9) - Ta(t, x)));
%Backward imp

Tao(t+1, (nx+1)-x) = (1/(1+XK1o))*(Tao(t, (nx+1)-x) + XK1o*Tao(t+1, (nx+1)-
(x-1)) + XK3o*(Td(t, (nx+1)-x, 1) -Tao(t, (nx+1)-x)) + XK3sh*(Tsh(t, (nx+1)-
x) -Tao(t, (nx+1)-x))); %Backward imp

end

%shell side heat balance, 1st step
for x = 1:nx

    Tsh(t+1, x) = Tsh(t, x) + XKsh*(Tao(t, x) - Tsh(t, x));

end

%DESICCANT heat and mass balance 1ST HALF

%HEAT

% input:
% e = subdiagonal vector
% f = diagonal vector
% g = superdiagonal vector
% r = right hand side vector
% output:
% Td = solution vector

%for every segment along x
for x=1:nx

for y=1:9

fp(t, x, y) = 1+2*XKd;

end

for y=1:7

    ep(t, x, y) = (-XKd);

    gp(t, x, y) = (-XKd);

end

end

%for left hand boundary
for x=1
for y=1:7
```

Appendices

```
rp(t, 1, y+1) = (1-2*XKc)*Td(t, 1, y+1)+2*XKc*Td(t, 2, y+1);
end
end

for x=1

for y = 1:9

e(t, 1, :) = [0; ep(t, 1, 1); ep(t, 1, 2); ep(t, 1, 3); ep(t, 1, 4); ep(t, 1,
5); ep(t, 1, 6); ep(t, 1, 7); (-2*XKd)];
f(t, 1, :) = fp(t, 1, :);
g(t, 1, :) = [(-2*XKd); gp(t, 1, 1); gp(t, 1, 2); gp(t, 1, 3); gp(t, 1, 4);
gp(t, 1, 5); gp(t, 1, 6); gp(t, 1, 7); 0];
r(t, 1, :) = [(1-2*XKc)*Td(t, 1, 1)+2*XKc*Td(t, 2, 1) - XKd*(Bilo*(Td(t, 1,
1)-Tao(t, 1))); rp(t, 1, 2); rp(t, 1, 3); rp(t, 1, 4); rp(t, 1, 5); rp(t, 1,
6); rp(t, 1, 7); rp(t, 1, 8); (1-2*XKc)*Td(t, 1, 9)+2*XKc*Td(t, 2, 9)-
XKd*(Bil*(Td(t, 1, 9)-Ta(t, 1))+Bi2*(Yd(t, 1, 9)-Ya(t, 1))*(Td(t, 1, 9)-Ta(t,
1))+Bi3*(Yd(t, 1, 9)-Ya(t, 1)))];

% TridiagHEAT: Tridiagonal equation solver banded system
% Td = TridiagHEAT(e,f,g,r): Tridiagonal system solver.

Td(t+1, 1, :) = TridiagHEAT (e(t, 1, :),f(t, 1, :),g(t, 1, :),r(t, 1, :));
%Call other function from other script

end

end

%for between left and right boundaries
for x=2:(nx-1)

for y=1:7

rp(t, x, y+1) = XKc*Td(t, x-1, y+1)+(1-2*XKc)*Td(t, x, y+1)+XKc*Td(t, x+1,
y+1);

end

e(t, x, :) = [0; ep(t, x, 1); ep(t, x, 2); ep(t, x, 3); ep(t, x, 4); ep(t, x,
5); ep(t, x, 6); ep(t, x, 7); (-2*XKd)];
f(t, x, :) = fp(t, x, :);
g(t, x, :) = [(-2*XKd); gp(t, x, 1); gp(t, x, 2); gp(t, x, 3); gp(t, x, 4);
gp(t, x, 5); gp(t, x, 6); gp(t, x, 7); 0];
r(t, x, :) = [XKc*Td(t, x-1, 1)+(1-2*XKc)*Td(t, x, 1)+XKc*Td(t, x+1, 1) -
XKd*(Bilo*(Td(t, x, 1)-Tao(t, x))); rp(t, x, 2); rp(t, x, 3); rp(t, x, 4);
rp(t, x, 5); rp(t, x, 6); rp(t, x, 7); rp(t, x, 8); XKc*Td(t, x-1, 9)+(1-
2*XKc)*Td(t, x, 9)+XKc*Td(t, x+1, 9)-XKd*(Bil*(Td(t, x, 9)-Ta(t,
x))+Bi2*(Yd(t, x, 9)-Ya(t, x))*(Td(t, x, 9)-Ta(t, x))+Bi3*(Yd(t, x, 9)-Ya(t,
x)))];

% TridiagHEAT: Tridiagonal equation solver banded system
% Td = TridiagHEAT(e,f,g,r): Tridiagonal system solver.

Td(t+1, x, :) = TridiagHEAT (e(t, x, :),f(t, x, :),g(t, x, :),r(t, x, :));
%Call other function from other script
end
```

Appendices

```
%for right hand boundary
for x=nx

for y=1:7

rp(t, nx, y+1) = 2*XKc*Td(t, (nx-1), y+1)+(1-2*XKc)*Td(t, nx, y+1);

end

e(t, nx, :) = [0; ep(t, nx, 1); ep(t, nx, 2); ep(t, nx, 3); ep(t, nx, 4);
ep(t, nx, 5); ep(t, nx, 6); ep(t, nx, 7); (-2*XKd)];
f(t, nx, :) = fp(t, nx, :);
g(t, nx, :) = [(-2*XKd); gp(t, nx, 1); gp(t, nx, 2); gp(t, nx, 3); gp(t, nx,
4); gp(t, nx, 5); gp(t, nx, 6); gp(t, nx, 7); 0];
r(t, nx, :) = [2*XKc*Td(t, (nx-1), 1)+(1-2*XKc)*Td(t, nx, 1) -
XKd*(Bilo*(Td(t, nx, 1)-Tao(t, nx))); rp(t, nx, 2); rp(t, nx, 3); rp(t, nx,
4); rp(t, nx, 5); rp(t, nx, 6); rp(t, nx, 7); rp(t, nx, 8); 2*XKc*Td(t, (nx-
1), 9)+(1-2*XKc)*Td(t, nx, 9)-XKd*(Bi1*(Td(t, nx, 9)-Ta(t, nx))+Bi2*(Yd(t,
nx, 9)-Ya(t, nx)))*(Td(t, nx, 9)-Ta(t, nx))+Bi3*(Yd(t, nx, 9)-Ya(t, nx))]];

% TridiagHEAT: Tridiagonal equation solver banded system
% Td = TridiagHEAT(e,f,g,r): Tridiagonal system solver.

Td(t+1, nx, :) = TridiagHEAT (e(t, nx, :),f(t, nx, :),g(t, nx, :),r(t, nx,
:)); %Call other function from other script

end

%MASS 1st HALF

% input:
% em = subdiagonal vector
% fm = diagonal vector
% gm = superdiagonal vector
% rm = right hand side vector
% output:
% W = solution vector

%for every segment along x
for x=1:nx

for y=1:9

fmp(t, x, y) = 1+2*XKb;

end

for y=1:7

emp(t, x, y) = (-XKb);

gmp(t, x, y) = (-XKb);

end

end
```

Appendices

```
%left hand boundary
```

```
for x=1
```

```
for y=1:8
```

```
    rmp(t, 1, y) = (1-2*XKa)*W(t, 1, y)+2*XKa*W(t, 2, y);
```

```
end
```

```
em(t, 1, :) = [0; emp(t, 1, 1); emp(t, 1, 2); emp(t, 1, 3); emp(t, 1, 4);
```

```
emp(t, 1, 5); emp(t, 1, 6); emp(t, 1, 7); (-2*XKb)];
```

```
fm(t, 1, :) = fmp(t, 1, :);
```

```
gm(t, 1, :) = [(-2*XKb); gmp(t, 1, 1); gmp(t, 1, 2); gmp(t, 1, 3); gmp(t, 1, 4);
```

```
gmp(t, 1, 5); gmp(t, 1, 6); gmp(t, 1, 7); 0];
```

```
rm(t, 1, :) = [rmp(t, 1, 1); rmp(t, 1, 2); rmp(t, 1, 3); rmp(t, 1, 4); rmp(t, 1, 5);
```

```
rmp(t, 1, 6); rmp(t, 1, 7); rmp(t, 1, 8); (1-2*XKa)*W(t, 1,
```

```
9)+2*XKa*W(t, 2, 9)-XKb*Bim*(Yd(t, 1, 9)-Ya(t, 1))];
```

```
% TridiagMASS: Tridiagonal equation solver banded system
```

```
% W = TridiagMASS(e,f,g,r): Tridiagonal system solver.
```

```
W(t+1, 1, :) = TridiagMASS (em(t, 1, :),fm(t, 1, :),gm(t, 1, :),rm(t, 1, :));
```

```
%Call other function from other script
```

```
end
```

```
%between left and right boundaries
```

```
for x=2:(nx-1)
```

```
for y=1:8
```

```
    rmp(t, x, y) = XKa*W(t, x-1, y)+(1-2*XKa)*W(t, x, y)+XKa*W(t, x+1, y);
```

```
end
```

```
em(t, x, :) = [0; emp(t, x, 1); emp(t, x, 2); emp(t, x, 3); emp(t, x, 4);
```

```
emp(t, x, 5); emp(t, x, 6); emp(t, x, 7); (-2*XKb)];
```

```
fm(t, x, :) = fmp(t, x, :);
```

```
gm(t, x, :) = [(-2*XKb); gmp(t, x, 1); gmp(t, x, 2); gmp(t, x, 3); gmp(t, x,
```

```
4); gmp(t, x, 5); gmp(t, x, 6); gmp(t, x, 7); 0];
```

```
rm(t, x, :) = [rmp(t, x, 1); rmp(t, x, 2); rmp(t, x, 3); rmp(t, x, 4); rmp(t,
```

```
x, 5); rmp(t, x, 6); rmp(t, x, 7); rmp(t, x, 8); XKa*W(t, x-1, 9)+(1-
```

```
2*XKa)*W(t, x, 9)+XKa*W(t, x+1, 9)-XKb*Bim*(Yd(t, x, 9)-Ya(t, x))];
```

```
% TridiagMASS: Tridiagonal equation solver banded system
```

```
% W = TridiagMASS(e,f,g,r): Tridiagonal system solver.
```

```
W(t+1, x, :) = TridiagMASS (em(t, x, :),fm(t, x, :),gm(t, x, :),rm(t, x, :));
```

```
%Call other function from other script
```

```
end
```

```
%right hand boundary
```

```
for x=nx
```

Appendices

```
for y=1:8

rmp(t, nx, y) = 2*XKa*W(t, (nx-1), y)+(1-2*XKa)*W(t, nx, y);

end

em(t, nx, :) = [0; emp(t, nx, 1); emp(t, nx, 2); emp(t, nx, 3); emp(t, nx,
4); emp(t, nx, 5); emp(t, nx, 6); emp(t, nx, 7); (-2*XKb)];
fm(t, nx, :) = fmp(t, nx, :);
gm(t, nx, :) = [(-2*XKb); gmp(t, nx, 1); gmp(t, nx, 2); gmp(t, nx, 3); gmp(t,
nx, 4); gmp(t, nx, 5); gmp(t, nx, 6); gmp(t, nx, 7); 0];
rm(t, nx, :) = [rmp(t, nx, 1); rmp(t, nx, 2); rmp(t, nx, 3); rmp(t, nx, 4);
rmp(t, nx, 5); rmp(t, nx, 6); rmp(t, nx, 7); rmp(t, nx, 8); 2*XKa*W(t, (nx-
1), 9)+(1-2*XKa)*W(t, nx, 9)-XKb*Bim*(Yd(t, nx, 9)-Ya(t, nx))];

% TridiagMASS: Tridiagonal equation solver banded system
% W = TridiagMASS(e,f,g,r): Tridiagonal system solver.

W(t+1, nx, :) = TridiagMASS (em(t, nx, :),fm(t, nx, :),gm(t, nx, :),rm(t, nx,
:)); %Call other function from other script

end

%Updating the other variables
for x=1:nx %space step

RHa(t+1, x) = Ya(t+1, x)*(10^-6*exp(5294/Ta(t+1, x)))/(1+1.61*Ya(t+1, x));
if RHa (t+1, x) > 1

    RHa(t+1, x) = 1;
    Ya(t+1, x)=RHa(t+1, x)/((10^-6*exp(5294/Ta(t+1, x)))-(1.61*RHa(t+1,
x)));

end

for y=1:9

    RH(t+1, x, y)= 0.0078-(0.05759*W(t+1, x, y))+(24.16554*(W(t+1, x, y)^2))-
(124.78*(W(t+1, x, y)^3))+(204.226*W(t+1, x, y)^4); %C/(C-1+(Wmax/W(t+1, x,
y))); %RH after each t

if RH (t+1, x, y) > 1

    RH(t+1, x, y) = 1;

end

end

Yd(t+1, x, 9)=RH(t+1, x, 9)/((10^-6*exp(5294/Td(t+1, x, 9)))-
(1.61*RH(t+1, x, 9)));

end
```

Appendices

```
%SECOND STEP
%air stream heat and mass transfer at 2nd half of time step
%inlet
for x = 1

    Ya(t+2, x) = Yinlet;

Ta(t+2, x) = Tinlet;

    Tao(t+2, (nx+1)-x) = Taoinlet;

end

%after inlet

for x = 2:nx

Ya(t+2, x) = (1/(1+XK1))*(Ya(t+1, x) + (XK2*(Yd(t+1, x, 9) - Ya(t+1, x))) +
(XK1*(Ya(t+2, (x-1))))); %backward implicit

    Ta(t+2, x) = (1/(1+XK1))*(Ta(t+1, x) + XK1*Ta(t+2, x-1) + XK3*(Td(t+1, x, 9)
-Ta(t+1, x)) + XK2h*(Yd(t+1, x, 9) - Ya(t+1, x))*(Td(t+1, x, 9) - Ta(t+1,
x))); %Backward imp

    Tao(t+2, (nx+1)-x) = (1/(1+XK1o))*(Tao(t+1, (nx+1)-x) + XK1o*Tao(t+2,
(nx+1)-(x-1)) + XK3o*(Td(t+1, (nx+1)-x, 1) -Tao(t+1, (nx+1)-x)) +
XK3sh*(Tsh(t+1, (nx+1)-x) -Tao(t+1, (nx+1)-x))); %Backward imp

end

%shell heat balance 2ND half step

for x = 1:nx

    Tsh(t+2, x) = Tsh(t+1, x) + XKsh*(Tao(t+1, x) - Tsh(t+1, x));

end

%MASS 2ND HALF

% input:
%     em = subdiagonal vector
%     fm = diagonal vector
%     gm = superdiagonal vector
%     rm = right hand side vector
% output:
%     W = solution vector

%for lower boundary
for x=1:nx

for y=1

fmp(t+1, x, y) = 1+2*XKa;
```

Appendices

```
        rmp(t+1, x, y) = (1-2*XKb)*W(t+1, x, 1)+2*XKb*W(t+1, x, 2);

end

end

for x=1:(nx-2)

for y=1

        emp(t+1, x, y) = (-XKa);

        gmp(t+1, x, y) = (-XKa);

end

end

for x=1:nx

for y=1

em(t+1, :, 1) = [0 emp(t+1, 1:(nx-2), 1) (-2*XKa)];
fm(t+1, :, 1) = fmp(t+1, :, 1);
gm(t+1, :, 1) = [(-2*XKa) gmp(t+1, 1:(nx-2), 1) 0];
rm(t+1, :, 1) = rmp(t+1, :, 1);

% TridiagMASS: Tridiagonal equation solver banded system
% W = TridiagMASS(e,f,g,r): Tridiagonal system solver.

W(t+2, :, 1) = TridiagMASS (em(t+1, :, 1),fm(t+1, :, 1),gm(t+1, :, 1),rm(t+1,
:, 1)); %Call other function from other script

end

end

%for between upper and lower boundaries
for x=1:nx

for y=2:8

fmp(t+1, x, y) = 1+2*XKa;
        rmp(t+1, x, y) = XKb*W(t+1, x, y-1)+(1-2*XKb)*W(t+1, x, y)+XKb*W(t+1,
x, y+1);

end

end

for x=1:(nx-2)

for y=2:8

        emp(t+1, x, y) = (-XKa);
```

Appendices

```
        gmp(t+1, x, y) = (-XKa);

end

end

for x=1:nx

for y=2:8

em(t+1, :, y) = [0 emp(t+1, 1:(nx-2), y) (-2*XKa)];
fm(t+1, :, y) = fmp(t+1, :, y);
gm(t+1, :, y) = [(-2*XKa) gmp(t+1, 1:(nx-2), y) 0];
rm(t+1, :, y) = rmp(t+1, :, y);

% TridiagMASS: Tridiagonal equation solver banded system
% W = TridiagMASS(e,f,g,r): Tridiagonal system solver.

W(t+2, :, y) = TridiagMASS (em(t+1, :, y),fm(t+1, :, y),gm(t+1, :, y),rm(t+1,
:, y)); %Call other function from other script

end

end

%for upper boundary
for x=1:nx

for y=9

fmp(t+1, x, y) = 1+2*XKa;
rmp(t+1, x, y) = 2*XKb*W(t+1, x, 8)+(1-2*XKb)*W(t+1, x, 9)-
XKb*(Bim*(Yd(t+1, x, 9)-Ya(t+1, x)));

end

end

for x=1:(nx-2)

for y=9

emp(t+1, x, y) = (-XKa);

gmp(t+1, x, y) = (-XKa);

end

end

for x=1:nx

for y=9

em(t+1, :, 9) = [0 emp(t+1, 1:(nx-2), 9) (-2*XKa)];
fm(t+1, :, 9) = fmp(t+1, :, 9);
gm(t+1, :, 9) = [(-2*XKa) gmp(t+1, 1:(nx-2), 9) 0];
```

Appendices

```
rm(t+1, :, 9) = rmp(t+1, :, 9);

% TridiagMASS: Tridiagonal equation solver banded system
% W = TridiagMASS(e,f,g,r): Tridiagonal system solver.

W(t+2, :, 9) = TridiagMASS (em(t+1, :, 9),fm(t+1, :, 9),gm(t+1, :, 9),rm(t+1,
:, 9)); %Call other function from other script

end

end

%HEAT 2ND STEP

% input:
% e = subdiagonal vector
% f = diagonal vector
% g = superdiagonal vector
% r = right hand side vector
% output:
% Td = solution vector

%lower boundary
for x=1:nx

for y=1

fp(t+1, x, y) = 1+2*XKc;
rp(t+1, x, y) = (1-2*XKd)*Td(t+1, x, 1)+2*XKd*Td(t+1, x, 2) -
XKd*(Bilo*(Td(t+1, x, 1)-Tao(t+1, x)));

end

end

for x=1:(nx-2)

for y=1

ep(t+1, x, y) = (-XKc);

gp(t+1, x, y) = (-XKc);

end

end

for x=1:nx

for y=1

e(t+1, :, 1) = [0 ep(t+1, 1:(nx-2), 1) (-2*XKc)];
f(t+1, :, 1) = fp(t+1, :, 1);
g(t+1, :, 1) = [(-2*XKc) gp(t+1, 1:(nx-2), 1) 0];
r(t+1, :, 1) = rp(t+1, :, 1);
```

Appendices

```
% TridiagHEAT: Tridiagonal equation solver banded system
% Td = TridiagHEAT(e,f,g,r): Tridiagonal system solver.

Td(t+2, :, 1) = TridiagHEAT (e(t+1, :, 1),f(t+1, :, 1),g(t+1, :, 1),r(t+1, :,
1)); %Call other function from other script

end

end

%between lower and upper boundaries
for x=1:nx

for y=2:8

fp(t+1, x, y) = 1+2*XKc;
rp(t+1, x, y) = XKd*Td(t+1, x, y-1)+(1-2*XKd)*Td(t+1, x,
y)+XKd*Td(t+1, x, y+1);

end

end

for x=1:(nx-2)

for y=2:8

ep(t+1, x, y) = (-XKc);

gp(t+1, x, y) = (-XKc);

end

end

for x=1:nx

for y=2:8

e(t+1, :, y) = [0 ep(t+1, 1:(nx-2), y) (-2*XKc)];
f(t+1, :, y) = fp(t+1, :, y);
g(t+1, :, y) = [(-2*XKc) gp(t+1, 1:(nx-2), y) 0];
r(t+1, :, y) = rp(t+1, :, y);

% TridiagHEAT: Tridiagonal equation solver banded system
% Td = TridiagHEAT(e,f,g,r): Tridiagonal system solver.

Td(t+2, :, y) = TridiagHEAT (e(t+1, :, y),f(t+1, :, y),g(t+1, :, y),r(t+1, :,
y)); %Call other function from other script

end

end
```

Appendices

```
%upper boundary
for x=1:nx

for y=9

fp(t+1, x, y) = 1+2*XKc;
    rp(t+1, x, y) = 2*XKd*Td(t+1, x, 8)+(1-2*XKd)*Td(t+1, x, 9)-
XKd*(Bi1*(Td(t+1, x, 9)-Ta(t+1, x))+Bi2*(Yd(t+1, x, 9)-Ya(t+1, x))*(Td(t+1,
x, 9)-Ta(t+1, x))+Bi3*(Yd(t+1, x, 9)-Ya(t+1, x)));

end

end

for x=1:(nx-2)

for y=9

    ep(t+1, x, y) = (-XKc);

    gp(t+1, x, y) = (-XKc);

end

end

for x=1:nx

for y=9

e(t+1, :, 9) = [0 ep(t+1, 1:(nx-2), 9) (-2*XKc)];
f(t+1, :, 9) = fp(t+1, :, 9);
g(t+1, :, 9) = [(-2*XKc) gp(t+1, 1:(nx-2), 9) 0];
r(t+1, :, 9) = rp(t+1, :, 9);

% TridiagHEAT: Tridiagonal equation solver banded system
% Td = TridiagHEAT(e,f,g,r): Tridiagonal system solver.

Td(t+2, :, 9) = TridiagHEAT (e(t+1, :, 9),f(t+1, :, 9),g(t+1, :, 9),r(t+1, :,
9)); %Call other function from other script

end

end

%Updating the other variables after 2nd step
for x=1:nx %space step

    RHa(t+2, x) = Ya(t+2, x)*(10^-6*exp(5294/Ta(t+2, x)))/(1+1.61*Ya(t+2, x));
if RHa (t+2, x) > 1

    RHa(t+2, x) = 1;
    Ya(t+2, x)=RHa(t+2, x)/((10^-6*exp(5294/Ta(t+2, x)))-(1.61*RHa(t+2,
x)));

end

end
```

Appendices

```
end

for y=1:9

    RH(t+2, x, y)= 0.0078-(0.05759*W(t+2, x, y))+(24.16554*(W(t+2, x, y)^2))-
    (124.78*(W(t+2, x, y)^3))+(204.226*W(t+2, x, y)^4); %C/(C-1+(Wmax/W(t+2, x,
    y))); %RH after each t

    if RH (t+2, x, y) > 1

        RH(t+2, x, y) = 1;

    end

end

end

    Yd(t+2, x, 9)=RH(t+2, x, 9)/((10^-6*exp(5294/Td(t+2, x, 9)))-(1.61*RH(t+2,
    x, 9)));

end

end
```

Appendix B – Thomas Algorithm to solve tridiagonal system of desiccant side heat balance

```
function Td = TridiagHEAT (e,f,g,r)

% Tridiag: Tridiagonal equation solver banded system
% Td = Tridiag(e,f,g,r): Tridiagonal system solver.
% input:
% e = subdiagonal vector
% f = diagonal vector
% g = superdiagonal vector
% r = right hand side vector
% output:
% Td = solution vector
n=length(f);
% forward elimination
for k = 2:n
    factor = e(k)/f(k-1);
    f(k) = f(k) - factor*g(k-1);
    r(k) = r(k) - factor*r(k-1);
end
% back substitution
Td(n) = r(n)/f(n);
for k = n-1:-1:1
    Td(k) = (r(k)-g(k)*Td(k+1))/f(k);
end
```

Appendix C - Thomas Algorithm to solve tridiagonal system of desiccant side moisture balance

```
function W = TridiagMASS (em, fm, gm, rm)

% Tridiag: Tridiagonal equation solver banded system
% W = Tridiag(em, fm, gm, rm): Tridiagonal system solver.
% input:
% em = subdiagonal vector
% fm = diagonal vector
% gm = superdiagonal vector
% rm = right hand side vector
% output:
% W = solution vector
n=length(fm);
% forward elimination
for k = 2:n
    factor = em(k)/fm(k-1);
    fm(k) = fm(k) - factor*gm(k-1);
    rm(k) = rm(k) - factor*rm(k-1);
end
% back substitution
W(n) = rm(n)/fm(n);
for k = n-1:-1:1
    W(k) = (rm(k)-gm(k)*W(k+1))/fm(k);
end
```